

Tentative Design Response Spectrum for Seismically Isolated FBR

K. Ishida, Y. Sawada, H. Shiojiri

Central Research Institute of Electric Power Industry, Abiko, Japan

Masayuki Takemura

Kajima Corporation, Tokyo, Japan

Introduction

In the present paper, the tentative velocity response spectrum formulated as input seismic motion for studying the following three items concerning verification test on seismically isolated FBR is discussed.

- (1) Determination of the scale of seismically isolated element testing apparatus and the dimensions of seismically isolated elements
- (2) Study on seismically isolating method and seismically isolated structure
- (3) Verification test on seismically isolated FBR

Basic conditions for formulating the tentative velocity response spectrum ($\eta=5\%$)

The velocity response spectrum for tentative study formulated this time is not aimed at a specific point but is based on a general design condition that seismically isolated FBR is constructed on the bedrock in any area of Japan. The following four conditions are established to formulate the tentative velocity response spectrum.

- (1) Regarding a slightly long-period seismic motion ($T = 2 \sim 10$ sec.), the one which give an impact of the largest class possible in Japan shall be subjected to evaluation. Limit values are not to be evaluated.
- (2) The subject point shall satisfy the siting conditions for light-water type power reactors in Japan as a general rule, provided that points which have an accumulation layer of several thousand meters and cause a slightly long-period seismic motion to be amplified extremely shall be excluded.
- (3) For short-period domain, the existing spectrum used in light-water type power reactors shall be respected.
- (4) The vertical motion established with respect to the horizontal motion shall be defined by the ratio of amplitude to the horizontal motion.

Method for formulating the tentative velocity response spectrum

Seismic scale subject to evaluation

Looking at the distribution of seismic damages in Japan, earthquakes of M8 class occur off the coast of Sanriku and along the Nankai trough, and many of them occur in the sea areas more than 50 km away off the coast of the Pacific Ocean. Also, from the seismo-tectonics map (Omote's map) for extreme earthquakes, all of M8 class earthquakes occur off the coast of the Pacific Ocean, except some parts in Central Japan. Unless special cases are considered, therefore, discussion here is carried out on the velocity response spectrum for tentative study aimed at the earthquake of M8 with epicentral distance of 50 km.

Method for estimating the velocity response spectrum

To estimate the tentative spectrum for M8 and epicentral distance (Δ) of 50 km, the results of the following methods were currently judged in general.

- (1) Using bedrock accelerograms for strong motion earthquakes, a record of moderate earthquake of about 50 km in epicenter distance is compensated into a record of M8 earthquake by a simple method for evaluation.
- (2) The pseudo velocity response spectrum in the bedrock accelerogram is subjected to regression analysis at M and Δ , and evaluation is performed by extrapolating the empirical equation thus obtained.
- (3) Evaluation is performed by a simple semi-empirical equation using a fault model.
- (4) Evaluation is performed by a semi-empirical equation relating love wave in accordance with the normal mode theory.
- (5) As for the short-period domain, evaluation is performed by the existing spectrum used in the light-water type power reactor.

Results of estimation by the tentative spectrum

Results of estimation using the accelerogram on bedrock

With respect to the accelerogram (88 components) of M6 or more, about 50 km in epicentral distance and 60 km or less in hypocenter depth obtained on the bedrock ($V_s = 700-1800$ m/sec), the spectrum amplitude of each observation record was compensated into equivalence of M8 using the coefficient (γ) expressed by equation (1), and the result thus obtained is shown in Fig. 2 together with the mean and standard deviation.

$$\gamma = 10^{\Delta^n} \quad (1)$$

Equation (1) considers only the term relating to amplitude and magnitude from the equation for determining the magnitude adopted by the Japanese Meteorological Agency (JMA), and an appropriate result can be obtained for the spectrum amplitude in the neighborhood of 5 seconds in period. The result was about 40 kine in mean value and about 60 kine in mean value + standard deviation ($+\sigma$) in the neighborhood of 5 seconds in period. In Fig. 3, regression analysis was made at M and Δ on 88 pseudo velocity response spectra ($b=5\%$) obtained from the above-mentioned observation record, and from the regression equation thus obtained the mean spectrum at M8 and 50 km in epicentral distance and its standard deviation were determined. Equation (2) was used as the regression equation.

$$\log S_v(T) = a(T)M - (b(T) + m \log R) + c(T) + \sum d_i(T) \quad (2)$$

Here, if the body wave is assumed, then $m = 1$, and R refers to hypocentral distance X; if the surface wave is assumed, then $m = 1/2$ and R refers to hypocentral distance Δ . Also, for differential factor versus observation point, $\sum d_i(T)$, difference in conditions at observation points was taken into consideration. S_v is a velocity response spectrum.

From this, the result obtained by the regression equation is about 40 kine in mean value, and about 70 kine if standard deviation ($+\sigma$) is also considered.

Results of estimation by the semi-empirical equation based on fault model

Ishida^{1,3)} proposed a method for calculating the seismic motion in bedrock by using a low pass-filter which compensates the short-period spectrum because the theoretical seismic motion spectrum based on a simple fault model (Haskell model) underestimates the amplitude of the short-period seismic motion spectrum. Moreover, as this method required many fault parameter, an evaluation equation was proposed by reducing the number of parameters and using magnitude (M), hypocentral distance (X) and stress drop ($\Delta \sigma$) as variables. According to this proposal, the acceleration Fourier spectrum in seismic bedrock can be expressed by the following equation:

$$\ddot{U}(\omega) \sim \left\{ (1.8 \times 10^{10} \cdot 5^{H-2} / X) / A(T) \right\} \cdot \exp(-\omega X / 2V_Q) \quad (3)$$

Where, v_s : shear wave velocity; Q : value Q which represents a decay drop in the propagation path; $A(T)$: low-pass filter shown by the following equation:

$$\left. \begin{aligned} A(T) &= aT / (1+aT) \\ a &= 0.023 \Delta \sigma + 0.22 \end{aligned} \right\} \quad (4)$$

The acceleration Fourier spectrum thus obtained is determined by a seismic moment in the long-period domain and by a stress drop in the short-period domain, as its characteristic.

Kudo²⁾ assumed as $d = 10$ km the mid-point depth of the underground structural model and fault width obtained by blasting test at Yumenoshima in Tokyo and determined the semi-empirical equation of acceleration spectrum intensity $\ddot{U}(\omega)$ (cm/s) on the ground surface against surface wave as shown below, with M and epicentral distance Δ as parameters.

$$\ddot{U}(\omega) \sim 7.2 \times 10^{10} \cdot 5^{H-2} \sqrt{\Delta} \quad (5)$$

Evaluation by the latter for M_0 and epicentral distance 50 km shows about 100 kine. However, considering the fact that this empirical equation relates to Tokyo which has a thick accumulation layer and that the evaluation corresponds to the response spectrum of $h = 0\%$, there is a strong possibility that this evaluation is considerably large. On the other hand, the former evaluates the incident wave equivalent to seismic bedrock to be 13 kine and assumes the amplification ratio of incident wave to amplitude to be about 4 times, thus expecting a seismic motion of 72 kine.

Tentative velocity response spectrum

The results of these studies are summarized in Fig. 4. Based on these results, the tentative value is set at 100 kine within the range of 2 to 10 seconds in period, with engineering judgment considered. It is evident from the figure that this value is almost equal to a velocity response spectrum value (mean value + 2 σ) which is the analytical result based on the seismic observation record. As for short-period domain, the spectrum including a short-period domain and slightly long-period domain is shown in Fig. 5 which adopts existing light-water type power reactor standards. As is clear from this figure, there is a large difference in the spectrum level at a period of 2 seconds. Because of this, both spectrums will be tentatively used as shown by the dotted line. Meanwhile, for reference, external observation records of Japan Sea Central Earthquake ($M_j = 7.7$) which occurred in 1983 and spectrums of La Union records on Mexican Earthquake ($M_s = 8.1$) which occurred in 1985 are shown in the figure.

Estimation of vertical motion velocity response spectrum

The vertical motion velocity response spectrum ($h = 5\%$) is defined by its ratio to the horizontal motion velocity response spectrum ($h = 5\%$). In Fig. 6, the ratio (vertical motion spectrum/horizontal motion spectrum) and the value \pm are shown. The seismic motion record is the same data-set as that used in estimating the tentative horizontal motion velocity response spectrum. The indicated ratio of the vertical motion spectrum to the horizontal motion spectrum is about 0.6 when the period is 2 seconds or more, and in the short-period domain that value is increasing gradually.

Here, considering the fact that attention is paid to the spectrum amplitude in a slightly long-period spectrum, the ratio of the vertical motion spectrum to the horizontal motion spectrum was tentatively set at 0.6.

Conclusion

The velocity response spectrum of a slightly long-period earthquake studied this time was tentatively set at 100 kine in the range of about 2 to 10 seconds in period. This is the result obtained by considering collectively the analytical results of seismic observation records on bedrock, the results of evaluation using a simple fault model ($M = 8.0$, epicentral distance = 50 kine) and the results of evaluation by a prediction equation concerning the spectrum amplitude of love wave ($M = 8.0$, epicentral distance = 50 km).

The present research was conducted under a contract given by the Ministry of International Trade and Industry.

References

- 1) K. Ishida: A study on estimating the characteristics of the strong motion spectrum. Trans. of A.I.J., 1982.
- 2) K. Kudo: A study on the estimation of surface wave related to the long-period structure. SJCEE, 1982.
- 3) K. Ishida: A study on estimating the characteristics of the strong motion spectrum. 7JCEE, 1986.

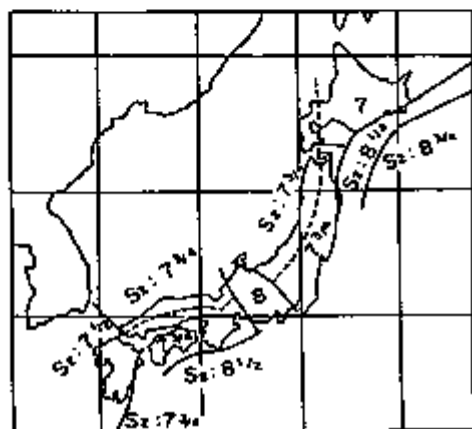


Fig.1 Map on Seismotectonics (Omote's map). Numeral of the figure indicated the extreme magnitude which is expected to occur.

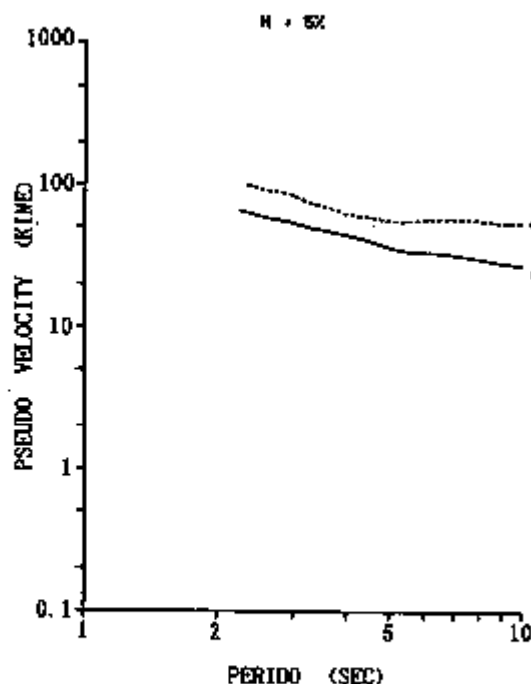


Fig.2 Pseudo velocity response spectra (mean (μ), mean + standard deviation (σ)) corrected by $\gamma = 10 \Delta^n$ (eq.1).

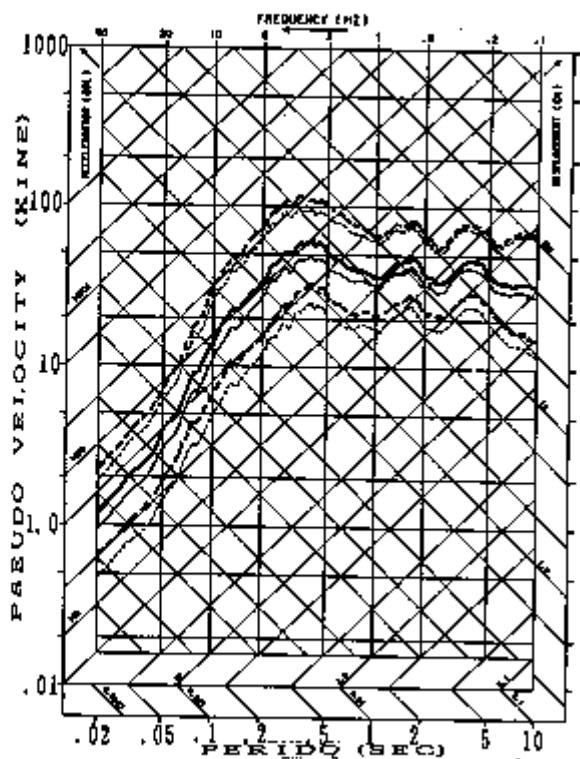


Fig.3 Pseudo velocity response spectra (mean (μ), mean + standard deviation (σ) estimated by regression analysis (eq.2). Thick lines are the results for $m=1$ (eq.2). Fine lines are the results for $m=2$ (eq.2).

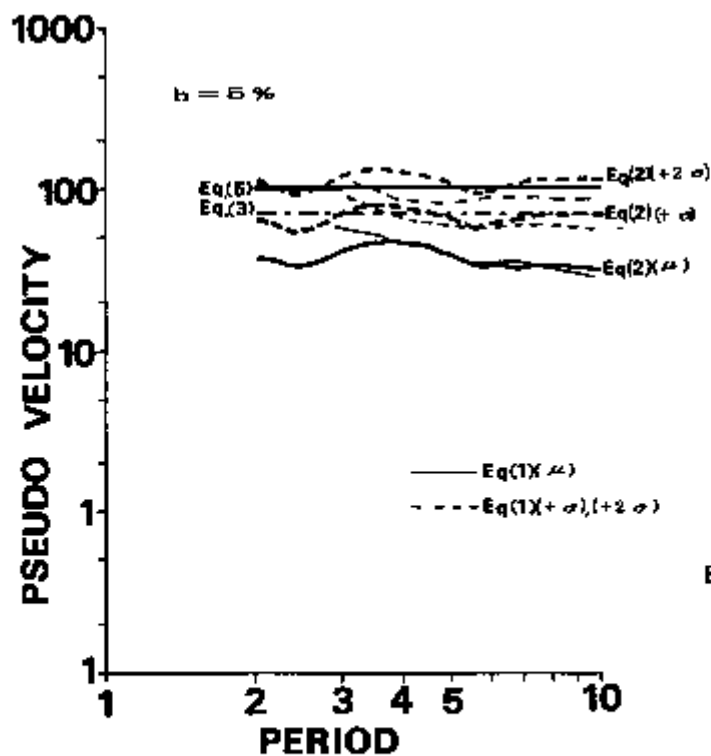


Fig.4 Comparisons of the results obtained various methods (eqs.1 ~ 5).

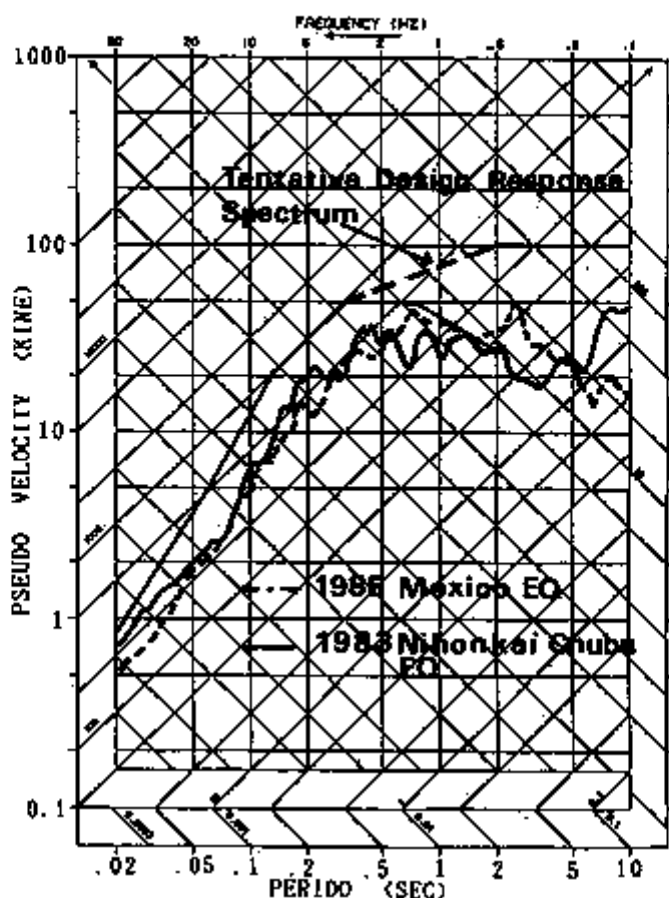


Fig.5 Tentative design base velocity response spectrum ($\eta=5\%$) and the comparisons of observed response spectra of 1983 Nihonkai-Chubu earthquake and 1985 Mexico earthquake.

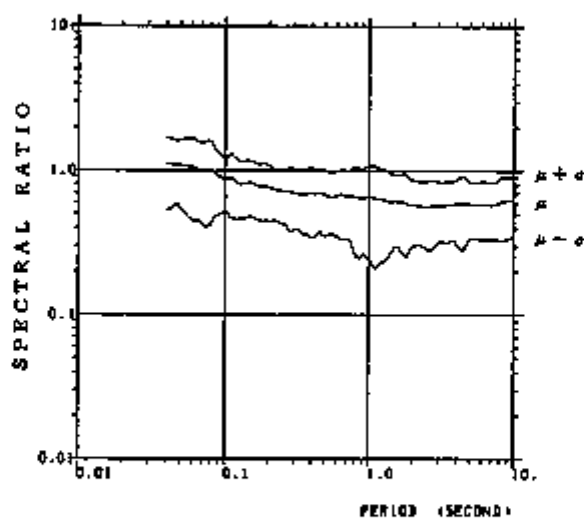


Fig.6 Spectral ratio (vertical / horizontal).

Dynamic Base Isolation of Panels Under Different Dynamic Excitations

M. Olivieri, C. Ravera, C. Mazzieri, E. Traversone
ANSALDO SpA, Genova, Italy

INTRODUCTION

The design of Nuclear Power Plants implies the structural integrity and operability verifications of structures, components and equipment against dynamic excitations caused by earthquakes, operational and accident transient conditions, external events such as pressure waves and missile impacts. For electrical equipment such as panels, the dynamic qualification of the internal instrumentation requires that the medium high frequency components of some design excitations do not cause significant local amplifications. The dynamic base isolation makes this requirement easier to be met. It consists of a combination of spring and damper elements put at the base of the panel (and eventually at the top for high rise configurations), providing a panel dynamic decoupling with respect to the medium high frequency components of the excitation and a displacement limitation against the low frequency components.

CRITERIA FOR ISOLATORS SELECTION

Type Selection

The isolator type selection is one specific phase of the qualification procedure for class 1E electrical equipment typically shown in Table 1.

Among various configurations of dynamic isolators available on the market, the specific choice is based on two main parameters:

- the isolator typical frequency, governing the global dynamic characteristics of the combined panel plus isolators system,
- the isolator intrinsic damping, mainly characterizing the global damping properties of the combined system.

The selection of such parameters relies on the theoretical fundamentals of the dynamic isolation (against sinusoidal excitation typically), indicating that:

- a good isolation efficiency requires that the ratio between the dominating frequency of the excitation and the fundamental frequency of the isolated system be sufficiently high (typically larger than 3).
- taking into account the opposite role of the system damping in the two regions a) of deamplification (required against medium/high frequency excitations) and b) of amplification (possible as a consequence of low frequency excitations) an isolator type exhibiting increasing damping values at higher strains is recommended.

Isolators with damping characteristics varying between 4% of critical at small strains and more than 10% for typical earthquake induced strains are, available on the market.

Isolators Characteristics

For a given type, isolators of a specific size are characterized both statically, by mean of axial and radial static deflection curves, and dynamically, by axial and radial response amplification curves, against sinusoidal or random excitations of suitable amplitude (typically ± 1 mm) in the interesting frequency range (for instance 1 : 70 Hz).

As an example such characteristics are shown in fig. 1 for a steel type isolator, made with a spring contained in a steel wire ball providing damping properties.

Layout considerations

The number, location and mounting directions of the chosen isolators can be defined for given geometrical and inertia properties of the panel and layout boundary conditions.

For high rise panels additional stabilizers may be required also.

For any principal direction a specific check of the resulting isolator stiffness is needed, to avoid excessive displacements and run-stop impacts but to allow strain levels compatible with the required damping magnitude. The resulting stiffness can be obtained from the deflection curves, taking into account the mounting direction and possible preloads for each element. A good distribution of the resulting stiffness must be finally verified to avoid concentrations on single elements.

ANALYSIS VALIDATION WITH TEST RESULTS

In order to validate an analysis procedure, to be extensively used for the dynamic qualification of isolated panels, a prototypical panel has been vibration tested with the PERSEUS shaking table at the Ansaldo Boschetto Facilities in Genoa.

After an independent experimental check of the static and dynamic characteristics provided by the isolator supplier, transmissibility characteristics and forced responses under several dynamic excitations with different frequency contents were evaluated for the isolated panel and for the panel rigidly connected to the shaking table.

Typical instructure responses spectra measured at the top and bottom of the panel are shown in fig. 1 and compared with the base excitation in case of assumed aircraft impact conditions. Following results are worth note:

- peak responses occur at the fundamental frequency of the isolated panel (about 6 Hz).
- A small variation with the panel height of the peak responses indicates that the dominating mode is a quasi rigid panel translation on the isolators.
- The dynamic decoupling obtained with the isolators significantly filters the high frequency components of the excitations.

The measured responses have been also satisfactorily compared with the results of a dynamic analysis of a FEM model of the isolated panel. Fig. 1 typically presents such a comparison for the X impact case.

The analysis procedure consists of a linearization of the isolators stiffness characteristics, a response spectrum analysis of the combined model with strain weighted average modal dampings (Ref./1/) and a direct development of the instructure response spectra for the device qualification (Ref.2).

APPLICATIONS

To show the advantages of the base isolation predictable with the validated analytical procedure, two typical different applications are presented:

- an Instrumentation Rack with a width dimension of 72" subject to seismic and medium/high frequency hydrodynamic excitations is analysed on a fixed base and with base isolation (see fig. 2).
- An Inverter Panel formed with 4 coupled units, resting on a common isolated base slab is analyzed against seismic and high frequency missile impact excitations (see fig. 3).

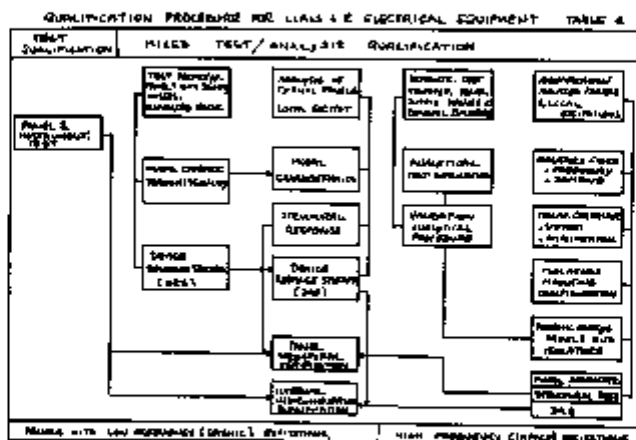
The dynamic decoupling and the redistribution of the modal participation factors towards the fundamental low frequency modes, obtained with the base isolators, significantly reduce the hydrodynamic and impact responses (by a factor of 4 for both horizontal and vertical hydrodynamic peak responses), whereas the additional damping effects of the isolators and the use of top stabilizers limit the maximum seismic responses to still acceptable levels.

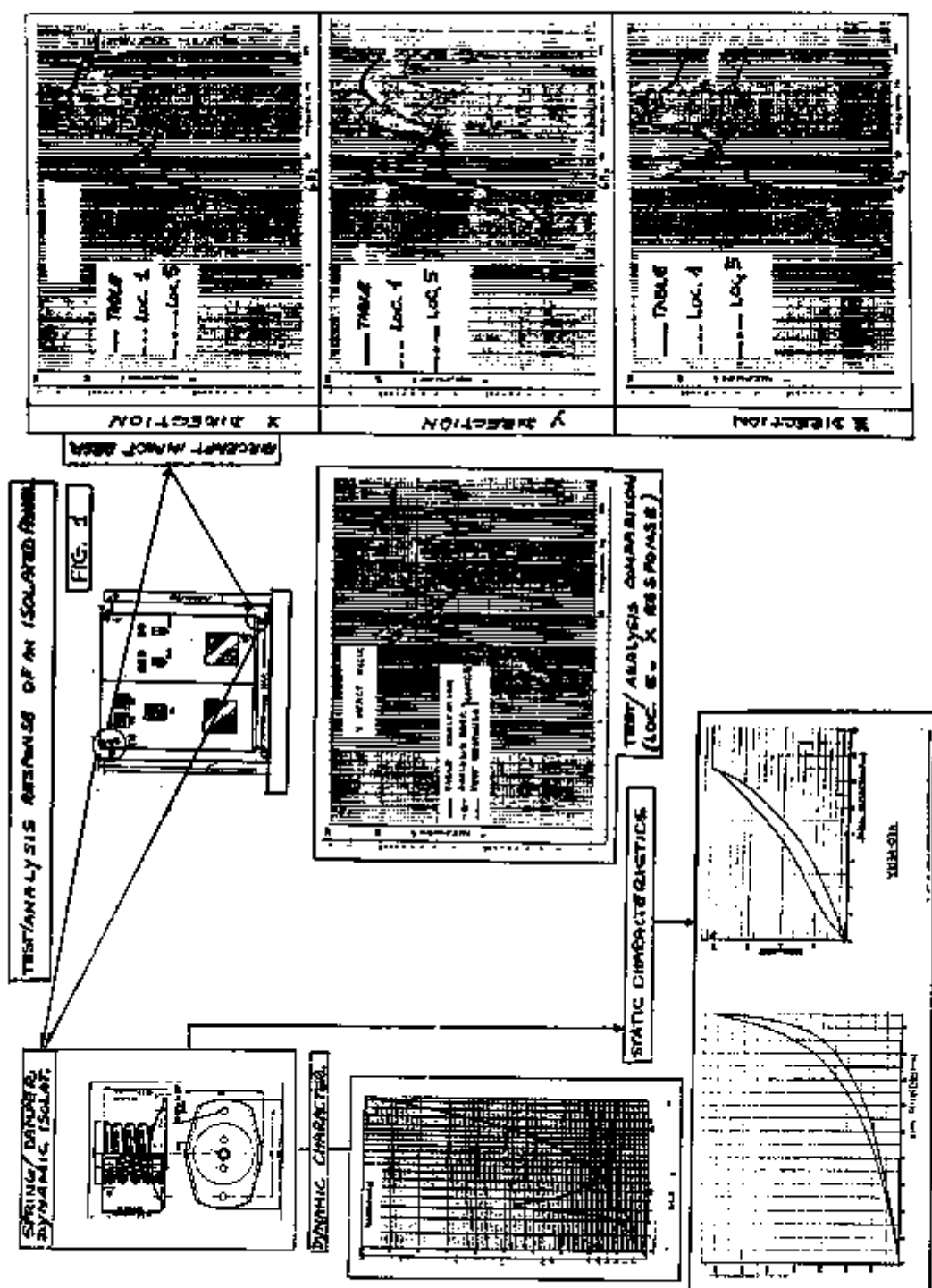
CONCLUSION

The base dynamic isolation of electrical panels is a practical tool to make easier the qualification of internal instruments under dynamic base excitations of different frequency characteristics.

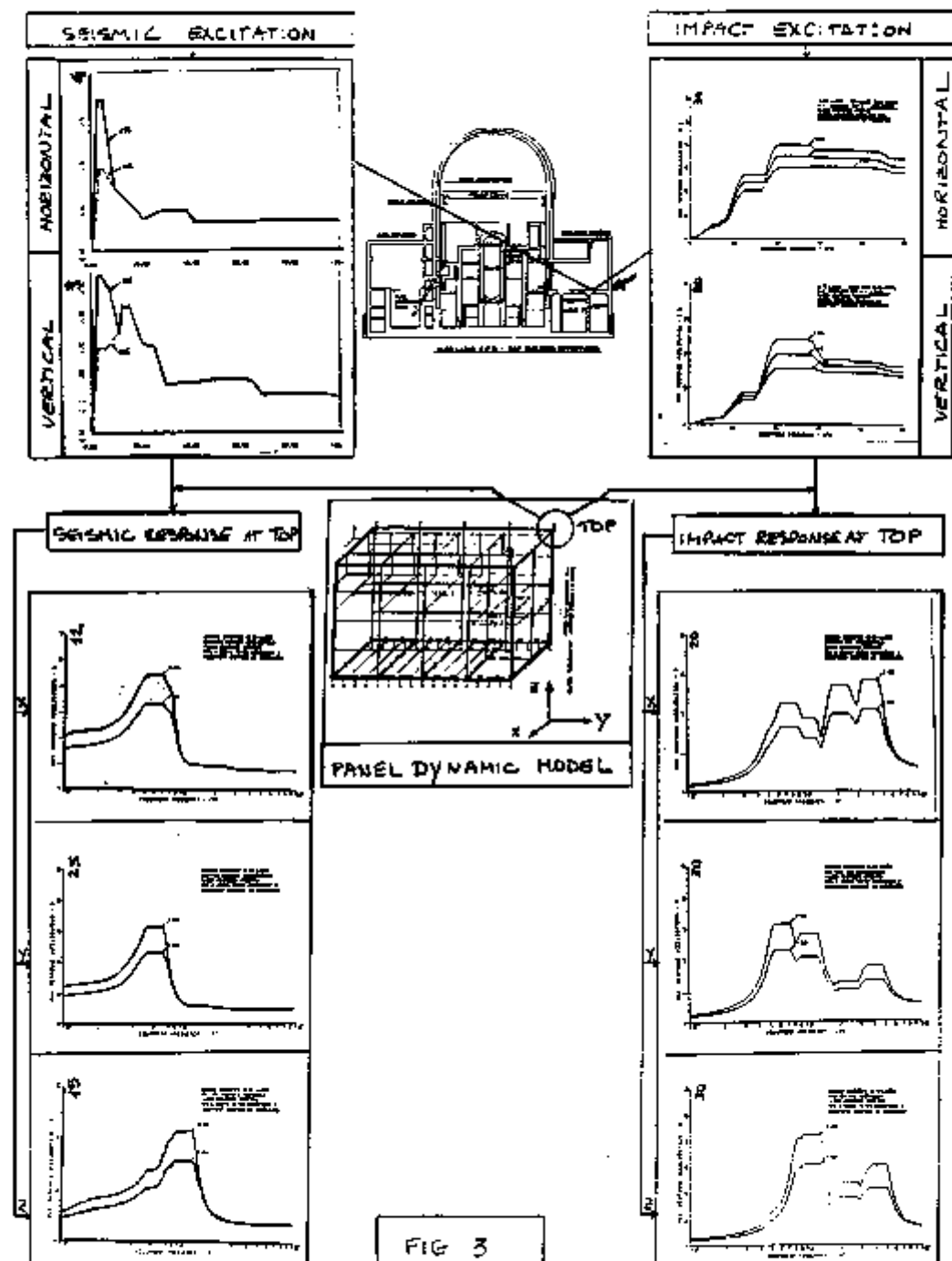
REFERENCES

- 1.-VITI et al "SAP 87" Ansaldo document n° NT-AST-87031
2.-VITI et al "CYRANO 2" Ansaldo document n° STUGAST 0010.





SEISMIC AND IMPACT RESPONSE OF AN ISOLATED "INVERTER" PANEL



Nonlinear Seismic Analysis of Base-Isolated Reactor Building by the Hybrid Frequency-Time-Domain Procedure

Georges R. Darbre
University of California, Berkeley, CA USA

INTRODUCTION

A sliding-type base isolation system can be used to isolate a reactor building from a seismic excitation. The seismic analysis of this type of structure is a challenging task when the radiation condition in the supporting soil must be appropriately accounted for. The reason is that the nonlinear effects of the sliding-type isolation mechanism are defined in the time domain while the contribution of the semi-infinite soil medium to the equation of motion is defined in the frequency domain. One way of performing the seismic analysis of a nonlinear structure interacting with a soil medium characterized by frequency-dependent stiffness coefficients is to disregard the frequency dependence of the stiffness coefficients of the soil. The soil is thus replaced by a set of springs and dashpots with constant coefficients. A time-stepping algorithm can then be used to solve the equation of motion. This approach is obviously only approximate and the results of the analysis performed in this fashion are not as accurate as the results obtained in a linear soil-structure interaction analysis in which the frequency-dependence of the soil contribution is duly accounted for.

In this paper, it is shown how the nonlinear seismic analysis of a base-isolated reactor building is performed when duly accounting for the frequency-dependence of the soil contribution to the equation of motion. The same degree of accuracy is then achieved as when performing a linear soil-structure interaction analysis in which this frequency dependence is considered. The nonlinear analysis is performed using the hybrid-frequency-time domain (HFTD) procedure which proves to be very effective in handling this type of problem.

SYSTEM INVESTIGATED: REACTOR BUILDING ON SLIDING-TYPE BASE ISOLATION

Model: The two-dimensional model of a reactor building on a sliding-type base isolation system shown in Fig. 1 is used to obtain the global response in a multistep seismic analysis. The reactor building with internals is modeled by beams and lumped masses. This superstructure rests on a rigid upper raft which is connected to a rigid lower raft through the isolation mechanism. The lower raft is bound to the soil.

Superstructure: The dynamic properties of the superstructure are characterized by fixed-base natural frequencies of 4.6 Hz for the fundamental frequency, 7.9 Hz for the second frequency and 14.4 Hz for the third frequency. The energy dissipation within the superstructure is taken as stiffness proportional with $[C] = 0.01 \text{ sec } [K]$ (5% critical damping at 1.6 Hz).

Isolation mechanism: The horizontal force/displacement relation of the sliding-type isolation mechanism is given by the elasto-plastic relation shown in Fig. 2. It is defined by the stiffness coefficient $k_h = 2 \cdot 10^6 \text{ N/m}$ and the sliding force $R_h = 60 \cdot 10^6 \text{ N}$. A viscous type of energy dissipation also occurs, with $c_h = 0.015 \text{ sec } k_h$. In the rocking direction, the moment/rotation relation is linear-

elastic with the stiffness coefficient $k_r = 150 \cdot 10^{12}$ Nm characterizing the relation. A viscous damper with $c_r = 0.015$ sec k_r is also present. The three lowest small-amplitude natural frequencies of the superstructure and isolation mechanism on rigid soil are 1.0 Hz, 4.8 Hz and 8.9 Hz, respectively.

Soil: The soil consists of a layer of depth equal to the radius of the foundation (17.5 m) resting on a semi-infinite halfspace. The properties of the layer are: shear modulus of $180 \cdot 10^6$ N/m², mass density of $2 \cdot 10^3$ kg/m³ ($C_s = 300$ m/s), Poisson's ratio of 1/3 and hysteretic damping ratio of 5%. The properties of the halfspace differ only in the value of the shear modulus equal to $720 \cdot 10^6$ N/m² ($C_s = 600$ m/s). The frequency-dependent stiffness coefficients characterizing the response of a massless circular rigid foundation welded to the layer are shown in Fig. 3. The stiffness coefficients form the 2x2 dynamic stiffness matrix $[S_{bb}(\omega)]_g = [K_{bb}(\omega)]_g + i\omega [C_{bb}(\omega)]_g$. The elements of $[K_{bb}(\omega)]_g$ are normalized with respect to the corresponding static values of $K_{hh} = 20 \cdot 10^9$ N/m, $K_{rr} = 4.6 \cdot 10^{12}$ Nm and $K_{hr} = K_{rh} = 13 \cdot 10^9$ N (the coupling coefficient is divided by 5 in the figure for better representation). The elements of $[C_{bb}(\omega)]_g$ are normalized through multiplication by C_s/a (shear wave velocity of layer divided by foundation radius) and division by the static value of the corresponding spring coefficient.

Seismic input: The vertically propagating input earthquake is given by the horizontal free-surface acceleration time history of Fig. 4 with a peak acceleration of 30% g.

METHOD OF ANALYSIS: HFTD PROCEDURE

The hybrid-frequency-time domain (HFTD) procedure has been presented in details elsewhere (Darbre, 1988a; Kawamoto, 1983) and only its fundamental concept as well as those implementation details pertinent to the present analysis are presented here.

Fundamental Concept: In the HFTD procedure, the nonlinear system which needs to be analyzed is replaced by a linear system. Because it is linear, this latter system can be analyzed in the frequency domain and any frequency-dependent quantity can be duly accounted for. The linear system which is introduced differs from the nonlinear system which needs to be analyzed. The resulting difference in response is replaced by the response produced by pseudo-forces. The latter depend on the response itself and the problem has thus to be solved iteratively. Symbolically, the procedure is written as (Darbre, 1988b):

$$\begin{array}{ccc} \{F_{\text{internal}}\} & = & \{F_{\text{external}}\} \\ \{F_{\text{internal}}\}_{\text{linear}} + \{\Delta F_{\text{internal}}\}_{\text{nonlinear}} & & \\ \{F_{\text{internal}}\}_{\text{linear}} & = & \{F_{\text{external}}\} - \{\Delta F_{\text{internal}}\}_{\text{nonlinear}} \\ \downarrow & & \downarrow \quad \downarrow \\ \text{solved in} & \text{defined in} & \text{evaluated in} \\ u\text{-domain} & t\text{-domain} & t\text{-domain} \end{array}$$

Implementation of procedure for system investigated: In this application, the pseudo-linear system is selected as the whole system with a non-sliding isolation mechanism (linear behavior). The equation of motion in the frequency domain is thus (in terms of total displacements):

$$\begin{bmatrix} [S_{aa}(\omega)]_s & [S_{ab}(\omega)]_s \\ [S_{ba}(\omega)]_s & [S_{bb}(\omega)]_s + [S_{bb}(\omega)]_g \end{bmatrix} \begin{Bmatrix} \{u_a(\omega)\} \\ \{u_b(\omega)\} \end{Bmatrix} = \begin{Bmatrix} Q(\omega) \\ 0 \end{Bmatrix} + \begin{Bmatrix} 0 \\ [S_{hb}(\omega)]_g \{u_b(\omega)\}_g \end{Bmatrix}$$

The elements of the matrices identified by the subscript s outside of the brackets refer to the structure composed of the superstructure, the pseudo-linear isolation mechanism and the rafts, while $[S_{bb}]_g$ refers to the dynamic stiffness of the massless foundation welded to the soil. $\{u_b\}_g$ is the input motion identified earlier.

The nonlinear effects are collected in the vector of pseudo forces $\{Q(u)\}$. The vector $\{Q(u)\}$ is the Fourier transform of the time-dependent vector $\{Q(t)\}$. Only two elements of this vector are non-zero, namely those referring to the degrees of freedom affected by the nonlinear sliding-type mechanism (horizontal direction of nodes 1 and 7). They are

$$\begin{Bmatrix} Q_{1h}(t) \\ Q_{7h}(t) \end{Bmatrix} = \begin{Bmatrix} (F_{1h}(t))_{\text{linear}} - (F_{1h}(t))_{\text{nonlinear}} \\ (F_{7h}(t))_{\text{linear}} - (F_{7h}(t))_{\text{nonlinear}} \end{Bmatrix}$$

where $(F_{1h})_{\text{linear}}$ and $(F_{7h})_{\text{linear}}$ are simply given by

$$\begin{Bmatrix} (F_{1h})_{\text{linear}} \\ (F_{7h})_{\text{linear}} \end{Bmatrix} = k_h \begin{bmatrix} 1 & -1 \\ -1 & 1 \end{bmatrix} \begin{Bmatrix} u_{1h} \\ u_{7h} \end{Bmatrix} + c_h \begin{bmatrix} 1 & -1 \\ -1 & 1 \end{bmatrix} \begin{Bmatrix} \dot{u}_{1h} \\ \dot{u}_{7h} \end{Bmatrix}$$

and where $(F_{1h})_{\text{nonlinear}}$ and $(F_{7h})_{\text{nonlinear}}$ are conveniently written as

$$\begin{Bmatrix} (F_{1h})_{\text{nonlinear}} \\ (F_{7h})_{\text{nonlinear}} \end{Bmatrix} = \begin{Bmatrix} (\bar{F}_{1h})_{\text{nonl.}} \\ (\bar{F}_{7h})_{\text{nonl.}} \end{Bmatrix} + c_h \begin{bmatrix} 1 & -1 \\ -1 & 1 \end{bmatrix} \begin{Bmatrix} \dot{u}_{1h} \\ \dot{u}_{7h} \end{Bmatrix}$$

The first part of the right-hand side of this latter equation refers to the stiffness contribution of the isolation mechanism while the second part refers to the viscous-damping contribution. The stiffness contribution is

$$(\bar{F}_{1h}(t+\Delta t))_{\text{nonl.}} = (\bar{F}_{1h}(t))_{\text{nonl.}} + k_h ((u_{1h}(t+\Delta t) - u_{7h}(t+\Delta t)) - (u_{1h}(t) - u_{7h}(t)))$$

$$(\bar{F}_{7h}(t+\Delta t))_{\text{nonl.}} = (\bar{F}_{7h}(t))_{\text{nonl.}} + k_h ((u_{7h}(t+\Delta t) - u_{1h}(t+\Delta t)) - (u_{7h}(t) - u_{1h}(t)))$$

with a limiting positive value of $+R_h$ and a limiting negative value of $-R_h$ imposed both on $(\bar{F}_{1h}(t+\Delta t))_{\text{nonl.}}$ and on $(\bar{F}_{7h}(t+\Delta t))_{\text{nonl.}}$.

RESULTS OF ANALYSIS

The acceleration time histories of nodes 1, 4 and 6 are shown in Figs. 5 to 7. Also shown are the relative horizontal displacement δ between nodes 1 and 7 (Fig. 8) and the sliding code with a value of +1 indicating sliding of the upper raft toward the right, a value of -1 indicating sliding toward the left and a value of 0 indicating no sliding (Fig. 9). Although sliding occurs at very few occasions and over short periods of time, the peak accelerations in the superstructure are substantially lower than when using a non-sliding isolation mechanism. This is shown in Table 1. Also shown in Table 1 is the case where the upper raft is rigidly connected to the lower raft, i.e. the case in which no isolation mechanism is introduced. The associated peak accelerations are then generally still larger.

Table 1: Peak response values for various isolation mechanisms

isolation mechanism	$(\ddot{u}_{1h})_{\text{max}}$ m/sec ² *2	$(\ddot{u}_{4h})_{\text{max}}$ m/sec ² *2	$(\ddot{u}_{6h})_{\text{max}}$ m/sec ² *2	$(\delta)_{\text{max}}$ cm
sliding	1.30	2.19	1.52	14.5
non-sliding	1.97	3.53	2.51	6.4
none	3.29	4.21	2.32	----

As indicated earlier, one can solve nonlinear soil-structure-interaction problems by disregarding the frequency dependence of the stiffness coefficients of the foundation. The peak accelerations obtained when introducing this approximation are shown in Table 2. The constant spring coefficients are selected as the zero-frequency values of the actual dynamic spring coefficients and the constant damping coefficients are taken equal to the infinite-frequency values of the actual dynamic

damping coefficients. Differences in peak accelerations are observed. Similar differences are also observed when analyzing the same superstructure with isolation mechanism resting on a softer soil ($C_s = 150$ m/s for the layer and $C_h = 300$ m/s for the halfspace) and on a stronger soil ($C_s = 600$ m/s for the layer and $C_h = 1200$ m/s for the halfspace).

Table 2: Peak response values with/without frequency dependence (various soils)

soil	frequency dependence	$(\ddot{u}_1)_{\max}$ m/sec ²	$(\ddot{u}_4)_{\max}$ m/sec ²	$(\ddot{u}_6)_{\max}$ m/sec ²	$(\delta)_{\max}$ cm
medium	yes	1.30	2.19	1.52	14.5
	no	1.37	2.37	1.61	15.8
soft	yes	1.77	2.49	1.64	4.4
	no	1.74	2.81	1.80	5.8
strong	yes	1.27	2.15	1.44	13.3
	no	1.31	2.24	1.47	13.6

The peak accelerations are generally lower when considering the frequency dependence of the stiffness coefficients of the soil than when disregarding it. It should however not be concluded, from these data, that disregarding this frequency dependence and using constant spring and damping coefficients leads to a conservative design. The above results apply only to the specific superstructure, isolation mechanism and sites investigated and do not form a large enough data base from which a general conclusion can be drawn.

CONCLUSIONS

This paper addresses the calculation of the global seismic response of a reactor building on a sliding-type base isolation which interacts with the surrounding semi-infinite soil. Two major conclusions are drawn from this study.

First, the HFTD procedure proves to be very effective in performing a nonlinear seismic analysis in which the frequency dependence of the stiffness coefficients of the soil is duly accounted for. The accuracy of the results is thus the same as the accuracy achieved in a linear analysis in which this frequency dependence is routinely considered.

Second, the comparison between the peak accelerations of selected nodes when accounting for the frequency dependence of the stiffness coefficients of the soil and when disregarding it shows that the results of the analysis are influenced by this frequency dependence. In the present case, this influence is however limited (difference in peak accelerations between 2% and 13%). This is not surprising as the purpose of an isolation system is to isolate the superstructure from the surrounding soil. Any reasonable changes in soil properties or modeling thereof thus does not strongly affect the calculated response of the superstructure.

ACKNOWLEDGMENT

The support of the Swiss National Science Foundation under grant No. 82.598.0.88 is gratefully acknowledged.

REFERENCES

- Darbra, G.R. and Wolf, J.P. (1988a). Criterion of Stability and Implementation Issues of Hybrid Frequency-Time-Domain Procedure for Nonlinear Dynamic Analysis. *Earthquake Engineering and Structural Dynamics*, Vol. 16, 569-581.
- Darbra, G.R. (1988b). Hybrid Frequency-Time-Domain Procedure for Nonlinear Dynamic Analysis with Application to Nonlinear Soil-Structure Interaction. 9th World Conference on Earthquake Engineering, Tokyo/Kyoto.
- Kawamoto, J.D. (1983). Solutions of nonlinear dynamic structural systems by a hybrid frequency-time-domain approach. Research Report R83-5, Massachusetts Institute of Technology, Department of Civil Engineering, Cambridge.

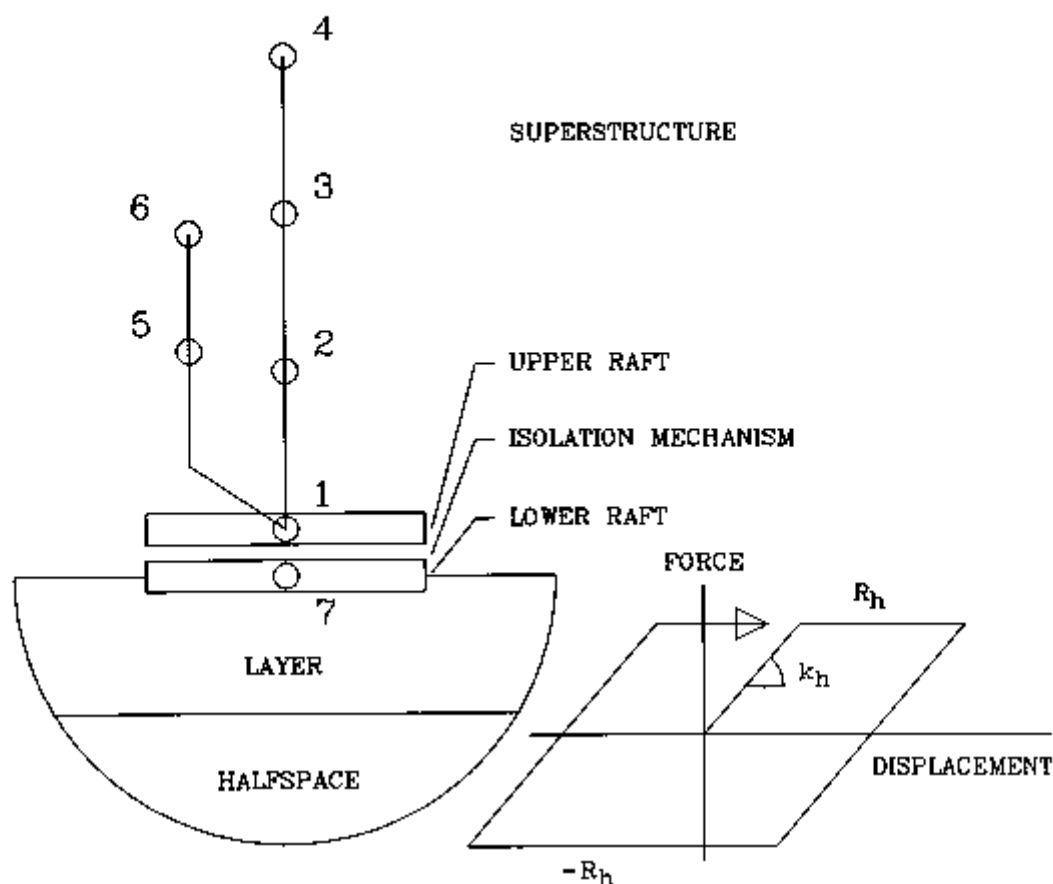


Fig. 1 - Two-dimensional model

Fig. 2 - Horizontal force/
displacement relation
of isolation mechanism

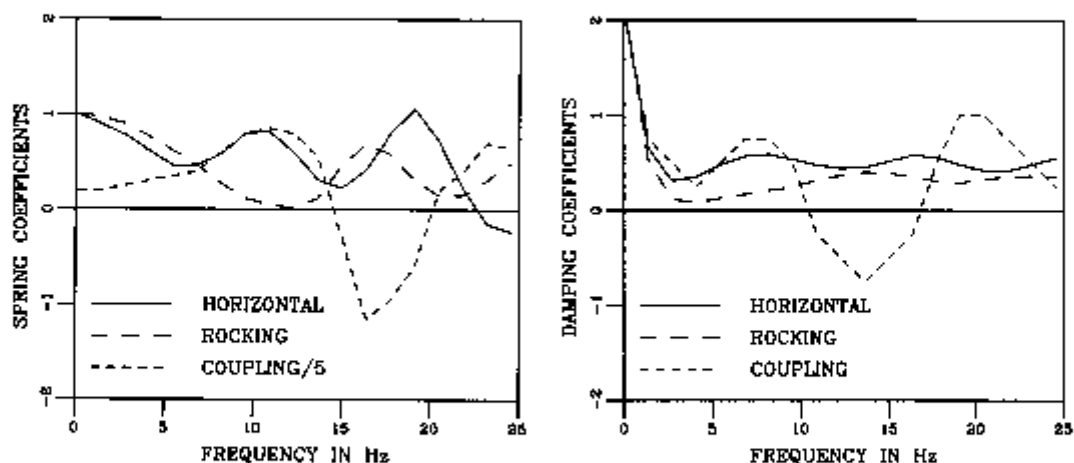


Fig. 3 - Dynamic stiffness coefficients of massless circular rigid foundation
a) spring coefficients
b) damping coefficients

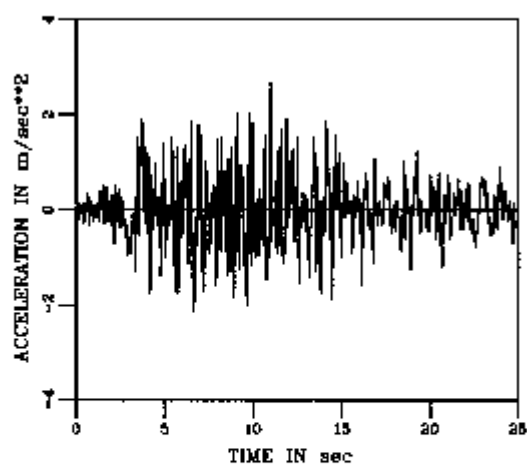


Fig. 4 - Earthquake input acceleration

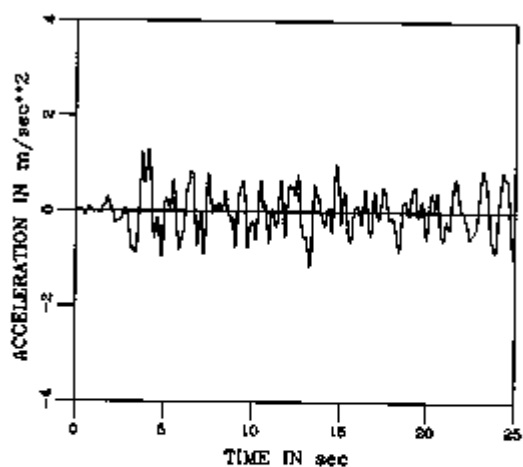


Fig. 5 - Horizontal acceleration of node 1

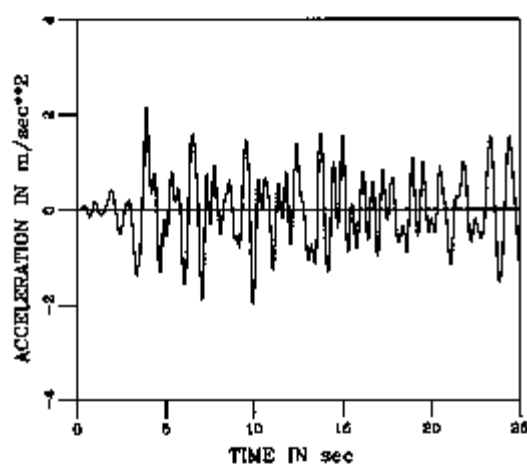


Fig. 6 - Horizontal acceleration of node 4

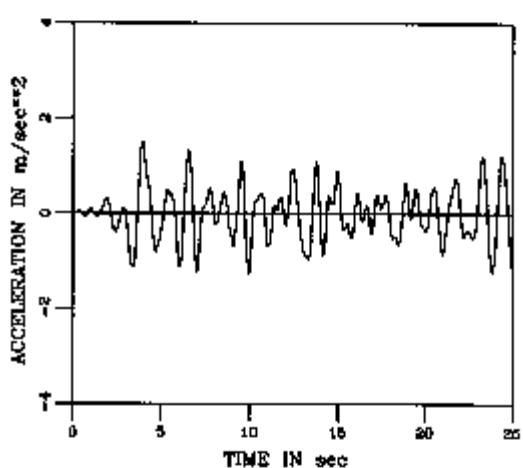


Fig. 7 - Horizontal acceleration of node 5

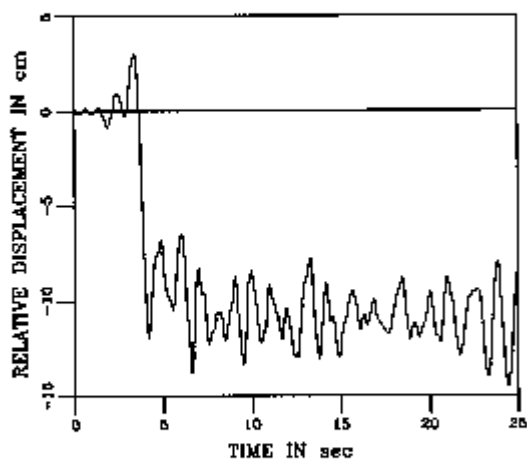


Fig. 8 - Relative isolation displacement

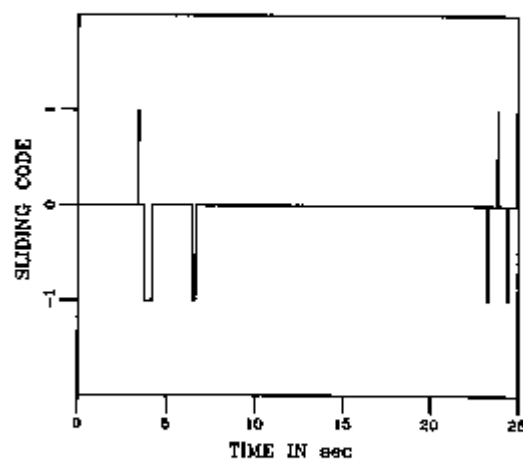


Fig. 9 - Sliding code for isolation mechanism

Study on Base Isolation for Torsional Response Reduction in Asymmetric Structures Under Earthquake Motion

Takashi Nakamura, Tetsuo Suzuki, Hiroshi Okada, T. Takeda
Obayashi Corporation, Tokyo, Japan

1. INTRODUCTION

Recently, several buildings with base isolation systems have been constructed and effectiveness of those systems to reduce earthquake input are reported by several observation results. However, the system is now adopted only in the regular shape building which is symmetry in stiffness and mass distribution in plan and elevation, where torsional response is negligible.

To apply this system to more general building, it is important to establish the design philosophy how to arrange the system so that the torsional effects can be minimized.

In this paper, torsional response characteristics of asymmetrical building models with base isolation systems and effectiveness of usage of those system in reducing the torsional earthquake response are described by dynamic tests and analyses.

2. EXPERIMENTAL MODELS

2.1 Outline of Experiments

Test Model

The test model consists of two floors as shown in Fig.-1 and Photo.-1. The upper floor supported by four steel columns represents a building and has 1 axis eccentricity in stiffness or mass distribution as follows.

- 1) An asymmetrical Model in stiffness distribution (Model A series)
Two pairs of different stiffness steel columns (Column L, Column S) are utilized. The eccentric rate R_x is 0.430.
- 2) An asymmetrical Model in mass distribution (Model B series)
Additional mass is eccentrically attached on the upper floor supported by four same stiffness steel columns (Column M). The eccentric rate R_x is 0.205.

The lower floor has a base isolation system underneath. Two types of isolation systems are employed, one of which is four laminated rubber bearings (Rubbers) usage only, and another is two cantilever type dampers of prestressing steel bar (Dampers) added together.

Regarding the arrangement of Rubbers, same stiffness rubbers are utilized to avoid stiffness eccentricity of base isolation system except Model B-3 and B-4 cases in which two different kinds of Rubbers are installed to coincide the centroid of stiffness of base isolation system with that of gravity of

superstructure.

Table-1 summarizes the test models and characteristics of model components such as Weight, Column, Rubber and Damper. In this table, Model A-1 and B-1 are base fixed case for comparison usage.

Measurement systems with regard to response accelerations, displacements, input acceleration and strains of steel columns and Dampers are also shown in Fig.-1.

Testing Program

One directional (X direction) input motions are applied on shaking table, where maximum accelerations are controlled so that the steel column and Rubber remains in elastic.

1) Resonance test

Natural frequencies and vibration modes of test models are examined by sine wave input motion.

2) Earthquake response test

Three earthquake waves such as El Centro 1940 NS, Taft 1952 EW and Nachinohe 1968 EW are employed where time scale is reduced to 1/2 to take account of scale effect. In this paper, El Centro 1940 NS tests are mainly explained.

2.2 Results of Dynamic Tests

Resonance Curve and Vibration Mode (Dynamic characteristic)

Eigen values obtained from resonance tests are shown in Table-2.

Earthquake Response

Fig.-2 show time history response displacements of upper floor, where input motion is El Centro 1940 NS 150gal and response direction is the same of that of input. In these figure, N means north and indicates weaker stiffness column side for Model A series and additional mass allocated side for Model B series.

In fixed base cases, the displacements of the weaker stiffness columns side in Model A-1 and the additional mass allocated side in Model B-1 are larger than those of the other side, then torsional deformations occur fairly. On the other hand, in base isolated cases, the response displacements of both sides are nearly equal, and no significant torsional deformations occur. In regard to Model B-3 and B-4, the centers of stiffness of the base isolation systems are set to coincide with those of gravity of superstructure.

Besides, when comparing displacements of base isolation systems between only Rubbers usage Model and Dampers added together Model, the latter displacements are smaller than those of the former as a result of energy absorption effect of Dampers.

From these results, it seems very effective to use the base isolation system for the reduction of torsional deformation of asymmetrical buildings.

3. SIMULATION ANALYSIS

Outline of Analysis

Simulation analysis is conducted using shear-type vibration model as shown in Fig.-3, where two translational and a rotational degrees of freedom are provided at the center of gravity of each floor¹⁾. Each column stiffness is evaluated by Multiple Shear Spring model (MSS model)²⁾ as shown in Fig.-3 to take account of the interaction effect between two-dimensional forces beyond elastic region. Viscous damping coefficients are assumed 0.4%, 6.0%, and 0.0% for steel column, laminated rubber bearing and prestressing steel bar, respectively.

Results of Simulation Analysis

Analytical results of eigen values, time history waves of earthquake response displacement are shown in Table-2 and Fig.-3, respectively, together with the test results. From these results, simulation analysis results provide good agreement with the test results in all cases.

4. ANALYTICAL MODEL

Outline of Analytical Models

Analytical model (Model C series) is shown in Fig.-4. The superstructure has 2 axis asymmetry in stiffness, consists of three pairs of different stiffness columns (Model C1, C2 and C3 in Table-3), but each model has the same eccentric rate $R_x = R_y = 0.420$. The base isolation system under the lower floor consists of nine pairs of Rubber and Damper, and has no stiffness eccentricity. The fundamental lateral period of isolation system is 1.5 sec. Each member stiffness is evaluated by WSS model and viscous damping coefficients are assumed 2.0%, 2.0%, and 0.0% for column, Rubber and Damper, respectively. El Centro 1940 earthquake waves are used, as NS-component is for X-direction input and EW-component is for Y-direction input.

Results of Analysis

Analytical results of eigen values are shown in Table-4. As the superstructure (Model C-1~3 series) becomes more flexible, the 1st mode period of base isolated model (Model C-4 ~6 series) becomes longer by the coupled effects with the lateral isolating period.

Maximum values of earthquake response at the center of gravity of each floor are shown in Table-5, and time history response accelerations and relative story displacement orbits at the diagonal corners of each floor are shown in Fig.-6.

To compare with fixed base models and base isolated models in Table-5 and Fig.-6, relative story displacements, rotational angle and response accelerations of superstructure are drastically reduced in base isolated model. As regards the relative story displacement, columns of fixed based models (Model C-1 ~3 series) show elasto-plastic response, but those of base isolated models (Model C-4~6 series) remain in elastic region.

From these results, base-isolation system is very effective for a building with 2 axis eccentricities to reduce its torsional response

5. CONCLUSION

Folloing are concluded through the present study :

1) Base isolation system provides great promise for the reduction in torsional and lateral forces of buildings. Therefore this system may lead cost effectiveness in the construction of torsionally unbalanced building.

2) Torsional deformation can be minimized when the structural design is carried out so that the center of stiffness and strength of isolation system coincide with that of gravity of superstructure.

3) Dynamic analysis method used in this study is effective to predict the response behavior of isolated system because of a good agreement obtained between simulation analysis and test results.

REFERENCES

1. Suzuki, T., Okada, H., etc. (1988). Torsional Response Characteristics of Building with Base Isolation System (Part 1). "Report of the Technical Research Institute OHBAYASHI CORP.", No. 35, pp.67-71.
2. Wada, A., Kinoshita, M. (1985). Elastic Plastic Dynamic 3-Dimensional Response Analysis by using a Multiple Shear Spring Model (Part 1, Parat 2). Summaries of Technical Papers of Annual Meeting, AIJ, B, pp.313-315.

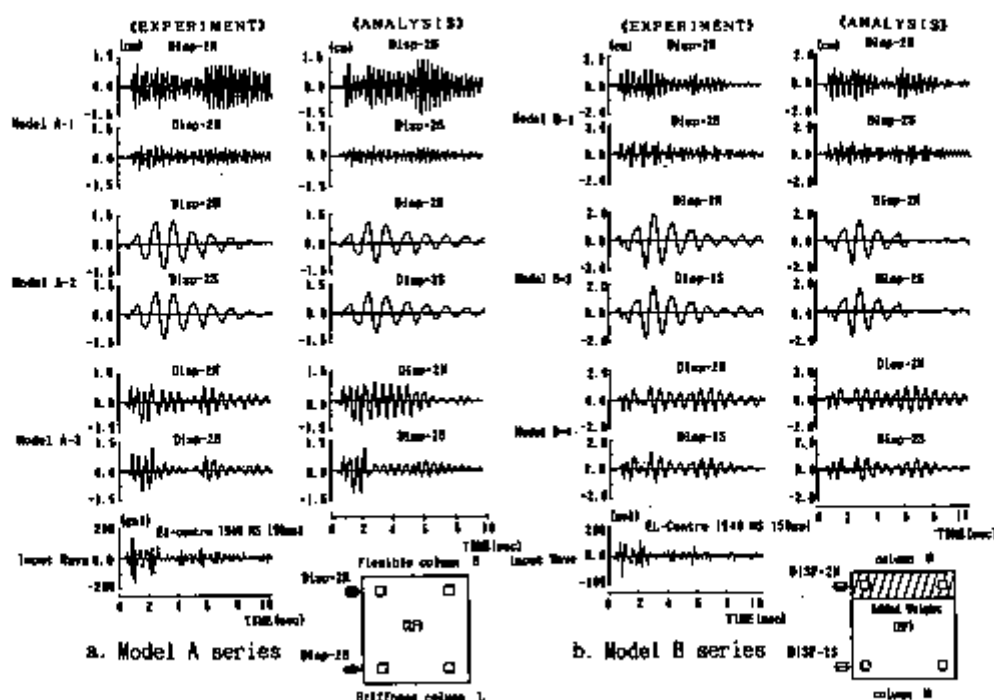
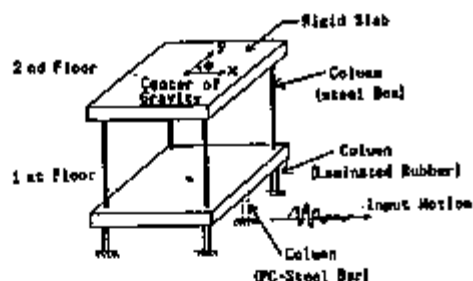
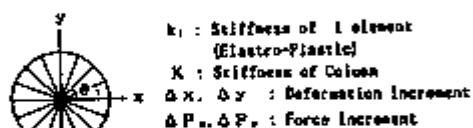


Fig-2 Test and Analysis results of earthquake response



a. Stiffness Vibration Model



$$\begin{Bmatrix} \Delta P_1 \\ \Delta P_2 \end{Bmatrix} = [K] \begin{Bmatrix} \Delta x \\ \Delta y \end{Bmatrix}$$

$$[K] = \begin{bmatrix} 2k \cos^2 \theta & 2k \cos \theta \sin \theta \\ 2k \cos \theta \sin \theta & 2k \sin^2 \theta \end{bmatrix}$$

b. Evaluation of column

Table-3 List of Superstructure Columns

Superstructure Model	Model C1	Model C2	Model C3
Column ①	80.0 t/cm	20.0 t/cm	5.0 t/cm
Column ②	480.0 t/cm	120.0 t/cm	30.0 t/cm
$\Sigma K = 3 \text{ Column } \oplus 6 \text{ Column } \ominus$	1820.0 t/cm	440.0 t/cm	120.0 t/cm
Yielding displacement δ_y	0.46 cm	1.84 cm	7.36 cm

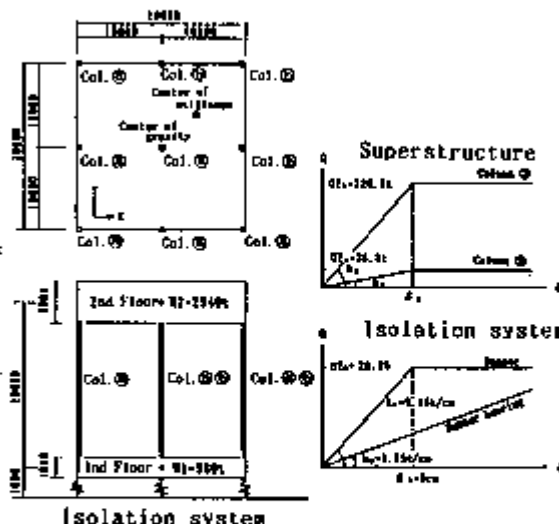


Fig-4 2 axis Eccentricity Model

Fig-3 Analytical Model

Table-4 Results of Eigen Value (2 axis asymmetry model in stiffness)

Analytical model			Vibration Mode (Hz)					
Base condition	Model C Series	Superstructure model	1st.	2nd.	3rd.	4th.	5th.	6th.
Fixed base Model	Model C-1	Model C1	3.18	4.83	6.21			
	Model C-2	Model C2	1.59	2.01	2.10			
	Model C-3	Model C3	0.794	1.01	1.95			
Base Isolated Model	Model C-4	Model C1	0.633	0.840	0.930	6.43	8.14	12.6
	Model C-5	Model C2	0.630	0.648	0.885	3.43	4.19	5.42
	Model C-6	Model C3	0.337	0.572	0.792	2.08	2.35	3.94

Table-5 Maximum value of earthquake response at center of gravity

		Fixed base model						Base isolated model						Comments
		Relative story displacement			Acceleration			Relative story displacement			Acceleration			
Superstructure model	S _y cm Yield point displacement	Analytical model	X cm Instn ratio	Y cm Plastic ratio	θ rad × 10 ⁻³	Xgal Response ratio	Ygal Response ratio	Analytical model	X cm Plastic ratio	Y cm Plastic ratio	θ rad × 10 ⁻³	Xgal Response ratio	Ygal Response ratio	Input earthquake wave = El-centro X = 341.7 gal Y = 216.1 gal
Model C1	2F δ _y = 8.96mm 1F δ _y = 5.6 cm	Model C-1	2.19 (4.77)	1.18 (2.61)	0.132	398.0 (1.00)	215.9 (1.00)	Model C-3	0.736 (2.512)	0.429 (0.487)	0.032	125.1 (1.368)	116.5 (0.500)	
	-		-	-	-	-	10.18 (2.094)		1.88 (0.10)	0.049	122.7 (1.897)	315.1 (0.849)		
	2F δ _y = 1.45cm 1F δ _y = 5.0 cm		Model C-2	5.04 (2.76)	3.28 (1.14)	0.449	306.3 (0.800)		111.1 (0.49)	Model C-5	0.969 (2.664)	0.849 (0.660)	0.053	
-	-	-		-	-	-	10.18 (2.19)	1.38 (0.10)	0.124		122.7 (1.902)	221.1 (0.596)		
2F δ _y = 2.35cm 1F δ _y = 5.0 cm	Model C-3	6.32 (0.305)		0.58 (0.18)	0.332	236.7 (0.596)	237.1 (0.13)	Model C-6	4.34 (0.636)		4.35 (0.594)	0.296	186.2 (1.902)	
-		-	-	-	-	-	12.28 (2.44)		13.21 (0.10)	0.295	238.3 (0.637)	185.1 (0.581)		

[] : Acceleration response ratio () : Damping factor

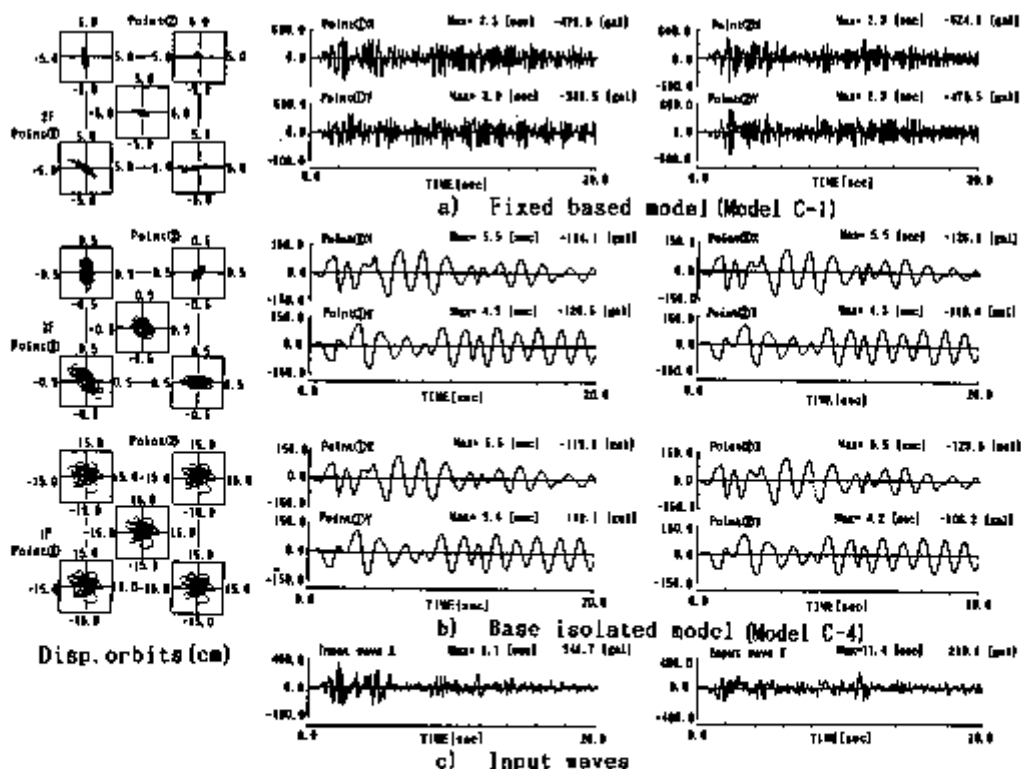


Fig.-6 Analysis results of earthquake response

Seismic Isolation Using the Friction Pendulum System

Victor A. Zayas, Stanley S. Low

Earthquake Protection Systems, San Francisco, CA USA

Stephen A. Mahin

University of California, Berkeley, CA USA

INTRODUCTION

An innovative seismic isolation system, the Friction Pendulum System (FPS), offers improvements in strength, versatility and ease of installation as compared to previous systems. Moreover, the approach offers several inherent performance benefits not available before. It is based on well known engineering principles of pendulum motion, and is constructed of materials with demonstrated longevity and resistance to environmental deterioration. The desirable isolation characteristics exhibited by FPS components hold the promise of an effective and practical system for significantly increasing the seismic resistance of nuclear power plants, reactor vessels, and equipment. This paper presents results from a four year research and testing program to assess the technical performance of the FPS.

FPS SEISMIC ISOLATION

The Friction Pendulum System (FPS) uses geometry and gravity to achieve the desired seismic isolation results. A photograph and cross section view of an FPS steel connection is shown in Fig. 1. The FPS concept is based on an innovative way of achieving a pendulum motion (Fig. 2). The supported structure or equipment item responds to earthquake motions with small amplitude pendulum motions. Friction damping absorbs the earthquake's energy. The result is a simple, predictable, and stable earthquake response. The operation of the connection is the same whether the concave surface is facing up or down. Fig. 3 illustrates the operation of the connection when installed at the top of a column, with the concave surface facing downward, as tested on the shake table at U.C. Berkeley's Earthquake Engineering Research Center.

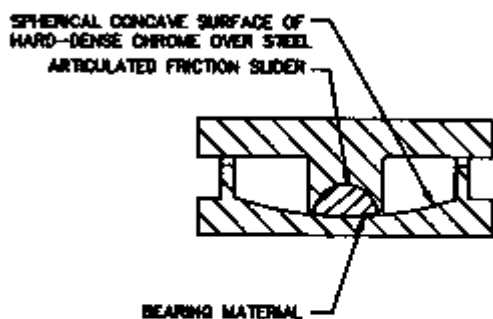
RESULTS

The FPS seismic isolation has been tested under more than 150 simulated earthquake loadings and conditions (Zayas, Low and Mahin, 1987). Seismic isolation is achieved by shifting the natural period. The natural period is controlled by the selection of the radius of curvature of the concave surface. The natural period of vibration of a rigid mass supported on FPS connections is determined from the pendulum equation, $T = 2\pi\sqrt{r/g}$, where g is the acceleration of gravity. This is the sliding period of the isolators, and the sliding or activated period of a relatively stiff structure supported on the FPS.

The force level at which sliding motion begins is controlled by the selection of the friction bearing material. When the earthquake forces are below the friction force level, an FPS supported structure responds like a conventionally supported structure. Once the friction force level is exceeded

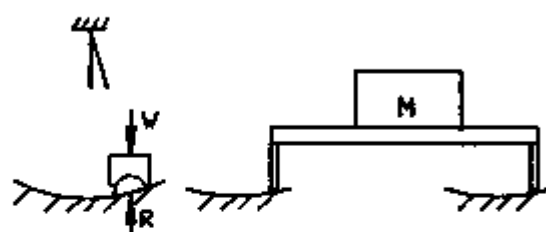
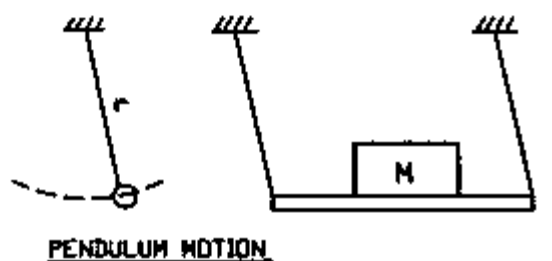


a.) Photograph



b.) Section

Fig. 1 FPS Isolator

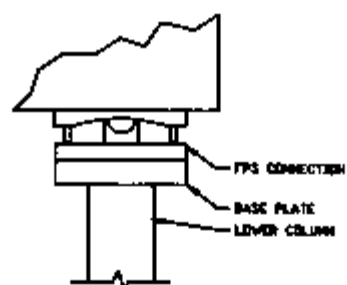


EQUATIONS

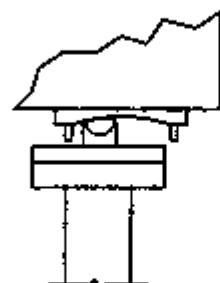
PERIOD $T = 2\pi\sqrt{r/g}$

STIFFNESS $k = W/r$

Fig. 2 Basic Principles



CENTERED POSITION



DISPLACED POSITION

Fig. 3 FPS Operation

the dynamic response is controlled by the FPS isolators. The steady state response of the FPS to harmonic ground motions is plotted in Fig. 4. As the strength of the ground accelerations increase, the percentage of acceleration transmitted to the structure decreases. When considering long period earthquake ground motions, or near field pulses, the friction coefficient and natural period can be chosen such that there is no amplification of motions with periods greater than .707 times the FPS period.

The experimentally measured hysteretic loops for the lateral force versus displacement response of the FPS are shown in Fig. 5. The results are shown for test Structure II, subjected to an earthquake loading scaled to twice the strength of the 1940 El Centro record. The experimental hysteretic loops demonstrate ideal bi-linear responses with no observable degradation under repeated cyclic loading. The base shear loads measured for the various test structures are plotted in Fig. 6, together with the elastic response spectra for non-isolated structures. The initial elastic structure period of the test structures (the non-isolated period) can be read from the horizontal axis.

During the earthquake simulation tests, the test structures underwent small amplitude pendulum motions which were hysterically damped by the friction bearing materials. The hysteretic friction damping minimized the seismic drifts and displacements. The drifts occurring in the FPS and the structure above are plotted in Fig. 7. The results reported in Figs. 5, 6, and 7 are for the test structures supported on FPS isolators with a 2 sec. period and a friction coefficient of 0.10. Of primary interest are the results for the test structures with initial elastic periods of less than 0.9 sec.

The FPS approach has the flexibility to achieve a wide range of isolator properties. The effect of varying the period and friction coefficient of the FPS isolators is shown in Fig. 8. Changing the FPS period from 2 to 3 sec. reduces the base shear and increases the displacement. Changing the friction coefficient from 0.10 to 0.05 further reduces the base shear and increases the displacement.

The lateral restoring stiffness of the activated FPS connection is, $K=W/r$, where W is the supported weight and r is the length of the radius of curvature of the concave surface. This is the stiffness of a simple pendulum. The fact that the stiffness is directly proportional to the supported weight, is an important and unique property of the FPS which has advantageous effects on the torsion response of a structure. The center of lateral stiffness of the FPS connections coincides with the center of mass. Since the friction force is also proportional to the supported weight, the center of rigidity of the connections acting as a group always coincides with the center of mass of the structure. This property makes the FPS connections particularly effective at minimizing adverse torsional motions which would otherwise occur in asymmetrical structures. The torsion responses for test Structure I, with different imposed mass and stiffness eccentricities, are shown in Fig. 9.

Another unique property of the FPS connections, as compared to other sliding supports, is the design of the articulated slider. The semi-spherical design of the slider results in uniform contact pressures between the slider and the concave surface for any combination of lateral and vertical loads. This avoids edge gouging, and reduces high frequency stick-slip motions which occur with other sliding support systems. The floor spectra for the second story in-structure response of test Structure I is shown in Fig. 10.

The fact that the period is independent of the structure mass is another important and unique property of the FPS which has advantages in controlling the response of a supported structure. The desired period can be selected by simply choosing the radius of curvature of the concave surface. The period does not change if the structure weight changes or is different than assumed.

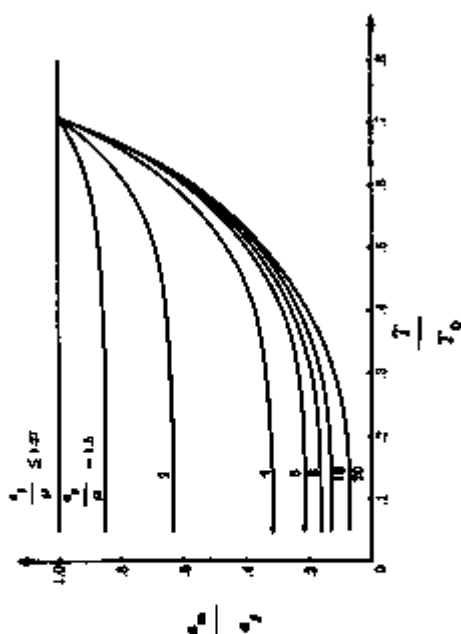


Fig. 4 Acceleration Transmissibility

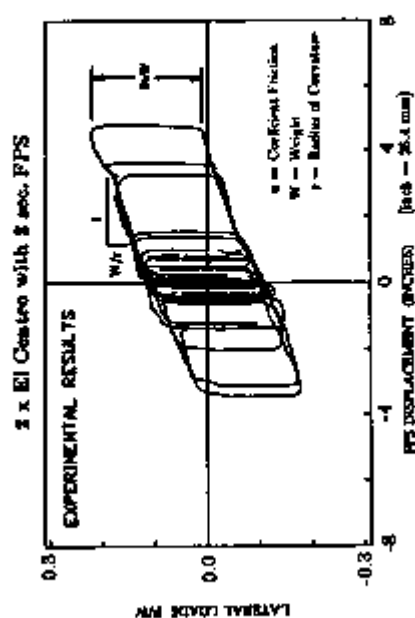


Fig. 6 Hysteresis Loops for the FPS

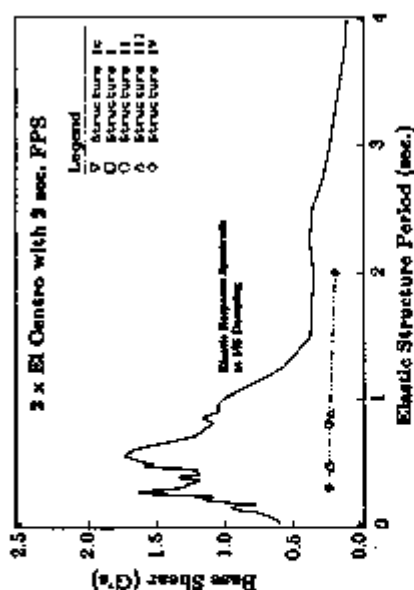


Fig. 4 Base Shear Response

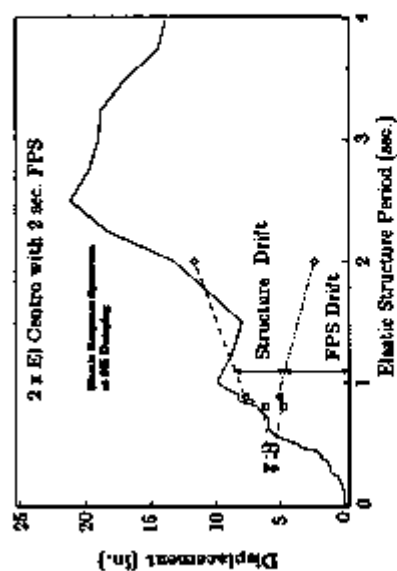


Fig. 7 Drift Response

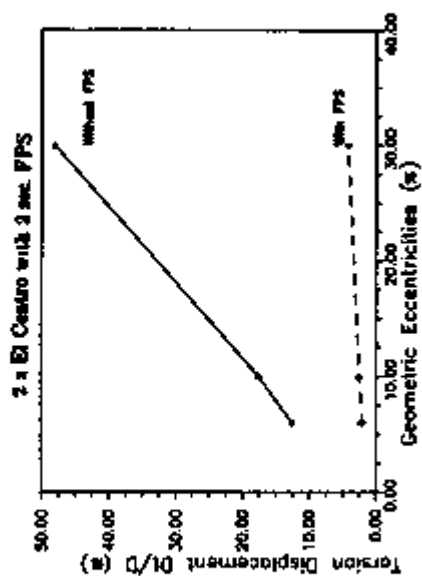


Fig. 9 Torsion Response

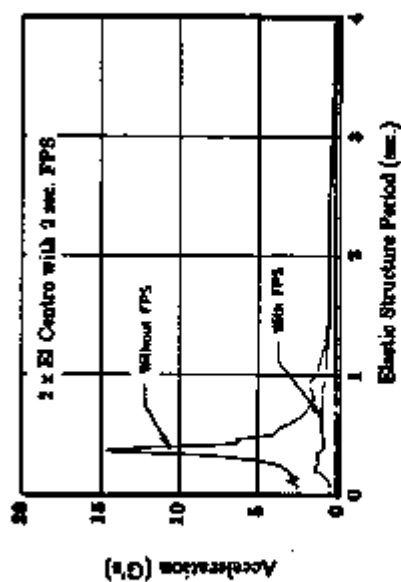


Fig. 10 Floor Spectra

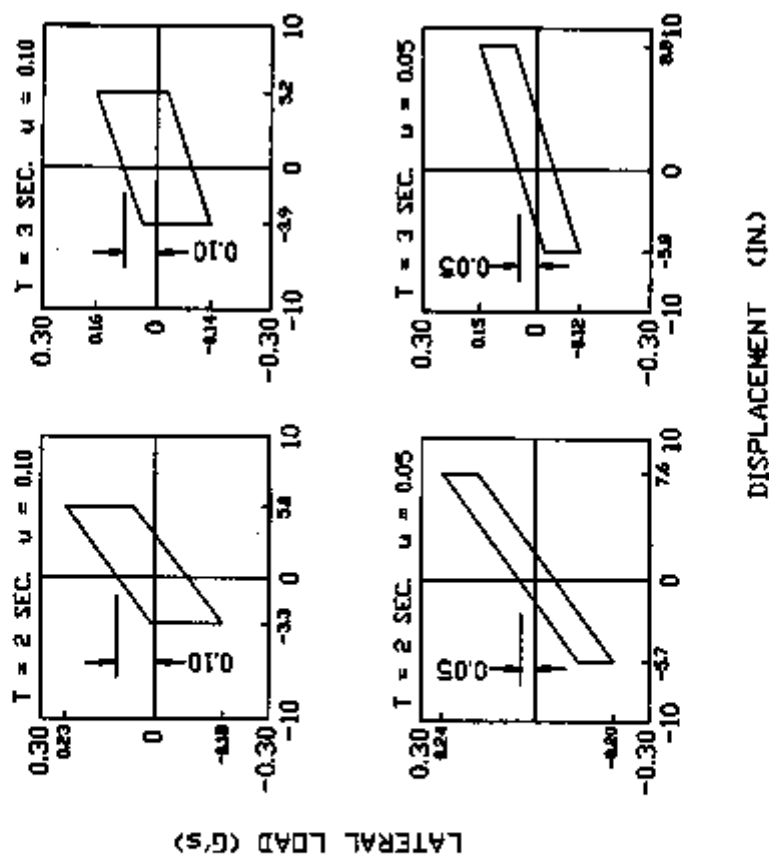


Fig. 8 Responses for Different FPS Periods and Friction Coefficients
(2 x El Centro)

The FPS approach permits the construction of compact isolators with small or very large load capacities, and which retain full strength and stability throughout their displacement range. The approach can be used to isolate light equipment items (Fig. 11), or heavy reactor buildings (Fig. 12).

The enclosing cylinder of the FPS isolator provides a lateral displacement restraint, and protects the interior components from environmental contamination. An uplift displacement restraint as used in an installation of the FPS is shown in Fig. 13. The displacement restraint provided by the enclosing cylinder provides an important safety feature in the event that earthquake loadings greatly exceed the design loads. In overload tests, when the isolator reached the lateral displacement restraint, the base shear loads increased, but the seismic loads and damage were always substantially less than would have occurred to the same structure without the FPS. Fig. 14 shows the response of Structure IV, with a 2 sec. FPS, subjected to the 1985 Mexico City earthquake.

CONCLUSIONS

The use of gravity and geometry to provide the restoring force achieves an effective and versatile seismic isolation system. FPS isolated structures demonstrate excellent seismic responses when subjected to severe earthquake ground motions including near field pulses, long period motions, and severe vertical motions. For properly designed structures, seismic loads are reduced by factors of 8 and greater. Torsional motions of eccentric and irregular structures are substantially reduced or eliminated. Because of the inherent simplicity, versatility, stability and durability of the FPS concept, it should become a major tool for the seismic resistant design of nuclear power facilities.

Reference: Zayas V.A.; Low S.S., and Mahin S.A., "The FPS Earthquake Resisting System: Experimental Report," UCB/EERC-87/01, Earthquake Engineering Research Center, University of California, Berkeley, June 1987.

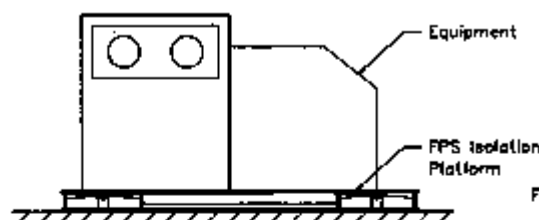


Fig. 11 Equipment Isolation

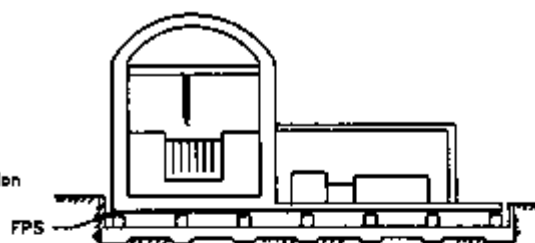


Fig. 12 Reactor Building Isolation

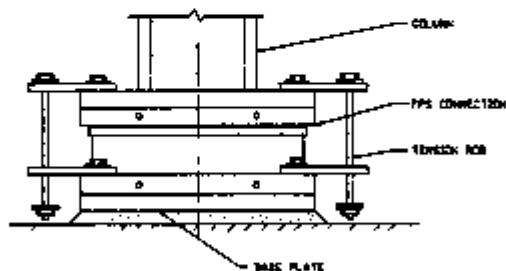


Fig. 13 FPS With Uplift Restraint

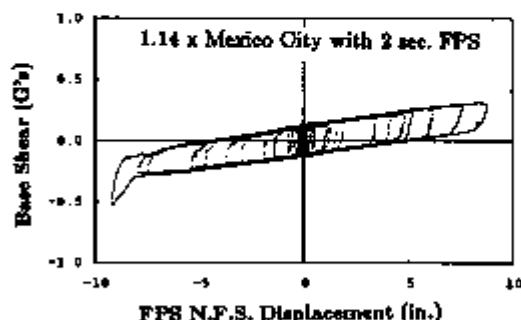


Fig. 14 Response of Displacement Restraint

Test on Large-Scale Seismic Isolation Elements

T. Mazda, H. Shiojiri, Y. Oka

Central Research Institute of Electric Power Industry, Abiko, Japan

T. Fujita

University of Tokyo, Tokyo, Japan

Matsutaro Seki

Ohbayashi Corporation, Tokyo, Japan

ABSTRACT

Demonstration test of seismic isolation elements is considered as one of the most important items in the application of seismic isolation system to Fast Breeder Reactor (FBR) plant. Facilities for testing seismic isolation elements are built in Abiko Research Laboratory of CRIEPI, and various tests for full-scale laminated rubber bearing and reduced scale models are conducted. From the result of the tests, the laminated rubber bearings turn out to satisfy the specification. Their basic characteristics are confirmed from the tests with full-scale and reduced scale models. And the ultimate capacity of the bearings under the condition of ordinary temperature are evaluated.

INTRODUCTION

Recently the seismic isolation has become one of the notable methods in the seismic design of important structures or equipment. And the research for the application of seismic isolation system to FBR plant has been conducted since 1987. This research program has various technical issues to be investigated. One of the most significant issues is to estimate the characteristics of seismic isolation element. In this test, the main objectives are followings. One is to clarify the basic characteristics of full-scale seismic isolation element under actual loading condition. And the other is to clarify the failure characteristics of reduced scale models under actual loading condition. Based on the above recognition, facilities for testing seismic isolation elements were built, and by using these facilities various static tests were conducted.

OUTLINE OF FACILITIES AND SEISMIC ISOLATION ELEMENT

Facilities for Testing Element

Facilities for testing seismic isolation element was built in Abiko Research Laboratory of CRIEPI. Two actuators can apply both horizontal load and vertical load on the element, the actuators are controlled in load control mode and displacement control mode. Maximum available load of each actuator is 600 tonf. Maximum achievable horizontal displacement is ± 600 mm or 1200 mm, and maximum achievable vertical displacement is ± 350 mm or 700 mm. Maximum velocity of loading of each actuator is 0.5 cm/sec. Fig 1 shows the facilities.

Seismic Isolation Element

In this program, concept of base isolation of FBR building was selected as the most feasible system. In this concept, natural rubber bearing, lead rubber

bearing and high damping rubber bearing are regarded as the promising seismic isolation element of the FBR building. Natural rubber bearing was tested at first. Because natural rubber bearing with damper is considered to be the most feasible system of the base isolation in Japan, and the scattering of the basic characteristics of the bearing are relatively small in comparison with other bearings.

Fig. 2 shows the natural rubber bearing consisting of thin natural rubber sheets and insert steel plates. One full-scale model and two kinds of reduced scale models were submitted for the test.

The full-scale model is designed to behave linearly up to the displacement of 500 mm, and designed to provide the 500 ton rated mass with the horizontal natural frequency of 0.5Hz and the vertical one of 20Hz.

Parameters of the bearings are summarized in Table 1.

RESULTS OF TESTS

Horizontal Stiffness Tests

The objectives of these tests are to estimate the horizontal stiffness and damping of the bearing and to confirm the similarity between a full-scale model and reduced scale models. The tests were performed under the condition of low frequency cyclic loading (under 0.01Hz).

Four cycles of sinusoidal horizontal displacement was applied under constant vertical load. The amplitude of horizontal displacements are varied from shear strain of rubber $\pm 25\%$ to shear strain of rubber $\pm 400\%$. And the amplitude of vertical loads are varied from -20% to $+200\%$ of design vertical load, and the record of third cycle was adopted as a data.

Fig. 3 shows the relationship between horizontal load and horizontal displacement of each model and Fig. 4 shows the relationship between normalized horizontal spring constant and shear strain of rubber.

From these results, the horizontal stiffness of the all bearings turned out to behave almost linearly within shear strains of 200%. But over shear strains of 300%, restoring force (horizontal load) increases sharply as shear strain increases.

Equivalent horizontal spring constant obtained by the tests of the bearings agree approximately with the design value within shear strain of 200%, but at shear strain of 400% the equivalent horizontal spring constant increases about 30% of the design value owing to the hardening of rubber.

Fig. 5 shows the relationship between equivalent damping ratio and shear strain of rubber. The equivalent damping ratio for the full-scale model in horizontal direction is between 1% and 2% within shear strain of 200%. But from the test result of 200ton model, it was made clear that the equivalent damping ratio is larger at shear strain over 300% by material non-linearity of rubber.

Differences of these characteristics between models of the same scale were small.

Vertical Stiffness Tests

The objectives of these tests are to evaluate the vertical stiffness and damping of the bearing and to investigate the similarity between a full-scale model and reduced scale models. The tests were performed under the condition of low frequency cyclic loading in the same way as horizontal stiffness tests. In the first test, four cycles of sinusoidal vertical load was applied under initial static vertical load and constant shear strain.

Amplitude of sinusoidal vertical load was $\pm 50\%$ of design vertical load. The initial vertical loads were varied from 50% to 150% of the design vertical load.

And the constant shear strain of the bearing were varied from 0% to 200%. In the second test, vertical load was increased gradually from 0% to 200% of the design vertical load.

Fig. 5 shows the relationship between vertical load and vertical displacement for each model, and Fig. 6 shows the relationship between normalized vertical

spring constant and shear strain of rubber.

From these results, the vertical stiffnesses of all bearings around design vertical load without shear strain turned out to be almost linear. And it was proved that the equivalent vertical spring constant agree approximately with the design value. However, the equivalent vertical spring constants decrease as shear strain increases, and are 50% of the design value at shear strain of 200%.

Breaking Tests

The objectives of these tests are to evaluate the strength of the bearings and the deformation characteristics around the breaking point and to confirm the similarity rule of two reduced scale models around the breaking point.

Fig. 7 shows the relationship between horizontal displacement and horizontal load of each reduced scale model up to the breaking point.

From these results, breaking points of each model were approximately between shear strain of 450% and 500%, and between shear stress of 50kgf/cm² and 75kgf/cm².

CONCLUSION

Horizontal stiffness tests, vertical stiffness tests and breaking tests for both full-scale model and reduced scale models were conducted.

As a result, followings were obtained.

1) Characteristics of a full-scale model used in design were made clear and agreed approximately with the design value.

2) Characteristics of reduced scale models around breaking point are clarified and the similarity rule between a full-scale model and reduced scale models were verified.

The present research was sponsored by the Ministry of International Trade and Industry, Japan.

REFERENCES

Sawada Y. et al., 1989, " Seismic Isolation Test Program ". Trans. 10th SMIRT, to appear.

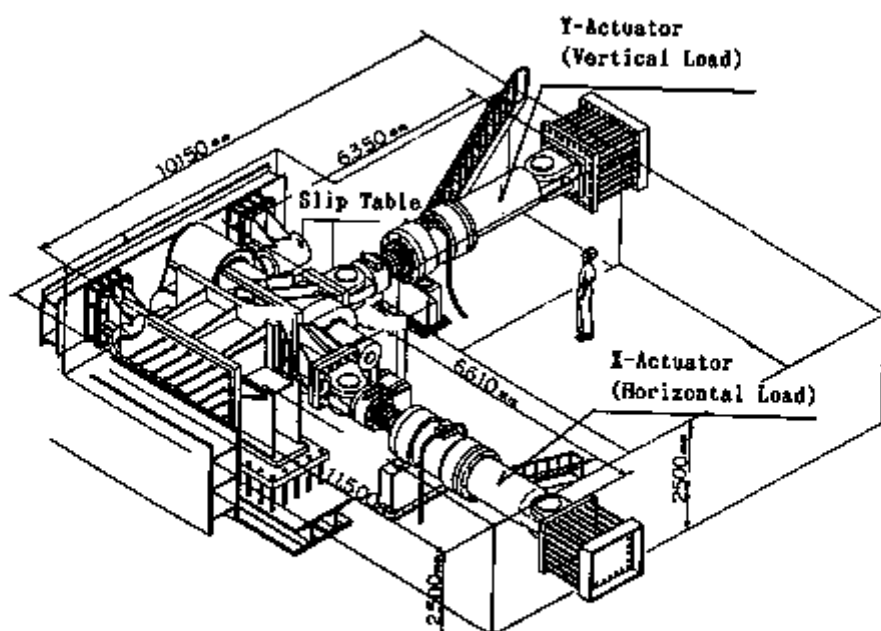


Fig.1 Facilities for Testing Element

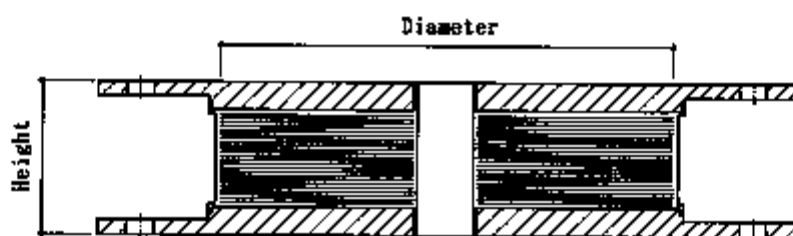


Fig.2 Natural Rubber Bearing

Table 1. Design Parameters of Bearings

Parameter	Type	full-scale model	1/1.58 reduced scale model	1/3.18 reduced scale model
Diameter (mm)		1600	1020	500
Height (mm)		560	340	160
Thickness of Rubber Sheet (mm)		8.0	5.7	2.8
No. of Rubber Sheet		25	25	26
Thickness of Steel Plate (mm)		5.8	3.1	1.6
No. of Steel Plate		24	24	24
Rated Vertical Load (tonf)		500	200	50
Horizontal Spring Constant (tonf/cm)		5.036	3.19*	1.59*
Horizontal natural frequency (Hz)		0.5	—	—
Vertical Spring Constant (tonf/cm)		8057	5099*	2550*
Vertical natural frequency (Hz)		20	—	—

* : Value is fixed from similarity

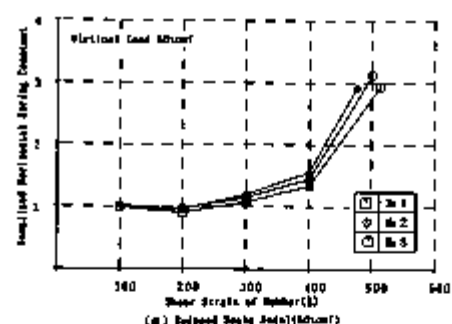
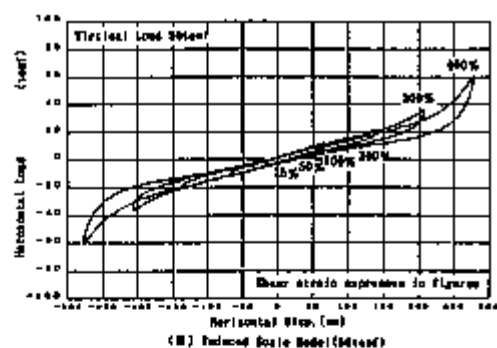
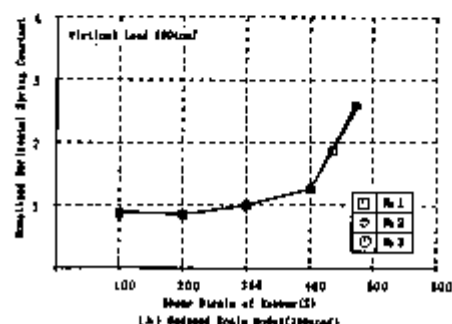
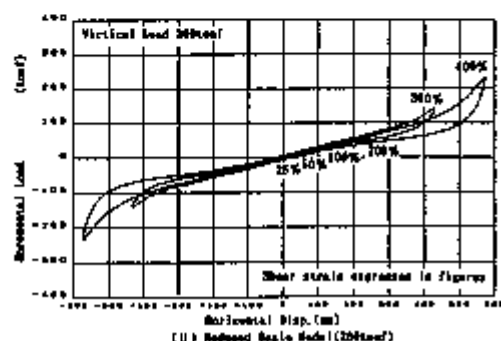
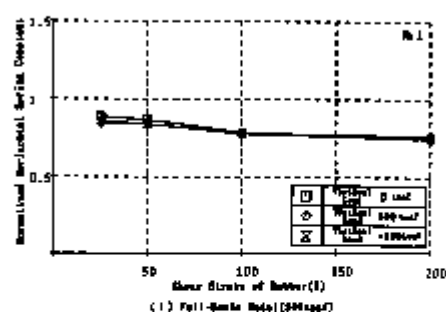
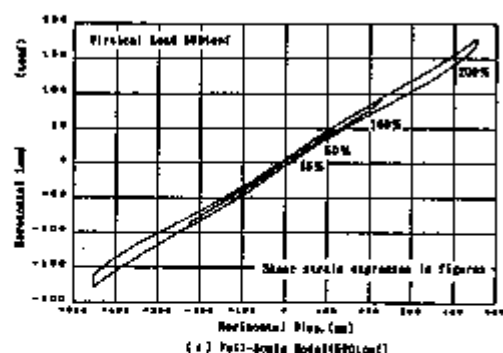


FIG.3 Relationship between Horizontal Load and Horizontal Displacement

FIG.4 Relationship between Normalized Horizontal Spring Coefficient and Shear Strain of Rubber

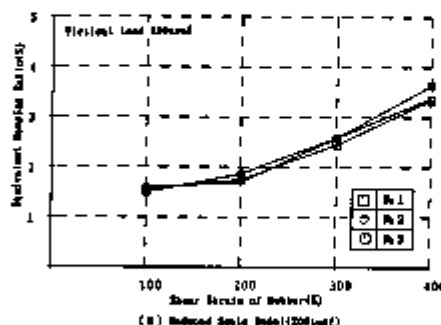
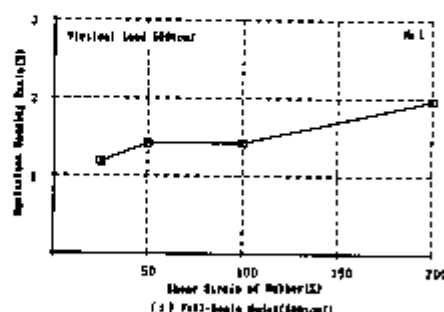


FIG.5 Relationship between Repetition Loading Ratio and Shear Strain of Rubber

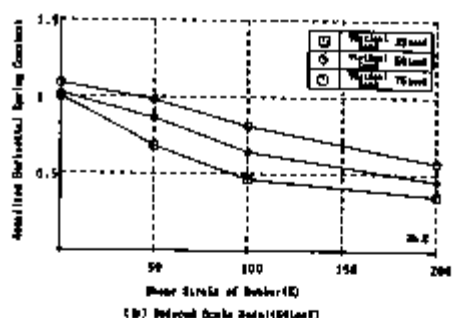
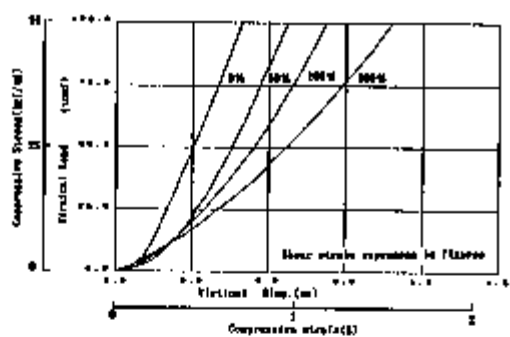
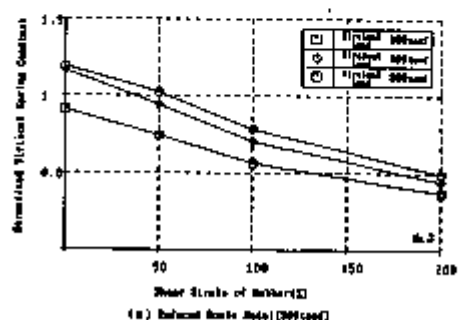
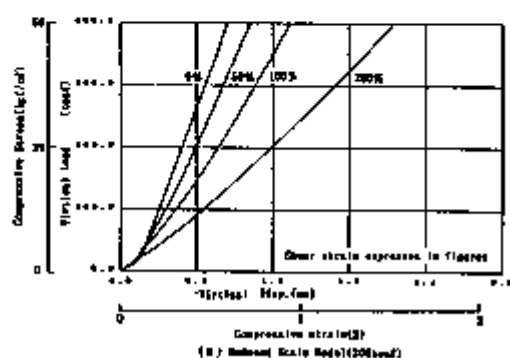
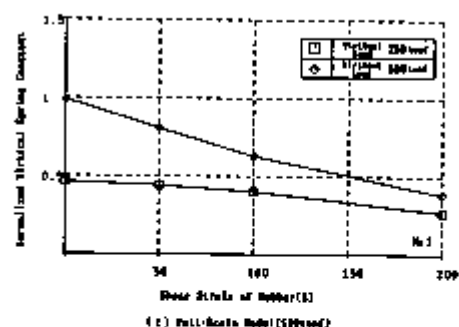
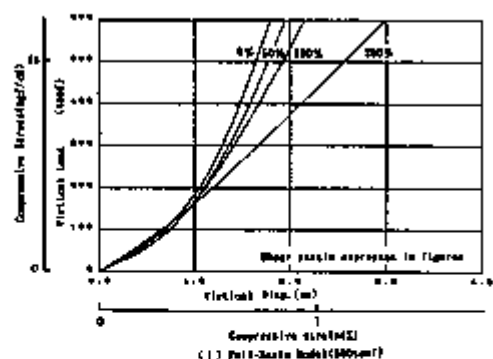


Fig. 4 Relationship between vertical load and vertical displacement

Fig. 5 Relationship between Normalized Vertical Spring Constant and Shear Strain of Rubber

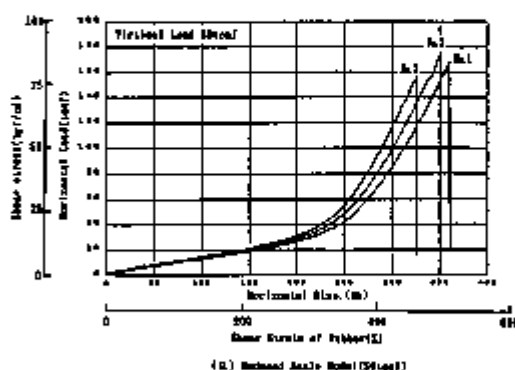
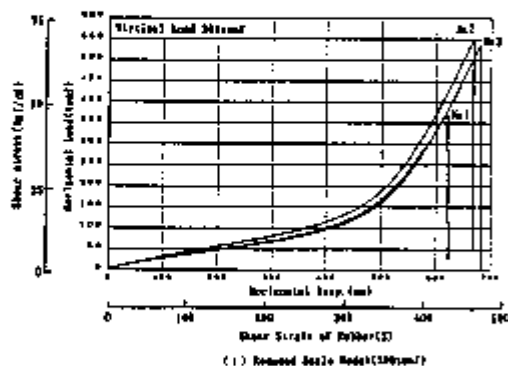


Fig. 8 Relationship between horizontal load and horizontal displacement

Earthquake Response Analysis of Base Isolated Building

T. Mazda, H. Shiojiri, Y. Sawada

Central Research Institute of Electric Power Industry, Abiko, Japan

O. Harada, N. Kawai,

Okumura Corporation, Ibaragi, Japan

S. Ohtsuka

Okumura Corporation, Tsukuba, Japan

1. INTRODUCTION

Recently, the seismic isolation has become one of the popular methods in the design of important structures or equipments against the earthquakes. However, it is desired to accumulate the demonstration data on reliability of seismically isolated structures and to establish the analysis methods of the these structures.

Based on the above recognition, the vibration tests of a base isolated building were carried out in Tsukuba Science City. After that, many earthquake records have been obtained at the building. In order to examine the validity of numerical models, earthquake response analyses were executed by using both Lumped Mass model, and Finite Element model.

2. OUTLINE OF BASE ISOLATED BUILDING AND ISOLATION DEVICE

(1) Base Isolated Building

The base isolated building, a object of test and observation, is a four-story reinforced concrete building. The floor area is 1,330 m² and the weight is 2,250 ton. Seismic isolation devices are installed between the basement and the first floor.

(2) Seismic Isolation Device

The seismic isolation devices consist of laminated rubber bearings and elasto-plastic steel dampers, which provide the functions to lengthen the natural period and to absorb the vibration energy during strong earthquakes, respectively. Fig.2 shows the laminated rubber bearing, consisting of thin natural rubber sheets and steel plates. Fig.3 shows the elasto-plastic damper consisting of four spiral steel bars which allows to provide almost the same functional characteristics for every direction. 25 rubber bearings and 12 dampers are installed as shown in Fig.1.

The rubber bearing is considered as a linear material up to the displacement of 200 mm from the results of element test conducted before installation. The average stiffness of the rubber bearings used for this isolated building is 0.82 ton/cm. The yielding displacement of the steel elasto-plastic damper is about 30 mm and the stiffness before yielding is about 2.0 ton/cm. Under the assumption that the damper behaves elasto-plastically, the horizontal periods of this building with the isolation devices are 1.4 sec and 2.1 sec corresponding to pre-yielding stiffness and post-yielding stiffness, respectively.

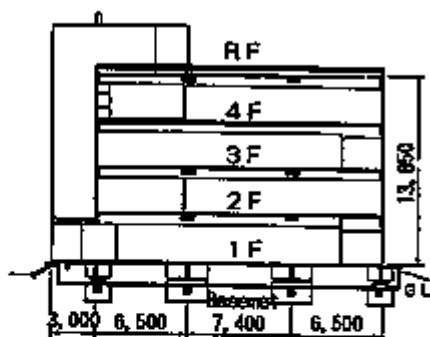


Fig. 1 Section and Plan of Building

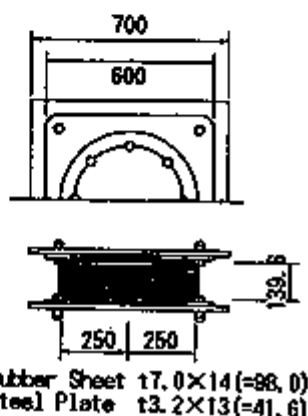


Fig. 2 Laminated Rubber Bearing

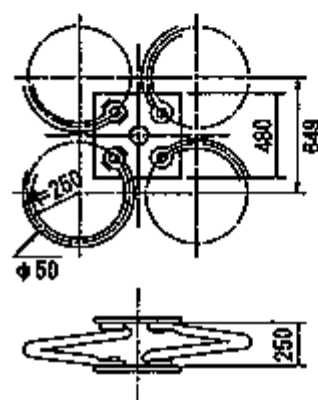


Fig. 3 Elasto-Plastic Steel Damper

3. EARTHQUAKE RESPONSE ANALYSIS

(1) Input Ground Motion

The steel dampers didn't yield during any observed earthquake. SW Ibaraki Earthquake (1987.6.30, Magnitude=5.1, Epicentral distance=11km) was adopted as input motion. This earthquake ground motion contains large amounts of high frequency components.

(2) Lumped Mass Model

1) Numerical model

The building above isolation devices was modeled into five lumped mass system. Weight of each floor was lumped at floor level. Each mass was connected by equivalent spring that considered effects of bending and shearing.

Isolation devices were modeled by a pair of sway and rocking spring. Fig. 4 shows the lumped mass model. Modal analysis was used to evaluate the earthquake response of the building. Newmark- β method was used in numerical integration of the response of each mode. Modal damping was estimated from both the forced vibration test and the earthquake response observation. As a result, it was assumed that damping ratio of first mode was 2.5%, and all of other modes were 0.3%.

Analysis condition of this model shows in Table 1.

SW Ibaraki Earthquake (1987.6.30, Magnitude=5.1, Epicentral distance=11km) was adopted as input motion. This earthquake ground motion contains large amounts of high frequency components.

2) Numerical results

Fig. 6 shows the mode shapes obtained by the analysis.

Every floor of the building moves in the same direction in the first mode, and roof floor and first floor moves in the opposite direction in the second mode.

Fig. 7 shows the comparison of the observed acceleration of first floor with calculated one.

High frequency component corresponding to the second mode is excited in observed record, but excitation of high frequency component is much less in lumped mass model. This is considered to be due to the effects of multi-input motion and three-dimensional vibration mode of the building which cannot be well considered by this model. As to the acceleration of the third floor, (See Fig. 8) the calculated result is well agreed with the observed record. As to the relative displacement between the base mat and the first floor, (See Fig. 8) the shape of calculated time history is quite similar to that of observed record. Also, Fourier spectrum, is very similar to observed one around first natural frequency. From above results, it can be said that lumped-mass model is useful in the simulation of the first mode response of isolated building. So, it will be possible to estimate the deformation of isolation devices during earthquakes by using this model.

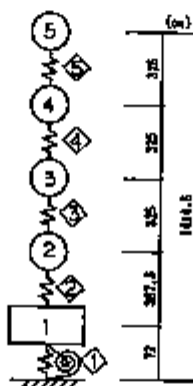


Fig. 4 Lumped Mass Model

Table 1 Analysis Condition of Lumped Mass Model

Mass or Member No	Weight (tonf)	Stiffness (tonf/cm)	Mode No	Damping Ratio(%)
5	408.9	1719	1	2.5
4	479.2	2718	2	0.3
3	424.0	3534	3	0.3
2	431.3	4515	4	0.3
1	502.5	71.68	5	0.3
	1.34×10^8 (tonf·cm ²)	2.05×10^{10} (tonf·cm)	6	0.3

Table 2 Analysis Condition of FEM Model

Isolation Device					
Rubber Bearing				Steel Damper	
Horizontal Stiffness (tonf/cm)	Damping Ratio (%)	Vertical Stiffness (tonf/cm)	Damping Ratio (%)	Horizontal Stiffness (tonf/cm)	Damping Ratio (%)
1.61	2.5	1304	1.0	2.51	2.5
Reinforced Concrete					
Modulus of Elasticity (kgf/cm ²)	Shearing Modulus of Elasticity (kgf/cm ²)	Poisson's Ratio	Density (g/cm ³)	Damping Ratio (%)	
6.8×10^4	2.7×10^4	0.167	2.9	0.3	

Fig. 5 FEM Model

(3) Finite Element Model

1) Numerical Model

In this case, Finite Element model is used for the upper structure.

Floors and main walls are modeled by shell elements, pillars and garters are modeled by three-dimensional beam elements. Stiffness and damping of the upper structure was estimated from both design values and the results of the forced vibration test.

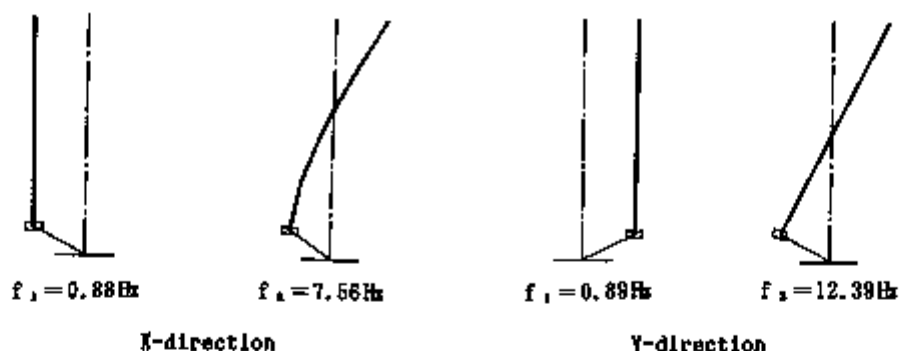
The models of 25 rubber bearings and 12 steel dampers are put in each position. Steel dampers are modelled by horizontal shearing springs. Rubber bearings are modelled by horizontal shearing springs and vertical springs. In time history analysis, the damping matrix proportional to the stiffness matrix is used. Fig. 5 shows the finite element model, and analysis condition shows in Table 2.

2) Numerical Results

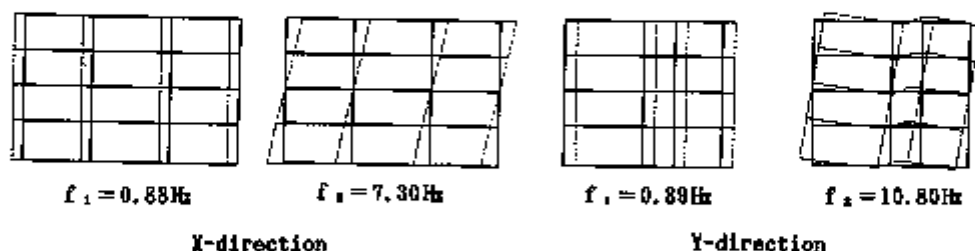
The result of finite element model is very similar to the observed record of the first floor. (See Fig. 7) Especially excitation of the second mode is expressed very well by the model.

As to Fourier spectra of responses, those of numerical results are similar to those of observed records not only around the first mode, but also around the second mode. The acceleration of the third floor and the relative displacement between the first floor and the base mat calculated by this model are almost the same as those by the lumped-mass model, since these responses are dominated by the first mode.

From above results, it can be said that evaluation of the second mode will be possible by finite element model.



1) Lumped Mass Model



ii) FEM Model

Fig. 6 Results of Modal Analysis

650

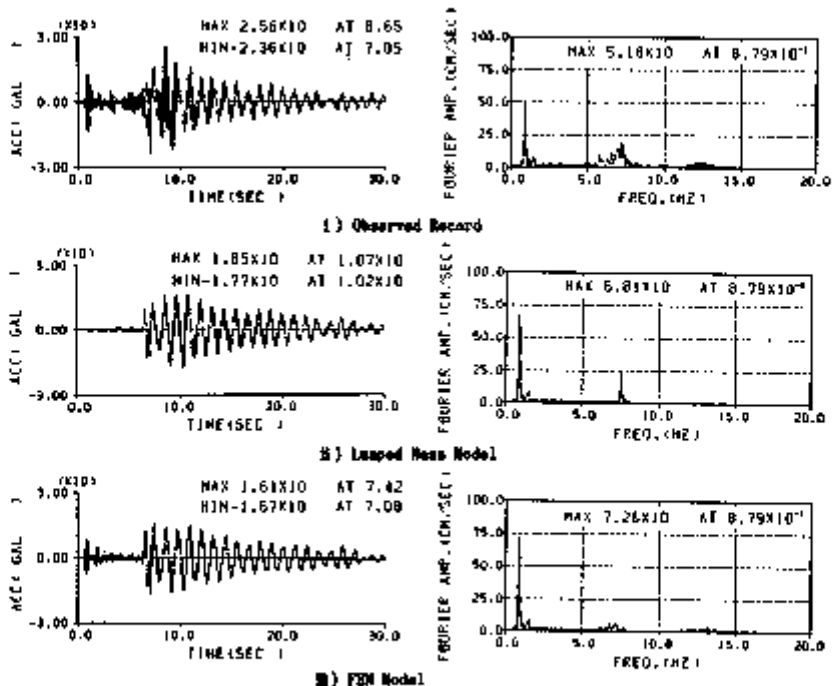


Fig. 7 Comparison of Observed Record with Calculated Results
(Acceleration of First Floor)

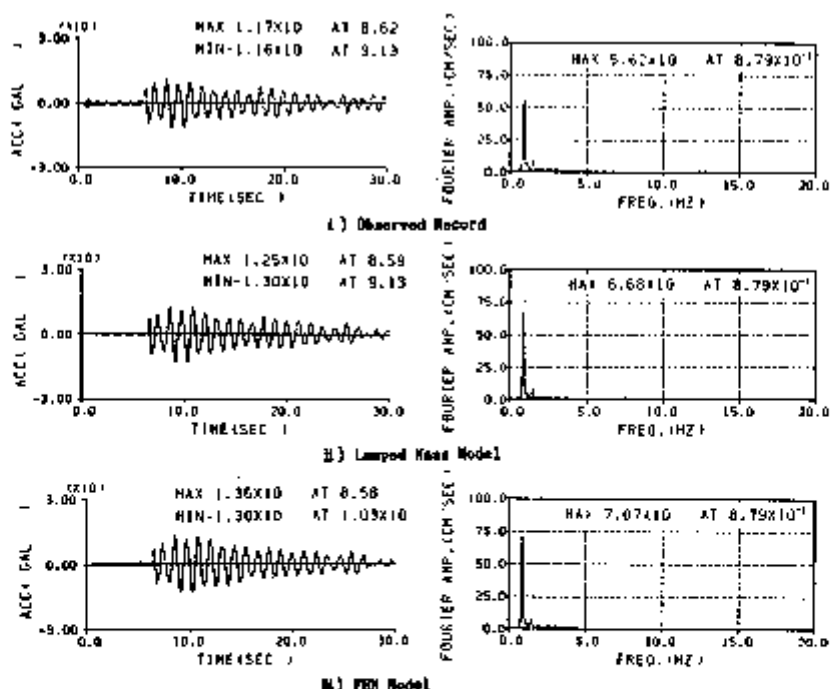


Fig. 8 Comparison of Observed Record with Calculated Results
(Acceleration of Third Floor)

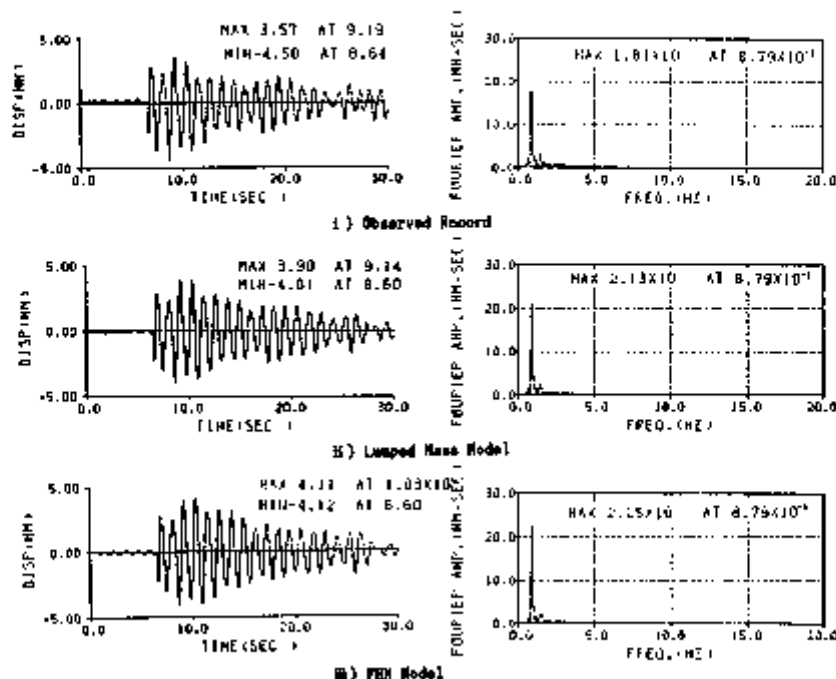


Fig. 8 Comparison of Observed Record with Calculated Results
(Relative Displacement between Base Mat and First Floor)

4. CONCLUSIONS

Earthquake response analyses by using both lumped mass model and finite element model are carried out. The results are compared with the observed one, and the followings are confirmed.

- Lumped mass model is available to estimate the response of the upper structure and the deformation of the isolation devices, as the dynamic behavior of the base isolated building is dominated by the first mode.
- Higher mode is more accurately simulated by finite element model, and the use of this model is recommended when the effect of high frequency mode is significant.

5. REFERENCES

- S. Aoyagi, T. Mazda, O. Harada, M. Takeuchi et al., Experimental Study on the Dynamic Behavior of the Base Isolated Building, 9th SMIRT (1987), pp.687-692.
- S. Aoyagi, T. Mazda, O. Harada, S. Ohtsuka, Vibration Test and Earthquake Response Observation of Base Isolated Building. 9th WCEE(1988).

Dynamic Characteristics of the Base-Isolated Building Constructed on a Soft Ground

Yoshihiro Sawada, Hiroo Shiojiri, Yoshio Mashiko, Taiji Matsuda
Central Research Institute of Electric Power Industry, Abiko, Japan
Nobuhiro Machida, Yotimasa Katano, Nobuyuki Ogino
Kumagai Gumi Company Ltd., Tokyo, Japan

1. Introduction

Construction of a base-isolated building on a soft ground has been thought of to be very difficult, considering its dynamic characteristics which the ground presents at an earthquake. This paper, in all aspects, discusses the dynamic characteristics of the base-isolated building constructed on a soft ground; for the purpose of spreading the use of the isolation system, December 1988, we have constructed a building which is isolated in its base from earthquake oscillation, in Edogawa Ward, typical soft ground in Tokyo (classified as the third class in Building Standard Law). Using this full-scale model, we studied its vibration-behavior and conducted an analysis by simulation on the basis of earthquake data obtained on the model building.

2. Description of the ground, building and isolation system

2.1. Outlines of the ground and building

The tested building is a dormitory of 10.5 m in eaves height, of three story reinforced concrete structure, weighing 1400 tons and covering 770 m² in total (Photo 1).

As shown in Figure 1, geologically, a thick alluvium extends on the diluvium which consists, from above, of the upper Tokyo formation, the Tokyo gravel bed and the lower Tokyo formation.

2.2. Isolation system

The proposed isolation system features combination of a standard type laminated rubber bearing and a steel damper, but the latter is designed and developed especially for this purpose. Details of the laminated rubber bearing and the steel damper are shown respectively in Figures 2 and 3. The layout of the isolation system is given in Figure 4.

3. Vibration test and its results

Through the test, we have conducted two kinds of vibration test, free vibration and forced vibration in order to know basic vibration characteristics of the base-isolated building and the performance of the isolators in a wide frequency range.

3.1. Free vibration test

(1) Test method

As shown in Figure 5, the upper footings are connected, with PC steelwires, to a hydraulic jack set in the lower footing. By using the jack, relative displacement was made occur between the foundation and the building, releasing restraining force by cutting the breaking pin at the joining part to produce

free vibration in the building. The relative displacement between foundation and building is 100 mm, equivalent to a response deformation appearing to the building when attacked by an earthquake of class VI (about 250 cm/s^2).

(2) Test results and observations

- The restoring force immediately after the free vibration and the analysis value are shown in Figure 6. As they demonstrate good agreement, featuring the bilinear type restoring force used for analysis.
- The deformation time history wave form in the isolation story and its analysis value are given in Figure 7 and the vibration mode in Figure 8. From the Figure 7, we understand that after the release, the amplitude rapidly converge at less than 20 mm in one cycle. The analysis value and the experimental value show good agreement. From the vibration mode, we can see that it demonstrates the rigidity behavior inherent in the isolation structure.

3.2. Forced vibration test

(1) Test method

A shaker of 50 tons was installed on the building roof. Parallel vibration is applied in the short sides (X direction) and long sides (Y direction). Excentric shaking is made in the X direction (Fig. 9).

(2) Test results and observations

- The resonance curves (parallel and excentric accelerations on each floor) are given in Figures 10, 11 and 12. The vibration mode at parallel acceleration is shown in Figure 13. The natural vibration of this building is 0.96 Hz, in X direction, 0.99 Hz in Y direction, having no difference in direction, they coincide well with the frequency (1.0 Hz) of the initial rigidity obtained by the free vibration test. Furthermore, the vibration mode shows, even in small amplitude, the rigidity behavior inherent in the isolation structure.
- As the torsion peak at each acceleration is 1.02 Hz, almost same as the resonance point obtained by the parallel acceleration, we can consider that torsion exerts almost no effect on the seismic behavior of the building.

4. Earthquake study on the base-isolated building and simulation analysis

This building is designed as a total system to experiment the ground, isolation system and building, performing a series of surveys and collecting the data concerning the behavior. Figure 14 shows the layout of seismometers. In this section, we discuss the analysis of the earthquake waves recorded on the building as well as the simulation analysis using the above results.

4.1. Seismic observation

(1) Characteristics of the earthquake waves recorded

After the completion of the building, it has experienced several earthquake attacks. Of them, the relatively larger attack, occurred at the south-east of Ibaragi-Prefecture, was selected to study the base-isolated building. The results of the study are given hereunder. Table 1 shows the specifications of the earthquake.

(2) Analysis results and observations

Through the analysis of the ground, a ground model is created as shown in Figure 15, taking into consideration the boring survey of the site and the in-laboratory test results. After inputting the earthquake wave obtained at 51.5 m under the ground level by one dimensional wave theory (SHAKE), the model is compared with the earthquake wave given at the building foundation. Figure 16 shows Fourier spectra of the both cases. For the analysis of the building, using the characteristics of an isolation system confirmed through the shaking test of the building, we produced a multiple particle system model (Figure 17).

We inputted the actual earthquake waves to the model to perform the earthquake response analysis. Its results are compared with the survey results (Figure 18). From the analysis, it is confirmed that its results coincide well with the measured values.

4.2. Simulation analysis of the building

In order to ensure the propriety of the characteristics discussed in the precedent chapter and the analysis method, and to study the dynamic characteristics of the building, we have prepared two kinds of artificial earthquake waves different in nature, but which can be assumed to occur on this ground. These waves are inputted to the model, providing two input levels of 25, 50 cm/s as standard, to perform the earthquake response analysis of the building. Figures 19 and 20 present the response analysis results. The analysis confirms that in each response value, Case B is larger than Case A, with a minor difference of 10 to 20%. By comparing with the conventional type aseismic structure, we know that the isolation system works effectively, because the acceleration of the building is reduced to one-third. The base-isolated building, even if attacked by larger earthquakes, may demonstrate a good isolation effectiveness to earthquake waves of different nature.

Conclusion

Through the vibration test, the following are demonstrated:

- The restoring force characteristics of the isolation system coincide well the design values. In the larger deformation field, a large attenuation is obtained by yielding of dampers.
- In the field of small amplitude, the natural vibration frequency in the parallel direction presents good agreement with the frequency calculated from the initial rigidity. The natural vibration frequency torsion approximates the peak in the parallel direction.
- The building features a rigid behavior with less inter-story displacement for the fields of small amplitude and large amplitude. The vibration observed in the building is shifted into the isolation frequency, and this means that the building has the isolation performance as designed.

In the seismic observation and the simulation analysis of the building, the following are confirmed:

- The analysis results of the ground and the building, using the seismic survey, shows good agreement with the measured values.
- The simulation analysis shows that the building can produce an isolation effect of high reliability.

As mentioned above, by means of the seismic observation and the vibration test, we can confirm that the base-isolated building constructed on the soft ground demonstrate a sufficient isolation effect.

Continuing the seismic observation, we will pursue our study on the isolation effect of our base-isolated building constructed on the soft ground, especially for large earthquake attacks.

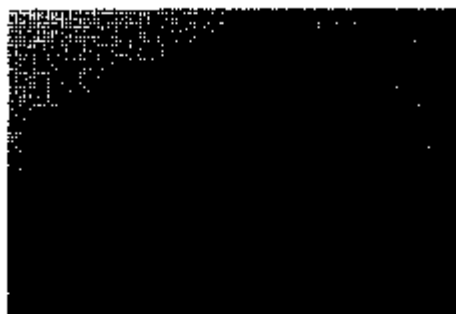


Photo 1 View of the building

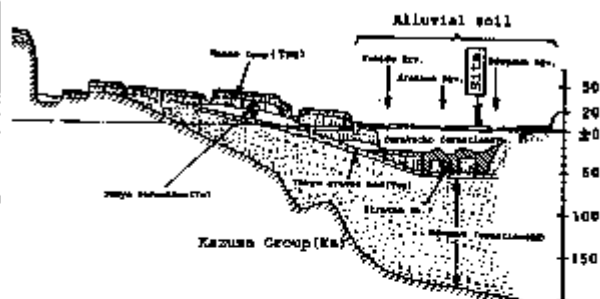


Fig. 1 Geologic profile

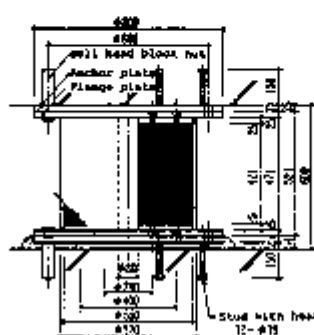


Fig. 2 Detail of the laminated rubber bearing

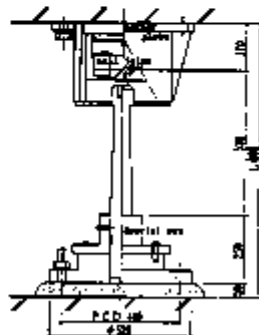


Fig. 3 Detail of the damper

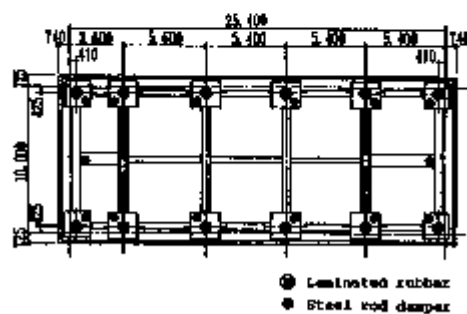


Fig. 4 Layout of the isolation system

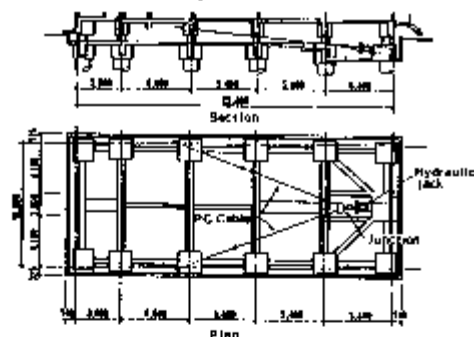


Fig. 5 Schematic diagram of the experiment system

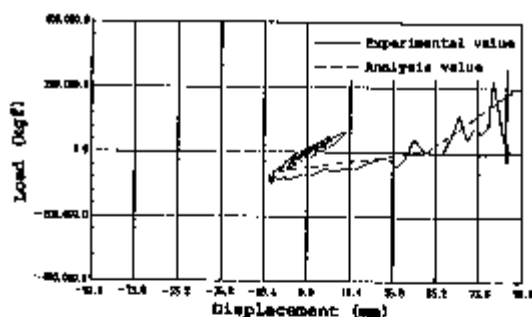


Fig. 6 Comparison of restoring characteristics (relative displacement: 100 mm)

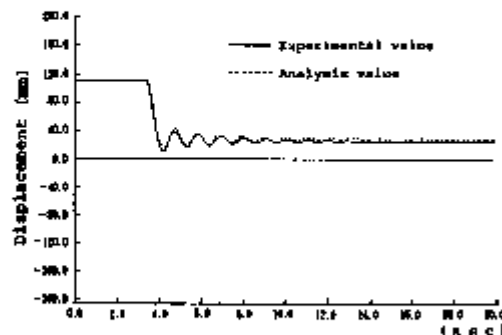


Fig. 7 Displacement-time history wave form in the isolation story (relative displacement: 100 mm)

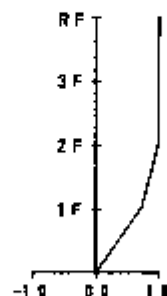


Fig. 8 Vibration mode (relative displacement: 100 mm)

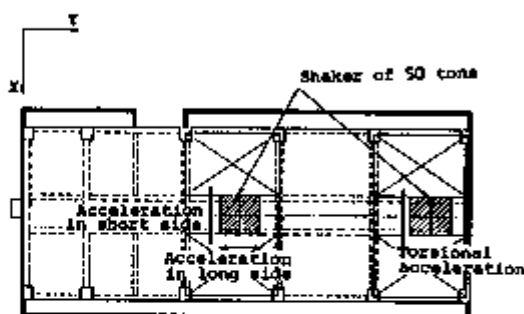


Fig. 9 Position of the shaker and acceleration direction

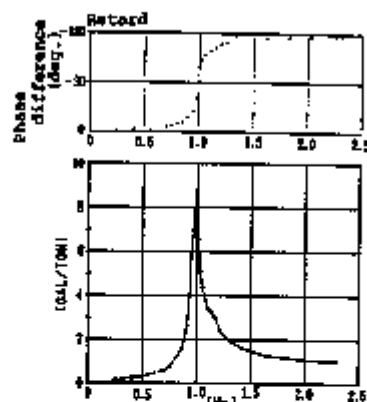


Fig. 10 Resonance curve (parallel acceleration in Y direction)

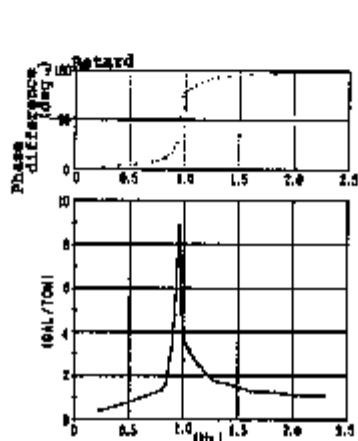


Fig. 11 Resonance curve (parallel acceleration in X direction)

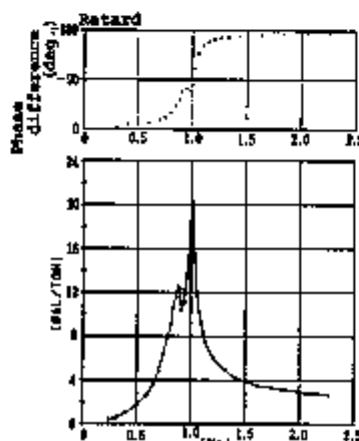


Fig. 12 Resonance curve (torsional acceleration)

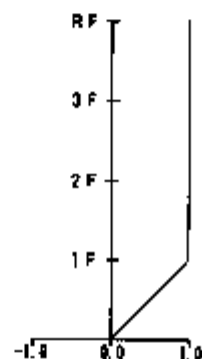


Fig. 13 Vibration mode (parallel acceleration in X direction)

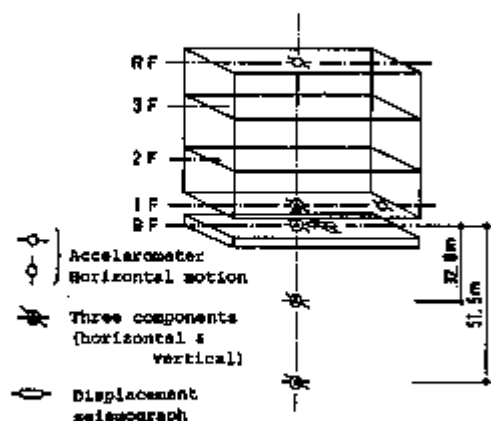


Fig. 14 Layout of the seismometers

Table 1 Specification of the earthquake

Occurrence of earthquake (time)	Epicenter latitude / longitude	Magni- tude (M)	Depth (km)	Epicen- ter dis- tance (km)	Inten- sity in China
sl. 2. 10 21:27	South-east of Ibareqi Pref. 36° 00'N 130° 55'E	5.6	54	34	III

Depth (m)	ρ (t/m ³)	V_s (m/sec)	H (m)	h (%)
-0.0	1.45	110	100	0
-10.0	1.6	150	140	0
-20.0	1.7	220	120	0
-30.0	2.0	410	325.0	2.0
-40.0	1.9	680	1157.0	1.9
-150.0	2.2	1,500	200.0	1.0
-270.0				
75	3,000	00		

* The above data are taken from the dynamic deformation curve obtained through the in-laboratory soil test.

Fig. 15 Ground model

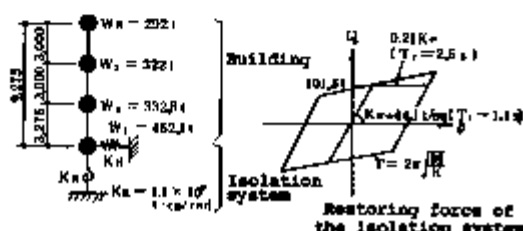


Fig. 17 Analysis model

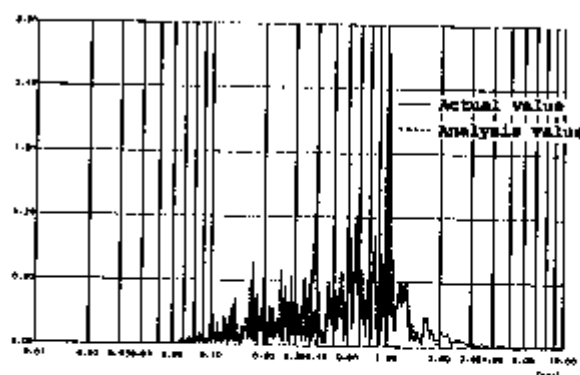


Fig. 16 Fourier spectra (building foundation)

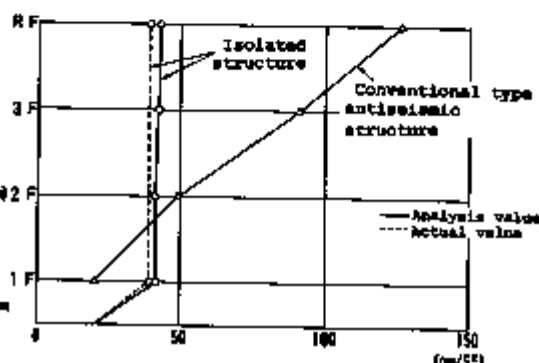


Fig. 18 Maximum acceleration response

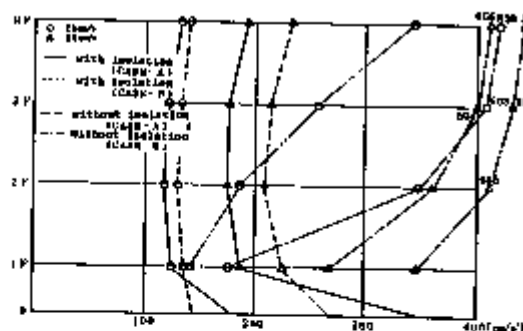


Fig. 19 Maximum response acceleration

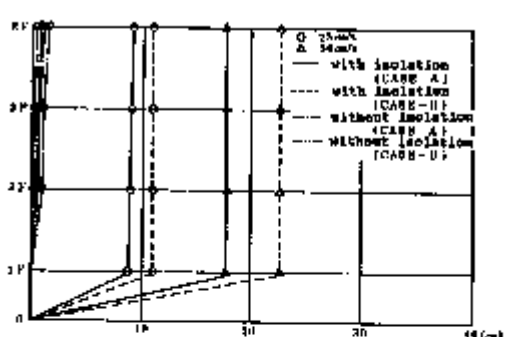


Fig. 20 Maximum response displacement

References

- Machida and Katano et al., "Study on Earthquake Base Isolation System",
Summaries of Technical Papers of Annual Meeting, Architectural Institute of
Japan 1986.8
- Seki and Okada et al., "Study on the seismic isolation of the structures"
(Part 1 to 11), Summaries of Technical Papers of Annual Meeting, Architectural
Institute of Japan 1984.10, 1985.10, 1986.8

Study of Base-Isolated Structures of Nuclear Power Plants (A Study on the Arrangement of Bearings and Stresses in the Basement)

Toru Nagano, Akira Kowada, Takao Matsumura
The Kansai Electric Power Company, Osaka, Japan

T. Nakamura, K. Kuroda
Mitsubishi Atomic Power Industries, Inc., Tokyo, Japan

Hidemasa Tomura, Tsutomu Iba
Ohbayashi Corporation, Tokyo, Japan

1. INTRODUCTION

The buildings of a nuclear power plant are much heavier than ordinary buildings. For example, the weight of the reactor building for a 4 loops PWR in Japan is about 200,000 tons. Many bearings are needed to support it and it is therefore important to study how to arrange the bearings. The characteristics of the three types of bearings arrangements considered in this study are as follows:

- a) an arrangement of 500 ton bearings under walls (Fig. 1)

Since the weight of the superstructure is transmitted to the base isolation layer through the walls, it is effective to arrange the bearings under the walls so that the bearings can support the weight directly. The variation in the bearing loads can be reduced by spacing the bearings under walls according to the weight of the superstructure.

- b) a uniformly distributed arrangement of 500 ton bearings (Fig. 2)

If we can arrange the bearings without any relation to the wall layout of the superstructure, many advantages can be expected. This arrangement makes use of the characteristics that the shear stiffness of laminated rubber is not very sensitive to the supported load.

- c) an arrangement of 1000 ton bearings under walls (Fig. 3)

There are advantages in using large capacity bearings such as simpler construction and maintenance, etc.

2. CONDITIONS and CASES ANALYSED

- (1) Reference building --- reactor building for a 4 loops PWR
- (2) Loads --- dead load + live load (D+L)
- (3) Thickness of the basemat
 - Type 1 upper basemat 2.5m, lower basemat 1.5m
 - Type 2 upper basemat under PCCV 2.5m, other places 1.5m
 - lower basemat 1.0m
- (4) Soil Conditions --- $V_s=2200\text{m/s}$, $V_s=1000\text{m/s}$, $V_s=500\text{m/s}$
- (5) Bearing Arrangements --- 3 types mentioned above
- (6) Cases of Analysed

Table 1 Cases Analysed

Models	bearings			basemat thickness		velocity of shear wave (m/s)
	standard load	arrangement	pieces	upper (m)	lower (m)	
Model 1	500t	under wall	95	2.5	1.5	2200
Model 2	500t	under wall	95	2.5	1.5	1000
Model 3	500t	under wall	95	2.5	1.5	500
Model 4	500t	under wall	95	under PCCV 2.5 other places 1.5	1.0	2200
Model 5	500t	uniformly distributed	95		1.0	2200
Model 6	1000t	under wall	47		1.0	2200

(7) Analytical model

A quarter of the reactor building is modeled by F.E.M. Basemat are modeled by plate elements. PCCV, internal concrete and the reactor external building are modeled by beam elements. Pedestals are modeled by beams, bearings by springs and soil by winker springs. The plan of the arrangement of the 500 ton bearings under walls is shown Fig. 1 and the conceptual model is shown in Fig. 4.

3. RESULTS

(1) Fig. 5 shows the variations in bearing loads. Models 1, 2, 3 show the changes in these variations due to soil conditions. The ratios of max. load to avg. load are 1.28 for model 1, 1.74 for model 2 and 2.33 for model 3. If the bearings must be designed to withstand the max. load, the bearings of model 3 will be the most expensive. Models 4, 5, 6 show the changes in the variation caused by bearing arrangements. The ratios of max. to avg. are 1.33 for model 4, 1.34 for model 5 and 1.28 for model 6. The difference between model 4 and model 5 is not important from the point of view of designing bearings. However, attention must be paid to the fact that there are a few bearings with extremely small loads in model 6. Fig. 6 shows the variations in bearing loads diagrammatically in plan view.

(2) Fig. 7 shows the changes in the displacements and deformations of the basemats due to soil conditions. Fig. 9 shows the corresponding changes in the stresses. The displacements and also the local deformations and stresses are smaller for hard soil than for soft soil.

(3) Fig. 8 shows the changes in the displacements and deformations of the basemats caused by the arrangements of the bearings. Local deformations in the upper basemat are smaller when bearings are located under the walls than those for when uniformly distributed, but the opposite applies to local deformations in the lower basemat. Fig. 10 shows a diagrammatical representation of a deformed basemat.

4. CONCLUSIONS

(1) Stiffness of soil

- As the stiffness of the soil increases, the variation in the bearing loads decreases.

- As the stiffness of the soil increases, the vertical displacements, local deformations and stresses in the basemat become smaller.
- The reactor building may be satisfactorily designed with an upper basemat 2.5m thick and the lower basemat 1.0m thick for all the cases in the study.

(2) Thickness of the basemat

- For hard soil ($V_s=2200\text{m/sec}$), the basemat thickness does not have any effect on the deformation of the total system.

(3) Bearing arrangements

- Arrangement of 500 ton bearings under walls

Because the weight of the upper building is transferred through the walls directly to the lower basemat, the deformation of the upper basemat is small and the variation of the bearing loads is small.

- Uniformly distributed arrangement of 500 ton bearings

The stresses in the lower basemat are smaller than in the case of bearings arranged under the walls, but the stresses in the upper basemat are greater. There is a large variation in the bearing loads.

- Arrangement of 1000 ton bearings under walls

There are a few bearings which have extremely small loads because the distance between bearings is limited by the design of the upper slab. Therefore, it is recommended that a combination of 500 ton and 1000 ton bearings should be used.

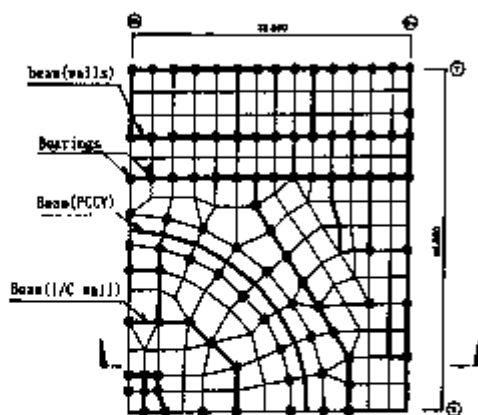


Fig. 1 500t bearings arranged under walls

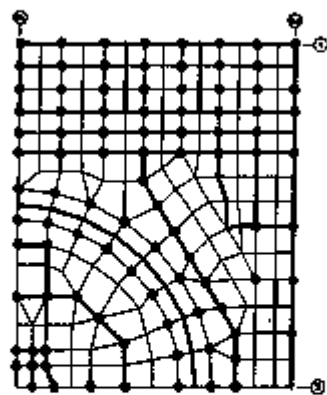


Fig. 2 Uniformly distributed arrangement of 500t bearings

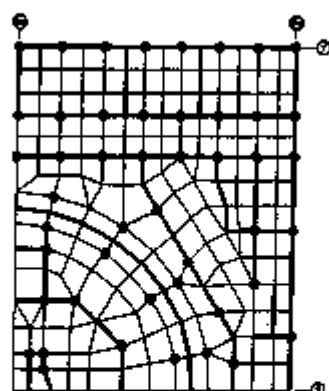


Fig. 3 1000t bearings arranged under walls

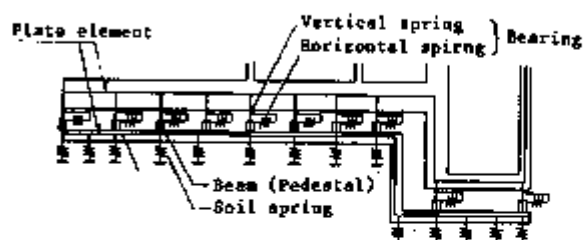


Fig. 4 Conceptual model

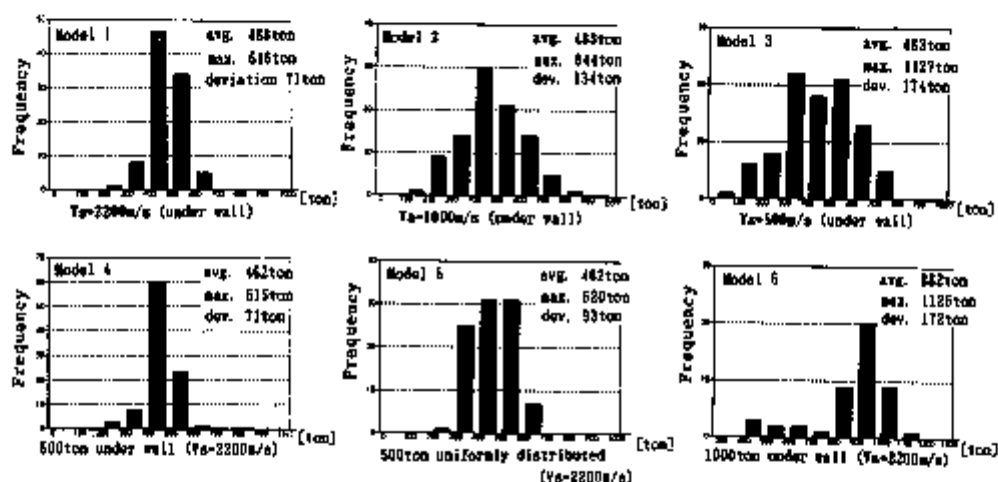


Fig. 5 Variations in bearing loads

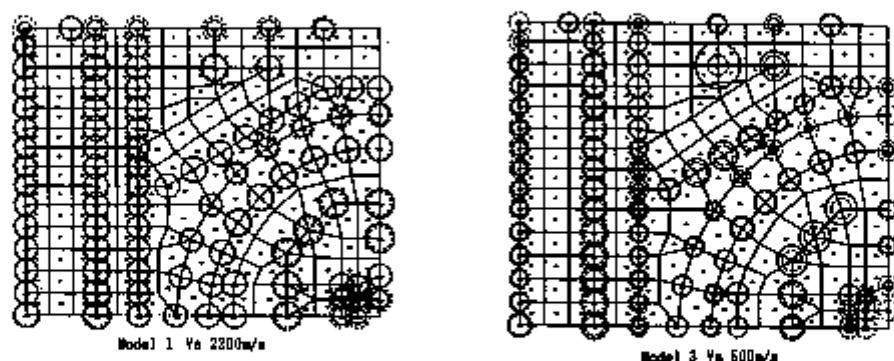


Fig. 6 Bearing loads due to soil conditions

(Diameter represents the bearing load. existing load 500t load)

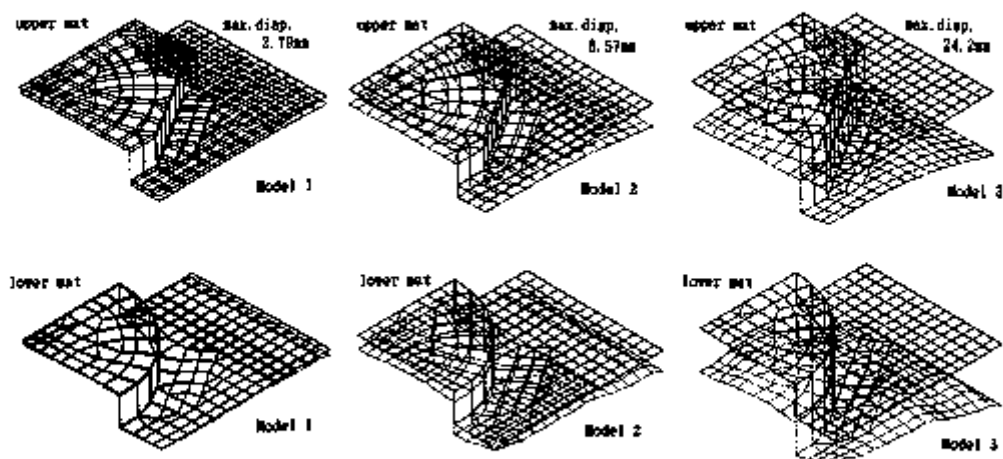


Fig. 7 Changes in the displacements and deformations of the basemats due to soil conditions

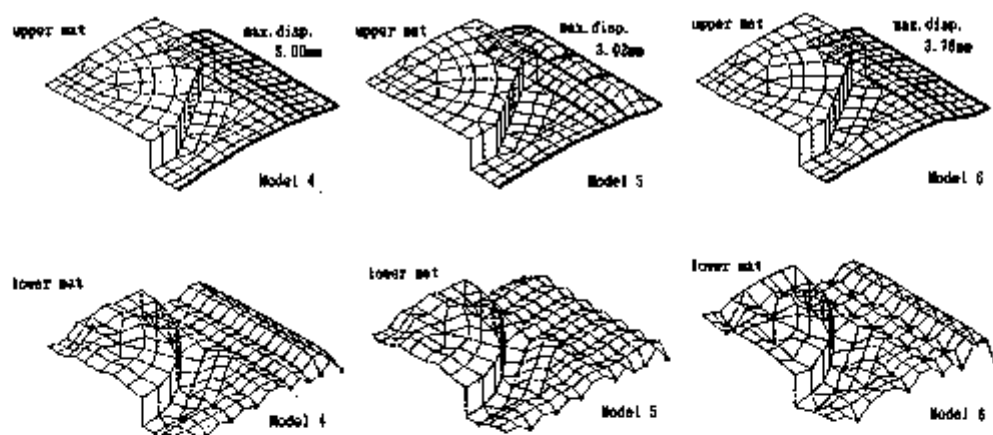


Fig. 8 Changes in the displacements and deformations of the basemats due to the arrangement of the bearings

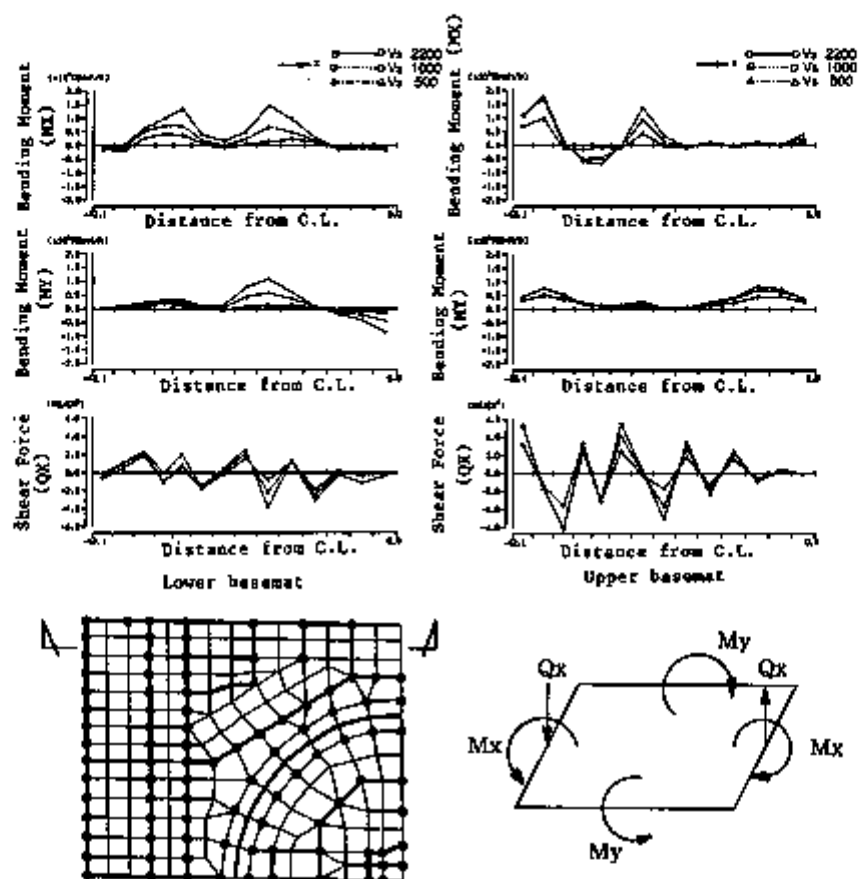


Fig. 9 Stresses in the basemat for different soil conditions

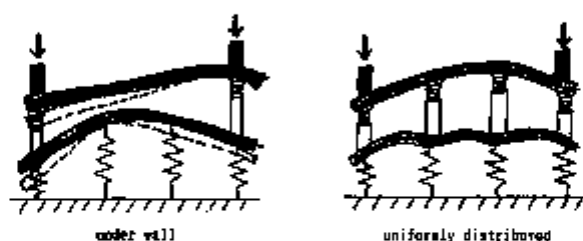


Fig.10 Diagrammatic representation of a deformed basemat

Earthquake Response Characteristics of a Base-Isolated Reactor Building with Eccentricities of Superstructure

H. Tomura, A. Miyamoto, T. Iba, K. En, T. Suzuki
Ohbayashi Corporation, Tokyo, Japan

1. INTRODUCTION

In designing a conventional non-isolated reactor building, it is always required to pay attention to the location of shear walls and the distribution of the weights to suppress torsional response under an earthquake. Due to this requirement, equipment cannot be freely arranged in the building, and the volume of the building has been larger than that actually needed. However, if the isolation devices are used, even in the case of a building with eccentricity, it may be oscillated only in the direction of excitation, and moreover, the acceleration response could be drastically reduced (Miyamoto et al, 1987).

In this paper, the torsional response behaviors of such building are discussed qualitatively and quantitatively, subjected to a severe ground motion. From numerical examples, it is concluded that the natural frequency of torsional motion depends on the arrangement of the isolation devices, and base-isolation system is effective to reduce the torsional response by decoupling the torsional stiffness of the devices from the lateral stiffness.

2. ANALYTICAL CONDITIONS

2-1. Analytical Model

A reactor building is modeled as a three-dimensional, two-lumped mass model which consists of a rigid basemat, superstructural slab and shear walls. Two eccentric types of superstructures are considered in this study, as shown in Fig. 1. The differences in both types are their eccentricity directions. The base-isolation devices, which are composed of laminated rubber bearings and steel dampers, are idealized as MSS (Multi-Shear-Spring) models (Fig. 2). They are effective in modeling bi-lateral coupled nonlinear system (Wada and Kinoshita, 1985). The restoring force characteristics of the isolation devices are set to be bi-linear (Fig. 3).

2-2. Torsional Stiffness of Isolation Devices

To investigate the torsional response, it is necessary to accurately estimate the torsional stiffness of the isolation devices. This is closely related to the arrangement of the devices, especially dampers. In designing a base-isolated structure, the rubber bearings should be arranged in proportion to the dead loads of the superstructure. On the other hand, the dampers may be arranged freely. Typical cases of the arrangements and their torsional to lateral modal period ratios are shown in Table 1.

2-3. Seismic Input

An artificial seismic wave is simulated using Ozaki spectrum (Ozaki, 1979). The wave is set for high seismic intensity zone ($M=7.0$, $\Delta=20\text{km}$) and has the same phase characteristics as El Centro (NS; 1940). Fig. 4 shows the acceleration time history (max: 267 Gal) and the corresponding velocity response spectrum. In this analysis, the amplitude is magnified to show 400 Gal as maximum.

2-4. Analytical Cases

The nonlinear earthquake response analyses are carried out in the time domain by direct integration using Newmark β method. The ratio of torsional modal period to lateral one of the isolation devices, and the natural modal period of the superstructure are taken as the indicators to discuss the coupling effects on the dynamic behaviors. (Table 2). The fundamental lateral period of the isolation devices is fixed at 1 sec .

2-5. Comparison between Elastic and Elasto-Plastic Model for Devices

For the typical cases, the results for elastic models are compared with those for elasto-plastic models (Fig. 5).

Using the elasto-plastic model, the response in the excited direction is reduced due to the stiffness degradation and hysteretic damping effects. This characteristic is common regardless eccentricity direction (Fig. 5-1, 2).

However, each model makes much difference in torsional response characteristics, although both elastic and elasto-plastic models show rigid-body behavior. Torsional displacement is estimated by the product of the torsional angle and the half width of the basement (Fig. 5-3, 4).

Even after 25 sec , at which seismic input motion ceases, the elasto-plastic model continues to show resonance phenomena with the period of 1 sec . Therefore, it cannot be expected to reduce the torsional response by plastic deformation.

3. ANALYTICAL RESULTS

3-1. Natural Mode Characteristics

Nominal modes are shown in Fig. 6 for one of the eccentric structures with the elastic devices. For fixed-base, torsional motion is excited and its center is located on the main axis of structural stiffness. On the other hand, base-isolated structure oscillates only in the translational mode along the main axis, and the torsional mode is negligibly small.

3-2. Response Characteristics

In each case shown in Table 2, the responses of the isolated buildings are estimated by the Fourier amplitude spectra (Fig. 7). They express the responses both in the directions of lateral excitation and torsion.

The responses in the excited direction are the same regardless the torsional isolating period. As the superstructure becomes more flexible, the response grows by the coupled effects with the lateral stiffness of the isolation devices. That also results in increase of the structural magnification factor.

On the other hand, when the torsional period of the isolating zone equals to the lateral one, the torsional response grows as mentioned in

2-5. Resonance phenomena are observed as the effect of the interaction between the lateral and torsional stiffness. Although it is only in the limited case that the superstructure is very flexible, whose lateral period is 0.4 sec , at the peak, the torsional response shows about $1/4$ of the maximum lateral component.

If both periods are separated enough, responses are decoupled. Moreover, as the superstructural stiffness is larger enough than that of the isolation devices, the absolute amplification factor is negligibly small and torsional resonance can be avoided.

3-3. Effects of Superstructural Eccentricity on Torsional Response

It is considered that the torsional response is excited and amplified due to the eccentricity of the superstructural stiffness. In order to estimate this effect, for the typical cases, the accumulated energy curves are indicated in Fig. 8. They are the results obtained from the acceleration response histories for both eccentric types of structure, the lateral period of which is 0.4 sec. They show the rates of energies consumed for the torsional to lateral response.

The torsional rate gradually increases on account of its resonance as shown in Fig. 5-3.4. In the case of two axis eccentricity, the torsional rate is larger to reach about 20 % compared with 12 % for one axis eccentricity, in spite that there is little difference in the amount of total consumed energy for any type of structure.

4. CONCLUSION

Base-isolation system is very effective for a reactor building with eccentricity to reduce its torsional response. The torsional response is excited only in the case that the torsional modal period of the isolating zone coincides with the lateral modal period and also when the superstructure is flexible.

However, when the dampers are arranged with each rubber pad in a large-scale structure such as a reactor building, the torsional period tends to coincide with the lateral period.

This suggests that the torsional stiffness of the isolation devices should be increased, for instance, by separating the dampers from the rubber pads and locating the dampers along the edges of the building.

5. REFERENCES

- Miyamoto, A. et al., Study on Reactor Building using Base-Isolation System, AIJ, Oct.1987
 Osaki, Y., "Guideline for Evaluation of Basic Design Earthquake Ground Motions", 1979
 Wada, A. and M.Kinoshita, Elastic Plastic Dynamic 3-Dimensional Response Analysis by using a Multiple Shear Spring Model, AIJ, Oct.1985

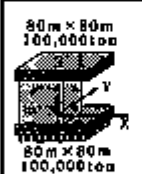
	center of gravity	●	1 axis eccentricity	2 axis eccentricity
	stiffness	⊗		
eccentric distance (m)	e _x		0.0	10.0
	e _y		10.0	10.0
eccentric rate	R _{ex}		0.200	0.236
	R _{ey}		0.0	0.236

Fig.1 Analytical Model.

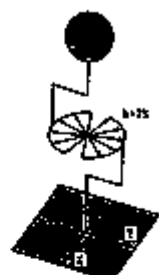


Fig.2 MSS Model

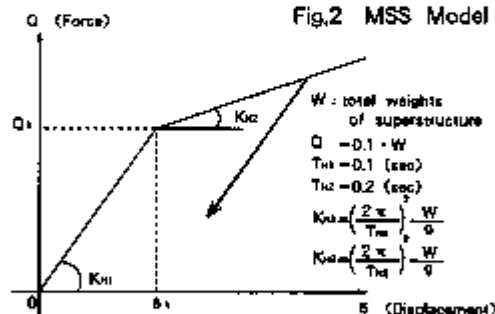

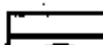




Fig.3 Restoring Force Characteristics

Table 1 Isolating Devices Arrangement
& Torsional/Lateral Period Ratio

arrangement of rubber pads & damper								
	rubber pads	damper	rubber pads	damper	rubber pads	damper	rubber pads	damper
dispersion	○	—	—	—	○	○	—	—
under wall	—	○ (edges)	○	○	—	—	○	○
T_T / T_L	0.76		0.99		1.00		1.00	

T_T : torsional period of isolation devices

T_L : lateral period of isolation devices

Table 2 Analytical Cases

1 axis eccentricity		torsional period of isolation devices(sec)		
		0.7	1.0	1.4
1st period of super-structure (sec)	0.1	○	○	○
	0.2	○	○	○
	0.4	○	●	○

lateral period of isolation devices: 1.0sec

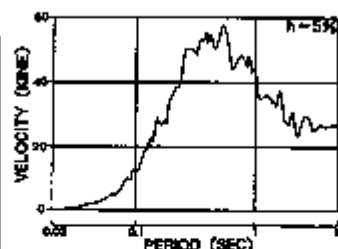


Fig.4-2 Velocity Response Spectrum

MAX. ACC.: 400.06GAL

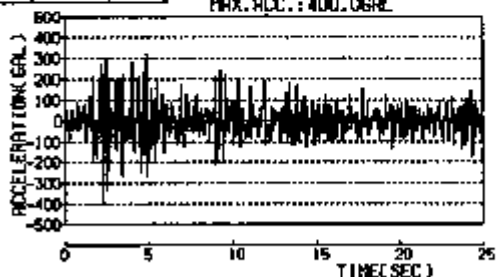


Fig.4-1 Acceleration Time History

Fig.4 Seismic Input Wave

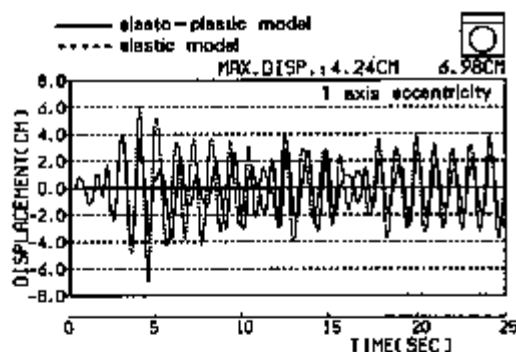


Fig.5-1 Excited Direc. Displacement Response

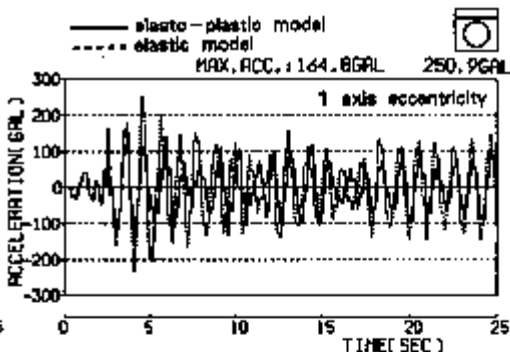
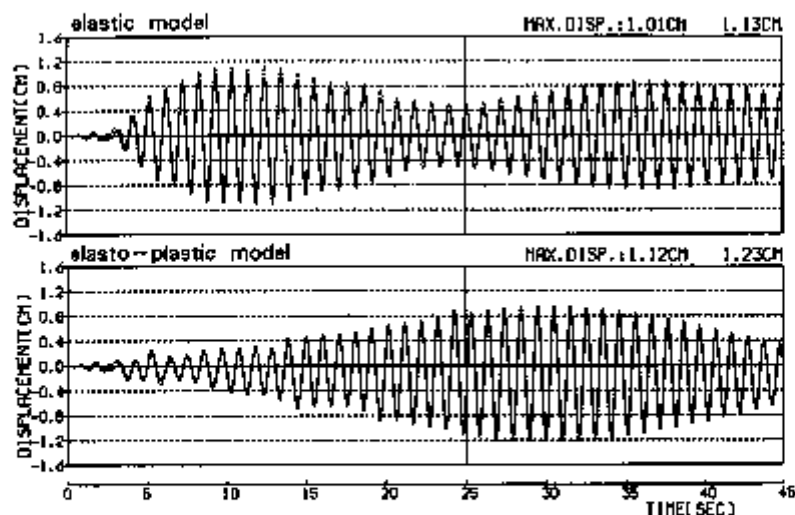


Fig.5-2 Excited Direc. Acceleration Response

(structural lateral period: 0.4sec)
(torsional period of isolation devices: 1.0sec)
(lateral period of isolation devices: 1.0sec)



structural lateral period
: 0.4 sec
torsional period of
devices : 1.0sec



Fig.5-3
Torsional Response
(1 axis eccentricity)

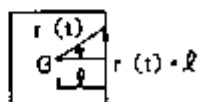
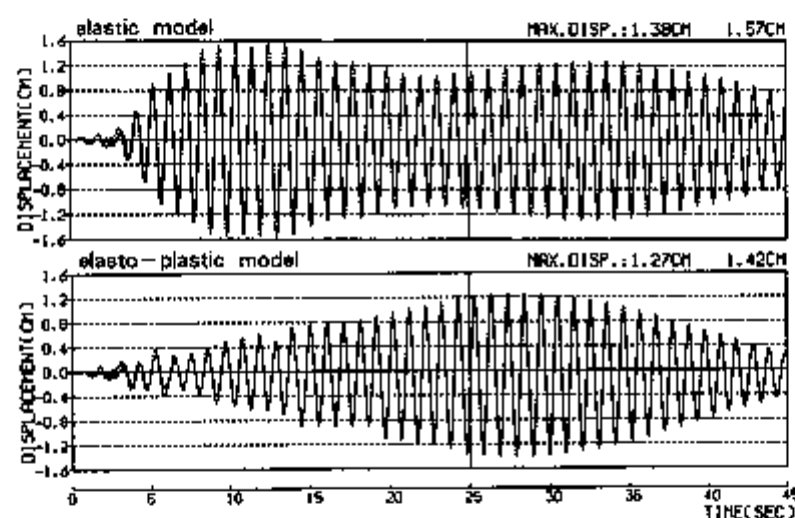


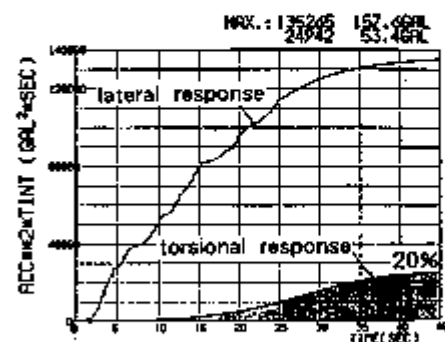
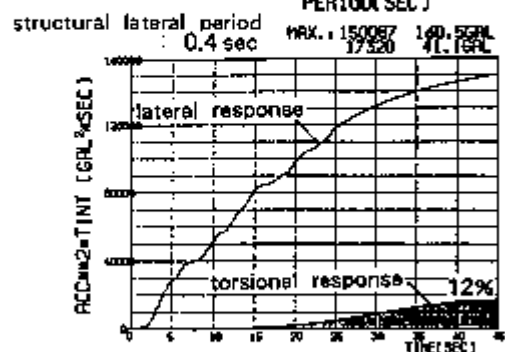
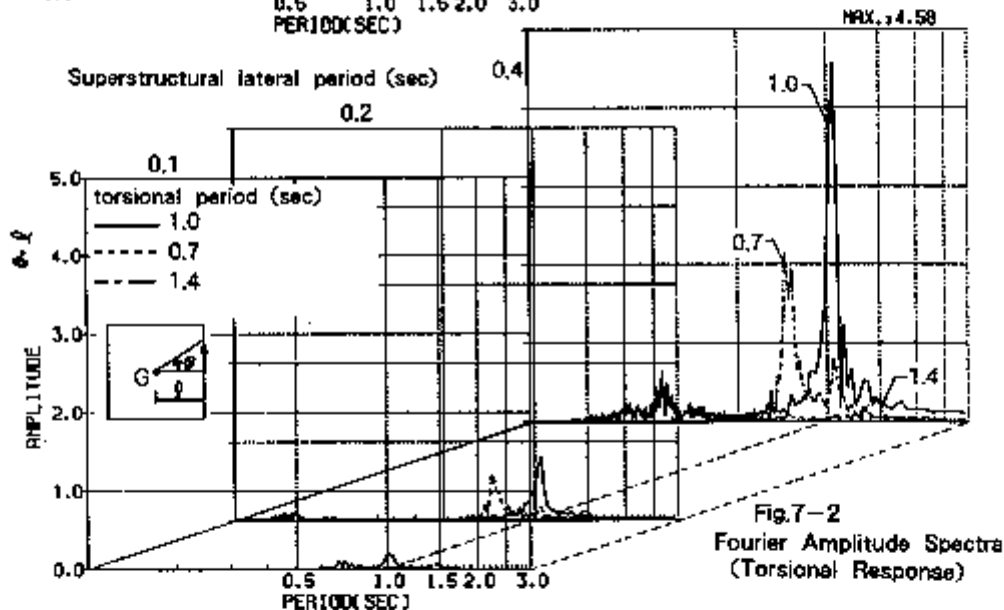
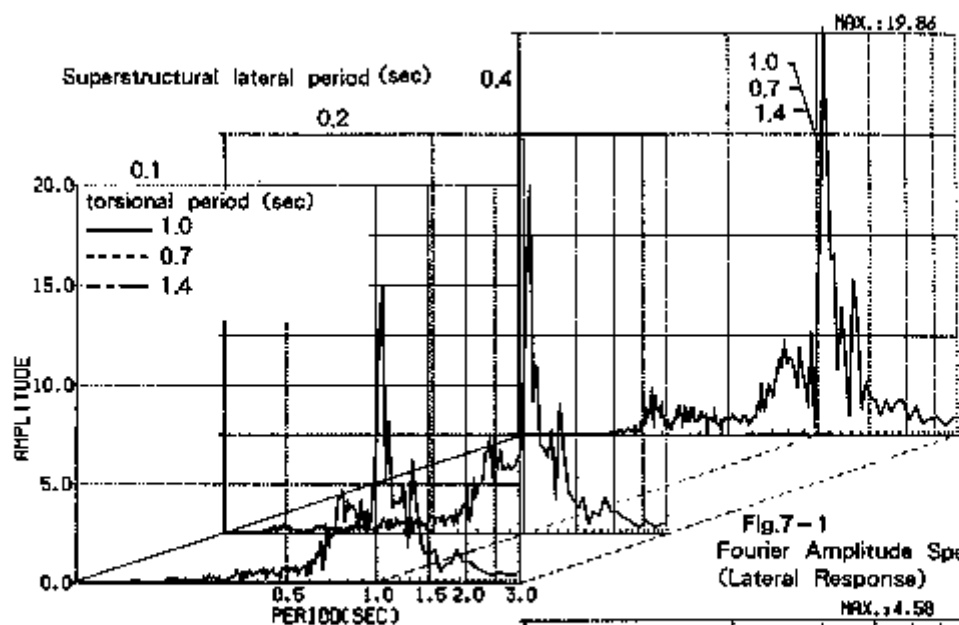
Fig.5-4
Torsional Response
(2 axis eccentricity)

		1 axis eccentricity			2 axis eccentricity		
Fixed	y						
	x						
	sec.	0.208	0.200	0.126	0.235	0.200	0.131
Isolated	y						
	x						
	sec.	1.011	1.010	1.004	1.014	1.010	1.005

structural lateral period
: 0.2 sec
lateral & torsional period
of devices : 1.0sec

Fig.6
Comparison of
Nomal Modes

X : torsional center



Seismic Isolation Test Program

Y. Sawada, H. Shiojiri, C. Kurihara, Y. Maeno, S. Aoyagi, H. Shimizu, T. Goto
Central Research Institute of Electric Power Industry, Abiko, Japan

H. Shibata, T. Fujita
University of Tokyo, Tokyo, Japan

Y. Kitagawa
Building Research Institute, Tsukuba, Japan

M. Shigeta
Hitachi Ltd., Hitachi, Japan

K. Takabayashi
Kajima Corporation, Tokyo, Japan

ABSTRACT

A test and research program was developed, and started in 1987 under the contract with Ministry of International Trade and Industry to verify the reliability and effectiveness of seismic isolation for FBR. It was intended to select appropriate seismic isolation concepts, to determine their effectiveness and feasibility, and to develop a rough draft of design technical guideline by 1989.

It is further intended to establish seismic isolation concepts, to verify their reliability and to prepare a design technical guideline by 1993 in order to reflect the results in the design of the demonstration reactor.

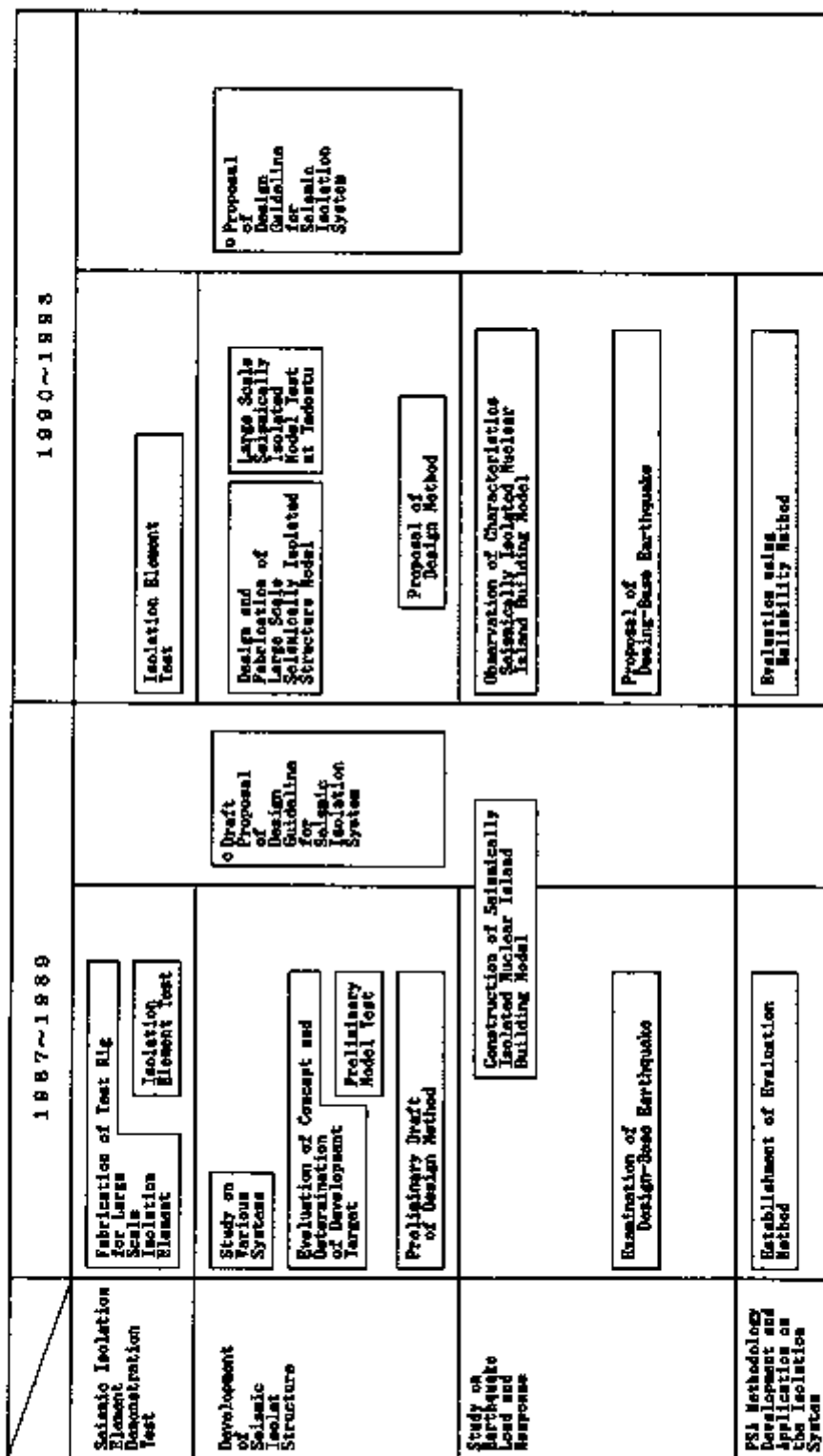
1. Introduction

Seismic isolation is expected to be effective in raising the reliability during earthquakes, reducing the cost, enlarging siting, and promoting the design standardization of FBR.

Although seismic isolation has been applied to several office buildings and residences in Japan, more research and demonstration are considered to be needed to verify the reliability and the effectiveness of seismic isolation for such important structures as FBR. A test and research program was developed, and started in 1987 sponsored by Ministry of International Trade and Industry so that the results could be reflected in the demonstration reactor. It was intended to select appropriate seismic isolation concepts, to determine their effectiveness and feasibility, and to develop a rough draft of design technical guideline within three years. It was further intended to establish seismic isolation concepts, to verify their reliability, and to prepare a design technical guideline(draft)within seven years. On the basis of a survey of past researches, designs, and seismic safety reviews of nuclear power stations, a research program were decided to consist of the following items. (Fig.1)

- 1) To prepare a FBR seismic isolation design technical guideline (draft) on the basis of a survey of domestic and overseas standards and codes and the results of the present research.
- 2) To select appropriate seismic isolation systems and seismic isolation elements on the basis of a survey of past cases and seismic response analyses.
- 3) To develop structural concepts and to investigate technical issues through analyses, model experiments, etc.
- 4) To demonstrate the reliability of FBR seismic isolation systems during strong earthquake by large-scale shaking table.
- 5) To demonstrate the reliability of the seismic isolation elements by conducting breaking tests with large-scale seismic isolation element models.

FIG. 1 SEISMIC ISOLATION STUDY PROGRAM



- 6) To evaluate relatively long period components of earthquake motion by collecting and analyzing seismic observation records and by applying analytical methods, and to propose a method for setting an appropriate design earthquake motion.
 - 7) To construct simulated seismically-isolated FBR buildings, and verify the reliability of the seismic isolation system under real working conditions by observing the response of the system during actual earthquakes.
 - 8) To develop seismic PSA techniques for seismic isolation system.
- In this paper, details of the program are described.

2. Proposal of Design Guideline for Seismic Isolation System

It is intended to propose a technical guideline which will be required in designing seismic isolation for FBR.

First, a comprehensive survey of aseismic design standards, guidelines and actual designs of nuclear power stations and seismically-isolated buildings in and out of Japan were conducted.

On the basis of the findings of the survey, terms to be covered by the guideline were picked up, the basic philosophy and framework of the guideline were formulated, and remaining technical tasks were clarified.

The tasks remained are to be investigated in this program, and by reflecting the results of the program, the design guideline will be proposed.

The principal contents of the technical guideline (draft) are as follows.

Section I Safety design policy for seismic isolation systems

- ① Safety design policy for seismic isolation systems

Section II Seismic isolation design policy for seismic isolation systems

- ① Basic policy
- ② Classification of importance
- ③ Methods for evaluating seismic isolation design
 - Methods for calculating seismic forces
 - Methods for evaluating design earthquake motion
 - Methods for evaluating seismic isolation system
- ④ Combination of loads and tolerances

Section III Engineering data

- (1) Evaluation of earthquake motion
- (2) Seismic isolation design methods
- (3) Seismic isolation elements design methods
- (4) Building design methods
- (5) Component design methods
- (6) Construction methods

3. Seismic Isolation Element Demonstration Test

It is intended to conduct tests on large-scale seismic isolation elements for FBR so as to demonstrate the safety against seismic load, and the durability of these elements in service life of the plant.

The tests on the elements are conducted according to the following procedure:

- 1) A survey of past tests on seismic isolation elements is made to select necessary test items and to develop a test program
- 2) A specification of a laminated elastomer for base isolation of FBR building is examined.
A full-scale (500t class) and reduced scale (200t and 50t class) models are fabricated, (Fig. 2)
- 3) A static biaxial load tester, which is capable of breaking large scale (200t class) isolation elements, is fabricated. (Fig. 3)
- 4) Scale law is confirmed by conducting tests on full-scale and reduced scale models using the load tester and by testing cut-out samples from the elastomers of different scales.

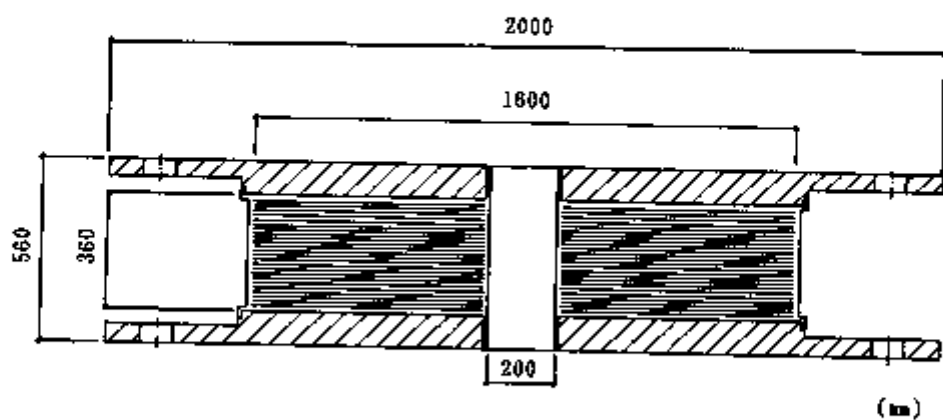


FIG. 2 A FULL-SCALE SEISMIC ISOLATION ELEMENT



FIG. 3 Biaxial Load Tester

- 5) The breaking loads and displacements are determined from the test results of reduced-scale models using the biaxial load tester, while load-displacement relationships for design loads are determined using full-scale models.

4. Development of Seismically Isolated structure

It is intended to select appropriate seismic isolation concepts for FBR, to develop an isolation structure, and to verify the reliability of the structure.

It is conducted according to the following procedure.

- 1) Several promising seismic isolation concepts and corresponding isolation devices are picked up based on existing knowledge.
- 2) Each plant concept is subjected to seismic response analysis using a tentative design spectrum for seismically isolated FBR, the applicability, cost reduction effects and future research and development items are evaluated on the basis of the results of their findings, and an isolation concept is selected.
- 3) The design of an isolation system for FBR is developed in some detail, (Fig. 4) and tasks for further investigation are identified.
- 4) Analytical studies and model tests are conducted for the identified tasks, and the design of the isolation system is revised.
- 5) The reliability of the isolation system are verified by large scale model tests using the shaking table of Nuclear Power Engineering Test Center at Tadotsu, Japan. (Table 1)

5. Study on Earthquake Load and Response.

In order to design seismic isolation systems for FBR, it is necessary to make rational design earthquake ground motion which includes relatively long-period components. It is also important to confirm the performance of isolation systems and to verify the response analysis method by observing the response of actual seismically isolated structures.

It is intended to propose a method to determine design earthquake ground motion for seismically isolated FBR, and to construct and observe the response of the about 1/3 scale seismically isolated nuclear island building model.

For investigation of design earthquake ground motion, seismic observation records of large earthquakes (Magnitude >6) are analyzed and comparison are made with the results of evaluation methods such as the semi-experimental formula for Love wave, semi-experimental formula for body wave, and a method for synthesizing strong ground motion using observed seismograms of small events.

6. PSA methodology development and application on the isolation system

It is intended to investigate the reliability of seismically isolated FBR structures during earthquakes from the view point of probabilistic safety assessment.

Following methods are employed in the study.

- 1) Estimation of probabilistic factor of safety which consists of capacity factor, response factor, and deterministic safety factor.
- 2) Simulation and evaluation of safety margin measures based on second moment reliability for estimating the reliability index of both isolated and non-isolated FBR structure.
- 3) Development of a Monte Carlo simulation technique for more accurate assessment and for investigation of the effect of randomness of isolation devices on the response of seismically-isolated FBR.

7. Conclusion

A test and research program is developed, and started under the contract with MITI in 1987.

This program is expected to verify the reliability and effectiveness of seismic isolation for FBR.

TABLE 1 SPECIFICATION OF SHAKING TABLE

Equipment	Major Specifications
Vibration Table	15m X 15m X 3.5m (H) Weight 420 ton
Horizontal Actuators	Exciting Force 450 ton f Stroke \pm 200mm
Vertical Actuators	Exciting Force 300 ton f Stroke \pm 100mm Built-in Balance Cylinder
Fixed Guide	Compression Force 350 ton f
Movable Guide	Compression Force 360 ton f Stroke 100mm

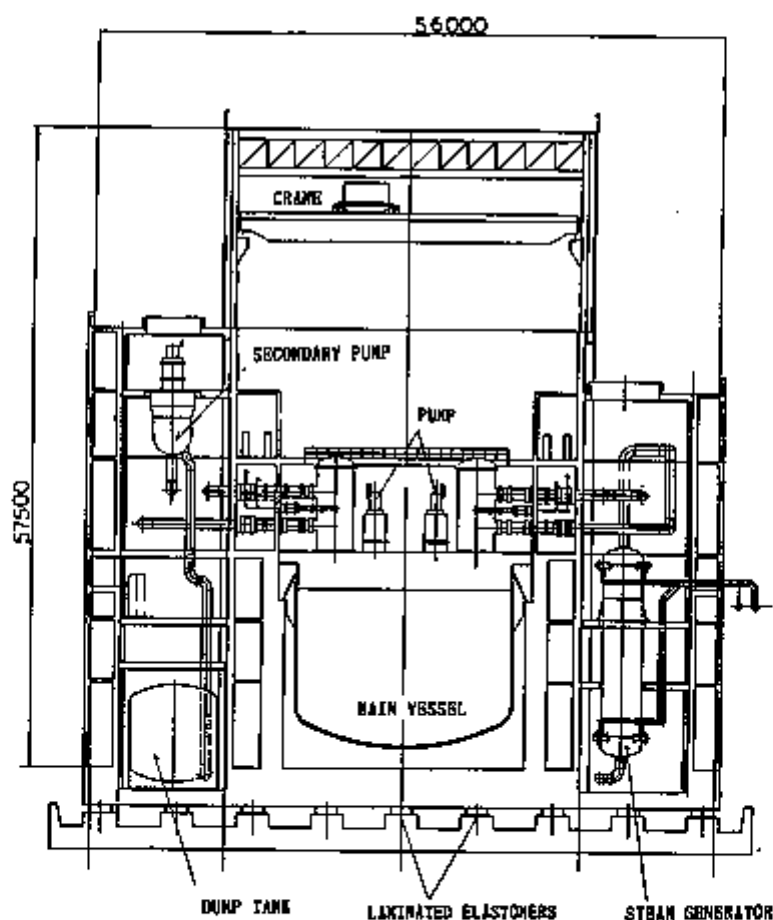


FIG. 4 SEISMICALLY ISOLATED FBR PLANT

Probabilistic Assessment on Torsional Vibration of a Base Isolated Structure for FBR

Shuichi Yabana

Central Research Institute of Electric Power Industry, Abiko, Japan

Heki Shibata

University of Tokyo, Tokyo, Japan

INTRODUCTION

Recently, electric power industry, universities and manufacturers discuss to introduce a base isolation system into a fast breeder reactor plant (FBR), because seismic load is more dominant and, maybe, critical than the other loads in the design of FBR. In some trial design of a base isolated structure for a large-scale FBR, several hundred pads are used. The pads' characteristics may not be uniform, because of randomness caused by the aging and other reasons. If the distribution of pads' characteristics is uneven, torsional vibration of super-structure shall occur during an earthquake. The torsional vibration may give some additional damage to the reactor vessel, piping and other equipment.

Base isolation system is generally inelastic system. Torsional response of inelastic system was studied by some researchers, but one of the system in which inelastic elements have random characteristics is investigated here. The aim of this paper is to investigate the relation to the randomness of pads' characteristics and the torsional vibration using Monte Carlo method, and to obtain the basic idea to decide the range of randomness of their characteristics for design guide of an isolation system.

3DOF MODEL OF THE ISOLATED STRUCTURE

As shown in Fig.1, the isolated structure is modeled as 3DOF hysteretic system which consists of a rigid slab and pads. The restoring characteristics of each pad is bi-linear with circular yielding curve, which is modeled on a lead rubber bearing. In elastic state, stiffness is always the first stiffness k_1 , and in plastic state (Fig.2), tangent stiffness is shown as,

$$k_x = k_1 \{ (\gamma-1) \cos\theta (\cos\theta + \frac{dy}{dx} \sin\theta) + 1 \} \quad (1)$$

$$k_y = k_1 \{ (\gamma-1) \sin\theta (\sin\theta + \frac{dx}{dy} \cos\theta) + 1 \} \quad (2)$$

where γ is ratio of first and second stiffness.

For the simulation, the model was chosen as follows: mean of k_1 and γ are decided so that mean natural frequency of this system in horizontal direction is 1.3 Hz in elastic state and 0.5 Hz in plastic state. Mean of displacement at yielding point is set so that a pad subjected to 50 gal input yields.

Monte Carlo Simulation

As there is no statistical data on the randomness of pads' characteristics by the aging, the distribution of the randomness is assumed log-normal

distribution. In each sample of Monte Carlo simulation, the first stiffness and/or the yielding displacement of each pad is given randomness in order to simulate the uneven distribution of the characteristics. Trial number of the simulation was decided to be 50 samples by the convergence of the mean and the standard deviation of maximum torsional angle. The inputs are two directional ground motions. Two sets of input ground motions chosen for the simulation are NS and EW components of time histories recorded at El Centro in 1940 (max. acc. NS: 341.7 gal, EW: 210.1 gal) and at Hachinohe, Japan in 1968 (max. acc. NS: 225.0 gal, EW: 182.9 gal).

In a model of a large FBR with a lot of pads, the amount of the calculation is very large, so that two types of isolated structure model are discussed. First, the basic relations between the maximum torsional angle and the variation of the pads' characteristics are discussed with the partial model as shown in Fig.3. In this case, number of pads is changed from 9 to 36, and the range of randomness of pads' characteristics, or the coefficient of variation (COV) is changed from 10% to 40%. Secondly, actual torsional vibration of the isolated structure is estimated with an actual size model. Fig.4 shows an actual size model of the base isolated structure for FBR. Number of pads is 16, 100 and 256. The COV of their pads' characteristics is set 40%. Wilson θ method is used with $\theta = 1.4$, and time interval for the simulation is 1 msec (partial model) and 2.5msec (actual model).

RESULTS OF SIMULATION

Simulation for Partial Model of the Base Isolated Structure

The responses at the center of gravity are almost equal to all cases. The relation between the mean of maximum torsional angle and the variation of the stiffness and yielding displacement is shown in Figs.6. The mean of maximum torsional angles is proportional to the variation. The COV of the maximum torsional angles is constant to the variation of the pads' characteristics. The maximum torsional angle in the case of random stiffness is about twice as big as one in the case of the random yielding displacement. That is, the variation of the stiffness is more effective to excite the torsional vibration than one of the yielding displacement. In the case that both the stiffness and the yielding displacement are given randomly, the maximum torsional angle is less than sum of those which occur where their randomnesses are independently given.

The mean of maximum torsional angles decreases according to increasing the number of the pads as shown in Table 1. It is found that the mean of maximum torsional angle is proportional to distance of the eccentric center which is the distance between the center of gravity and the center of torsion in elastic state. The normalized distance of eccentric center, based on where the number of pads is 9, is almost as same as normalized maximum torsional angle, so that maximum torsional angle in the case of multi-pads can be estimated by the result of the maximum torsional angle for 9 pads obtained by Monte Carlo simulation. The estimated torsional angle a_e for other cases can be written as

$$a_e = a_g e \quad (3)$$

where a_g : the maximum torsional angle calculated by Monte Carlo simulation for 9 pads in normalizing number,

e : normalized distance of eccentric center based on 9 pads for other multi-pad cases.

The authors call this method the simplified estimation method.

By using two sets of input ground motions, the distributions of maximum torsional angles are different, as shown in Fig.6. Although the peak acceleration of Hachinohe waves are smaller than those of El Centro, the torsional responses are almost same. This reason may be that Hachinohe waves include long period components.

Simulation for Actual Size Model

The maximum responses are shown in Table 2, in the case that the stiffness is given randomness. Horizontal acceleration is reduced by about 1/3 to input ground motion. The mean of maximum torsional accelerations and angles are 3.0×10^{-3} rad/sec² and 1.2×10^{-4} rad, so that the incremental acceleration and displacement at the corner of the slab are about 10 gal and 3 cm. Considering to add the variation of the responses to the mean, these values are not large. Table 3 shows relation between number of pads and distance of the eccentric center. Table 4 shows the comparison of the maximum torsional angles estimated by the simplified method from normalized distance of the eccentric center and those obtained by Monte Carlo simulation. They are almost consistent, so that the simplified estimation method can be said to be verified.

The shear buckling of a reactor vessel in a pool type large FBR plant, as shown in Fig.7, is examined, as an example of the effect of torsional response of the building to the equipment of FBR. The maximum stress of the vessel section at the upper edge is 3.0×10^{-4} kg/mm², when the maximum torsional acceleration is 3.0×10^{-3} rad/sec² in COV of stiffness 40%. In spite of large limit variation of their characteristics, the maximum stress is much smaller than the limit of its shear buckling stress.

CONCLUSIONS

The torsional vibration of a base isolated structure for FBR caused by the aging of pads was simulated by Monte Carlo method, and the relation between the torsional vibration and the variation of pads was investigated. The following results from the simulation for several levels of model are obtained:

- (1) The mean of the maximum torsional angles is proportional and the coefficient of their variation is almost constant to the variation of the stiffness and yielding displacement.
- (2) The randomness of the stiffness is more effective to excite the torsional vibration than that of yielding displacement.
- (3) The maximum torsional angle decreases according to increasing the number of the pads, and is proportional to the distance of the eccentric center. From this result, the simplified estimation method of maximum torsional angle has been presented.
- (4) Using two sets of input ground motions, the distributions of maximum torsional angles are different. Hachinohe waves which include long period component, tend to excite more the torsional vibration response.

In the actual size model, the torsional response is small, so that the reactor vessel in pool type FBR may not suffer damage. Through applying to the actual size model, the simplified estimation method of the maximum torsional angle was verified.

ACKNOWLEDGEMENT

The authors want to express their gratitude to Dr. Sawada, CRIEPI, to give a chance for Mr. Yabana to study at Shibata's Laboratory, Inst. of Ind. Sci., University of Tokyo. They sent the manuscript, which is the same to this paper, to the Bulletin of ERS for internal material of Earthquake Resistant Structure Research Center, Inst. of Ind. Sci..

REFERENCES

- Tso, W.K. and Bozorgnia, Y. (1986). Effective Eccentricity for Inelastic Seismic Response of Building. *Earthq. Eng'g. and Struct. Dyn.*, Vol.14, No.3, pp.413-427.
- Yabana, S. and Shibata, H. (Mar. 1989). Probabilistic Assessment on Torsional Response Due to Aging of Base Isolation Pads for Large Fast Breeder Reactor. *Bull of ERS, Inst. of Ind. Sci., Univ. of Tokyo*, No.22. (in printing)
- Yamazaki, Y. (1981). Inelastic Torsional Response of Structures Subjected to Earthquake Ground Motions. *Trans. of AIJ*, No.310, pp.61-68. (in Japanese)

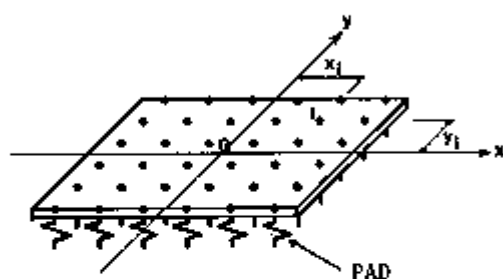


Fig.1. Isolated Structure Model

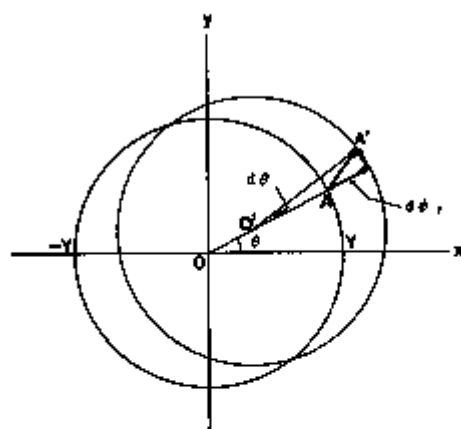
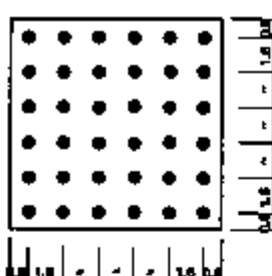
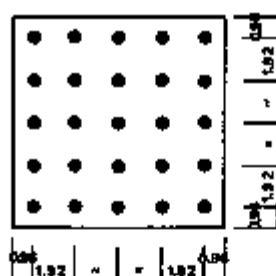
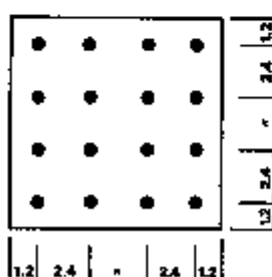
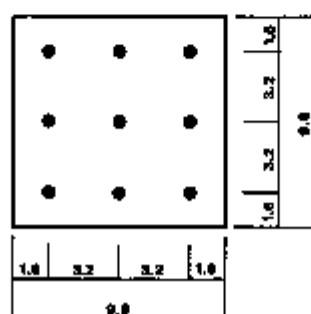
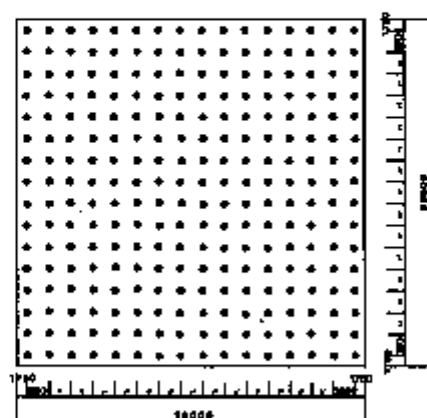


Fig.2. Yielding Displacement Circle



Weight of Slab : 4,500ton

Fig.3. Partial model



Weight of Slab : 128,000ton
Number of Pads : 256

Fig.4. Actual Size Model

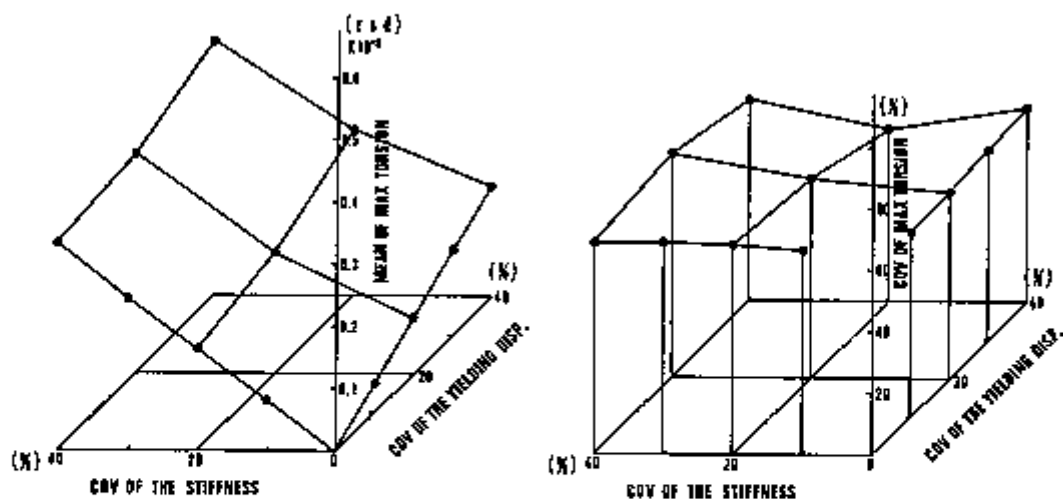


Fig.5. Relation Between Maximum Torsional Angle and Variation of Pads' Characteristics (Input: El Centro, Number of Pads: 9)

(a) Mean of Maximum torsional Angles (b) COV of Maximum torsional Angles

Table 1. Normalized Distance of Eccentric Center v.s. Normalized Maximum Torsional Angle (COV of Stiffness : 40%)

Pad No.	9	16	25	36
Dis. of Ecc. Center (cm)	40.31	34.62	28.28	22.45
Normalized Dis. of Ecc. Center	1.0	0.86	0.65	0.56
El Centro: Norm. Max. Tor. Angle	1.0	0.82	0.61	0.49
Hachinohe: Norm. Max. Tor. Angle	1.0	0.72	0.55	0.46

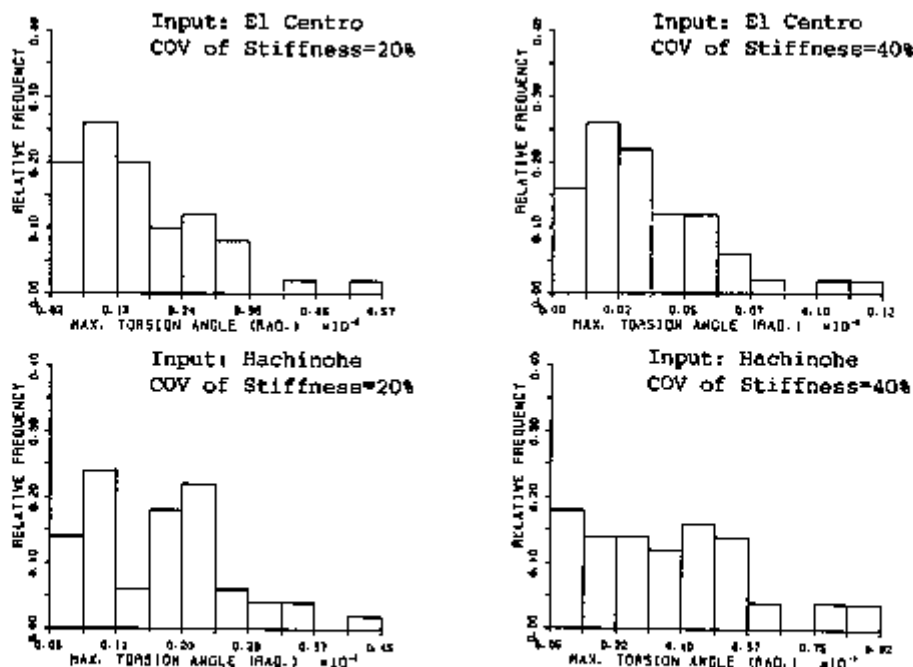


Fig.6. Distribution of Maximum Torsional Angle

Table 2. Maximum Responses of Actual Size Model
(Input: El Centro, COV of Stiffness= 40%)

Pad No.		15	100	256
Max. Acc. at Gravity Center (gal)	x	117.877 8.636	117.808 0.828	117.381 0.492
	y	109.269 4.158	109.636 1.948	109.580 1.159
Max. Disp. at Gravity Center (cm)	x	7.385 0.829	7.636 0.378	7.590 0.225
	y	7.703 0.810	7.549 0.326	7.561 0.188
Max. Acc. at Slab Corner (gal)	x	124.625 5.226	118.873 1.862	119.108 1.247
	y	112.808 4.896	110.815 1.953	110.864 1.767
Max. Disp. at Slab Corner (cm)	x	8.564 1.144	7.877 0.511	7.757 0.269
	y	8.653 1.178	7.870 0.454	7.768 0.235
Max. Torsional Acc. (rad/s ²)		0.978×10^{-2} 0.419×10^{-2}	0.502×10^{-2} 0.283×10^{-2}	0.354×10^{-2} 0.164×10^{-2}
		0.502×10^{-3} 0.327×10^{-3}	0.177×10^{-3} 0.114×10^{-3}	0.124×10^{-3} 0.725×10^{-4}

Upper Values: Mean, Lower Values: Standard Deviation

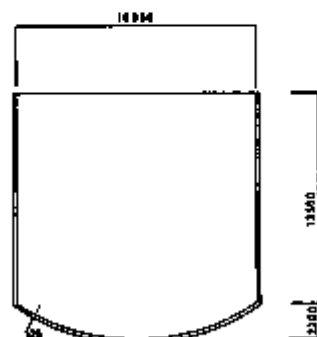


Fig.7. An Example of Schematic Drawings of Reactor Vessel in a Fast Breeder Reactor Vessel

Table 3. Distance of Eccentric Center for Actual Size Model

Pad No.	15	100	256
Dis. of Ecc. Center (cm)	202.0	77.5	51.9
Normalized Dis. of Ecc. Center	1.0	0.384	0.257

Table 4. Estimated Maximum Torsional Angle by Monte Carlo Simulation and Simplified Estimation Method

Input	Pad No.	15	100	256
El Centro	Monte Carlo Sim. (rad)	5.02×10^{-4}	1.77×10^{-4}	1.24×10^{-4}
	Simplified Estimation(rad)	—	1.93×10^{-4}	1.29×10^{-4}
Hachinohe	Monte Carlo Sim. (rad)	5.11×10^{-4}	1.80×10^{-4}	1.18×10^{-4}
	Simplified Estimation(rad)	—	1.96×10^{-4}	1.91×10^{-4}

Response of a Base-Isolated Large Liquid Metal Reactor Plant to Seismic Loads

Y. W. Chang, J. Gvildys

Argonne National Laboratory, Argonne, IL USA

INTRODUCTION

In recent years, base isolation has been applied to various civil structures such as bridges and buildings for the purpose of reducing its acceleration to below the level of ground accelerations during seismic events. The basic principal of base isolation is to introduce a soft layer of material between structure and foundation to allow a degree of flexibility in horizontal motions which could reduce the seismic accelerations during earthquakes. If base isolation is properly designed, it shifts the fundamental frequency of the structure away from the damaging frequency range of earthquakes. Thus, the seismic loads transmitted to the structure can be greatly reduced. This is particularly important in Liquid Metal Reactor (LMR) plants, because the components of primary system such as reactor vessel and piping loops are designed to be thin-walled structures and have little inherent seismic resistance. Thus, the use of base isolation offers a viable and effective approach that permits the reactor structures to better withstand the seismic loading.

This paper deals with the seismic response of a base isolated large-scale LMR plant. The analysis model was based on a preliminary nuclear island layout developed by EPRI during the concept development phase of the large-scale prototype breeder (LSPB) project. The nuclear island has a dimension of 184'-0" x 210'-6"; the reactor vessel has an ID of 62 ft and an overall length of 70 ft. Two soil conditions have been considered in the analysis. One is a hard-soil site having a shear wave velocity of 6000 ft/s, and the other is a soft-soil site having a shear wave velocity of 2000 ft/s. For comparison purposes, the response of a conventional plant (unisolated) was also analyzed.

MODEL OF LSPB PLANT

The LSPB plant consists of a single basemat which supports the reactor containment building (RCB), the steam generator building (SGB), the reactor service building (RSB), and the crane enclosure building (CEB). The mathematical model of the nuclear island is shown in Fig. 1. The buildings and reactor vessel are modeled with finite elements. They are represented by a number of beams and springs interconnected at their nodes and a number of masses lumped at floor levels, and are placed at the nodes as shown in Fig. 1. The reactor containment building, the steam generator building, and the reactor service building, are represented by beams 1-5 whereas the crane enclosure building is represented by beams 6-9 connecting nodes 8 and 302. The reactor vessel and its internals are represented by beams 101-117 together with springs K1, K2, and K4-10. Spring K3 represents the reactor vessel support skirt.

*Work supported by the U.S. Department of Energy, Office of Technology Support Program, under Contract W-31-109-Eng-38.

Under seismic excitation, the response of the plant is affected by the stiffness of the soil around it. Thus, the surrounding soil must also be properly included in the mathematical model. Here, we assume that the soil can be represented by a frequency independent spring and dashpot as shown in Fig. 1. For isolated plants, the nuclear island has two concrete foundation mats, and the isolators are placed between the two mats. The fundamental frequency of an isolated nuclear island ranges from 0.2 to 0.5 Hz. Here, we assume that the isolated plant has a fundamental frequency of 0.50 Hz.

SEISMIC INPUT

The seismic input used in the LSPB analyses is a synthetic earthquake acceleration time history which has a 19-s duration and 3801 data points digitized at 0.005 s intervals. The maximum peak acceleration of the time history has a zero period ground acceleration (ZPGA) of 0.3 g for sites with a low shear velocity of 2000 ft/s or less and a ZPGA of 0.2 g for sites with a high shear wave velocity of 6000 ft/s or greater.

DISCUSSION OF RESULTS

Four Cases have been studied. They are:

Case	Site Condition	Peak Ground Acc.	Base Isolation
1	Hard Soil, $V_s=6000$ ft/s	0.2 g	No
2	Hard Soil, $V_s=6000$ ft/s	0.2 g	Yes
3	Soft Soil, $V_s=2000$ ft/s	0.3 g	No
4	Soft Soil, $V_s=2000$ ft/s	0.3 g	Yes

The system frequencies are given in Table I.

Table I. System Frequencies, Hz

Case	Frequency, Hz				
	ω_{isolator}	ω_{building}	$\omega_{\text{foundation mat}}$	$\omega_{\text{reactor vessel}}$	ω_{core}
1	---	16.02	---	22.15	16.20
2	0.50	15.56	65.26	22.15	16.20
3	---	5.34	---	22.15	16.20
4	0.50	5.18	21.75	22.15	16.20

These frequencies were obtained from eigenvalue analysis. With this background information, we can now discuss the results of the analyses. The maximum peak accelerations at the top of the basemat (Node 1), reactor vessel support (Node 5), top of the reactor vessel (Node 102), core support structure (Node 107), top of the core barrel (Node 111), bottom of the reactor core (Node 123), and top of the core (Node 117) for cases 1-4 are shown in Table II. It can be seen in Table II that for hard soil sites, the base isolation with isolator frequency of .50 Hz can reduce the horizontal accelerations by a factor of two or more. However, for soft soil sites, the maximum peak accelerations at the top of the basemat and reactor vessel support are reduced very slightly, whereas at reactor components, the peak accelerations are greatly increased.

Table II. Peak Acceleration, g

Site Condition	Base Isolation	Structural Mode			Component Mode			
	Isolator freq. = .50 Hz	Node 1	Node 5	Node 102	Node 107	Node 111	Node 123	Node 117
Hard Soil Site	No	.23	.22	.35	.45	.41	.47	1.10
$V_s = 6000$ ft/s	Yes	.14	.12	.15	.21	.20	.25	.45
SSE = .2g								
Soft Soil Site	No	.38	.41	.68	2.03	1.21	1.94	2.94
$V_s = 2000$ ft/s	Yes, in-tune	.34	.38	2.20	3.30	2.34	3.69	6.22
SSE = .3 g	Yes, detuned 1/2 cut-off	.20	.15	.20	.59	.45	.60	.63

It should be pointed out that the increase in component accelerations is not due to the dynamic characteristics of the isolators which are unsuitable for soft soil sites. It is due to tuning and interaction of the frequency of the containment building (primary) with the frequencies of the reactor vessel and reactor core (secondary). It has been pointed out (Sachman & Kelly, 1978) that if the equipment frequency (secondary) is tuned to a structure frequency (primary), there exist two closely spaced frequencies on either side of the tuning frequency around which a band of high amplification appears. A typical result of a tuned equipment - structure system is shown in Fig. 2 in which the equipment was tuned to the third structure frequency, and γ is the mass ratio of the equipment to structure. It can be seen from the Fourier frequency spectrum curve shown in Fig. 3 that tuning and interaction of component and structure frequencies occurred in the present analysis. The two high-amplification regions around the tuned frequency are clearly shown.

As mentioned earlier, the reactor core has a frequency of 16.20 Hz, and the reactor vessel has a frequency of 22.15 Hz. The two frequencies introduced by the use of isolators on a hard soil site are 0.50 Hz of isolator frequency and 65.26 Hz of basemat frequency. They are not in tune with the component frequencies. However, on a soft soil site, the two new frequencies introduced by base isolation are 0.50 Hz of isolator frequency and 21.75 Hz of basemat frequency. The basemat frequency is in tune with the reactor vessel and reactor core. Thus, due to tuning and interaction, the responses of the components, especially the reactor vessel and reactor core, are greatly amplified. It is this amplification which makes the results of component responses unacceptable.

To prove that tuning and interaction of frequencies between the components and lower basemat are the main reason for the occurring of amplifications, we use a detuned system in which the reactor vessel frequency is reduced to about 6.5 Hz by using a softer spring at the reactor vessel support. Actually, detuning of the system frequencies can be achieved in several ways. For example, one can detune the lower basemat frequency. Since the frequency of the lower basemat is related to the surrounding soil, detuning its frequency would involve changing the mass of the basemat and the spring constant of the soil. Changing the soil spring constant is considered to be undesirable because we want to be able to use the LSPB base isolation design under all soil conditions. Thus, detuning is accomplished through the use of a softer spring at the reactor vessel support. The spring constant, K_3 , of the reactor vessel support in the detuned system has a value of 0.112 E7 kips/ft . Therefore, the reactor vessel has a frequency of 6.5 Hz which is not in tune with the lower basemat frequency. The maximum peak accelerations on reactor components of the detuned system are given in Table 1. It can be seen that they are also reduced by a factor of two or more.

CONCLUSIONS

It has been demonstrated that seismic base isolation is a useful device for reducing the structures and components accelerations to below the level of ground accelerations. The results of the LSPB analyses show that the base isolation can reduce horizontal accelerations by a factor of two or more.

The basic principal of base isolation is to shift the fundamental frequencies of the structures and components away from the damaging frequency range of earthquakes, so that seismic loads transmitted to the structures and components would not be amplified. Since base isolators act as a soft layer of material separating the structure with the surrounding soil and allowing a degree of flexibility in horizontal motions, it also introduces two new frequencies in the isolated system. One is the fundamental frequency of the isolators which is usually in the range of 0.20-0.50 Hz and has no effects on structural response. The other is the frequency of the lower basemat which is in the range of 20-60 Hz depending on the soil stiffness and will affect the structural response. If the frequency of the lower basemat is in-tune with one of the component frequencies, tuning and interaction of frequency can occur in the isolated system and the seismic response can be greatly amplified. This has been demonstrated by the results of the in-tuned and detuned analysis. Thus, one should be very careful in the application of base isolation to reactor plant that the frequencies of the components should be detuned from the lower basemat frequency.

REFERENCE

- Sachman, J. L. and Kelly, J. M. (1978). Rational Design Methods for Light Equipment in Structures Subject to Ground Motion. VCB/EER-78/19.

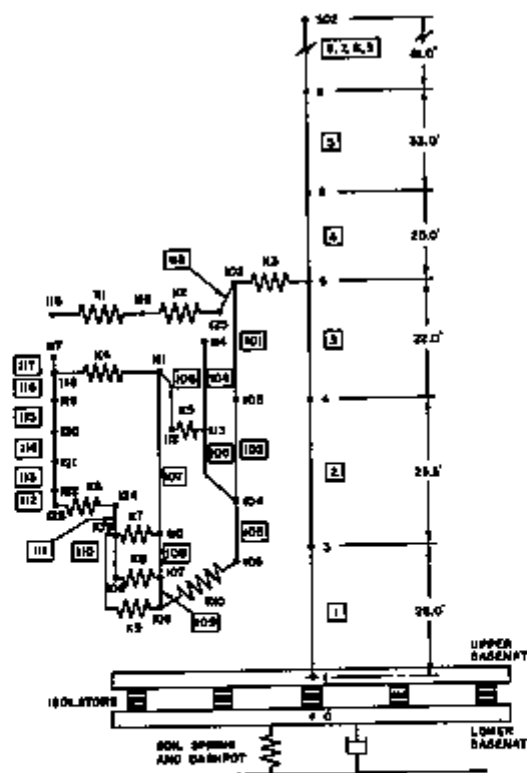


Fig. 1. Mathematical Model of LSPB Plant

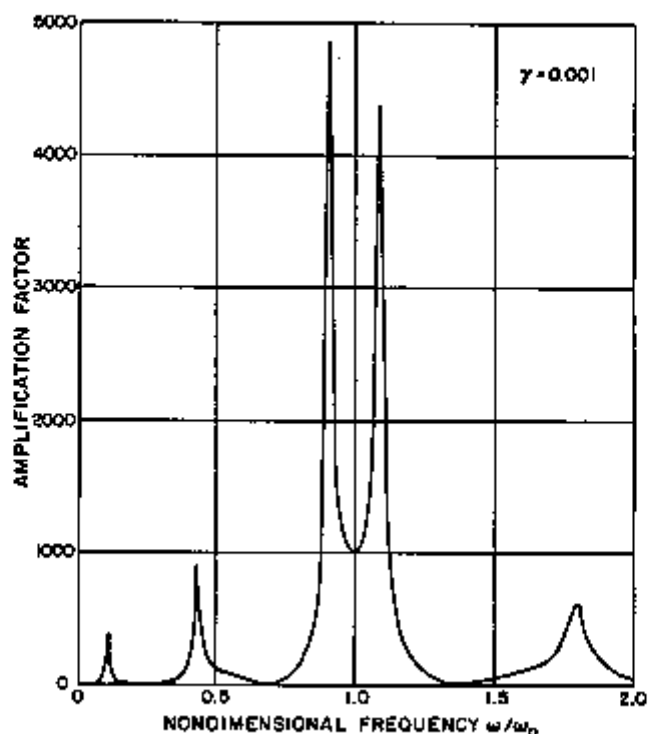


Fig. 2. Amplification Factor for Equipment Acceleration as a Function of Frequency -- Equipment Tuned to Third Structure Frequency

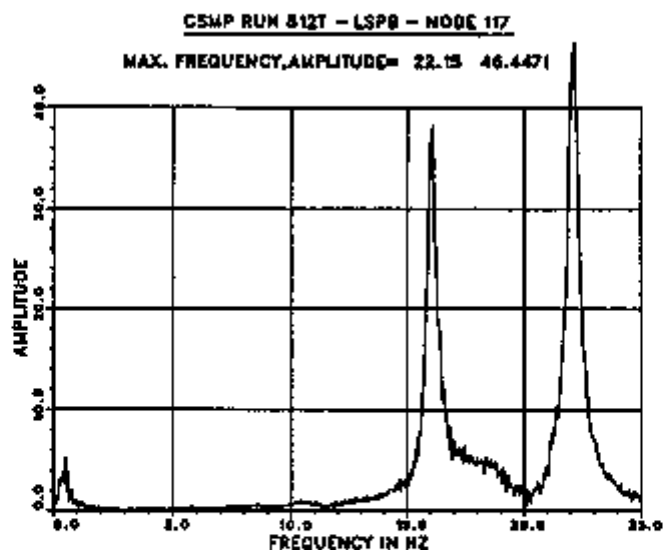


Fig. 3. Acceleration Time History and Frequency Spectrum, Node 117, Case 4, In-time

Seismic Isolation System with Rubber Bearings and Friction Dampers

Yoshio Itoh, Tetsuo Uno, Kiyoshi Nagai
HAZAMA-GUMI, Ltd., Yono, Saitama, Japan

INTRODUCTION

Many proposals for base isolation systems have been provided for reducing the response of buildings subjected to strong earthquake motions. Laminated rubber bearings are considered to be practical supporting devices for a base isolation system. For a base isolation system using laminated rubber bearings, energy absorbing devices to reduce maximum displacement during earthquake are important. Many types of dampers have been developed, for example, hysteretic dampers using steel bars or lead plugs, viscous dampers, and accelerated liquid mass dampers (Kawamata, 1987), and others.

We have developed a new-type friction damper whose friction force can be controlled easily (Uno et al, 1988). The friction damper provides a large capability for energy absorption and high durability for cyclic loading. A base isolated reinforced concrete structure with friction dampers and four laminated rubber bearings supporting 470 tons of weight was constructed for tests and observations to grasp the dynamic characteristics of the system. This report describes the results of alternate loading tests on dampers, free vibration tests on a base isolated structure with friction dampers, and earthquake observation of the structure.

FRICITION DAMPER

Figure 1 shows details of the newly developed friction damper. This damper transforms straight-line motion of the mounting devices into rotational motion of friction plates. Friction plates consist of sintered metal discs and

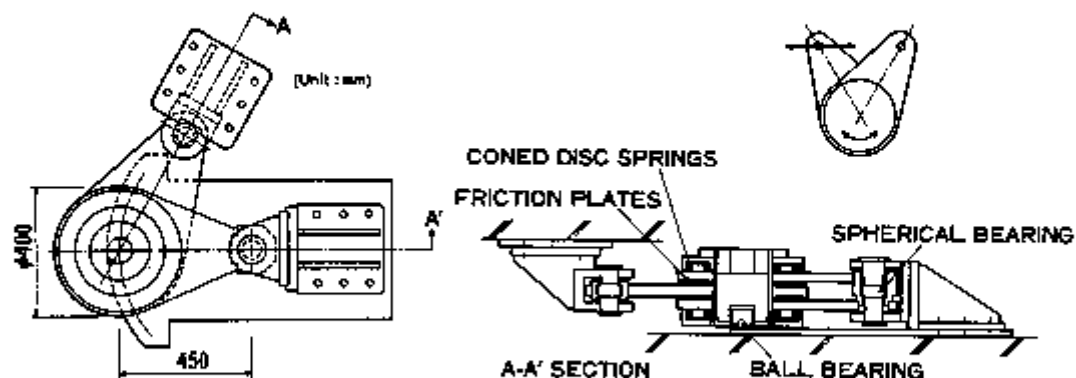


Figure 1 Friction Damper

stainless steel discs. Friction plates are fixed steel plates tightened by screwing a bolt through coned disc springs. The friction force can be controlled by adjusting the tightening torque. The friction damper is supported by the ball bearing, and two spherical bearings connect the damper and the mounting devices fixed on the base and the superstructure; the damper, therefore, does not restrict vertical movement of the superstructure. Friction forces of the damper are independent of velocity of sliding speed, and the friction forces of the damper depend on the direction of loading (Takai et al, 1988). The directional property of the dampers shall be considered in designing actual buildings.

LOADING TESTS ON FRICTION DAMPERS

Figure 2 shows the test apparatus for loading tests on the friction dampers. Figure 3 shows a hysteresis loop of ten cycles at a loading speed of 50mm/sec and a clamping force of 70tonf (surface pressure : 8.8kgf/cm²). The friction force of the damper slightly increased by repeating cycles, however, it is considered that this slight change is not a serious problem in practical use. The temperature of the friction plate rose by 20 C during the test, which was measured by a thermo-couple fixed on a side face of a friction plate. The friction force in Figure 3 is dependent on the displacement, that is caused by change of the distance between the loading axis and the rotational axis of friction plates. The amount of change of friction force can be reduced by making the length between the spherical bearings and the rotational axis of friction plates longer.

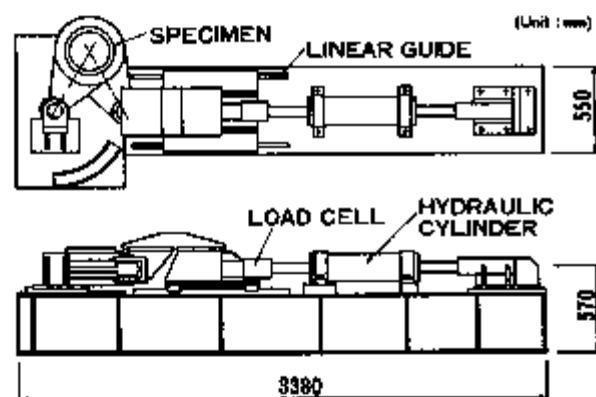


Figure 2 Test Apparatus

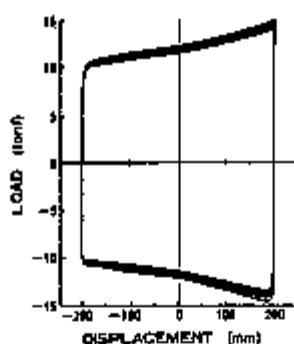


Figure 3 Hysteresis Loop of a Friction Damper

FREE VIBRATION TESTS ON A BASE ISOLATED STRUCTURE

Figure 4 shows the base isolated structure, and Table 1 lists the specifications of the base isolated structure. Dimensions of the superstructure were determined for another experiment that has no connection with this study, and it has columns with a 90cm by 90cm section. The stiffness of the superstructure is stiff enough to consider the system as a single degree of freedom. Four laminated rubber bearings supported the superstructure whose weight was 470 tons. Two free vibration tests were done on the X-direction, one was on the structure without a damper, and the other was on the structure with two dampers which were effective for the X-direction and the friction forces of which were 0.5tonf/unit. Photo 1 shows the friction damper and the laminated rubber bearing installed in the structure. A notched PC steel rod was set between the superstructure and the base. This notched section was cut by pulling the rod with a jack; a free vibration was then generated.

Table 1 Specifications of the Base Isolated Structure

Weight of the superstructure		:	470tonf
Laminated rubber bearing	Thickness of a rubber layer	:	4.0mm
	Thickness of a steel plate	:	2.2mm
	Diameter of a steel plate	:	420mm
	Number of rubber layers	:	38
	Horizontal stiffness	:	0.5tonf/cm
Friction damper	Free vibration test	Friction force	: 0.5tonf/unit 2 units were installed for the X-direction (A and C in Figure 4)
	Earthquake observation	Friction force	: 2.25tonf/unit 4 units were installed for the X,Y-directions (A,B,C and D in Figure 4)

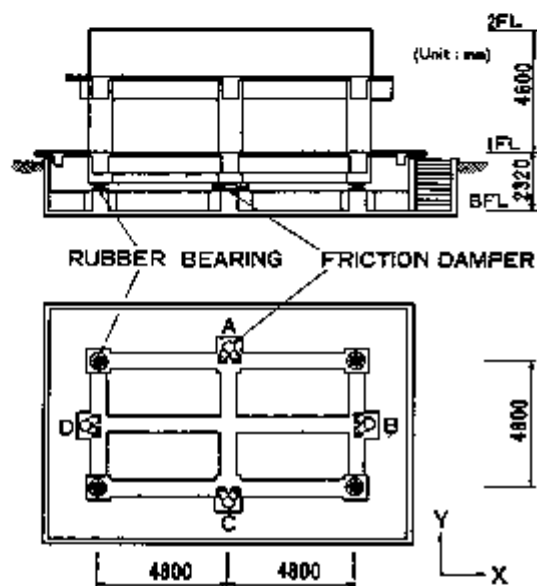


Figure 4 A Base Isolated Structure with Friction Dampers



Photo 1 Isolation Devices installed in the structure

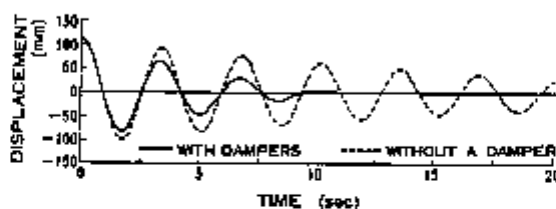


Figure 5 Displacement Time Histories of Free Vibration Tests

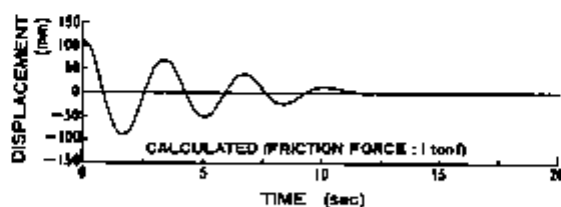


Figure 6 A Calculated Time History (with dampers)

Figure 5 shows the free vibration time histories of the relative displacement between the first floor and the base. The broken line indicates the free vibration waveform without a friction damper, and the solid line indicates the waveform with friction dampers.

Displacement(X) of a free vibration of a single degree of freedom with viscous damping with a damping ratio h and a Coulomb friction force F for each half cycle is

$$X = (X_0 + a)e^{-h\omega t} \left(\cos \sqrt{1-h^2} \omega t + \frac{h}{1-h^2} \sin \sqrt{1-h^2} \omega t \right) - a \quad (1)$$

in which X_0 is the initial displacement, and

$$a = \frac{F \operatorname{sgn}(\dot{X})}{k}, \quad \omega = \sqrt{k/m}$$

where m , k are the mass and the stiffness (Jacobsen et al, 1958). If a system has no damping, the amplitude of displacement decreases monotonously by $2F/k$ each half cycle.

Figure 6 shows a displacement calculated using the above expression. The natural frequency and the damping ratio were obtained from the results of free vibration tests without a friction damper. Figure 7 shows the decrease of amplitude of test results and calculation results using the above expression. Equivalent damping ratios are plotted in the figure, and that of the system increases with the decrease of the displacement amplitude. Experimental values agree well with the calculated result. This shows that friction dampers have worked well.

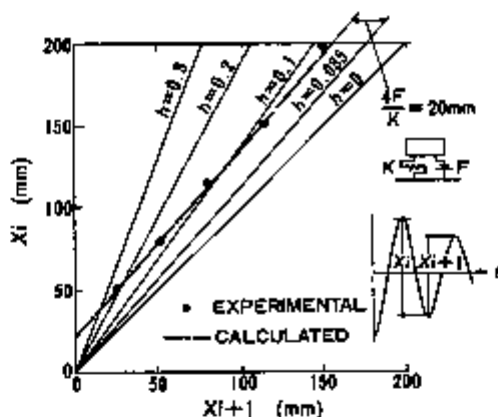


Figure 7 Decrease of Amplitude of a Free Vibration Test

EARTHQUAKE OBSERVATION OF A BASE ISOLATED STRUCTURE

In the base isolated structure, 17 seismometers were installed to observe the acceleration responses of the base, first and second floors, and the relative displacement response between the base and the first floor. Four dampers whose friction forces were 2.25tonf/unit were installed for the X,Y-directions. In several earthquake motions observed, the CHIBAKEN-TOUHOUKI earthquake on December 17, 1987, was comparatively large. The magnitude, the focal depth, and epicentral distance were 6.7, 58km, and 103km respectively.

Figure 8 shows acceleration records of each floor and relative displacement record between the base and the first floor. The maximum acceleration of the base was 31.3gal and that of the superstructure was at the limit of acceleration about 12-15gal. The dotted lines of figure 8 indicate analytical results based on the simple lumped mass system (see Figure 9). In this analysis, initial stiffness of the skeleton curve was obtained from the loading test results of the isolated structure, and the damping ratio of superstructure was 0.02. The

maximum acceleration and relative displacement shown in the analytical results agree with that of the observation records. On comparing observed and analytical waveform, the analytical results agree with the observed records when amplitude was comparatively large, but at the early weak motions, values of analytical results were larger than that of observed records. We consider that this difference was caused by the backlash of the mounting devices and the spherical bearings.

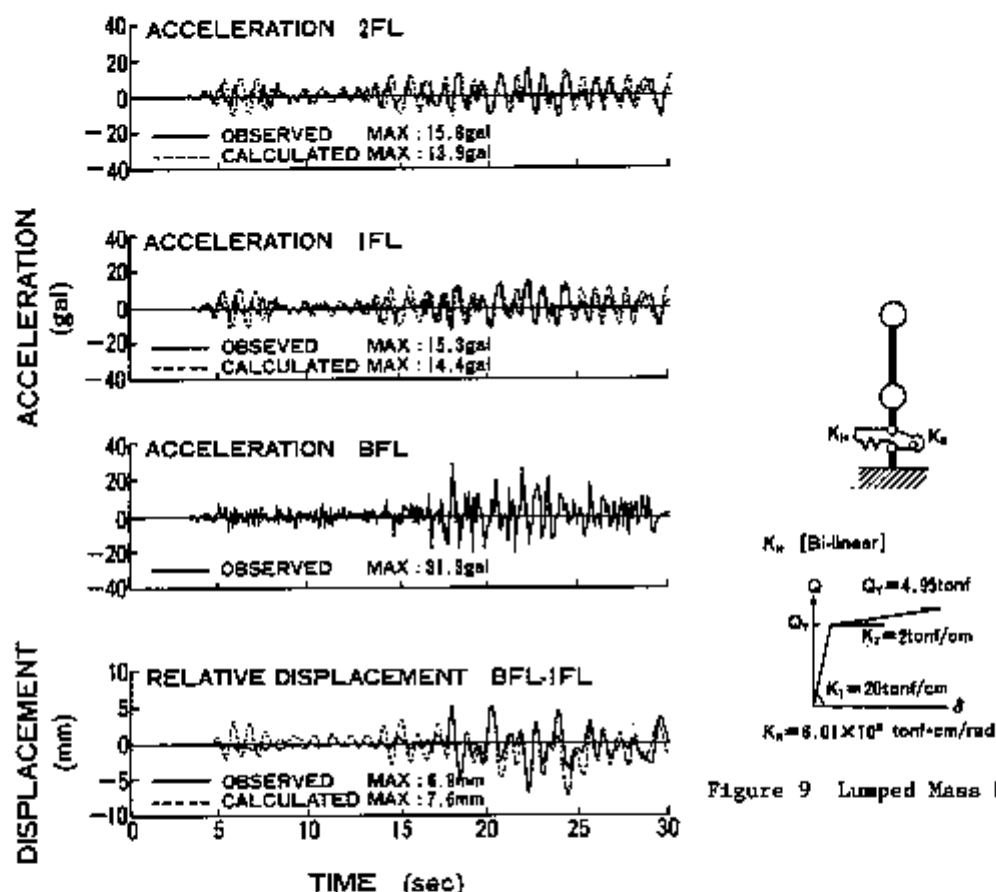


Figure 8 Comparison between Observed Records and Calculated Waveform

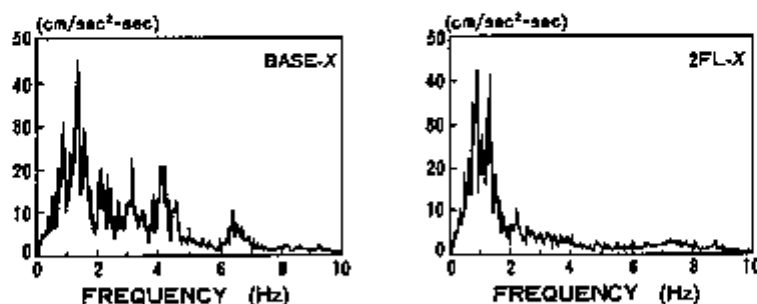


Figure 10 Fourier Spectrum

Figure 10 shows the Fourier spectrum of acceleration records of the base and the second floor. The Fourier spectrum of the superstructure was reduced to between 2Hz and 10Hz.

CONCLUSIONS

The results of loading tests on the newly developed friction dampers shows that it has a stable hysteresis property. Friction forces are slightly increased with repeating cycles, however, it is considered that this slight change is not a serious problem in practical use. From the free vibration tests and earthquake observations of the base isolated structure with laminated rubber bearings and the friction dampers, it was confirmed that this seismic isolation system worked well. The results of the simple simulation analysis agree with the observation records except for early weak motions. The response characteristics of a structure with this system subjected to strong earthquake motions can be estimated easily at the designing stage.

ACKNOWLEDGMENT

This study was carried out as a part of research series of the Experimental Research Committee on the Feasibility of Base Isolation System (Chairman: Prof. Kawamata of the Tohoku Institute of Technology) organized by Japan Association for Building Research Promotion. The authors wish to express their gratitude to the members of this Committee for their valuable suggestions. The support for the loading tests on the dampers provided by Sumitomo Metal Industries, Ltd. is also gratefully acknowledged.

REFERENCES

- Jacobsen, L.S. and Ayre, R.S. (1958). Engineering Vibrations with Application to Structures and Machinery. McGraw-Hill.
- Kawamata, S. (1987). Accelerated Liquid Mass Damper and Principles of Structural Vibration Control. Proc. 9th SMIRT Conf. K2, pp.737-742.
- Takai, H., Uno, T. and Nagai, K. (1988). Study on the Friction Damper as the Device of a Base Isolation System. Proc. 9th WCEE, Tokyo-Kyoto, to be published.
- Uno, T., Takai, H., Asano, K., Itoh, Y. and Nagai, K. (1988). Study on the Feasibility of a Base Isolation System (Part 5, 6, 7 and 8). Summaries of Technical Papers of Annual Meeting AIJ, B, pp.435-442.

Investigation of Base Isolation for Fast Breeder Reactor Building

M. Morishita

Power Reactor and Nuclear Fuel Development Corporation, Ibaraki, Japan

M. Kobatake, K. Ohta, Y. Okada

Shimizu Corporation, Tokyo, Japan

INTRODUCTION

Achievement of great rationalization for seismic-resistant design of equipment system is necessary and indispensable from the viewpoints of economical and structural validity for a fast breeder reactor to be made practical. The method of reducing seismic loads on the building and equipment by application of base isolation may be an effective method, but in application to nuclear facilities, it will become necessary to examine the feasibility to actual design considering the severe seismic design requirements in Japan.

With these considerations as the background, the authors carried out analytical studies from various viewpoints such as restoring force characteristics of base isolation device, influence of input earthquake motion, soil-structure interaction in base-isolated structure, etc. in case of providing base isolation system for a fast breeder reactor building (Morishita et al, 1987). Based on these analytical studies, vibration tests on a base-isolated structure using a triaxial shaking table and simulation analyses of the tests were performed attempting to verify the effectiveness of the base isolation system and appropriateness of the analysis method.

APPLICATION OF BASE ISOLATION TO FBR BUILDING

Construction of base-isolated buildings has been going on actively in Japan in recent years. In many of the buildings, the base isolation system adopted is that of combining laminated natural rubber bearings and various types of dampers, and buildings using lead rubber bearings or high-damping rubber bearings are now gradually increasing. It is considered that a base isolation method for ordinary buildings will be also suitable for a fast breeder reactor building, and in particular, the combination of laminated natural rubber bearings and steel hysteretic dampers, which have clearer mechanical properties and durability, has sufficient examples in ordinary base-isolated buildings, and it is thought possible to apply this system to nuclear facilities which are important structures and particularly requires reliability. The study of the combination of laminated natural rubber bearings and steel hysteretic dampers as the first stage in examining the applicability of base isolation to a fast breeder reactor building is reported in this paper.

In order to select the appropriate restoring force characteristics in case of combining laminated rubber bearings and steel hysteretic dampers, modeling was done by a two-lumped-mass system as shown in Fig.1, with the base isolation device modeled by a bilinear type spring shown in Fig.2, and analyses were made with device characteristics, soil properties, and maximum input acceleration of input waves as parameters. As for base isolation device, laminated rubber bearings were modeled as a linear spring, and steel dampers were modeled as an elasto-plastic spring, then the total device was represented as a bilinear spring synthesizing both elements. The artificial wave (Magnitude;8.4, Epicentral Distance;90km) and the EW component of the Hachinohe Harbor record in Tokachi-oki Earthquake in 1968 shown in Fig.3 were used in the analyses. Base isolation frequency(f)=1.0 Hz, yielding coefficient(β)=0.1, and

second stiffness ratio(α)=0.1 were selected as appropriate restoring force characteristics based on the analysis results.

Next, the case of applying these base isolation device characteristics to the 1,000MWe class loop-type fast breeder reactor building was assumed and earthquake response analyses were performed inputting the artificial wave to the multiple-lumped-mass model shown in Fig.4. Regarding the base-isolated building, analyses were performed for two cases of wall thickness, one was the same as no base isolation and the other was reduced considering the effect of reduction in response due to base isolation. The weight of the superstructure (including the upper base mat) was reduced from about 210,000tons to 140,000tons and the first natural frequency was lowered from 7.71Hz to 4.41Hz by reducing wall thickness. The results of earthquake response analysis (maximum response acceleration and floor response spectra at the support position of the reactor containment vessel) are shown in Fig.5. Through these, it was ascertained that by adopting base isolation, maximum response acceleration and floor response spectra in short period range could be greatly reduced, and that the reduction in wall thickness hardly affected on response values in base-isolated building. The maximum relative displacement of the base isolation device at this time was approximately 6cm, while the ductility factor of the steel damper was approximately 2.5.

DESIGN OF SHAKING TABLE TEST MODEL

With the base isolation device selected as the object, reduced specimens used in shaking table tests were designed and fabricated. The shaking table used was a large-sized triaxial shaking table of load capacity 20tons. And the base-isolated building, which was 16tons in weight, adopted a structure supported by four laminated rubber bearings of 4tons rated load. On the other hand, laminated rubber bearings used for the actual building were designed for 300tons rated load in consideration of the layout of the devices and fabrication, so the reduced model was designed in accordance with the reduction ratio shown in Table I.

The reduced models of the superstructure, laminated rubber bearing, and steel hysteretic damper are shown in Fig.6. The superstructure was designed as a steel frame structure to satisfy the reduction ratio with regard to the primary natural frequency of the superstructure of the fast breeder reactor building reduced in wall thickness. For the laminated rubber bearing, a precise model was designed with regard to rubber thickness, number of rubber layers, etc. in relation to the actual one of 300tons rated load. The steel hysteretic damper was made of three mild steel bars of diameter 13mm used as beams having both ends fixed for 4tons of upper weight, with the system of absorbing vibrational energy by bending deformation in the horizontal direction while absorbing axial deformation by a cylinder at the upper part. The configuration of the reduced model was determined to satisfy the scale effect with regard to stiffness, yielding displacement, etc.

TEST RESULTS

Before the shaking table tests, the static loading tests were performed to grasp the properties of each device element. The hysteresis curves obtained in the tests are shown in Fig.7. As a result of the tests, characteristics approximately according to the design values were obtained regarding elastic stiffness etc. for each element.

Concerning the superstructure of the steel frame, natural frequency and other properties were ascertained by resonance tests using the shaking table. The transfer functions of base-isolated and non base-isolated buildings in the horizontal direction of each story obtained from the white-noise wave excitation tests are shown in Fig.8.

Next, earthquake excitation tests were performed inputting the Tokachi-oki Earthquake wave to the shaking table reducing the time axis in accordance with the reduction ratio. Test cases are shown in Table II and the results (maximum response acceleration and floor response spectra at the top of the building) are shown in Figs.9 to 12. The test results are summarized as follows.

- 1) The comparison of responses by existence of the base isolation device is shown in Fig.9. It was confirmed that the response acceleration at the top of the building was reduced to approximately 1/2 and the short period range of the floor response spectrum was greatly reduced by adoption of the base isolation system.
- 2) The comparison of responses according to input level is shown in Fig.10. The ratio of increase in response acceleration of the building was lower than that of

increase in input level, and the base isolation device acted more effectively the higher the input level. The deformation of the laminated rubber bearing was about 3.6cm and within the allowable limit (7cm) even in inputting triple the original wave.

- 3) The comparison of responses in the EW direction in cases of horizontal one-directional (EW), horizontal two-directional (EW+NS), and horizontal two-directional and vertical (EW+NS+UD) input is shown in Fig.11. The figure shows that the influence of orthogonal input on one-directional maximum response value was small, and that the vertical motion input hardly affected on horizontal responses.
- 4) The comparison of responses in inputting the same wave repeatedly is shown in Fig.12. The difference between the 1st and 2nd excitation tests was almost negligible and it was found that the steel dampers had sufficient durability.

SIMULATION ANALYSES

One-directional simulation analyses for the cases of three input levels were performed with the three-lumped-mass model shown in Fig.13. For the stiffness and damping of the superstructure, properties modifying the design values based on resonance test results were used. Regarding the rubber bearings, the average value obtained by the static loading tests, which was almost same as the design value, were used, and as for the steel dampers, two types of hysteretic models, one was elasto-plastic model used as the design model, and the other was a Ramberg-Osgood (R-O) type set up to conform to the hysteresis curve obtained by static loading tests, were considered. Regarding the characteristics of steel dampers, the comparisons of the test results and the calculated values by the two kinds of analysis models are shown in Fig.14. According to the figures, values of the design model were larger than experimental values regarding damping factor, but by using the Ramberg-Osgood model, it became possible to represent the properties of the actual damper more precisely.

The results of analyses are shown in Figs.15 to 18. According to the figures, it was found possible to simulate the maximum response accelerations and the floor response spectra of the shaking table tests for each input level by modeling steel dampers by R-O model and that the analysis results by the design model were a little larger than the test results especially in large input level, but approximate response characteristics of the building could be sufficiently evaluated by each model.

CONCLUSIONS

Analytical and experimental studies were made for application of a base isolation system to a fast breeder reactor building, and the basic properties and effectiveness of laminated rubber bearings and steel hysteretic dampers proposed as one of the base isolation systems were ascertained. Then by the simulation analyses, the appropriateness of the analysis method was verified. It is planned that the shaking table tests and simulation analyses using the superstructure in this paper with high-damping rubber bearings or lead rubber bearings are to be performed hereafter.

ACKNOWLEDGEMENTS

This paper is a part of the results of research carried out by Shimizu Corporation under contract to the Power Reactor and Nuclear Fuel Development Corporation, and the authors wish to express their appreciation to the many persons who participated in the study and provided much valuable advice.

REFERENCES

- M. Morishita, T. Kuroda, M. Kobatake, Y. Okada (1987). Investigation of Base Isolation for Fast Breeder Reactor (Part 1-3). Annual Meeting of Atomic Energy Society of Japan, Nagoya
- M. Morishita, M. Kobatake, Y. Okada, S. Aoki (1987). Investigation of Base Isolation for Fast Breeder Reactor (Part 4-6). Fall Meeting of Atomic Energy Society of Japan, Sapporo
- M. Morishita, M. Kobatake, K. Ohta, Y. Okada (1988). Seismic Base Isolation Tests of Fast Breeder Reactor Building (Part 1-3). Fall Meeting of Atomic Energy Society of Japan, Kobe

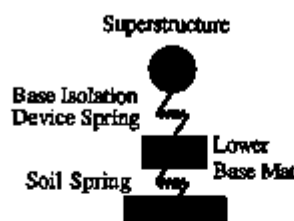


Fig.1 Analysis Model of Parametric Study

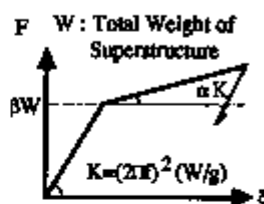


Fig.2 Hysteresis of Base Isolation Device

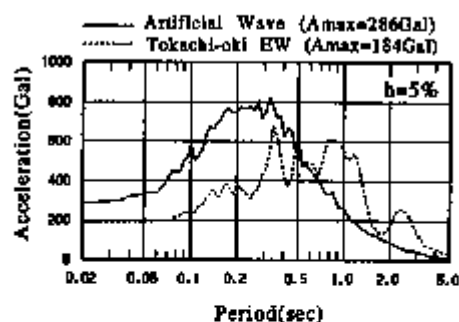


Fig.3 Acceleration Response Spectra of Input Earthquake Motions

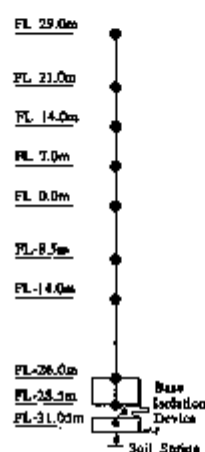
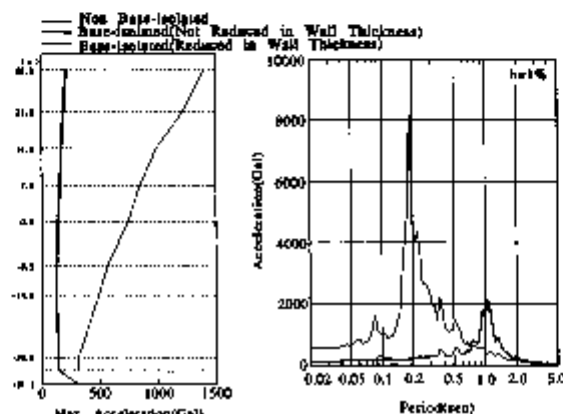


Fig.4 Analysis Model



(a) Max. Response Acceleration

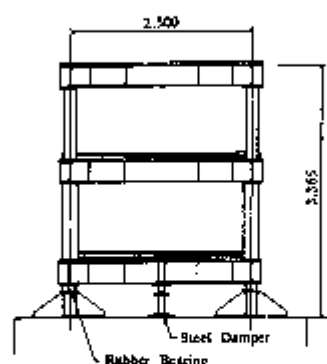
(b) Floor Response Spectra

Table I. Reduction Ratio from the Actual Building

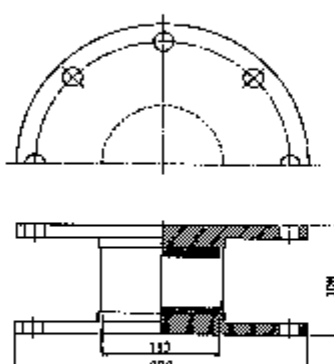
	Reduction Ratio
Weight	$1/\lambda^2$
Length	$1/\lambda$
Density	1.0
Frequency	λ
Stiffness	$1/\lambda$

$$\lambda^2 = 300/4 = 75 = 8.66$$

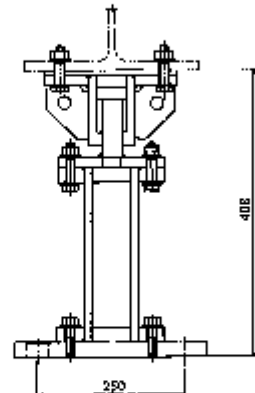
Fig.5 Results of Response Analysis



(a) Superstructure

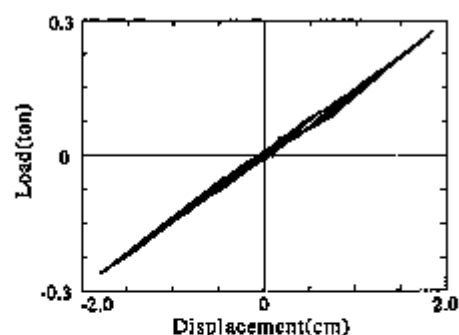


(b) Laminated Rubber Bearing

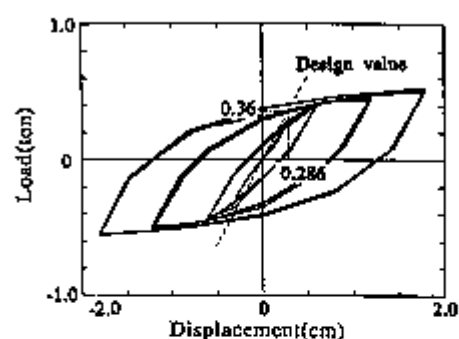


(c) Steel Hysteretic Damper

Fig.6 Specimens of Base-isolated Structure Model



(a) Laminated Rubber Bearing



(b) Steel Hysteretic Damper

Fig.7 Hysteresis Loop of Device

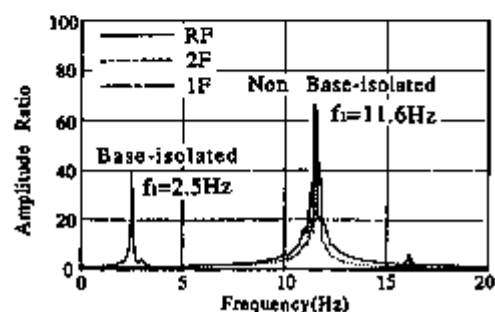
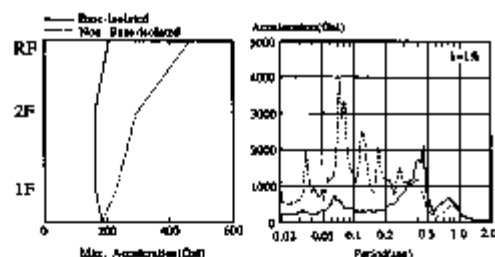


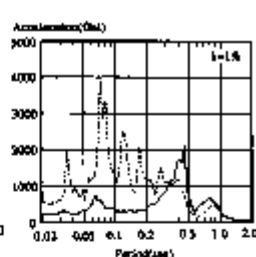
Fig.8 Horizontal Transfer Function

Table II. Test Cases of Earthquake Excitation

Model	Input	Max. Acc. (Gal)	Input Direction etc.
Non Base-isolated		184	EW
Base-isolated	A	184	EW
	B	368	EW (2.0 X original wave)
	C	552	EW (3.0 X original wave)
	D	184	EW+NS (2-D input)
	E	184	EW+NS+UD (3-D input)
	F	184	EW (2nd excitation of A)

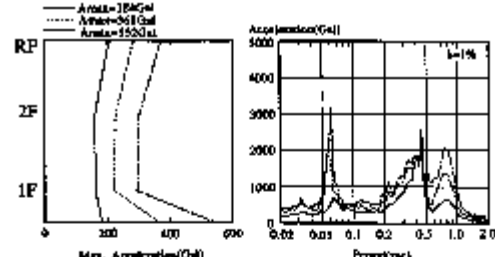


(a) Max. Response

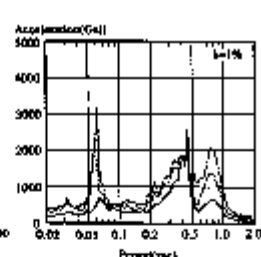


(b) Floor Response Spectra

Fig.9 Comparison of Base-isolated and Non Base-isolated

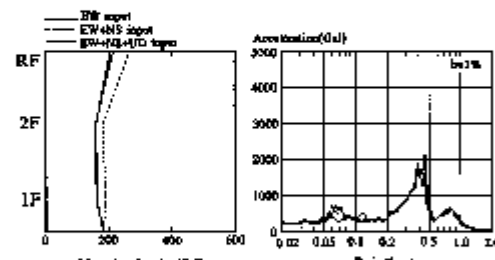


(a) Max. Response

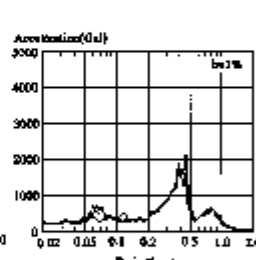


(b) Floor Response Spectra

Fig.10 Comparison by Maximum Input Acceleration

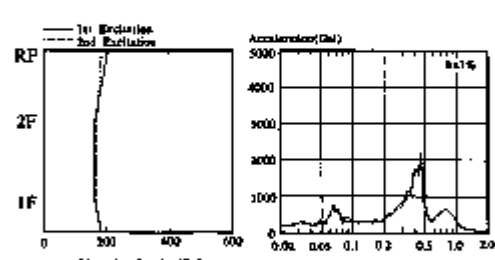


(a) Max. Response

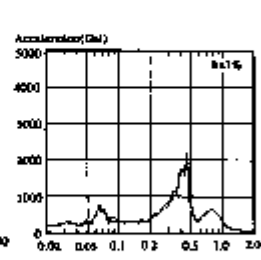


(b) Floor Response Spectra

Fig.11 Comparison by Input Direction

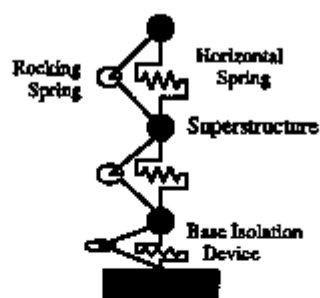


(a) Max. Response

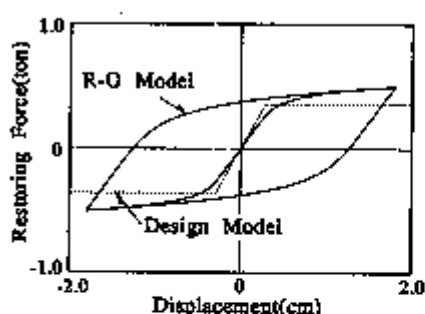


(b) Floor Response Spectra

Fig.12 Comparison of 1st and 2nd Excitation



(a) Base-isolated Building



(b) Hysteresis of Steel Damper

Fig.13 Simulation Analysis Model

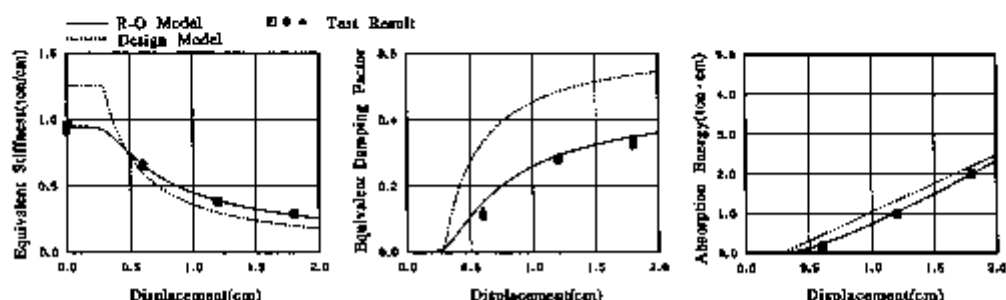


Fig.14 Characteristics of Steel Damper

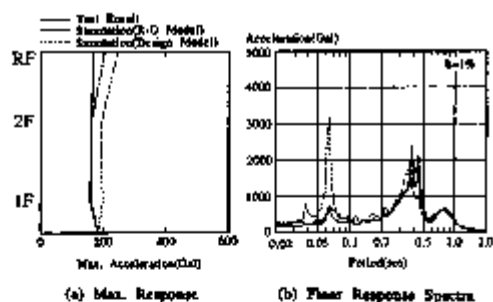


Fig.15 Results of Simulation Analysis
(Input $A_{max}=184\text{Gal}$)

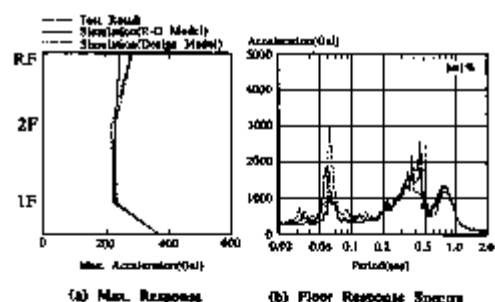


Fig.16 Results of Simulation Analysis
(Input $A_{max}=368\text{Gal}$)

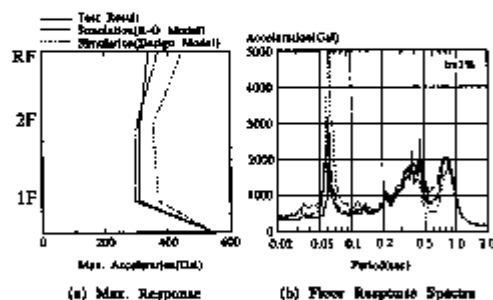


Fig.17 Results of Simulation Analysis
(Input $A_{max}=552\text{Gal}$)

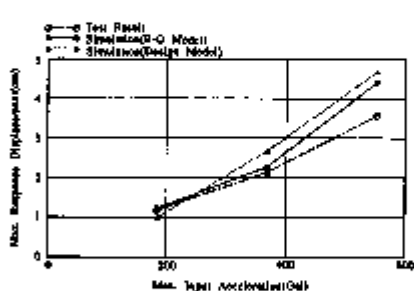


Fig.18 Maximum Displacement
of Base Isolation Device

Proof Test of Base-Isolated Building Using High Damping Rubber Bearing

Masaaki Saruta, Hiroyuki Watanabe
Shimizu Corporation, Tokyo, Japan

Masanori Izumi
Tohoku University, Sendai, Japan

INTRODUCTION

Growing expectations have recently arisen concerning the base isolation system, and as a consequence, more than twenty base-isolated buildings have been built in Japan. The present research is intended to prove the effectiveness of the base isolation system by on-site experiments and the observation of actual earthquakes for full-sized structure.

We used a system consisting of six rubber bearings and twelve oil dampers. After several experiments, we conducted the earthquake observations. Totally, thirty earthquakes were recorded from June 1986 to July 1988. From the results of these tests and the earthquake observations, the base isolation system was provided to be very effective in reducing the response acceleration (Tamura et al., 1987).

The system was replaced with the high damping rubber bearings in July 1987. In this paper, we report the dynamic loading test and the earthquake observation of these high damping rubber bearings.

TEST BUILDINGS

Two test buildings, one a base-isolated and the other an ordinary structure were constructed side by side in a yard of Tohoku University. The buildings are full-sized three-story reinforced concrete structures and the dimensions and construction method of the superstructures were exactly the same for both buildings.

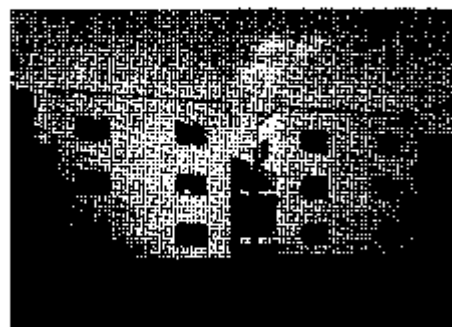


Fig. 1 General view of the test buildings

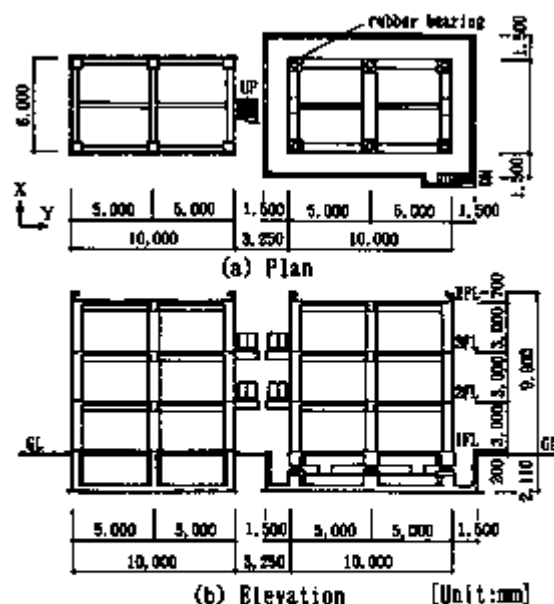


Fig. 2 Plan and elevation of test buildings

The buildings were constructed as frame structures with outer walls made of autoclaved light weight concrete. The plane dimensions of the buildings are 6 by 10 meters, and the total combined floor area is 180m². The buildings were completed in May 1986.

The general view of the buildings is shown Fig. 1. The building on the right is the base-isolated building and the one on the left is the ordinary one. The plan and elevation of the test buildings are shown in Fig. 2, with the installation of the high damping rubber bearings indicated.

The details of the location of the test buildings and soil profiles are discussed in the reference.

BASE ISOLATION ELEMENTS

The high damping rubber bearing functions as both bearing and damper. The damping of the bearing is enhanced by additives to the rubber compound. The configuration of the bearings is the same as that of the former normal bearings. The bearing consists of 18 layers of 6.7-mm thick rubber which diameter is 435 mm, 17 steel plates of 3.0-mm thickness, and 24-mm thick top and bottom flange plates. The dimensions of the bearings used in the test buildings are shown in Fig. 3. These bearings are designed to have the same dynamic properties as the former system involving the normal bearings and oil dampers. The equivalent horizontal stiffness at a 10-cm displacement is 640 kgf/cm, and the equivalent hysteresis damping coefficient is 0.15.

EXPERIMENT

Before setting the rubber bearings under the building, the static loading test was carried out at the laboratory. After installation, a forced vibration test was performed.

Loading test

The horizontal loading test was conducted under the constant vertical load of 50 tf. The load-displacement relation is shown in Fig. 4. The average of the equivalent horizontal stiffness and the equivalent hysteresis damping at each displacement are listed in Table 1. The average of the vertical stiffness under compressive loads of 50 tf \pm 15 tf is 910 tf/cm. The horizontal load-displacement relation of the high damping rubber bearing have

Table 1 Equivalent Stiffness and Hysteresis Damping

Displacement (cm)	1	3	5	10	15	20
Horizontal Stiffness (kgf/cm)	2060	1110	823	569	465	409
Hysteresis Damping Ratio (%)	18	15	13	13	12	12

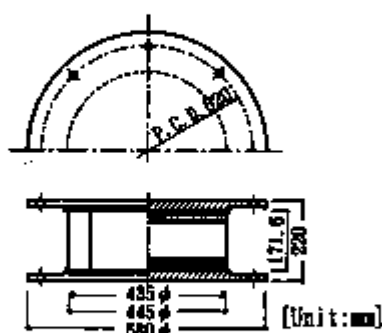


Fig. 3 Dimensions of high damping rubber bearing

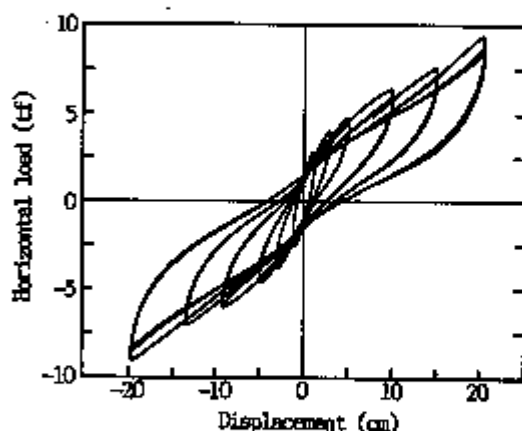


Fig. 4 Hysteresis Loop

the property of nonlinearity. The horizontal stiffness at 1-cm was approximately 4 times larger than the stiffness at 10-cm. The damping coefficient decreases according to the increase of the displacement. The average of the equivalent horizontal stiffness and the equivalent hysteresis damping at a 10-cm deformation are 569 kgf/cm and 0.13. These values are slightly lower than the designed values.

Vibration test

A vibration exciter was installed at the center of the roof slab to apply sinusoidal forces horizontally to each building.

Figure 5 shows the change in resonance curves of the base-isolated building in accordance with the levels of eccentric moment of the exciter for the X-direction. As is evident, the resonant frequency clearly decreases with the increase in loading force, i.e., the amplitude of horizontal displacement.

Figure 6 shows the difference in resonance curves caused by increasing and decreasing of sweep frequency. The resonance frequency is low in the case of the decreasing of sweep frequency. As is clear, these results depend on the nonlinearity of the high damping rubber bearing.

The natural frequencies and the damping ratios for both directions obtained experimentally are summarized in Table 2. These values were affected by the amplitude of vibration. The natural frequency decreased, but the damping ratio increased with the increase of the displacement. The damping of at a 10-kgfm eccentric moment is only 1/3 to the damping of at a 200-kgfm. Both values of the natural frequency and the damping ratio for the Y-direction of 1st vibration mode agreed with those for the X-direction.

Table 2 Natural Frequency and Damping Ratio

Direction	X							Y	
Vibration Mode	1 st				2 nd			1st	2nd
Eccentric Moment (kgfm)	10	20	100	200	2	4	10	200	10
Amplitude (mm)	0.38	0.60	1.78	3.27	0.18	0.38	1.08	3.35	0.87
Natural Frequency (Hz)	1.68	1.57	1.33	1.21	5.80	5.69	5.50	1.23	6.45
Damping Ratio (%)	5.1	6.4	10.9	11.9	2.0	2.0	1.8	11.6	2.2

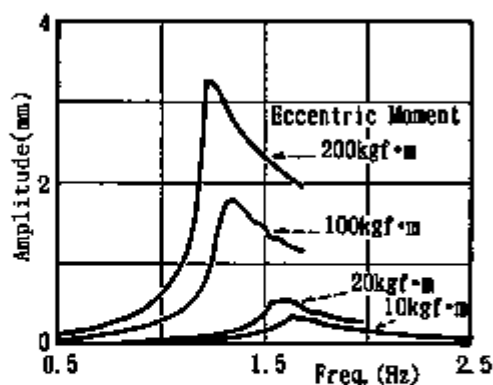


Fig. 5 Resonance curve of different eccentric moment

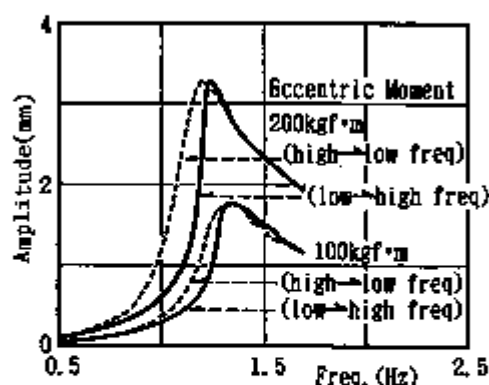


Fig. 6 Resonance curve of different sweep direction

EARTHQUAKE OBSERVATION

Accelerometer setup

At the start of the observation, the accelerations of eleven points were observed. The accelerometers were in the hard soil stratum (GL-27m), on the surface of the surrounding ground, on the base slab of the base-isolated building, and at the first floor and the roof of each building. Total observations were 27 components of earthquake motion, including 20 horizontal and seven vertical. Five accelerometers were added in March 1988, in order to observe vertical components on the base-slab of the base-isolated building and on the 1st floor of each building.

Recorded earthquake data

Seventeen earthquakes were recorded from August 15, 1987 to October 19, 1988. Nine earthquakes occurred off Fukushima Prefecture. Five of them were recorded more than an acceleration of 5 Gal on the ground surface.

The largest acceleration recorded on the ground surface was 27 Gal, and the corresponding peak accelerations at the roofs of buildings were 114 Gal for the ordinary building and the 43 Gal for the base-isolated.

Distribution of maximum accelerations

The maximum accelerations of all components during the earthquake on October 4, 1987 (magnitude = 5.8, epicentral distance = 128 km, focal depth = 51 km) are shown in Fig. 7.

The maximum accelerations on the roof of the ordinary building were 139 Gal in the X-direction and 114 Gal in the Y-direction. Those of the isolated building, however, were only 27 Gal and 43 Gal. The reduction of response acceleration is from 1/5 to 1/3. During the other earthquakes as well, the accelerations of the base-isolated buildings were also reduced.

The accelerograms at several points are shown in Fig. 8 for the X-direction and Fig. 9 for the Y-direction. The accelerograms recorded in the base-isolated building proved that the period of vibration became longer.

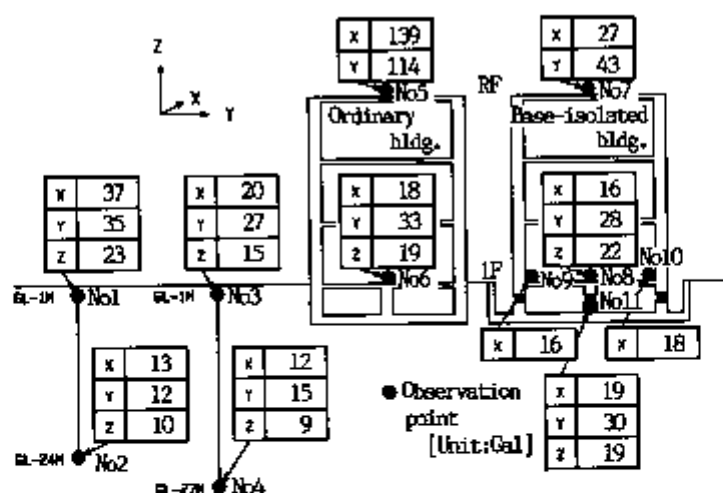


Fig. 7 Maximum acceleration distribution of the earthquake on October 4, 1987

Amplification Factor

The amplification factor of the building(A.F.) is defined as the ratio of the maximum acceleration on the roof to the maximum one on the ground surface. The amplification factors of the both buildings in earthquakes are shown in Fig. 10 for the X-direction and Fig. 11 for the Y-direction.

The solid and dotted lines in figures respectively show the regression for the isolated building and for the ordinary one. The dotted line is almost flat or a little inclined, whereas the solid line presents a clear the tendency to decrease along the X-axis indicating the maximum acceleration on the ground surface. In a case of larger earthquakes, the high damping rubber bearings are distinctly more effective in reducing the response acceleration.

Analysis of Observed Motions

The relative displacement of the base-isolated element was calculated by the integration of the relative acceleration between the base-slab and the 1st floor. The relative displacement by the integration is shown in Fig. 12 for five earthquakes, of which, the maximum acceleration on the ground surface was more than 5 Gal. The maximum value of them is only about 3 mm. Figure 13 shows the shear force - relative displacement relation for the earthquake on October 4, 1987 in the Y-direction. The equivalent stiffness decreases with the increase in displacement.

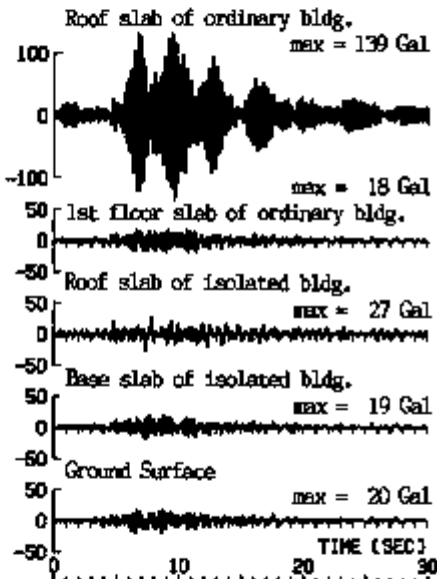


Fig. 8 Time history for X-direction of the earthquake on October 4, 1987

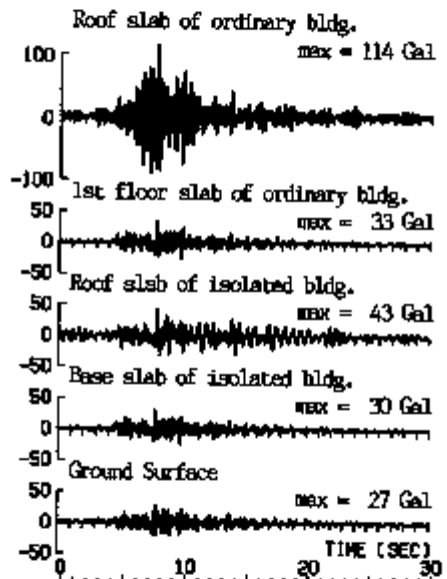


Fig. 9 Time history for Y-direction of the earthquake on October 4, 1987

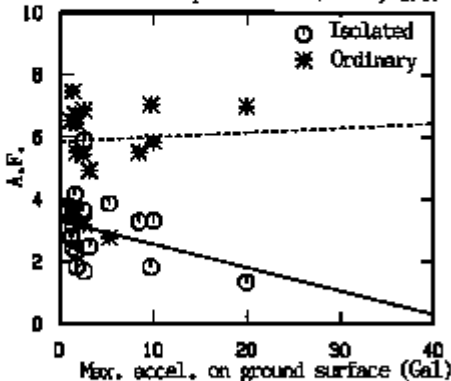


Fig. 10 Amplification factor in X-direction

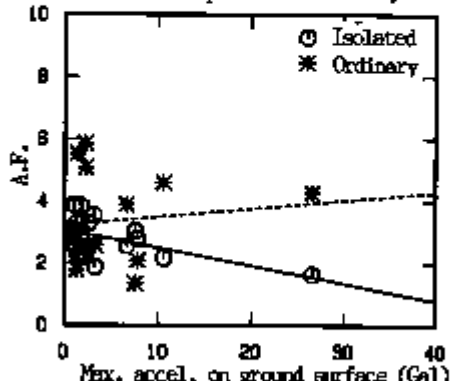


Fig. 11 Amplification factor in Y-direction

Figure 14 presents the Fourier spectra of the ground motion and the earthquake response at the roof of each building for the earthquake on October 4, 1987 in the Y-direction. The fundamental frequency of the isolated building is estimated to be within from 1.5 Hz to 2 Hz, and that of the ordinary one is 4.3 Hz.

CONCLUSION

From these results of the various tests and earthquake observations, following conclusions can be made.

- (1) The nonlinearity of the high damping rubber bearing for the horizontal stiffness is revealed at a small displacement.
- (2) The damping ratio of the bearing depends on the horizontal displacement. Especially, in the region of a small displacement under a 3-mm, the damping is only 1/3 of the design value.
- (3) The amplification factor of the base-isolated building was very small compared to that of the ordinary one.
- (4) The amplification factor of the base-isolated building has a tendency to decrease with the maximum acceleration on the ground surface.

ACKNOWLEDGMENT

This research was carried out as a joint research project of Tohoku University and Shimizu Corporation. The authors would like to express our appreciation to Shoji Hayashi and Keiichi Okada for their valuable help with the experiments, to Haruhiko Yokota and Kazuo Tamura for their helpful discussions, and to Bridgestone Corporation for providing the data of the high damping rubber bearings.

REFERENCE

Tamura K., Yamahara H. and Izumi M. "PROOF TEST OF THE BASE-ISOLATED BUILDING USING FULL-SIZED MODEL", Proc. Seismic, Vibration and Shock Isolation - 1988, ASME, PVP-Vol.147, pp.21-28

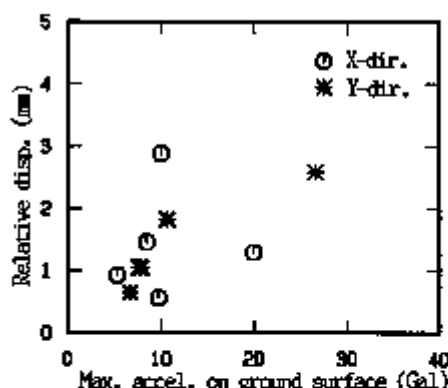


Fig. 12 Relative displacement by integration

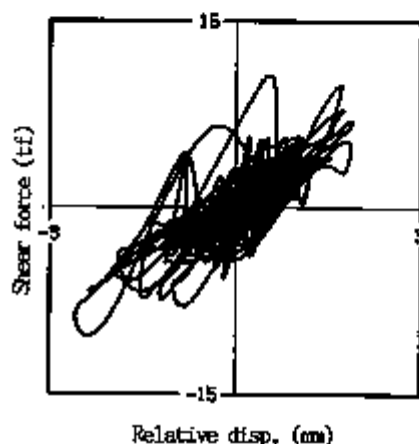


Fig. 13 Load-displacement relationship of isolation element

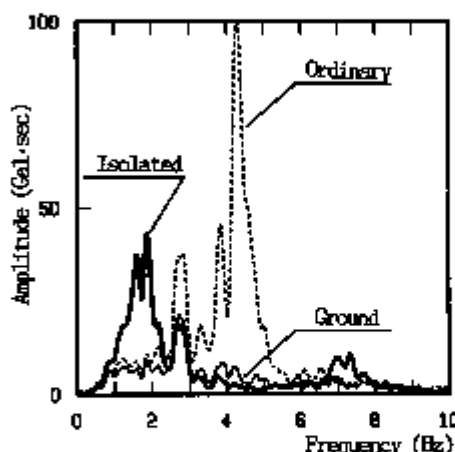


Fig. 14 Fourier amplitude for Y-direction of the earthquake on October 4, 1987

Reliability Analysis for Seismically Isolated FBR System

K. Hirata

Central Research Institute of Electric Power Industry, Abiko, Japan

Y. Kobayashi

Taisei Corporation, Tokyo, Japan

H. Kameda

Kyoto University, Kyoto, Japan

H. Shiojiri

Central Research Institute of Electric Power Industry, Abiko, Japan

INTRODUCTION

In recent years base isolation system has been applied for important structures such as those of nuclear facilities, and introducing the isolation system to FBR system to be constructed in seismically active region is planned. And for those structures evaluation of reliability for earthquakes is emerging as a matter of concern. For non-isolated LWR systems extensive studies have been conducted and the methodology regarding to seismic PSA has been developed so far[1][2]. However, for the isolated structures with natural period considerably longer than that of non-isolated structure and isolators behaving inelastically under design earthquake motion, the method developed for non-isolated structure can not be applied directly.

In this paper a simplified method for the evaluation of fragility of the isolated structure is presented, and the result of fragility analysis is shown.

Studies presented in this paper forms a part of a research project "Aseismic Proving Test of Seismic Isolation System for Fast Breeder Reactor(FY 1987-1993)" sponsored by Ministry of International Trade and Industry of Japan. Outline of the project is presented in Ref. [3].

SELECTION OF INPUT PARAMETER IN FRAGILITY ANALYSIS

In the seismic PSA of non-isolated structure, usually probability of failure is expressed as a function of peak ground acceleration A_p which is considered as the "best" parameter in describing ground motion intensity-response relationship. However, for the isolated structure of which the natural period is 1.0-2.0 second, and behaves inelastically under design earthquake motion, A_p might no more be the best parameter, and peak ground velocity V_p might be the best parameter. To verify this we conducted response analyses of isolated FBR building(Fig. 1) using 12 observed earthquake records and 3 artificial earthquakes, where restoring characteristics of the isolator is modeled with bi-linear model(Fig. 2). Natural periods of the isolated building corresponding to the first and the second stiffness K_1 , K_2 of the bi-linear spring are 1.0 sec. and 2.0 sec., and the yield displacement δ_y of the bi-linear spring is 1.24 cm.

Observed earthquake records are scaled to 10 and 20 times as large as the original ones so that the isolator will deform beyond its elastic limit and the ductility factor (defined as the ratio of maximum displacement to yield displacement) will be considerably large. Maximum acceleration of the artificial earthquake waves is scaled to several levels, and 35 earthquake waves with different peak acceleration are used in all. The ratios of A_p to V_p of the input motion range from 4.1 to 25.6. For the artificial earthquakes which are rich in long period components, the ratio A_p/V_p is smaller than

that of the observed ones(Fig. 3).

Result of non-linear response analyses shows the maximum displacement of the isolator has stronger correlation with V_p than with A_p (Figs. 4 and 5). Linear relationship between the maximum acceleration at the support level of the reactor vessel(Fig. 1) and the maximum displacement of the isolator(Fig. 6) indicates other response quantity such as inter-story shear force also has strong correlation with the peak ground velocity V_p (Fig. 7).

Description of Method

In the estimation of reliability for elasto-plastically behaving structure under strong earthquake motion, a method using reliability index is proposed by Kanda[4][5]. Here the method is applied in the estimation of the fragility of the isolated structure. Outline of the method is as follows.

Regression Analysis between Input Motion Intensity and Response

Using the results of non-linear response analyses, relationship between input motion intensity and the response is evaluated via regression analysis(e.g., linear regression). And in this case usually the response is converted to "equivalent linear response" which is defined as the response of linear system with the same potential energy as that of the elasto-plastic system(Fig. 2).

Estimation of Reliability Index under Given Input Motion Intensity

Safety margin of the member of the structure S_f which is defined as the ratio of the ultimate strength to the response is given as

$$S_f = R^*/Q^* \quad [1]$$

where R^* and Q^* are the ultimate capacity and the response, and $*$ stands for the equivalent linear response or equivalent linear capacity.

Assuming that R^* and Q^* follow log-normal distribution, reliability index β of the member is given as

$$\begin{aligned} \beta &= E[\ln R^*/Q^*(e)]/D[\ln R^*/Q^*(e)] \\ &= E[\ln R^* - \ln Q^*(e)]/\sqrt{D^2[\ln R^*] + D^2[\ln Q^*(e)]} \end{aligned} \quad [2]$$

where $E[\cdot]$ and $D[\cdot]$ mean the expectation and the standard deviation. From the assumption of log-normal distribution,

$$E[\ln R^*] = \ln E[R^*] - (1/2)D^2[\ln R^*], \quad D^2[\ln R^*] = \ln(1 + \delta_{R^*}^2) \quad [3]$$

where $\delta_{R^*}^2$ is c.o.v. of R^* . Equivalent response Q^* is expressed as a function of intensity of input earthquake e (e.g., peak ground velocity V_p or peak ground acceleration A_p) by regression analysis (Figs. 7 and 8) and the reliability index is given as a function of e . Probability of failure P_f of the member is given using the reliability index β as

$$P_f(e) = 1 - \Phi(\beta(e)) \quad [4]$$

where Φ is the normal distribution function. Using Eq.[4], fragility of the member of the structure is evaluated.

Confidence Interval of Probability of Failure

Functional relation between the response Q^* and the intensity of earthquake motion is given by the regression analyses of sample of size n which is the number of earthquake waves used in the response analyses, where the regression curve is considered to give the best estimate. Scatter of Q^* around the regression curve (Figs. 7 and 8) shows uncertainty of response for specified ground motion intensity, and the uncertainty is evaluated by confidence interval.

Suppose that the functional relation between Q^* and e (intensity of earthquake ground motion) is linear as

$$Q^* = \alpha_0 + \alpha_1 e \quad [5]$$

then the estimation interval of Q^* for specified intensity of input motion e , with the confidence interval of $100(1-\alpha)\%$ is given as [6]

$$\hat{\alpha}_0 + \hat{\alpha}_1 e \pm t(n-2, \alpha) \sqrt{[1 + 1/n + (\bar{e} - e)^2/S_{..}]/N_{..}} \quad [6]$$

where $\hat{\alpha}_0$ and $\hat{\alpha}_1$ are the least square estimates of α_0 and α_1 , $t(n-2, \alpha)$ is the α percentile value of the t -distribution with $(n-2)$ degrees of freedom, \bar{e} is the mean of intensity of each input earthquake motion e_i . See is given by

$$S_{..} = \sum (e_i - \bar{e})^2 \quad [7]$$

And V_e is the unbiased estimate of variance of error given as

$$V_e = S_{..}/(n-2) \quad [8]$$

and S_e is the sum of the squared errors given as

$$S_e = \sum (Q_i^* - (\hat{\alpha}_0 + \hat{\alpha}_1 e_i))^2 \quad [9]$$

Estimation of Fragility

Modeling of the Isolated Structure

Reference FBR building for the fragility estimation is modeled with 17-lumped mass system (Fig. 1). Restoring characteristics of the isolator is given by bi-linear model and the ultimate displacement of the isolator is 1.0m. The skeleton curve for the member of the upper structure is modeled with tri-linear curve. And the result of response analyses shown in "SELECTION OF INPUT PARAMETER IN FRAGILITY ANALYSIS" is made use of in the estimation of fragility.

Although within the level of the input earthquake used in the analyses, upper structure behaved elastically, the skeleton curve is made use of in the assessment of the ultimate strength of the member in terms of the "equivalent elastic ultimate strength".

Result of Estimation

Linear regression analysis between peak ground velocity V_p and response of each member is conducted and the functional relation is evaluated (Figs. 7 and 8). The fragility estimated using Eqs. [2] through [4] and these functional relations gives median fragility (indicating 50% non-exceedance probability of failure) of the member. And the upper and lower limit of the confidence interval of the fragility is estimated by Eq. [6]. The confidence interval is 90% and the upper and the lower limits correspond to 95% and 5% non-exceedance probability of failure. Probability of failure for the upper structure is smaller than that for the isolation element (Figs 9 and 10), which is explained

from the concentration of earthquake energy to the isolators indicating that the reliability of the isolation system is largely dependent on that of the isolator. As an example of sensitivity study, fragility of the isolator is estimated with median value of the ultimate displacement D_r as a parameter[Fig. 11]. Using the method proposed in this paper such parametric survey can easily be conducted once a set of response analyses are made.

CONCLUSIONS

Conclusions of this paper are summarized as follows.

- (a) Response of the isolated reactor building has strong correlation with peak ground velocity V_p , and the fragility of the isolated building is proper to be estimated in terms of V_p rather than peak ground acceleration A_p .
- (b) Estimation method of reliability for non-linear structure using reliability index is applied to the estimation of the fragility of the isolated FBR building and the reliability of the isolator proved to be influential in the total reliability of the isolated FBR system.

REFERENCES

- [1] PRA PROCEDURES GUIDE, NUREG/CR-2300, vol.1,2
- [2] R. P. Kennedy, C. A. Cornell, et al., Probabilistic Safety Study of an Existing Nuclear Power Plant, Nuclear Eng. and Design, 59, pp.315-338, 1980
- [3] Y. Sawada, et al., Seismic Isolation Test Program, Trans. 10th SMIRT, Div. K 1989
- [4] J. Kanda, Probability-based Seismic Margin Index for Inelastic Members of Reactor Buildings, Trans. 8th SMIRT, MK2/5, pp.353-359, 1985
- [5] J. Kanda, R. Iwasaki, and H. Sunohara, Stochastic Evaluation of Inelastic Seismic Response of a Simplified Reactor Building Model, Trans. 9th SMIRT, K1, pp. 403-408, 1987
- [6] R. Kume and Y. Iizuka, Regression Analysis(In Japanese), Iwanami, 1987

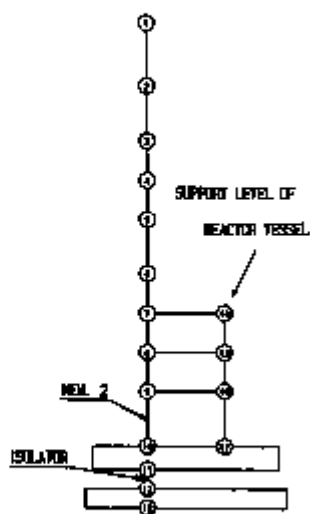


FIG. 1 LUMPED MASS MODEL FOR FBR BUILDING

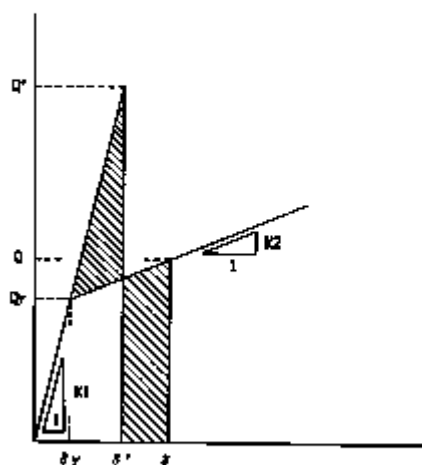


FIG. 2 BI-LINEAR MODEL FOR ISOLATOR AND CONCEPT OF EQUIVALENT LINEAR RESPONSE

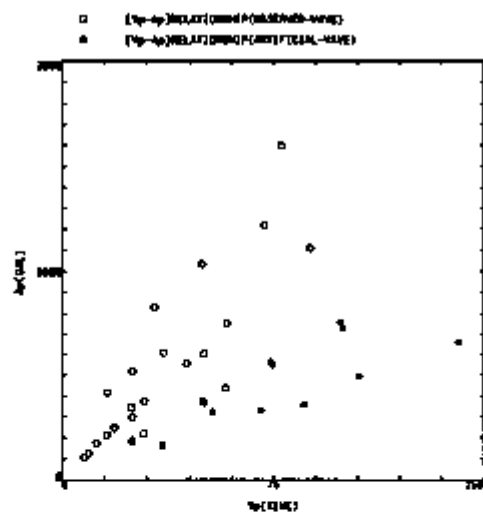


FIG. 3 Y_p vs A_p OF EARTHQ. WAVES

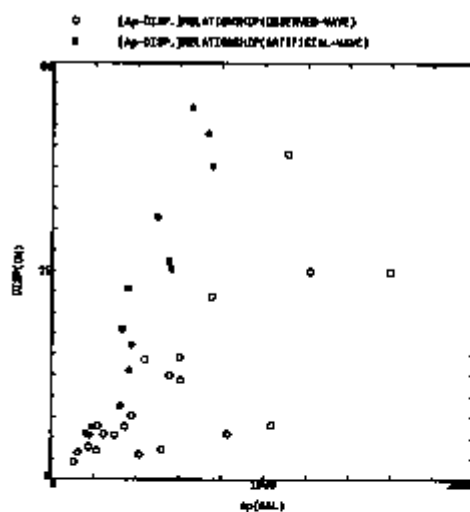


FIG. 4 A_p vs MAX. DISP. OF ISOLATOR

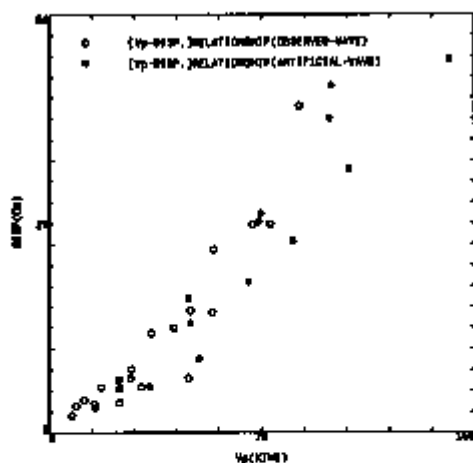


FIG. 5 V_p vs MAX. DISP. OF ISOLATOR

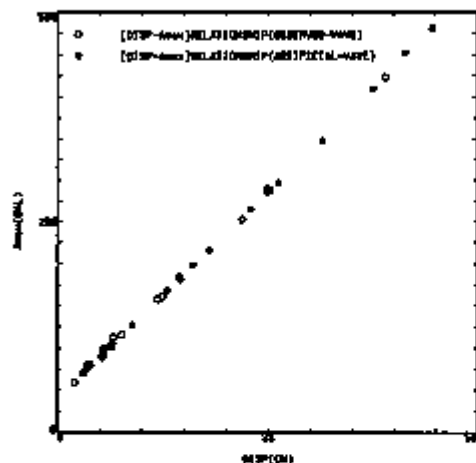


FIG. 6 MAX. DISP. OF ISOLATOR vs AN_4 AT SUPPORT LEVEL OF REACTOR

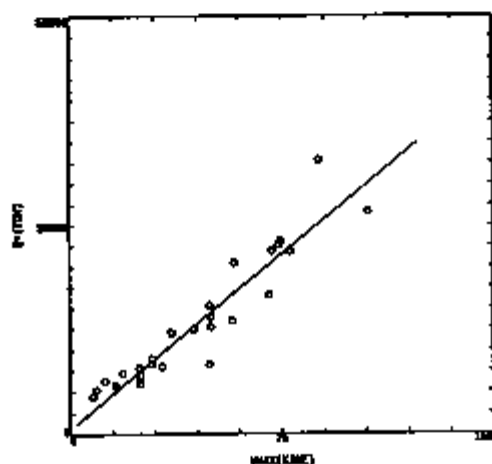


FIG. 7 LINEAR REGRESSION OF Q^* ON V_p (BUD. MEM. 2)

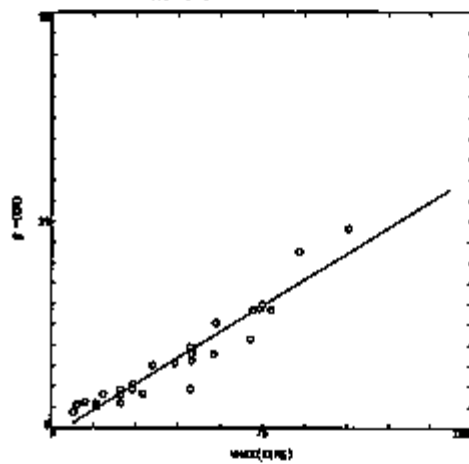


FIG. 8 LINEAR REGRESSION OF Q^* ON V_p (ISOLATOR)

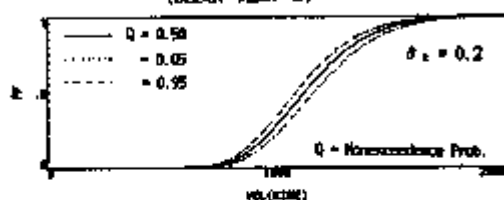


FIG. 9 FRAGILITY CURVE FOR BUD. MEM. 2

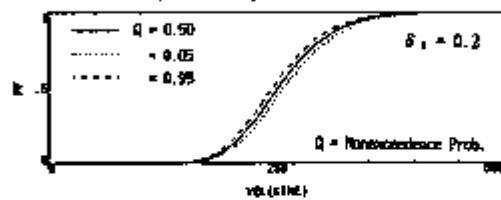


FIG. 10 FRAGILITY CURVE FOR ISOLATOR

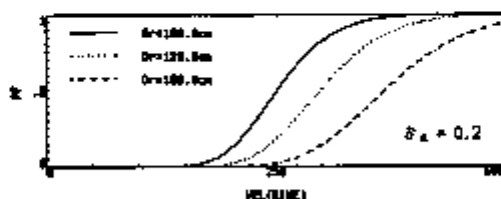


FIG. 11 FRAGILITY CURVE FOR ISOLATOR (PARAMETER: DISP. CAPACITY)

Earthquake Response Observation of Isolated Building

N. Kawai, O. Harada

Okumura Corporation, Tokyo, Japan

T. Ishii

Okumura Corporation, Tsukuba, Japan

Y. Sawada, H. Shiojiri, T. Mazda

Central Research Institute of Electric Power Industry, Abiko, Japan

1. INTRODUCTION

Base isolation system is expected to be one of the key technology for a rational design of FBR plant. In order to apply this system to important structures, accumulation of verification data is necessary.

From this point of view, the vibration test and the earthquake response observation of the actual isolated building using laminated rubber bearings and elasto-plastic steel dampers were conducted for the purpose of investigating its dynamic behavior and of proving the reliability of the base isolation system. Since September in 1986, more than thirty earthquakes have been observed. This paper presents the results of the earthquake response observation.

2. OUTLINE OF BASE ISOLATED BUILDING AND ISOLATION DEVICE

Base Isolated Building The base isolated building, an object of test and observation, is a four-story reinforced concrete building with dimensions of 15m in width, 20m in length and 14m in height as shown in Fig.1. Total floor area is 1,330m² and the weight is 2,250ton. Seismic isolation devices are installed between the basement and the first floor.

Seismic Isolation Device The seismic isolation devices consist of 25 laminated rubber bearings and 12 elasto-plastic steel dampers as shown in Fig.2 and Fig.3. The average horizontal stiffness of the rubber bearing used for this isolated building is 0.82ton/cm. The stiffness of the damper before yielding is about 2.0ton/cm and the yielding displacement is about 30mm. Under the assumption that the damper behaves elasto-plastically, the design horizontal natural frequencies of this building with the isolation devices are 0.71Hz(1.4sec) and 0.48Hz(2.1sec) corresponding to pre-yielding stiffness and post-yielding stiffness, respectively.

3. EARTHQUAKE RESPONSE OBSERVATION

3.1 Observed Earthquakes

More than thirty earthquakes have been observed since September in 1986 in the base isolated building. Epicenter of each earthquake is shown in Fig.4. Observed earthquakes are classified and characterized as shown in table 2.

Fig. 5 shows the averaged acceleration fourier spectra on the basement of each group earthquakes. Each spectrum is normalized such that a maximum spectrum value be 1.0. Low frequency components below 1.0Hz of group III are larger than that of group I and II.

Table 1. Classification of Observed Earthquakes

Group No.	Type	Epicentral Distance	Focal Depth	Magnitude ^a
I	Near	0 ~ 50km	50 ~ 80km	~ 8.0
II	Intermediate	50 ~ 150km	40 ~ 60km	~ 8.0
III	Far	150km ~	0 ~ 50km	6.0 ~ 7.0

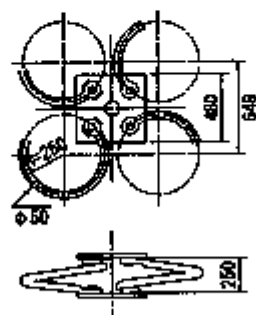
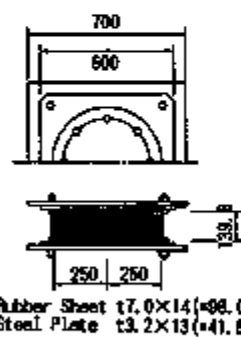
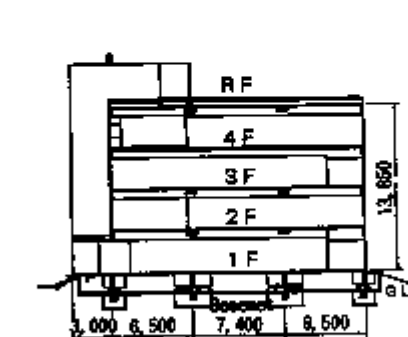
^a Magnitude of Japan Meteorological Agency

Fig. 2 Laminated Rubber Bearing Fig. 3 Elasto-Plastic Steel Damper

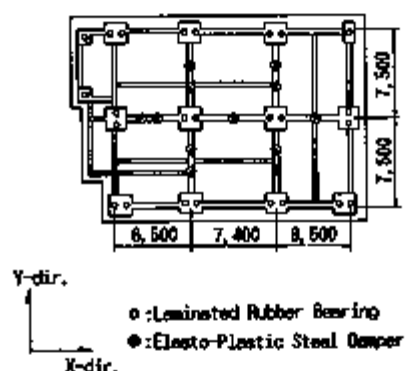


Fig. 1 Section and Plan of Building

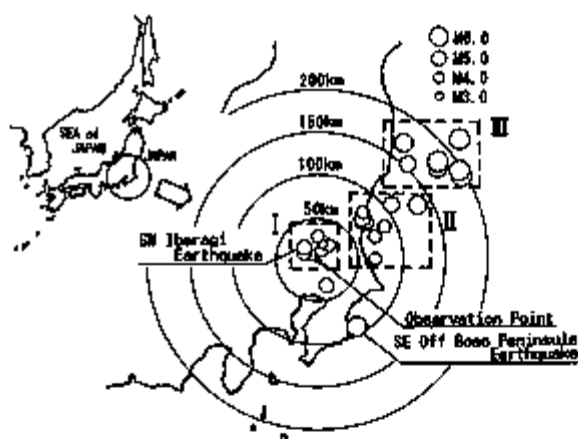


Fig. 4 Epicenter of Observed Earthquakes

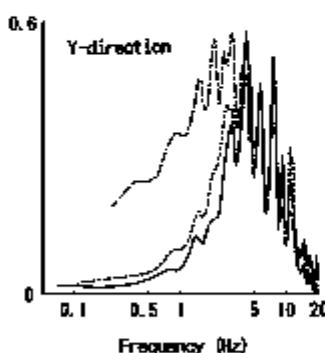
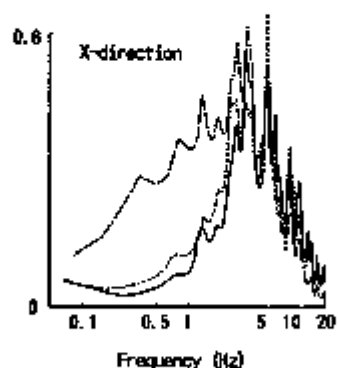


Fig. 5 Normalized Acceleration spectra on Basement

3.2 Response of the building

Fig. 6 shows the relationship between the ratio of the maximum acceleration (1st floor / basemat) and the maximum acceleration on the basemat. It can be seen that the horizontal acceleration ratio of both group I and II earthquakes are less than 0.5, that is, the acceleration on first floor is reduced sufficiently. But, in case of group III earthquakes, acceleration is not so reduced. This is because they contain much low frequency components as is shown in Fig. 5. The average ratio is around 0.6 in both X and Y-direction. On the other hand, the vertical acceleration ratio is almost constant and the average ratio is 1.24.

Fig. 7 shows the relationship between the maximum relative displacement (basemat-1F) and the maximum acceleration and velocity on the basemat, respectively. Strong correlation is observed between displacement of the isolation device and input velocity. This suggests that the deformation of the isolation device can be predicted by the velocity of input earthquakes.

It must be noted here that the relative displacement of the isolation device in these earthquakes are all less than yielding displacement of the dampers of 30mm, so in these cases, dampers do not work as damping devices for any observed earthquakes.

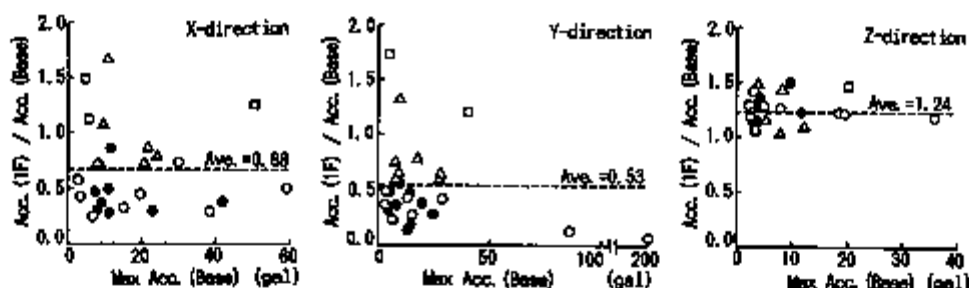


Fig. 6 Relationship between Acceleration Response Ratio of First Floor and Maximum Acceleration on Basemat

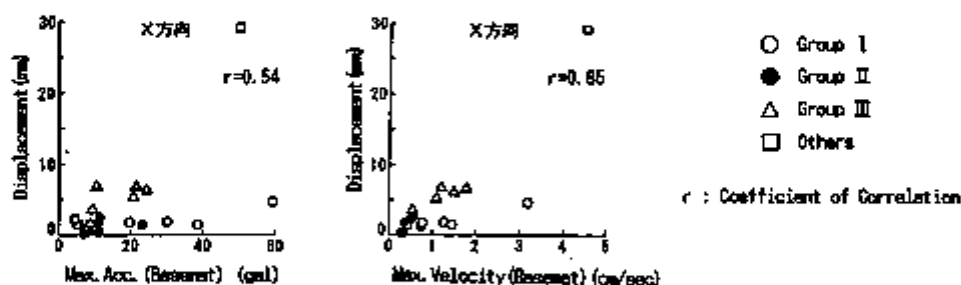


Fig. 7 Relationship between Maximum Displacement (1F-Basemat) and Maximum Acceleration and Velocity on Basemat

3.3 Typical Response Records

Two typical response records are introduced. One is the response for the SW Ibaraki Earthquake on June 30, 1987, the epicenter of it is very close to the observation point. Another is for the SE Off Boso Peninsula on Dec. 17, 1987 which includes much low frequency components compared with the other earthquakes. Data of both earthquakes are shown in table 2. The maximum acceleration distribution, time histories and acceleration response spectrum for 5% damping on each floor level are shown in Fig.8,9 and 10 respectively.

SW Ibaraki Earthquake, June 30, 1987 This is a typical high-frequency earthquake as seen in the time history and the acceleration response spectrum on the basemat. The maximum horizontal acceleration of 269gal was recorded on the ground surface at the beginning of a main shock. On the other hand, those in the building were around 20gal, showing a remarkable seismic isolation effect, especially in y-direction. The response spectrum on the first floor and the roof have a peak at the frequency around 7.0Hz(0.15sec), due to the second mode excitation. However, the acceleration response spectra in the building are reduced compared with that on the basemat in higher range than 1.5Hz.

SE Off Boso Peninsula Earthquake, December 17, 1987 The maximum horizontal ground surface acceleration is 83gal and those in the building are around 60gal in x-direction. In this case, acceleration reduction effect is not so large as the case of June 30, 1987 earthquake, however, the acceleration is not amplified in the building, which differ from the case of non-isolated building. As for the acceleration response spectra, the first mode frequency of 0.83Hz(1.2sec) is especially predominated. It is because the ground motion has a peak at this frequency. However, at the higher range than 1.5Hz (0.67sec), acceleration response spectra in the building are not higher than that on the basemat.

Table 2 Data of the Earthquakes

NAME	DATE	Magnitude	Focal Distance	Epicentral Distance	Depth
SW Ibaraki	June 30, 1987	5.1	55km	11km	55km
SE Off Boso Peninsula	Dec. 17, 1987	6.6	125km	104km	70km

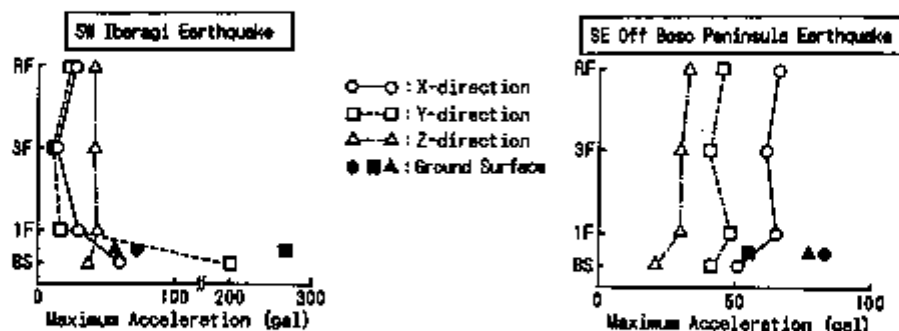


Fig. 8 Distribution of Maximum Acceleration

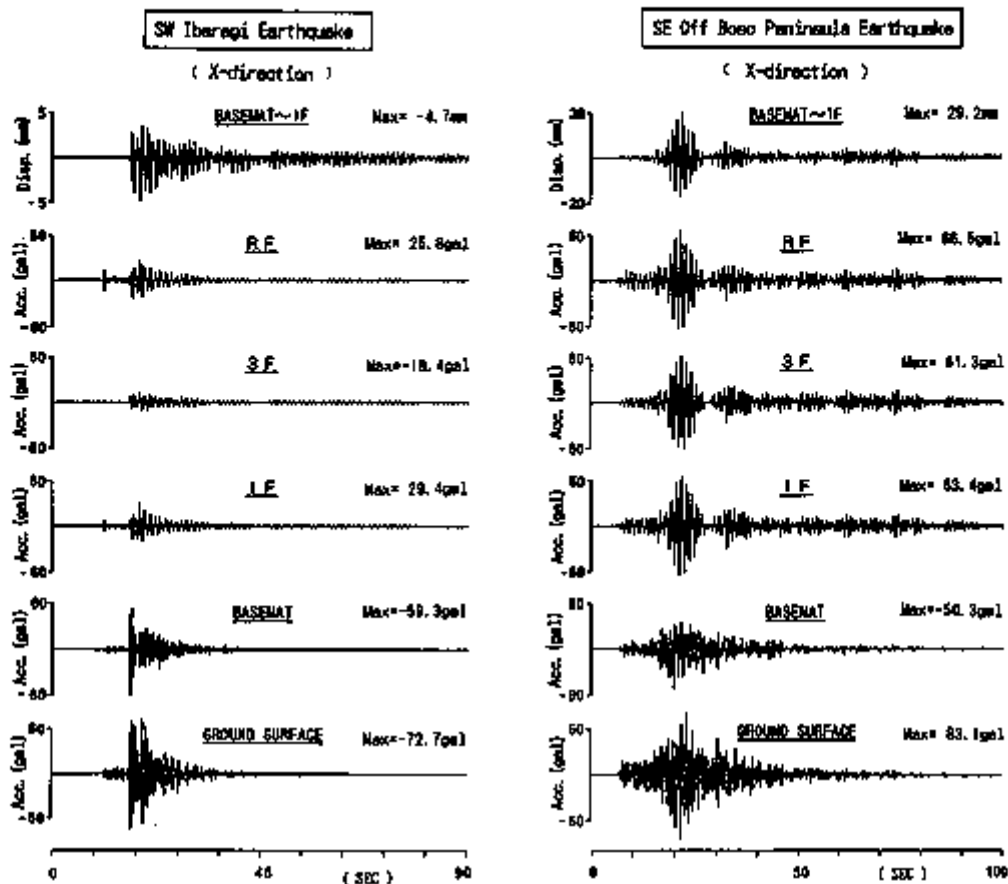


Fig.9 Time Histories of Acceleration and Displacement

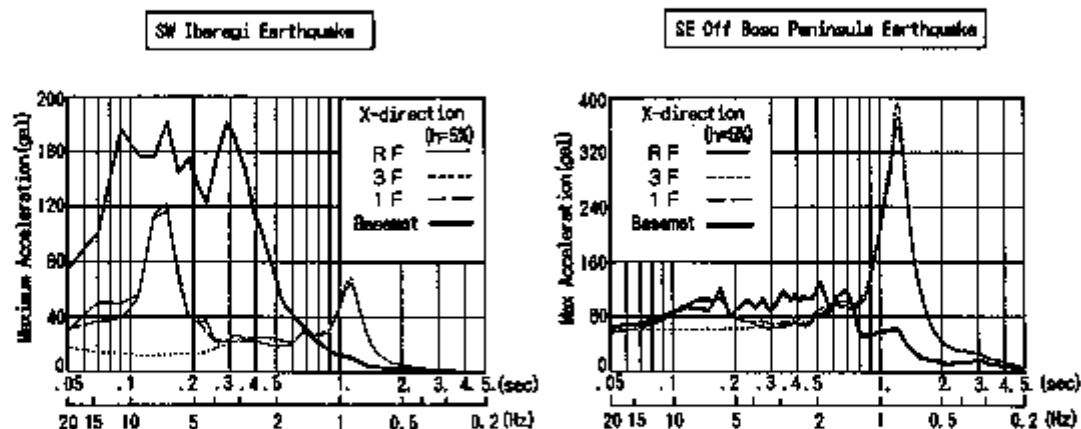


Fig.10 Acceleration Response Spectra

3.4 Torsional Behavior of the Building

The base isolated building is supposed to perform the torsional behavior due to the eccentricity during earthquake. In this building, the eccentric distance between the stiffness center of the isolation devices and the gravity center of the upper structure is about 30cm. Fig.11 shows the time histories of the translational displacement and the torsional angle at the center of the gravity on the first floor in the case of Dec.17,1987 earthquake. The maximum horizontal displacement due to torsional motion is about 3.0mm at the edge of the building which corresponds 15% of the recorded displacement. This is not so large as to make influence on the base isolation devices. And if needed, the torsional behavior can be reduced by adequate arrangement of the isolation devices.

Fig.12 shows the time history of the relative torsional angle between the first and the roof floor which indicates torsional behavior in the upper structure. Maximum torsional angle of 7×10^{-3} rad. is an order smaller than that of the first floor of 3×10^{-4} rad. in fig.14. This means that the torsional deformation of the base isolated building concentrate at the isolation devices and that of the upper structure is very small.

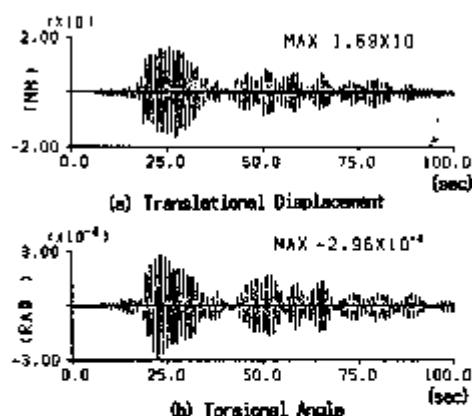
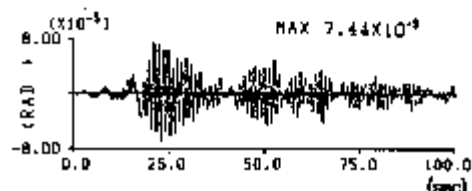


Fig.11 Translational Displacement and Torsional Angle at the Center of Gravity on First Floor



4. CONCLUSIONS

Through the earthquake response observation of the base isolated building, the followings are confirmed.

- i) Acceleration response during earthquake is strongly influenced by the frequency characteristics of the ground motion, especially, intensity of the component around the first natural frequency of the base isolated building. However, for any earthquake, it is sufficiently reduced in comparison with that of the ground surface.
- ii) The maximum relative displacement of the isolation device is almost in proportion to the maximum velocity of input earthquake.
- iii) Torsional deformation of the base isolated building is concentrated at the isolation devices and that of the upper structure is very small.

REFERENCES

1. S. Aoyagi, T. Mazda, O. Harada, M. Takeuchi et al., Experimental Study on the Dynamic Behavior of the Base Isolated Building, 9th SMIRT(1987), pp.687-692.
2. S. Aoyagi, T. Mazda, O. Harada, S. Ohtsuka, Vibration Test and Earthquake Response Observation of Base Isolated Building. 9th WCEE(1988).

On Problems to be Solved for Utilizing Shock Isolation System to NPP

Heki Shibata

Institute of Industrial Science, University of Tokyo, Tokyo, Japan

Shuichi Yabana

Central Research Institute of Electric Power Industry, Abiko, Japan

Tatsuya Shigeta, Hisanao Komine

Institute of Industrial Science, University of Tokyo, Tokyo, Japan

§1 INTRODUCTION

Since the success of Super-phenix, the interest to develop a large fast reactor, so called LFBR, has become more realistic one in Japan. However, the anti-earthquake design of a pool-type large fast reactor is more difficult than that of light water reactors for high seismicity areas like Japan. The reason of difficulties come from the difference of the structural requirement for LFBR. Three major points are as follows:

- i) Thin wall reactor vessel,
- ii) Thin wall sodium loops,
- iii) Large sodium pool with free surface.

If we apply the Japanese practice for light water reactors, the wall of a reactor vessel should be two or three times thicker than the thickness which is limited by the thermal stress requirement.

The minimum level of the S_1 earthquake, that is, Design Basis Earthquake, in Japan is 180 gal at the free surface of foundation rock layer. If this value will be cut down near to 100 gal, the design of main items would be easy. This fact is well known, however it is the problem how to reduce the seismic input to such a level.

Two methods have been considered since the project started. One is to lower the center of gravity as practical and to be embedding in soil. Another one is the use of a shock isolation system. We consider both methods will be practical for the purpose.

For a shock isolation, there are several choices, that is, from the isolation of a whole reactor building to that of a reactor vessel alone. Those were examined, and we understood that a simple, whole building isolation is most feasible for the first or second LFBR, which will operate from 2007 to 2010 in Japan.

In this paper, the authors will describe this subject along the conclusion above. However, it doesn't mean for us to abandon other choices. The isolation of main components including a reactor vessel, the second sodium loop and steam generator is still attractive.

§2 MERIT OF APPLYING SHOCK ISOLATING PADS

The authors believe that the principal part of Super-phenix I was designed to endure 0.1 G ground motion. On the other hand, the design basis earthquakes of nuclear power plants in Japan were evaluated from 180 gal to 480 gal, except very special cases of Mimaoka and Tokai #1. These figures are shown in Table 1. Also, the design procedure to decide the response and seismic load of main equipment in the reactor building is severer than other countries for light-water nuclear power plants in Japan. If we apply this standard procedure and design technique to the pool-type LFBR, the thickness of the wall of main

reactor vessels may exceed over 100mm. Of course, this value is depending on the details of its vessel support and other components surrounding the vessel. One of the target of preliminary design is to reduce it to approximately 50mm.

Such a heavy vessel may cause problems of thermal stress, and ratcheting induced by sloshing of the sodium surface. On the contrary, if the vessel is thinner than this limit, shear-type buckling may occur. To avoid these failures, the shock isolation system is useful as described in the introduction. The shock isolation system is a kind of low-pass filter whose folding frequency f_0 is designed in the range of 0.3 ~ 1 Hz. Transmissibility of sinusoidal acceleration input is easy to calculate as shown in Fig. 1 for a linear damping system.

To seismic inputs, the transmissibility of a filtering system depends on the wave form of inputs as we know the response analysis. Anyway, a peak ground acceleration may reduce into the level of 100 gal against S_1 earthquake, that is, the design basis earthquakes in Japan as shown in Table 1.

This means that a LFBR plant designed like Super-phenix may construct in a high seismic region in Japan by using an adequately designed shock isolation system. There are various combinations of design concepts as follows;

- i) structure: whole building
significant part
reactor vessel
- ii) direction of axes of isolater: horizontal
vertical
horizontal and vertical

The authors had been studying several types as a member of the committee in the Central Research Institute of Electric Power Industries (CRIEPI).⁽¹⁾ The final but current decision is the use of the horizontal isolation of the whole building, because this is the simplest technique even though the total weight of superstructure may be 200,000 to 250,000 ton. Also there will be several merits, for example, no flexible piping connection for main steam and other significant circuits is required, and all components mounted in the reactor building can be designed by lower design basis floor motion, and psychological and physical shocks to operational personnel may be reduced.

Of course, there would be many merits by employing other schemes, but we should solve some additional engineering problems such as flexible connection for the secondary main sodium circuit or the main steam line. The authors feel the necessity of the development of a partial structure isolation including a main reactor vessel and first and second sodium circuits at least.

Also the combination of use of isolating pads and servo-control system to suppress the sloshing phenomenon should be examined. As described later, the authors studied on a servo-controlled system.⁽²⁾

It was evaluated whether or not the design basis response can be recuded to this level without using shock isolation system in Japan. One idea is to look for low seismicity areas in Japan. We found that such sites will be found in the far-north area of Hokkaido island as shown in Fig. 2.⁽³⁾ This figure shows only a possibility obtained by a preliminary survey. Another idea is that decreasing the response of a reactor building as low as possible by embedding it. Japan Atomic Power Co. reported some examples of their design according to this design practice.

The choice of these methods have never been examined on with their merits and difficulties quantitatively until now. Even though, the use of a shock isolating system is one of realistic approaches to realize the pool-type large fast breeder plant in a high seismicity area like Japan.

53 PROBLEMS TO BE SOLVED

In the previous chapter, the authors mentioned that there are many choices how to combine which shock isolation system with which portion for being isolated in the whole plant. The most significant problem is the estimation of response of structure and equipment including piping systems in relation to potential seismic inputs. It is true that many specialists in this field have a

doubt on results of its response analysis. Especially, they consider whether or not the estimation of its relative displacement response will be highly reliable.

A sloshing phenomenon of sodium liquid surface has many unknown factors at this moment. Except the estimation of input ground motion, the sloshing phenomenon without any internal structure and the surface flow is clear for ordinary cylindrical vessels such as a cylindrical storage tank for oil and liquified gases. There are some discussions on input ground motions in the range of eigen-frequency of the fundamental sloshing mode and its response factor. (4)(5) There have been various examples of very large responses of liquid surface or a floating roof to the strong earthquakes through the world. (6)(7) A recent example in Japan, the response of floating roofs, whose eigen period are approximately 9 sec, reached to five meters in single amplitude even in the site which is more than 200 km from the epi-center. On the other hand, the results of response analyses obtained by using famous earthquake time histories like El Centro, Taft and others have shown very low levels since TID 7024 reported on this subject. As the authors have reported in various occasion since 4WCEE in Chili, (8) there are two main reasons. Most of time histories which have been used for the analyses are accelerogram, and don't contain significant level of wave components in this range of periods, two ~ ten seconds, because its level in acceleration is low and it is difficult to separate those components it from measuring error. Also the long period components depend on the source mechanism, especially its magnitude, and the geological structure, that is, the distribution of shear wave velocity in 1 ~ 2 km depth at the site. In the worst case, the maximum single amplitude may be considered to reach to a half meter or 60 kine in this frequency range, and this value is employed for the code of liquified gas storages in Japan. (8)(9) If the damping factor is 0.5% or less like liquid storage without any significant internal structure's flow disturbance, the response factor in displacement is over ten. In a case of a LFR reactor vessel, a critical damping ratio of the fundamental mode has not been clear, and the response factor may be smaller than the above case because of the effect of internal structures. For preventing this phenomenon, a simple shock isolation system is not effective as discussing in Chapter 8.

Aging effect on isolation pads is not so clear at this moment, even though the manufacturers are studying it very hard. The quality assurance of large isolation pads in Japan is fairly well, but still there is some difficulty to cure large size pads, like 500 ton capacity (in Fig.3), uniformly. Of course, its characteristics at the beginning is within a limit of the specification, but there would be a possibility to scatter their characteristics in certain extents after thirty or forty years use. The authors checked the effect of scattering its performance to the possibility to induce undesired torsional response, as will be reported in Div.K. (10)

Another problem is unevenly setting of pads. This may cause some incline of a reactor building or a part of structures supported by deteriorated pads. A pool-type reactor is very sensitive to the incline of the reactor vessel because of its primary design scheme. This effect has not been exactly evaluated, but it is estimated not to be so large compare to uneven settlement induced by the ordinary defect of civil engineering construction procedure.

Other problems to be solved are more detailed ones. Those subjects are condensed to the following input problem except aging of the pad.

- i) Setting the design basis earthquake including the frequency regions to govern the sloshing effect.
- ii) Examining the probability of exceedence of the response over the design basis earthquake.

These two subjects are completely seismological problems. They have been one of main reasons to oppose the use of shock isolation system for highly critical systems like nuclear power plants. The authors believe that the adequate engineering assumption based on current, but exact knowledges on seismology may overcome this problem. However, the design basis response spectrum approach using for light water reactors either in the U.S. or in Japan

is insufficient, because it is not the site and source dependent one completely.

54 DESIGN GROUND MOTION

For the light water reactor, the regulatory guideline for aseismic design of nuclear power plants⁽¹¹⁾ designates to specify the following three items:

- i) Peak amplitude of the ground motion,
- ii) Frequency distribution characteristics and
- iii) Duration of ground motions.

These parameters are considered as a function of the magnitude and the epicenter distance of the earthquake assumed for the design basis earthquake motion. As we know well, the effect of the change of a magnitude to the amplitude is most significant. If the value of a magnitude is changing by 0.3, the amplitude of ground motions, for example, PGA value changes by 2.8 times. This is more than the range of engineering allowance. Usually the estimation error of magnitude of a particular earthquake is said to be 1/4, and this value means the difference of 2.37 in an amplitude. One of the authors mentioned this fact in his early paper on the seismic-PRA problem. Again this becomes a very key issue on the reliability of a shock isolation system.

Before to discuss on the relation of such uncertainties to the design of a shock isolation system, the authors want to review Japanese practice⁽¹³⁾ quickly.

The Japanese practice is similar to the U.S. practice in the view point of using a design basis response spectrum, so-called "Ohsaki" spectrum. This spectrum was defined based on accumulated informations on peak accelerations of ground motions in near-fields as described in his paper.⁽¹⁴⁾ In Japan, it is understood that the shorter period of this response curve gives lower response compare to the results experienced in actual earthquakes. The attenuation formula officially used is based on Kanai's equation.⁽¹⁵⁾ However, there are many uncertainties which come from the individual site-source relation, and this equation gives only an average relation. Several attenuation equations were presented even for the Japanese region, the uncertainty was evaluated from 0.3 to 0.7 in the variation coefficient under an assumption of lognormal distribution.⁽¹⁶⁾

Magnitude and attenuation factor are directly related to the design uncertainty problem as well as the shape of the design response factor. Other parameters are not so seriously affected to the design of a shock isolation system. Also it is necessary to discuss on cumulative damage of components of the system. This will be described in Chapter 6.

Uncertainties of ground motions will be never solved as a deterministic prediction problem, however, we can estimate them in a probabilistic sense, maybe, as upper bounds of PGA. Most of models for PRA study are assumed to be rather simple mathematical form, but it should have some upper bound as a physical model. We can not conclude this discussion on the upper bounds in the deterministic sense so sharply at this moment, but we need to conclude it based on the exact knowledge of seismology.

55 DESIGN AND TESTING OF SYSTEM

A shock isolation system is expressed by a mass-spring model with a damping device. Therefore, its response estimation is rather simple, even if it has a non-linear component in it. Damping devices may be categorized into the following two. One is an ordinary viscous damper whose hysteresis curve is shown in Fig.4(a). The energy absorbed by this device is proportional to the square of the amplitude. In the case of higher order relation including the square, the amplitude of a resonator is balanced at least one equilibrium state against the input sinusoidal motions. Another model is a friction type damper whose hysteresis curve is shown in Fig. 4(b).

In this case the energy absorption rate is proportional to the amplitude, therefore, the response doesn't reach to equilibrium, and it is going to

deverge, if the input is sinusoidal and continues. Most of devices using the yielding phenomenon of metal have the similar characteristics to this case. Therefore, if the input is similar to sinusoidal waves, that means, in the case of components responding to slightly damped building motion, they may behave in unfavorable way.

For the shock isolation system of a building structure, input ground motions may not bring such a problem to its behavior in general, but we should pay attention to the system for components in a building.

Some typical responses of a model building with different combination of damping devices are shown in Fig.5. This result of testings and simulations shows that the use of a high viscous shear type damper is better than the simple use of a lead metal damping device as the response of an isolated structure. If the eigen period is near to one of the dominant periods of ground motions, the peak of response of the system with a lead metal damping device becomes higher than that with the viscous damper. But in other viewpoints, the use of viscous material has more practical difficulties. To avoid this problem, the combined use of several levels of yielding metal type damper will be practical.

Against the input over the design level, the authors feel the necessity of more systematic study. One is on the multi-level damping device above-mentioned. And another one is the use of a non-linear spring which has a hardening characteristics like a leaf spring. Both may induce higher acceleration by its braking effect, and also higher harmonic frequency components. The longer buffer stroke is the better to decrease these effects, of course. How we choose this stroke is a matter of the confidence of the designer on the amount of the excess input. Other back-up devices have been considered. To protect an isolator pad itself, the use of a sliding pad is a typical one. But this can not avoid the shock caused by hitting the stopping device. Additional friction pad to brake the motion using lowering the height of rubber pads was considered and tested. The design of this system should depend on the behavior of a rubber pad.

56 DESIGN AND TESTING OF COMPONENTS

The design and proof-testing of components, especially an isolator pad is very significant. This has been studied by Fujita and Fujita for last several years with its fabricator.⁽¹⁷⁾ They designed 500 ton capacity pad at this moment. And the Central Research Institute of Electric Power Industries is going to test it as described in Chapter 9.

One problem is the detailed analysis of strain distribution in a pad, and another is its quality assurance during fabrication, especially curing stage. The size of 500 ton pad is 1800mm in diameter and 500mm thick. The uniformity of curing is very important as well as those of auxiliary damping devices. Some major manufacturers of rubber tires have this capability, for example, the breaking limit of deformation can be controlled within 10% ranges. Parameters like stiffnesses can be controlled within this limit also. Adequate value of the safety factor for their strain, including connection between rubber and metal, has not been known, but usually it is taken as two.

Both round shape and square shape have been used. The fabrication cost for square shape is cheaper than round one's. However, there is a problem of skin or edge strain distribution of the square shape pad for a building which has similar vibration characteristics to both orthogonal directions, and this is the significant difference to the bridge bearing. At this moment, it is considered in Japan that the round shape pad is more reliable.

Tie bolts or anchor bolts are one of the key items for the safety of structures. This subject including the failure of concrete has been studied for a part of nuclear power plant safety projects last ten years in Japan.⁽¹⁸⁾ Even though we believe that we know the detailed practice well, we had many examples of the tension-type failure of a bolt as shown in Fig. 6 caused by pure shear force-type load. The design practice obtained by the project above covers this problem sufficiently in Japan.

The behavior of lead plug has been tested for bridge pads in New Zealand.

The recrystallizing of lead had been studied for cover metal of telephone and power cables for long years. It is considered that the higher purity of the metal the better damping plug. This may be true in the viewpoint of brittification at the grain boundary after repeating the recrystallization. The effect of impurity in lead metal to damping has not been studied so seriously.

Various types of metal are planned to be used for yielding-type damping mechanism. Bending and torsional types of deformation are using for this purpose, but it is difficult to get large yielding volume by bending type from the same size metal piece. Ordinary mild carbon steel is used, but austenite stainless steel is also appropriate metal except its cost. The yielding curve is also different to that of mild carbon steel, and is crispy as we know.

Use of visco-elastic material for a nuclear power plant is under the study. Aging including by radiation for long years has not been known with high engineering confidence. It should be studied on the property as well as the detailed design of devices.

§7 SYSTEM RELIABILITY

This subject includes both the response reliability and the component reliability. The response reliability is depending on uncertainties of ground motions as described in Chapter 3. However, it should be noticed that the shock isolation system improves the uncertainty of the response of components in the building by the filtering effect of the system as shown in Fig. 7. If the shock isolation system is not applied to the building, uncertainties including distribution of eigen-periods of the building, that is, peaks A and B in Fig. 7(A) may affect the response of components whose eigen-periods are in the region Z. On the other hand, as shown in Fig. 7(B), the filtering effect may decrease the variation of response level as well as level itself.

The peak C in Fig. 7(B) will be affected by the uncertainties both on the ground motions and the characteristics of shock isolation components. The former one affects to the height of the peak mainly, and the latter one to the position of the peak and the height. The latter one may be controlled by engineering knowledges and techniques.

The effect of non-uniformity of isolation pads⁽¹⁰⁾ was studied by the authors as reported in Division K, they are not so significant, because of the number of pads, for example, we need 400 pads for a 200,000 ton super-structure. This number reduces the effect by the random distribution of parameters of components under the structure. The authors' study was made for torsional response induced by the non-uniformity of pads' parameters, horizontal stiffness and yielding point. This conclusion may extend to other subjects, like uneven settlement of the super-structure, shifting of eigen-periods.

However, the authors assume that the aging effect would be non-biased and random. If the tendency of changing the parameters of each pads is one-direction, such as stiffness hardening and some other effects, then the shifting of the response peak should be considered.

For the components, based on the final result of PSA study in level one, we can present the limit values of variations of performance parameters on pads and other components. And their manufacturers control their products within the limit. It is more reasonable way compare to the way which has been done usually, that is, starting from the evaluation of the degree of the fluctuation of their performance.

§8 ACTIVE CONTROL SYSTEM

The fundamental idea is a feed back control as a servo-mechanism. By sensing acceleration on the structure, and compensating the response of the structure so as to minimize the acceleration response. The way of feeding back has a variety from an ordinary PID control to an adaptive control.

Several kinds of type of filter effect were mentioned.⁽²⁾⁽²⁰⁾ The active control system can be realized by any of them. Recently, a tuned mass type one

using an actuator was demonstrated. A tuned mass-spring type device compensates the response which is expected to sinusoidal one in its eigen-frequency. A servo-type mass device compensates the more irregular response. It is also considered that the mass is acting as an assumed wall fixed to the absolute coordinate by its inertia, and can overcome not only sinusoidal waves, but also random type input motions.

The authors have been studying on high-pass type servo mechanism for avoiding sloshing in a reactor vessel of LFBR. He used a linear motor instead of a hydraulic actuator, because it doesn't need to keep the hydraulic system under the stand-by operating condition. It is great energy loss to operate its oil pump through the life of it.

They employed "Linear Induction Motor (LIM)" at first. LIM has a non-linear characteristic including a dead zone in the relation of input signal to force output. By using a computer, such non-linearities are linearized, and the ordinary techniques like PI control were applied. To cover the response characteristics of a sloshing phenomenon, Housner model,⁽⁴⁾ which is famous sloshing model introduced by Housner and is simple than the theoretical model, was used for the model to control adaptively.

§9 CURRENT R & D PROJECTS IN JAPAN

The Central Research Institute of Electric Power Industry⁽¹⁾ have been studied this subject last three years under the sponsorship of MITI. In advance to this project, Power Reactor and Nuclear Fuel Development Corp. (PNC) made the preliminary survey project in 1983 and 1984.⁽¹⁹⁾ One of the authors, SHIBATA, has been working for these projects as a member committees. And also he organized a research committee on the aseismic design of FBR in 1982 by the supports of some utilities under the management of System Corp.. Fundamental study on the detailed designs of equipment and piping systems has been done by the three major manufactures of nuclear power plants under the sponsorship of electric power utilities. The use of the shock isolation system is proposed for the second LFBR for proving in principle.

The choice whether the use of a shock isolation system or reducing the seismic input to a reactor vessel and main components by the modification of the geometry and structural layout, especially lowering its center of gravity is a key issue for the design of the first LFBR which will be expect to be completed in 2008 ~ 2010.

The whole project including the choice whether pool-type one, like Superphenix, or a loop-type one, like Monju which is the Japanese proto-type FBR under construction, or a hybrid-type is going to be reviewed at the end of this F.Y., March 1990. And we are expecting to decide whether or not the shock isolation system will be applicable to the first LFBR or to the later one. We are planning to test several size models on shaking tables and in the field next four or five years. The exact schedule will be decided based on the decision above.

§10 ECONOMICAL CONSIDERATION

Because of the restriction by the Building Code in Japan, it is not clear how far we can reduce the total amount of super-structure, and the trial design with high accuracy has not been made. The design of base-mat and the distribution of wall and pads was discussed in the PNC report.⁽¹⁹⁾ Even though, a thick uniform mat and a uniform distribution of pads are considered for systems employed in most of R & D studies.

If we can reduce the amount of the super-structure as well as equipment, by the guess of the authors, the cost for the aseismic design of 10,000MW light water reactor in Japan is less than ¥100B (= \$1B). This amount may be not much difference to LFBR. The use of a shock isolation system may reduce 30% cost of this. However, the cost for a shock isolation system and supplemental components, such as lower mat, flexible connection pipings, may reach to 70% ~ 80% of the reduced cost. Therefore, the reduction of total cost may be

approximately ¥20B or \$0.2B, for the first one including some part of R&D cost.

This reduction is not so large as we are expecting. But it is important to mention that the structural design of a main vessel, other auxiliary components, sodium piping systems and so on is very critical to the seismic input considered in Japan. It is rather difficult to design such structures to satisfy both seismic and thermal conditions. There is a possibility to overcome this difficulty only by employing the shock isolation system. Also it should be mentioned that the use of the shock isolation system may reduce the uncertainty for the aseismic design by its filtering effect. Structural design problems caused by sloshing effect are also significant in some cases in Japan. But it is impossible to suppress this phenomenon by an ordinary passive type shock isolator in general. The choice of the site condition in the sense of engineering seismology is significant. The authors tried to develop an active control system for a main vessel and surrounding systems as mentioned,⁽²⁾ and it was proven that some active control systems are theoretically available, and required electric power is in the practical range. The cost has never been estimated, but it should be expensive compare to the cost which will be reduced.

§11 CONCLUDING REMARKS

The use of a shock isolation system is necessary to obtain the reasonably designed Large Fast Breeder Reactor in a high seismicity area like Japan. It is feasible in the engineering sense within a scope of R&D in Japan. The prototype of 500 ton isolation pad has been developed and tested already. We need several years more for developing the plant design itself. During these years, we are going to have more experiences on conventional buildings and industrial facilities. More practical R&Ds on related items will be made during this period. This means that the development of the plant itself may need more time than that for the shock isolation system.

Technical details for such systems were discussed in Ref.(20) and presented in a conference in Seoul last year.

The authors greatly appreciate the co-operations of Professor Fujita, Inst. of Ind. Sci., Univ. of Tokyo, and of Mr. Sawada and others, Central Research Institute of Electric Power Industry, for preparing this manuscript as well as daily research works.

§12 References

- 1) Sawada, Y., Shibata, H. and others : Seismic Isolation Test Program, Preprint of SMIRT-10, K28/4 (Aug. 1989) (in printing).
- 2) Shibata, H. and others : Study of Active Control System for Suppressing Earthquake-Induced Sloshing in Liquid Tanks, Report of ERS, Inst. of Ind. Sci., Univ. of Tokyo, No.III-7 (Mar. 1985) 45pp..
- 3) Shibata, H. ed. : Basic Study on Selection of Reactor-type of Large Fast Breeder Reactor --- Part IV, Report of FS Research Group, System Corp. Inc., (Mar. 1985), p.IV-3 (in Japanese).
- 4) US AEC ed. : Nuclear Reactors and Earthquake-chapter 6, TID-7024 (Aug. 1963) p.183.
- 5) Sogabe, K. and Shibata, H. : Aseismic Design of Cylindrical and Spherical Storages for their Sloshing Phenomenon, Proc. of 6 World Conf. on Earthq. Eng'g., Vol. III (Jan. 1977) pp.3356-3363.
- 6) Hanson, R.D. : Behavior of Liquid Storage Tanks, The Great Alaska Earthquake of 1964, Engineering, National Acad. of Sci. (1973) p.331.
- 7) Shibata, H. : Observation of Damages of Industrial Firms in Niigata Earthquake, 4WCEE, Vol. 3 (Jan. 1969) p.J-2-2.
- 8) Ministry of International Trade and Industry : Guideline for Aseismic Design of High-pressure Gas Facilities, MITI Notice, No. 515 (Oct. 1981) (in Japanese).
- 9) Shibata, H. trans. : Draft of Anti-earthquake Design Code for High-pressure Gas Manufacturing Facilities, Rept. of ERS, No.III-5 (July 1981) 30pp..

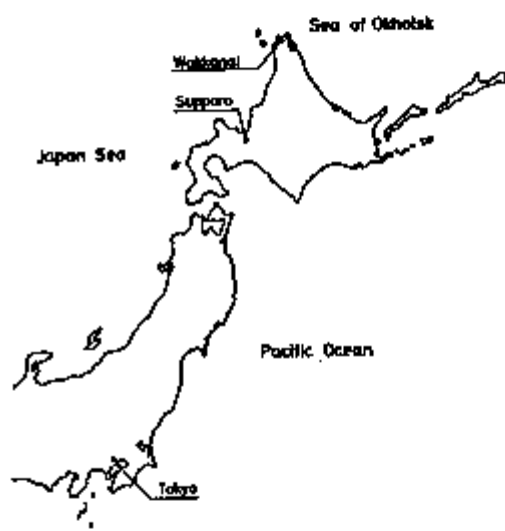
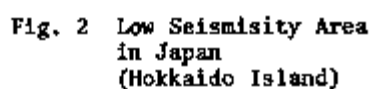
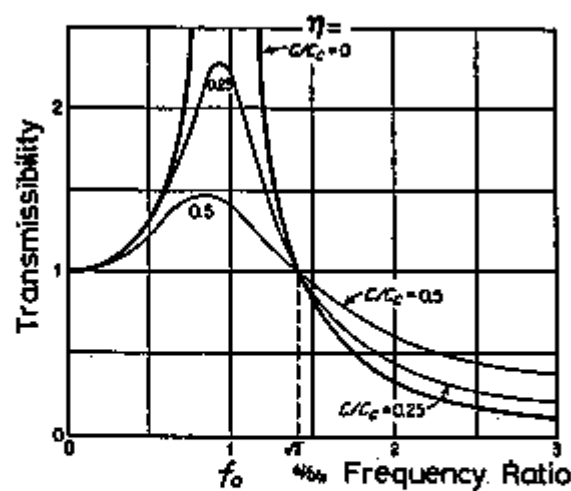
- 10) Yabana, S. and Shibata, H. : Probabilistic Assessment on Torsional Response due to Aging of Base Isolation Pads for Large Fast Breeder Reactor, *Report of ERS*, No. 22 (Mar. 1989) p.49.
- 11) Nucl. Safety Comm. : Guideline for Aseismic Design of Nuclear Power Plant (Sept. 1981).
- 12) Shibata, H. : On Response Analysis for Structural Design and its Reliability, *Proc. of 3SMIRT*, K4/3 (Sept. 1975).
- 13) Shibata, H. and Kato, M. : Recent Development of Fundamental Philosophy of Anti-earthquake Design for Nuclear Power Plant in Japan, *Working Material of IAEA*, IAEA-TC-472-1, Moscow (Mar. 1986).
- 14) Ohsaki, Y. and others : Design Spectra for Stiff Structures on Rock, *Proc. of 2nd Int. Conf. on Microzonation*, Vol.III (Nov. 1978) p.1187.
- 15) Udaguchi, T. and others : The Aseismic Design of Nuclear Power Plants in Japan, *Proc. of Peaceful Uses of Atomic Energy*, UN/IAEA, A/Conf.49, Vol. 3 (Sept. 1972) p.297.
- 16) Abe, K. and others : Development of Seismic Risk Analysis Methodologies at JAERI, *Proc. of Int. ENS/ANS Conf. on Thermal Reactor Safety* (Sept. 1988).
- 17) Fujita, T. : Collected Papers on Shock Isolation Technique, *Text for Seiken Seminar*, Inst. of Ind. Sci., C.129 (Dec. 1987) 192pp. (in Japanese).
- 18) Shibata, H. : Foundation Design Practice of Nuclear Power Plants in Japan -- in the view point of anti-earthquake design of mechanical components in the building, *Preprint for FMDL Conf.*, Leningrad, USSR (May 1989).
- 19) Technical Research Assoc. for Integrity of Structures at Elevated Service Temperatures : Study on Applicability of Shock Isolation System to Large Fast Breeder Reactor, Power Reactor and Nuclear Fuel Development Corp., PNC SJ 272 84-01/85-01 (Mar. 1984, Feb. 1985) 175pp. & 341pp. (in Japanese).
- 20) Shibata, H. : Some Comments on Application of Shock Isolation Systems, *Proc. of Korea-Japan Joint Seminar on Emergency Technology in Structural Eng'g. and Mechanics*, Seoul, Korea (Nov. 1988) p.354.

Table 1 Typical Level of S_1 and S_2 in Japan

Earthquake	Design Basis Seismic Coef. (Static)	Dynamic Zero-period Ground Acc. gal
S_2 Upper bound e. (Margin Check e.)	0.9	240 ~ 480 , 600)* ¹
S_1 Design basis e. (Maximum level e./ Historical Max.)	0.6	180 ~ 300 , 450)* ¹
S_0 * ² Operating e.	---	50 ~ 60

*¹ : Hamaoka Nuclear Stations in Earthquake Predicted Area.

*² : Not officially defined, as a reference.



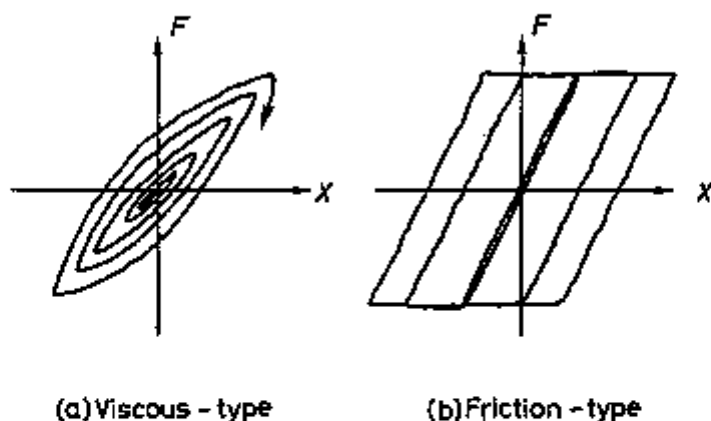


Fig. 4 Schematic Diagrams of Force vs Displacement of Damping Devices

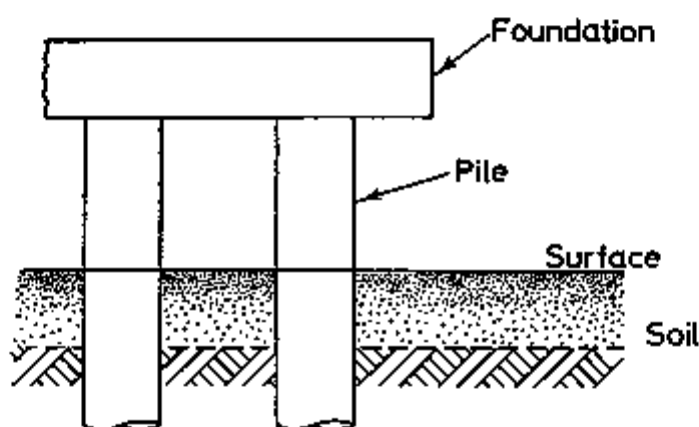


Fig. 6 Typical Failure Modes of Anchoring

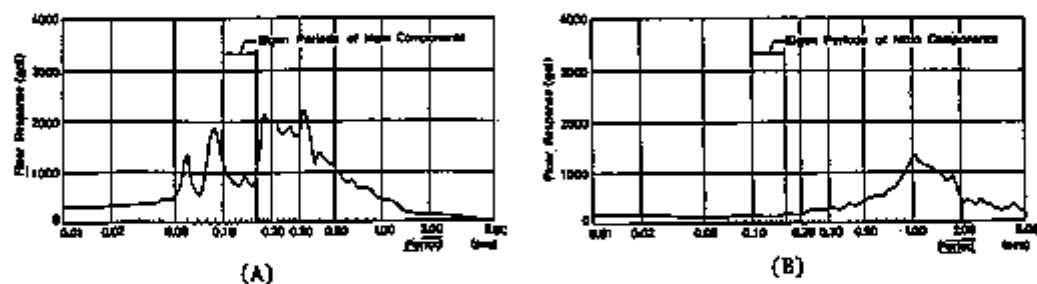


Fig.7 Schematic Drawings of Floor Response with/without Shock Isolation System; at Reactor Floor Level of LFR [Redrawn from CRIEPI's Data]

Testing of Seismic Isolation Bearings for the PRISM Advanced Liquid Metal Reactor Under Extreme Loads

F. F. Tajirian

Bechtel National Inc., San Francisco, CA USA

J. M. Kelly

University of California, Berkeley, CA USA

E. L. Glueckler

GE Nuclear Energy, San Jose, CA USA

INTRODUCTION

This paper presents the results of a series of tests performed to evaluate the response of high damping natural rubber seismic isolation bearings subjected to extreme horizontal displacements. Bearings of this type were included in the design of the reference U.S. advanced liquid metal reactor (ALMR), PRISM, to mitigate horizontal seismic loads and to enhance structural margins. The purpose of the tests was to determine the maximum shear strains and vertical load that the bearings could sustain before failure, to characterize the stiffness and damping of the bearings when subjected to extreme horizontal displacements representative of beyond design basis earthquakes, and to assess available performance margins.

PRISM is a compact standardized ALMR reactor installed in blocks consisting of three reactor modules per 465 MWe power block (Berglund et al., 1988). Each reactor module incorporates a horizontal isolation system to isolate the reactor module with its key safety functions of reactor shutdown, shutdown heat removal, and containment systems from potentially damaging ground motions. The entire isolated structure is housed in an underground silo as shown in Fig. 1. The small diameter of the PRISM vessel provides sufficient intrinsic resistance in the vertical direction to minimize amplifications in vertical ground motions which makes vertical isolation unnecessary. The total weight of these structures is approximately 9000 kips and is supported on 20 large diameter high damping steel laminated elastomeric bearings (Kelly, 1987). The bearings have a diameter of 52 in. and a total height of 23.1 in. and consist of thirty layers of rubber 1/2 in. thick and 29 steel plates 1/8 in. thick. The bearing dimensions were selected to give a horizontal frequency of 0.75 Hz and a vertical frequency over 20 Hz. The elastomeric compound used consists of a highly filled natural rubber with high damping. The properties of this compound were presented elsewhere (Tarics et al., 1984 and Tajirian and Kelly, 1988). Lateral loads from the isolated structure are transferred to the bearings through dowels which under large horizontal displacements would allow the top and bottom plates to bend and limit tensile stresses in the elastomer.

The design safe shutdown earthquake (SSE) for PRISM is a maximum horizontal and vertical acceleration of 0.3 g anchored to a design earthquake that envelopes the NRC Regulatory Guide 1.60 spectra. Options for siting in higher seismic zones are being investigated. Analytical results show that horizontal accelerations are substantially reduced in all the reactor components with isolation (Tajirian and Schrag, 1987). The peak spectral acceleration at the core support plate for 2 percent damping was reduced from 16.5 g to 0.25 g. Furthermore, horizontal spectral peaks above 2 Hz are eliminated. Incorporation of seismic isolation in the PRISM design results in reactor design simplification, improvements in reactor safety and facilitates design standardization for broad geographic deployment.

SEISMIC ISOLATION BEARING TESTS

A series of quasi-static tests was performed at the University of California Earthquake Engineering Research Center (EERC) in Richmond using the test fixture shown in Fig. 2. The maximum vertical capacity of the fixture is 1500 kips. Four bearings stacked in two tiers are loaded simultaneously in the horizontal direction using two large hydraulic actuators located between the top and bottom bearings. A maximum horizontal load of 400 kips can be applied to the bearings, while producing cyclic horizontal displacements up to ± 9 in., or 18 in. in any one direction. The bearings tested so far are half-scale, have a diameter of 26 in., and consist of thirty alternating layers of rubber 0.238 in. thick and 29 steel plates, see Fig. 3. The bearings are designed for a shear strain of 50 percent at the maximum SSE displacement. A series of vertical and cyclic horizontal stiffness tests were performed to verify the bearing properties under normal design loads. The results have been previously reported in (Tajirian and Kelly, 1988). The tests verified that the bearings are capable of undergoing several cycles of varying shear strain without appreciable change to their stiffness or damping. The tests also showed that the first cycle of each test gave a slightly higher initial average

stiffness. This is not expected to affect the design. Furthermore, the bearings have 10 percent damping or more for all applicable shear strains.

Extreme Displacement Tests

The bearings were then subjected to a series of extreme horizontal loads to determine the maximum shear strain that the dowelled bearings could sustain before delamination or other types of failure such as geometric instability would occur. The tests consisted of half cycles to maximize the achievable displacement with the actuators. Increasing horizontal loads were applied under a constant vertical load. The tests were performed for the vertical loads and shear strain levels defined in Table 1. It should be noted that the vertical load at the higher strains was increased beyond the design load to prevent rollout of the bearing and to induce failure of the elastomer in shear. The relationship between average horizontal bearing stiffness and shear strain is shown in Fig. 4. The average bearing stiffness at 50% strain is about 11.5 kips/in. and is reduced to 9.5 kips/in. at the higher strains. The stiffness is highly nonlinear at low strains, but is fairly constant for strains above 30%. The high stiffness at low strains is sufficient to resist strong wind and small earthquakes without movement. It can also be seen that the average horizontal stiffness is not sensitive to the vertical load.

The maximum shear strain achieved was 200 percent which corresponded to a maximum horizontal displacement of 14.4 in. which is four times larger than the displacement computed for the SSE (actual displacements are equal to the scaled displacements times the scaling factor of 2). Fig. 5 shows a bearing under a vertical load of 420 kips and displaced 14.4 in. There is substantial warping of the bearing end plates and disengagement of the dowels; however, even under these extreme conditions failure could not be induced. The hysteresis loops for 161, 176, and 200 percent shear strain are shown in Fig. 6. It can be seen that the stiffness of the bearing starts increasing at high strains due to stiffening of the elastomer. Additionally, the area of the hysteresis loop at higher strains is larger. This is caused by bending of the steel end plates beyond yield point and represents an increase in damping. This deformation of the end plates should produce an overall reduction of the horizontal stiffness of the bearing since the deformable system should be less stiff than a system with rigid elements but the increasing shear modulus of the elastomer at high shear strains more than compensates for the reduction in stiffness due to yielding of the plates. This provides an inherent stabilizing effect for controlling displacements in extreme events in contrast to other systems which soften with increased shear.

Even after several cycles of extreme displacements no damage could be observed in the bearings. To verify this, each extreme test was preceded and followed by a 50 percent nominal shear test and the hysteresis loops were plotted, see Fig. 7. No change in the stiffness or the hysteresis loops was observed. Larger loads could not be applied to fail the bearings due to load limitations of the test machine. Tests in Japan performed on 1/11 scale bolted elastomeric bearings with large aspect ratios have shown that the elastomer does not fail unless the shear strain exceeds 400 percent (Kurihara et al., 1987). For the PRISM half-scale bearings, this would correspond to a horizontal displacement of 30 in. Additionally, half-scale bearings with bolted type connection instead of dowelled connection were tested to compare the failure mechanism of the two systems and the results are currently being evaluated. The base PRISM design, which currently uses dowelled connections will be reassessed depending on the outcome of these tests.

Ultimate Vertical Load Test

To assess the ultimate load capacity of a single bearing under vertical load, one bearing out of the four previously used in the shear tests was tested in the four million pound Southwark-Emery test machine at EERC. The bearing was loaded at a rate of around 400 kips per minute. The vertical displacements were measured at four points equidistantly spaced around the periphery of the bearing. The bearing was loaded to the limit of the machine, 4000 kips which corresponds to 7500 psi pressure, without causing any apparent damage to the bearing. This corresponds to a margin of safety under direct vertical load of around 32. The load deflection curve for this test is shown in Fig. 8. It can be seen that the vertical stiffness is fairly constant even at high levels of vertical loading. On unloading and removal of the bearing from the machine it was found that the steel layer at the bottom of the dowel holes, which has a thickness of 1/16 in. was permanently distorted. No evidence of any damage to the elastomer or the internal steel shims was apparent. It is anticipated that the mode of failure under the ultimate load would be tensile bursting of the internal shims. To determine the actual failure pressure it will be necessary to use a smaller bearing and scale the results.

Buckling Load Test

The boundary conditions for bearings supporting a structure have a lower boundary which is fixed to the foundation and an upper boundary which is free to move laterally. In this condition, when the vertical load on the bearing exceeds the buckling load, the bearing buckles. To determine the buckling load for a single bearing two of the bearings used in the shear tests were loaded one on top of the other in the Southwark-Emery machine in direct compression. This simulates the boundary conditions in an isolated building described above. Vertical displacements were measured at four equidistant points around the bearings. Horizontal displacements at the mid-plane were measured in two orthogonal directions since the direction of horizontal displacement was not known a priori.

The bearings were loaded in four stages; first, to 1000 kips and then increasing the load in 1000 kips increments. During the fourth stage, the bearings buckled laterally at a maximum load of 3550 kips. The load deflection curve is

shown in Fig. 9. It should be noted that the vertical displacement noted in this figure is the total displacement in two bearings. The margin against buckling of a single bearing is 28. Fig. 10 shows the bearings in their buckled form.

SEISMIC ISOLATION SYSTEM QUALIFICATION

Other programs planned to qualify the PRISM seismic isolation design include: tests of full size bearings, shake table performance tests to evaluate system performance during real earthquakes, and evaluation of the effects of input with strong long period energy, seismic hazard assessment, and the development of design guidelines (Glueckler et al., 1988). As part of this program, Argonne National Laboratory (ANL) is working with Shimizu Corporation of Japan on a joint U.S./Japanese program for testing scale size PRISM type bearings in a unique facility built by Shimizu at Tohoku University in Sendai, Japan. The features of this facility are described by Tamura et al., 1988. ANL's effort is funded by the National Science Foundation; the program is expected to last two years and the results will be reported by ANL. Additional work is in progress at ANL to develop nonlinear finite element models for the prediction of elastomeric bearing performance that can be used for optimization of the bearing geometry.

CONCLUSIONS

Several recent technological advancements and developments are responsible for making seismic isolation a practical design alternative for earthquake damage mitigation. One important factor has been the development of large test machines which can test large scale bearings under a variety of loading conditions up to failure. The results of these tests have given designers much more confidence in selecting the necessary design parameters while ensuring satisfactory performance for the largest possible earthquakes. The high performance margins of the PRISM bearings were demonstrated by the fact that the bearings were capable of sustaining several cycles of displacements four times the SSE without failure or damage. Furthermore no loss of stiffness or damping was observed under all applicable conditions. The high available margins beyond the SSE was clearly demonstrated. The test results confirmed that both bearing horizontal stiffness and damping were not affected by changes in the magnitude of vertical load or number of cycles of loading. The results of these tests and other planned tests will be used to further optimize the design of the PRISM bearings.

REFERENCES

- Berglund, R. C., Tippets, F. E., and Salerno, L. N. (1988). PRISM, A Safe, Economic, and Testable Liquid Metal Fast Breeder Reactor Plant. ANS Topical Meeting on Safety of Next Generation Power Reactors, Seattle.
- Glueckler, E. L., Tajirian, F. F., and Kelly, J. M. (1988). Seismic Isolation for a Modular Liquid Metal Reactor Concept (PRISM). ANS Topical Meeting on Safety of Next Generation Power Reactors, Seattle, Washington.
- Kelly, J. M. (1987). Recent Developments in Seismic Isolation. Seismic Engineering, Recent Advances in Design, Analysis, Testing and Qualification Method, ASME PVP-Vol 127.
- Kurihara, M., et al. (1987). Feasibility Study on the Seismic Isolation of Pool-Type LMFBR, 2. Development of a Rubber Bearing and a Friction Damper. SMIRT 9, Vol K2, Lausanne.
- Tajirian, F. F., and Schrag M. R. (1987). Conceptual Design of Seismic Isolation for the PRISM Liquid Metal Reactor. SMIRT 9, Vol K2, Lausanne.
- Tajirian, F. F., and Kelly, J. M. (1988). Testing of Seismic Isolation Bearings for Advanced Liquid Metal Reactor PRISM. Seismic, Shock, and Vibration Isolation, PVP Conference (ASME), Pittsburgh, Vol. 147, pp. 95-99.
- Tamura, K., Yamahara, H., and Izumi, M. (1988). Proof Tests of the Base-Isolated Building Using Full-Sized Model. Seismic, Shock, and Vibration Isolation, PVP Conference (ASME), Pittsburgh, Vol. 147, pp. 21-28.
- Tarcs, A. G., Way, D., and Kelly, J. M. (1984). The Implementation of Base Isolation for the Foothill Communities Law and Justice Center. A Report to the National Science Foundation.

Table 1 Half Cycle Large Horizontal Stiffness Tests

TEST NUMBER	VERTICAL LOAD PER BEARING (KIPS)	SHEAR STRAIN PERCENT	HORIZONTAL STIFFNESS (KIP/IN.)
1	70	108.1	9.4
2	70	133.4	9.8
3	70	153.1	***
4	140	107.9	8.7
5	140	133.4	9.2
6	210	108.2	8.4
7	210	133.0	9.2
8	280	107.8	8.5
9	280	133.6	9.2
10	280	158.6	9.9
11	350	160.4	9.6
12	420	161.3	9.4
13	420	175.9	9.5
14	420	197.8	9.4

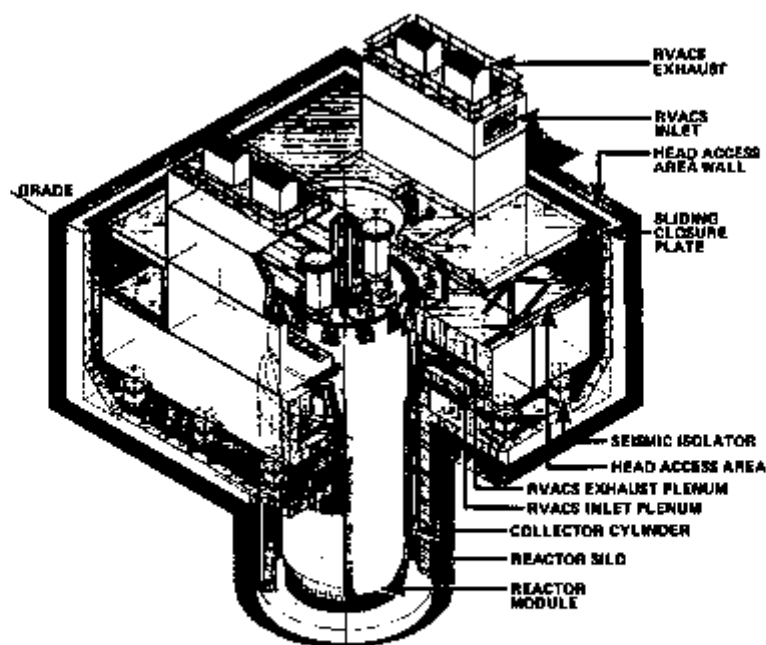


Fig. 1 PRISM Reactor Module

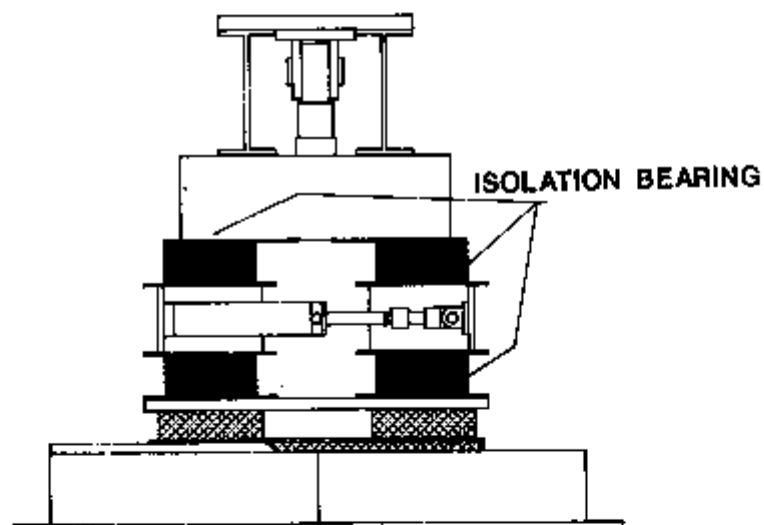


Fig. 2 EERC Test Fixture

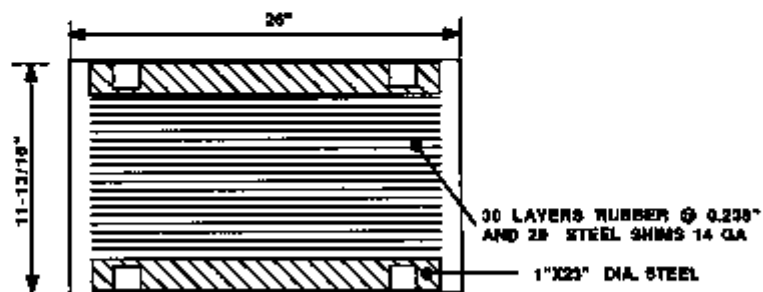


Fig. 3 Typical Half-Scale Bearing

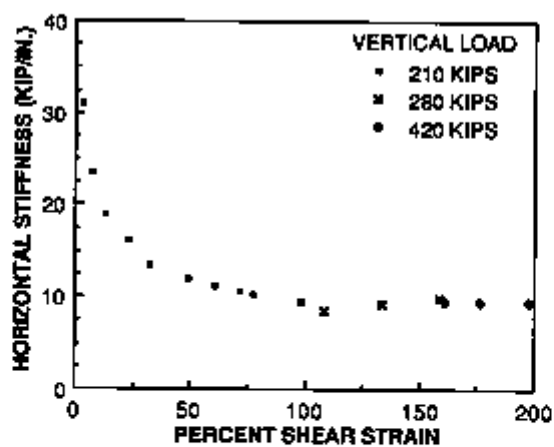


Fig. 4 Measured Horizontal Stiffness Versus Shear Strain



Fig. 5 Bearing Subjected to 420 Kips Vertical Load and 14.4 in. Displacement

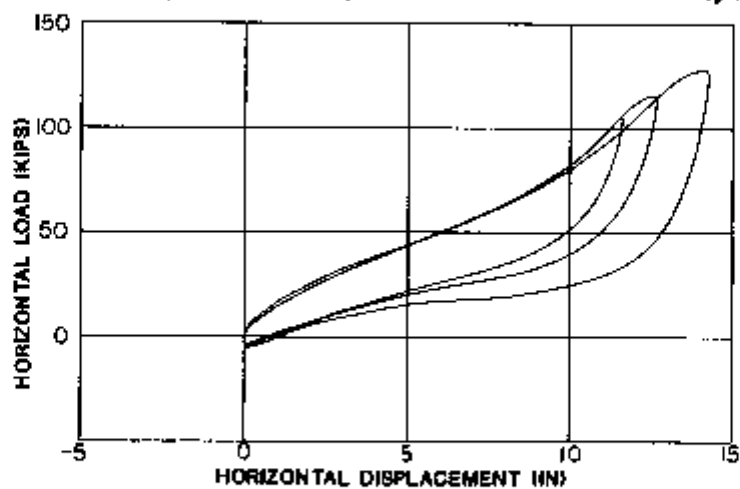


Fig. 6 Large Strain Hysteresis Loops

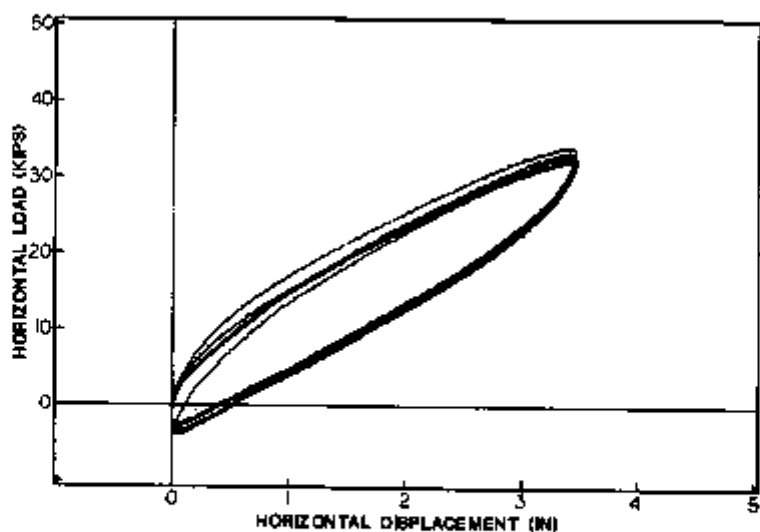


Fig. 7 Superposition of 50% Shear Strain Hysteresis Loops

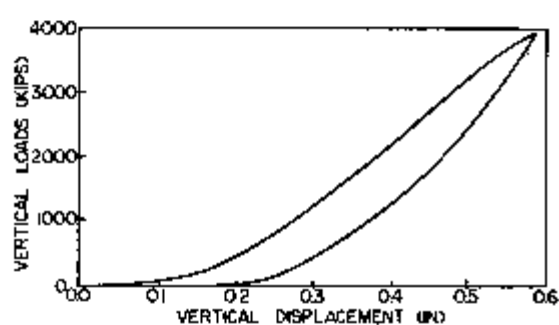


Fig. 8 Vertical Load versus Vertical Deflection for Single Bearing

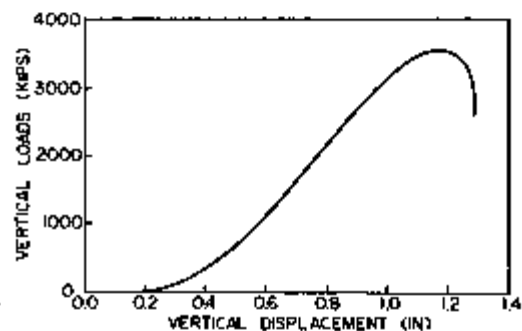


Fig. 9 Buckling Test Vertical Load versus Vertical Deflection

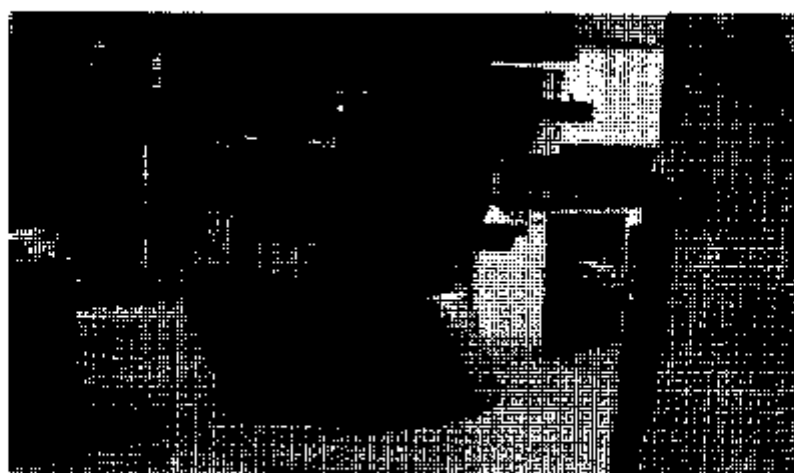


Fig. 10 Buckling of Bearings

Comparison of Seismic Isolation Concepts for FBR

H. Shiojiri, T. Mazda, H. Kasai

Central Research Institute of Electric Power Industry, Abiko, Japan

J. N. Kanda

University of Tokyo, Tokyo, Japan

T. Kubo

Nagoya Institute of Technology, Nagoya, Japan

M. Madokoro

Hitachi Ltd., Ibaraki, Japan

T. Shimomura

Mitsubishi Heavy Industries, Ltd., Kobe, Japan

Y. Kawamura

Toshiba Corporation, Yokohama, Japan

O. Nojima

Takenaka Komuten Company, Ltd., Tokyo, Japan

N. Kawai

Okumura Corporation, Tokyo, Japan

1. Introduction

Seismic isolation is expected to be effective in raising the reliability during earthquake, reducing the construction cost, enlarging the siting possibility, and promoting the design standardization for FBR.

A test and research program was started in 1987 (1), to verify the reliability and effectiveness of seismic isolation for FBR.

In this paper, some results of the preliminary study of the program are described.

First, seismic isolation concepts and corresponding seismic isolation devices were selected. Three kinds of seismically-isolated FBR plant concepts were developed by applying promising seismic isolation concepts to the non-isolated FBR plant, which was proposed in the past, and by developing plant component layout plans and building structural designs. Each plant was subjected to seismic response analysis, and on the basis of the results of their responses, reduction in the amount of material of components and buildings were estimated for each seismic isolation concepts. Furthermore, research and development items, which will be required on applying these seismic isolation concepts, were evaluated.

2. Selection of Candidate Seismic Isolation Concepts and Devices

2.1 Selection of Isolation Concepts

Possible seismic isolation concepts are classified by the scope of isolation as shown in Table 1. Of these concepts, concept ① through ⑥ correspond to component isolation, ⑦ and ⑧ to building isolation, and ⑨ and ⑩ to combined isolation. Since horizontal ground motion has dominant effect on the design of buildings and components, concepts in which buildings or some of components are isolated only in vertical direction were excluded.

(1) Building Isolation

At present, there are no effective isolation system which are capable of supporting a load of about 150,000 tons and at the same time achieving three-dimensional seismic isolation. Development of such a system will require many tasks such as devising an effective anti-rocking measure.

As for the horizontal seismic isolation of buildings, there exist LWR plants (Cruas and Koeberg) which adopt such system in addition to some experiences of conventional buildings in and out of Japan. It is expected to allow material reduction of building structure and many components. Hence the horizontal seismic isolation of buildings (⑦ of Table 1) was selected for the present investigation.

(2) Component Isolation

It was considered inadequate to use three dimensional isolation devices, since it will be difficult to adjust them in such a way to avoid rocking, since the isolation devices may have material or geometric nonlinearity. It is also difficult to obtain the optimal horizontal and vertical isolation properties since the horizontal and vertical vibrations are coupled with each other.

In the present investigation, concepts for seismically isolating the primary system alone (① and ③ of Table 1) were examined. Evaluation of concepts of which seismic isolation covers both primary and secondary systems were made by reflecting the findings of the combined isolation described next subsection.

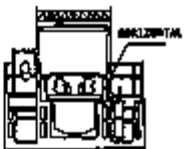
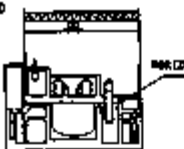
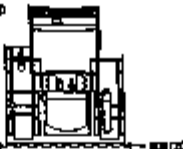

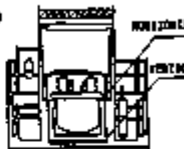
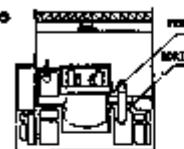
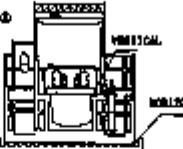
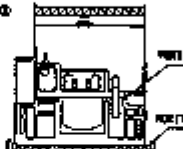
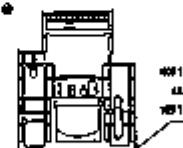
(3) Combined Isolation

The building is given a horizontal isolation for the reason stated above. Hence components are given a vertical isolation.

As the seismic isolation of the primary system is mainly examined in component isolation, a system for vertical isolation of the primary and secondary systems (④ of Table 1) is examined in combined isolation.

This system prevents any relative displacement of the sodium system piping. (④ of Table 1)

TABLE 1 CANDIDATE ISOLATION CONCEPT

ISOLATION TYPE	NO ISOLATION	COMPONENT ISOLATION		BUILDING ISOLATION
		PRIMARY COMPONENT	SECONDARY COMPONENT	BUILDING
NO ISOLATION	NO-ISOLATION PLANT	① 	② 	③ 
COMPONENT ISOLATION	PRIMARY COMPONENT	④  ⑤ 	⑥ 	⑦ 
	SECONDARY COMPONENT			⑧ 
BUILDING ISOLATION	BUILDING			⑨ 

2.2 Seismic Isolation Devices

(1) Devices for Horizontal Isolation of Buildings

The basic requirements of a device for horizontal isolation of buildings are that the device has a large capacity sufficient to bear the building weight, that the device has a high vertical rigidity and a low horizontal rigidity and that devices are reliable and durable. Furthermore, the device needs to have a large deformability which can cope with a relative displacement, since a relative displacement of several tens of centimeters is expected. Since the device is placed in an outdoor environment, any special high temperature or radiation are not expected.

At present, a laminated elastomer is most appropriate as a spring or a load-bearing device which meets all of basic requirements, in terms of reliability, load-bearing capacity, stiffness, deformability, and durability.

Since laminated elastomers does not have the damping capability, a combined use of some damping devices (dampers) is required. Possible separated dampers include hysteresis type dampers (elasto-plastic dampers, a friction damper, and combination of the two) and viscous type dampers (an oil damper and a viscous damper). The formers are generally simple in construction and inexpensive, and have excellent weatherability and durability. On the other hand, viscous type dampers have larger damping capability and have an excellent acceleration-reducing effect since their load-displacement curves are smooth and they do not excite high frequencies in components. Oil dampers have advantages in that their characteristics are independent of the frequency and amplitude. However, as one device has its damping effect in only one direction, many devices are needed. Furthermore, the oil dampers have a larger construction and are expensive in comparison with elasto-plastic dampers. Viscous dampers, in general, have a high temperature-dependency, and extra care is needed in maintenance to assure a long-term reliability. In general, the deformability of dampers is significantly less than that of laminated elastomers.

The laminated elastomer with lead plug and the laminated high-damping rubber bearing have damping capacity, in addition to the above-mentioned properties of a laminated elastomer. It is compact and allows easier arrangement and installation.

For the present study, the laminated elastomers with damping capability were selected.

(2) Devices for Horizontal Isolation of Components

The basic requirements of the devices for horizontal isolation of components are generally identical to those of the devices for horizontal isolation of buildings. In comparison with the devices for buildings, however, the devices for components are required to be more compact and have a smaller relative displacement, since their installation space is limited. The environmental conditions such as temperature and radiation are more severe.

Combinations of slide supports and coil springs are compact and have excellent environmental properties, but they pose problems of a large dispersion of friction coefficient, and of excitation of high frequencies in components. On the other hand, the laminated elastomer may be applicable, provided that the arrangement plan, radiation shielding design, and air conditioning design are made appropriately.

In the present study, the laminated elastomer with lead plug is under investigation.

(3) Devices for Vertical Isolation of Components

The basic performance requirements of a device for vertical isolation of components are to lower the vertical natural frequency, and to damp the vibration, as well as to bear the load. Smaller flexural displacement response

of the vertically-isolated floors are desirable.

To achieve them, it is necessary to have a relatively smooth load-displacement relationship and to achieve fabrication with small variation of the properties from the design values.

As for a spring or a load bearing device, the coil spring was selected on the ground that there are many experience and the dispersion of the properties are small and that it is compact and inexpensive.

As for the damping device, the oil damper is selected, since it is excellent in vibration characteristics, damping capability and fatigue characteristics. In the case of vertical isolation, it is sufficient to be effective in one direction only. In contrast with the oil damper, elastoplastic dampers are compact and inexpensive, but yielding points of dampers can scatter and rather abrupt change of stiffness at the point can excite flexural vibration of the floor. The friction damper, at present, has large variation in its characteristics, and is not selected.

3. Evaluation of Isolation Concepts

Response reduction, relative displacement, material reduction, and necessary technical development item were selected as the items for evaluating the applicability of a seismic isolation system to FBR plants.

To make a comparative evaluation of various systems under the same conditions, the seismically-isolated FBR with respective isolation systems were set according to the following rules, on the basis of a 1000 MWe semi-underground non-isolated FBR system.

- I) Each seismically-isolated FBR is to be installed on the ground surface.
- II) The structure of the proposed FBR is to be modified to allow the introduction of the isolation system and to enhance its effects. However, no modification of the structure of any systems or components irrelevant to the introduction of the isolation system will be made.

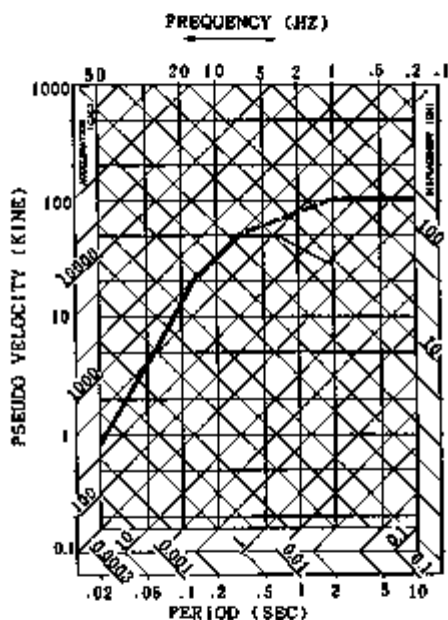


Fig. 3 TENTATIVE DESIGN
RESPONSE SPECTRUM

Table 2 RESPONSE OF ISOLATED PLANTS TO S1 EARTHQUAKE

ITEM		BUILDING ISOLATION	COMPONENT ISOLATION		COMBINED ISOLATION
			HORIZONTAL	HORIZONTAL AND VERTICAL	
DEVICE CHARACTERISTICS	NATURAL FREQUENCY	0.5 Hz	1.0 Hz	HORIZONTAL 1.0 Hz VERTICAL 1.5 Hz	HORIZONTAL 0.5 Hz VERTICAL 1.5 Hz
	DAMPING			VERTICAL 30%	VERTICAL 30%
	YIELDING ACCEL.	5.0 GAL	1.0 GAL	HORIZONTAL 1.0 GAL	HORIZONTAL 1.0 GAL
MAX. RESPONSE ACCEL. AT REACTOR SUPPORT		21.6 GAL	3.3 GAL	HORIZONTAL 3.3 GAL VERTICAL 1.75 GAL	HORIZONTAL 2.17 GAL VERTICAL 1.7 GAL
MAX. RELATIVE DISP.		1.8 cm	6.1 cm	HORIZONTAL 6.1 cm VERTICAL 1.7 cm	HORIZONTAL 1.8 cm VERTICAL 1.7 cm

TABLE 3 FINDINGS OF EVALUATION OF RATIONALIZING EFFECTS AND APPLICABILITY

SYSTEM	BUILDING ISOLATION	COMBINED ISOLATION		COMPONENT ISOLATION				REMARKS	
SEMI-SEPTAL	BUILDING	BUILDING	BUILDING	PRIMARY SYSTEM	PRIMARY SYSTEM	PRIMARY + SECONDARY SYSTEM	PRIMARY + SECONDARY SYSTEM		
DIRECTION	VERTICAL	PRIMARY SYSTEM	PRIMARY + SECONDARY SYSTEM	PRIMARY SYSTEM	PRIMARY SYSTEM	PRIMARY SYSTEM	PRIMARY SYSTEM		
MATERIAL REDUCTION	REACTION TIME (SEE WALL)	IT IS POSSIBLE TO REDUCE THE WALL THICKNESS OF THE REACTION TIME TO 1/2 TO 1/4 BY ADOPTING BRIDGE ISOLATION.	30 MM APPROX.	25 MM APPROX.	30 MM APPROX.	25 MM APPROX.	30 MM APPROX.	25 MM APPROX.	VERTICAL ISOLATION EFFECT IS SMALL.
	REACTION TIME (BOTTOM)	30 MM APPROX.	25 MM APPROX.	25 MM APPROX.	30 MM APPROX.	25 MM APPROX.	30 MM APPROX.	25 MM APPROX.	IF BY HORIZONTAL ISOLATION, REDUCTION OF ABOUT 1/4 INCH VERTICAL ISOLATION IS COMBINED.
	BOO FLOOR	125 MM APPROX.	25 MM APPROX.	25 MM APPROX.	125 MM APPROX.	25 MM APPROX.	125 MM APPROX.	25 MM APPROX.	EFFECT OF VERTICAL ISOLATION ON BOO FLOOR REACTION TIME IS GREAT. EFFECTS ON BOO TYPE ARE SMALL.
	VERTICAL ISOLATION (HWT)	IT IS POSSIBLE TO REDUCE THE WALL THICKNESS TO ABOUT ONE THIRD BY ADOPTING BRIDGE ISOLATION.	40 MM APPROX.	40 MM APPROX.	40 MM APPROX.	40 MM APPROX.	40 MM APPROX.	40 MM APPROX.	VERTICAL ISOLATION EFFECT IS SMALL.
	QUANTITY OF BUILDING MATERIALS	UPPER BUILDING: 1.000, LOWER FOUNDATION: 1.000	UPPER BUILDING: 1.000, LOWER FOUNDATION: 1.000	UPPER BUILDING: 1.000, LOWER FOUNDATION: 1.000	UPPER BUILDING: 1.000, LOWER FOUNDATION: 1.000	UPPER BUILDING: 1.000, LOWER FOUNDATION: 1.000	UPPER BUILDING: 1.000, LOWER FOUNDATION: 1.000	UPPER BUILDING: 1.000, LOWER FOUNDATION: 1.000	BUILDING ISOLATION REDUCES CONCRETE QUANTITY ABOUT 30% IN BOO FLOOR TYPE. FRAME QUANTITY.
	CONCRETE (C1)	1.000	1.000	1.000	1.000	1.000	1.000	1.000	
	STEEL FRAME (C1)	1.000	1.000	1.000	1.000	1.000	1.000	1.000	
	STEEL FRAME (C2)	1.000	1.000	1.000	1.000	1.000	1.000	1.000	
	STEEL FRAME (C3)	1.000	1.000	1.000	1.000	1.000	1.000	1.000	
	STEEL FRAME (C4)	1.000	1.000	1.000	1.000	1.000	1.000	1.000	
STEEL FRAME (C5)	1.000	1.000	1.000	1.000	1.000	1.000	1.000		
STEEL FRAME (C6)	1.000	1.000	1.000	1.000	1.000	1.000	1.000		
STEEL FRAME (C7)	1.000	1.000	1.000	1.000	1.000	1.000	1.000		
STEEL FRAME (C8)	1.000	1.000	1.000	1.000	1.000	1.000	1.000		
STEEL FRAME (C9)	1.000	1.000	1.000	1.000	1.000	1.000	1.000		
STEEL FRAME (C10)	1.000	1.000	1.000	1.000	1.000	1.000	1.000		
STEEL FRAME (C11)	1.000	1.000	1.000	1.000	1.000	1.000	1.000		
STEEL FRAME (C12)	1.000	1.000	1.000	1.000	1.000	1.000	1.000		
STEEL FRAME (C13)	1.000	1.000	1.000	1.000	1.000	1.000	1.000		
STEEL FRAME (C14)	1.000	1.000	1.000	1.000	1.000	1.000	1.000		
STEEL FRAME (C15)	1.000	1.000	1.000	1.000	1.000	1.000	1.000		
STEEL FRAME (C16)	1.000	1.000	1.000	1.000	1.000	1.000	1.000		
STEEL FRAME (C17)	1.000	1.000	1.000	1.000	1.000	1.000	1.000		
STEEL FRAME (C18)	1.000	1.000	1.000	1.000	1.000	1.000	1.000		
STEEL FRAME (C19)	1.000	1.000	1.000	1.000	1.000	1.000	1.000		
STEEL FRAME (C20)	1.000	1.000	1.000	1.000	1.000	1.000	1.000		
STEEL FRAME (C21)	1.000	1.000	1.000	1.000	1.000	1.000	1.000		
STEEL FRAME (C22)	1.000	1.000	1.000	1.000	1.000	1.000	1.000		
STEEL FRAME (C23)	1.000	1.000	1.000	1.000	1.000	1.000	1.000		
STEEL FRAME (C24)	1.000	1.000	1.000	1.000	1.000	1.000	1.000		
STEEL FRAME (C25)	1.000	1.000	1.000	1.000	1.000	1.000	1.000		
STEEL FRAME (C26)	1.000	1.000	1.000	1.000	1.000	1.000	1.000		
STEEL FRAME (C27)	1.000	1.000	1.000	1.000	1.000	1.000	1.000		
STEEL FRAME (C28)	1.000	1.000	1.000	1.000	1.000	1.000	1.000		
STEEL FRAME (C29)	1.000	1.000	1.000	1.000	1.000	1.000	1.000		
STEEL FRAME (C30)	1.000	1.000	1.000	1.000	1.000	1.000	1.000		
STEEL FRAME (C31)	1.000	1.000	1.000	1.000	1.000	1.000	1.000		
STEEL FRAME (C32)	1.000	1.000	1.000	1.000	1.000	1.000	1.000		
STEEL FRAME (C33)	1.000	1.000	1.000	1.000	1.000	1.000	1.000		
STEEL FRAME (C34)	1.000	1.000	1.000	1.000	1.000	1.000	1.000		
STEEL FRAME (C35)	1.000	1.000	1.000	1.000	1.000	1.000	1.000		
STEEL FRAME (C36)	1.000	1.000	1.000	1.000	1.000	1.000	1.000		
STEEL FRAME (C37)	1.000	1.000	1.000	1.000	1.000	1.000	1.000		
STEEL FRAME (C38)	1.000	1.000	1.000	1.000	1.000	1.000	1.000		
STEEL FRAME (C39)	1.000	1.000	1.000	1.000	1.000	1.000	1.000		
STEEL FRAME (C40)	1.000	1.000	1.000	1.000	1.000	1.000	1.000		
STEEL FRAME (C41)	1.000	1.000	1.000	1.000	1.000	1.000	1.000		
STEEL FRAME (C42)	1.000	1.000	1.000	1.000	1.000	1.000	1.000		
STEEL FRAME (C43)	1.000	1.000	1.000	1.000	1.000	1.000	1.000		
STEEL FRAME (C44)	1.000	1.000	1.000	1.000	1.000	1.000	1.000		
STEEL FRAME (C45)	1.000	1.000	1.000	1.000	1.000	1.000	1.000		
STEEL FRAME (C46)	1.000	1.000	1.000	1.000	1.000	1.000	1.000		
STEEL FRAME (C47)	1.000	1.000	1.000	1.000	1.000	1.000	1.000		
STEEL FRAME (C48)	1.000	1.000	1.000	1.000	1.000	1.000	1.000		
STEEL FRAME (C49)	1.000	1.000	1.000	1.000	1.000	1.000	1.000		
STEEL FRAME (C50)	1.000	1.000	1.000	1.000	1.000	1.000	1.000		
STEEL FRAME (C51)	1.000	1.000	1.000	1.000	1.000	1.000	1.000		
STEEL FRAME (C52)	1.000	1.000	1.000	1.000	1.000	1.000	1.000		
STEEL FRAME (C53)	1.000	1.000	1.000	1.000	1.000	1.000	1.000		
STEEL FRAME (C54)	1.000	1.000	1.000	1.000	1.000	1.000	1.000		
STEEL FRAME (C55)	1.000	1.000	1.000	1.000	1.000	1.000	1.000		
STEEL FRAME (C56)	1.000	1.000	1.000	1.000	1.000	1.000	1.000		
STEEL FRAME (C57)	1.000	1.000	1.000	1.000	1.000	1.000	1.000		
STEEL FRAME (C58)	1.000	1.000	1.000	1.000	1.000	1.000	1.000		
STEEL FRAME (C59)	1.000	1.000	1.000	1.000	1.000	1.000	1.000		
STEEL FRAME (C60)	1.000	1.000	1.000	1.000	1.000	1.000	1.000		
STEEL FRAME (C61)	1.000	1.000	1.000	1.000	1.000	1.000	1.000		
STEEL FRAME (C62)	1.000	1.000	1.000	1.000	1.000	1.000	1.000		
STEEL FRAME (C63)	1.000	1.000	1.000	1.000	1.000	1.000	1.000		
STEEL FRAME (C64)	1.000	1.000	1.000	1.000	1.000	1.000	1.000		
STEEL FRAME (C65)	1.000	1.000	1.000	1.000	1.000	1.000	1.000		
STEEL FRAME (C66)	1.000	1.000	1.000	1.000	1.000	1.000	1.000		
STEEL FRAME (C67)	1.000	1.000	1.000	1.000	1.000	1.000	1.000		
STEEL FRAME (C68)	1.000	1.000	1.000	1.000	1.000	1.000	1.000		
STEEL FRAME (C69)	1.000	1.000	1.000	1.000	1.000	1.000	1.000		
STEEL FRAME (C70)	1.000	1.000	1.000	1.000	1.000	1.000	1.000		
STEEL FRAME (C71)	1.000	1.000	1.000	1.000	1.000	1.000	1.000		
STEEL FRAME (C72)	1.000	1.000	1.000	1.000	1.000	1.000	1.000		
STEEL FRAME (C73)	1.000	1.000	1.000	1.000	1.000	1.000	1.000		
STEEL FRAME (C74)	1.000	1.000	1.000	1.000	1.000	1.000	1.000		
STEEL FRAME (C75)	1.000	1.000	1.000	1.000	1.000	1.000	1.000		
STEEL FRAME (C76)	1.000	1.000	1.000	1.000	1.000	1.000	1.000		
STEEL FRAME (C77)	1.000	1.000	1.000	1.000	1.000	1.000	1.000		
STEEL FRAME (C78)	1.000	1.000	1.000	1.000	1.000	1.000	1.000		
STEEL FRAME (C79)	1.000	1.000	1.000	1.000	1.000	1.000	1.000		
STEEL FRAME (C80)	1.000	1.000	1.000	1.000	1.000	1.000	1.000		
STEEL FRAME (C81)	1.000	1.000	1.000	1.000	1.000	1.000	1.000		
STEEL FRAME (C82)	1.000	1.000	1.000	1.000	1.000	1.000	1.000		
STEEL FRAME (C83)	1.000	1.000	1.000	1.000	1.000	1.000	1.000		
STEEL FRAME (C84)	1.000	1.000	1.000	1.000	1.000	1.000	1.000		
STEEL FRAME (C85)	1.000	1.000	1.000	1.000	1.000	1.000	1.000		
STEEL FRAME (C86)	1.000	1.000	1.000	1.000	1.000	1.000	1.000		
STEEL FRAME (C87)	1.000	1.000	1.000	1.000	1.000	1.000	1.000		
STEEL FRAME (C88)	1.000	1.000	1.000	1.000	1.000	1.000	1.000		
STEEL FRAME (C89)	1.000	1.000	1.000	1.000	1.000	1.000	1.000		
STEEL FRAME (C90)	1.000	1.000	1.000	1.000	1.000	1.000	1.000		
STEEL FRAME (C91)	1.000	1.000	1.000	1.000	1.000	1.000	1.000		
STEEL FRAME (C92)	1.000	1.000	1.000	1.000	1.000	1.000	1.000		
STEEL FRAME (C93)	1.000	1.000	1.000	1.000	1.000	1.000	1.000		
STEEL FRAME (C94)	1.000	1.000	1.000	1.000	1.000	1.000	1.000		
STEEL FRAME (C95)	1.000	1.000	1.000	1.000	1.000	1.000	1.000		
STEEL FRAME (C96)	1.000	1.000	1.000	1.000	1.000	1.000	1.000		
STEEL FRAME (C97)	1.000	1.000	1.000	1.000	1.000	1.000	1.000		
STEEL FRAME (C98)	1.000	1.000	1.000	1.000	1.000	1.000	1.000		
STEEL FRAME (C99)	1.000	1.000	1.000	1.000	1.000	1.000	1.000		
STEEL FRAME (C100)	1.000	1.000	1.000	1.000	1.000	1.000	1.000		
STEEL FRAME (C101)	1.000	1.000	1.000	1.000	1.000	1.000	1.000		
STEEL FRAME (C102)	1.000	1.000	1.000	1.000	1.000	1.000	1.000		
STEEL FRAME (C103)	1.000	1.000	1.000	1.000	1.000	1.000	1.000		
STEEL FRAME (C104)	1.000	1.000	1.000	1.000	1.000	1.000	1.000		
STEEL FRAME (C105)	1.000	1.000	1.000	1.000	1.000	1.000	1.000		
STEEL FRAME (C106)	1.000	1.000	1.000	1.000	1.000	1.000	1.000		
STEEL FRAME (C107)	1.000	1.000	1.000	1.000	1.000	1.000	1.000		
STEEL FRAME (C108)	1.000	1.000	1.000	1.000	1.000	1.000	1.000		
STEEL FRAME (C109)	1.000	1.000	1.000	1.000	1.000	1.000	1.000		
STEEL FRAME (C110)	1.000	1.000	1.000	1.000	1.000	1.000	1.000		
STEEL FRAME (C111)	1.000	1.000	1.000	1.000	1.000	1.000	1.000		
STEEL FRAME (C112)	1.000	1.000	1.000	1.000	1.000	1.000	1.000		
STEEL FRAME (C113)	1.000	1.000	1.000	1.000	1.000	1.000	1.000		
STEEL FRAME (C114)	1.000	1.000	1.000	1.000	1.000	1.000	1.000		
STEEL FRAME (C115)	1.000	1.000	1.000	1.000	1.000	1.000	1.000		
STEEL FRAME (C116)	1.000	1.000	1.000	1.000	1.000	1.000	1.000		
STEEL FRAME (C117)	1.000	1.000	1.000	1.000	1.000	1.000	1.000		
STEEL FRAME (C118)	1.000	1.000	1.000	1.000	1.000	1.000	1.000		
STEEL FRAME (C119)	1.000	1.000	1.000	1.000	1.000	1.000	1.000		
STEEL FRAME (C120)	1.000	1.000	1.000	1.000	1.000	1.000	1.000		
STEEL FRAME (C121)	1.000	1.000	1.000	1.000	1.000	1.000	1.000		
STEEL FRAME (C122)	1.000	1.000	1.000	1.000	1.000	1.000	1.000		
STEEL FRAME (C123)	1.000	1.000	1.000	1.000	1.000	1.000	1.000		
STEEL FRAME (C124)	1.000	1.000	1.000	1.000	1.000	1.000	1.000		
STEEL FRAME (C125)	1.000	1.000	1.000	1.000	1.000	1.000	1.000		
STEEL FRAME (C126)	1.000	1.000	1.000	1.000	1.000	1.000	1.000		

The resulting seismically-isolated plants of the respective systems were subjected to response analysis to evaluate their response characteristics. The design spectrum for horizontal ground motion is shown in Fig 1. The ratio of the vertical component spectrum to the horizontal one was assumed to be 0.6 (Ishida, 1989). The results are shown in Table 2.

On the basis of these findings, each isolation system was examined in terms of its material reduction effects, its applicability, and technical tasks to be examined in the future. A comparative evaluation was shown in Table 3.

The findings may be summarized as follows:

(i) As for horizontal isolation, building isolation, component isolation and combined isolation are virtually identical in terms of material reduction of isolated portions and improvement of the reliability of such portions. The wider the scope of the isolation, the greater the material reduction and the reliability improving effects.

(ii) The material reduction due to vertical isolation are relatively small. Expected effects are reduction relative displacement between the core and control rods, prevention of lifting of the core elements, and reduction of axial compression of vessels.

(iii) As for the relative displacement, it is expected to be accommodated by deformation of the piping in each isolation system. However, when the primary system components only are isolated, it will be necessary to make detailed investigation of methods for accommodating relative displacements of the secondary cooling system piping, which contains sodium, and fuel handling systems.

(iv) Required R & D items are relatively few for building isolation. Component isolation needs some measures for shielding and air conditioning of the seismic isolation elements. The addition of vertical isolation will add more R & D items, such as the reliability of vertical isolation elements, and confirmation of performance of vertical isolation mechanisms.

4. Conclusion

Isolation concepts were evaluated. As a preliminary study for applying seismic isolation to FBR,

At present, horizontal building isolation requires the smallest number of R & D items, and is expected to have ample cost reduction effects. It, therefore, is considered to have a high feasibility. Furthermore, there is a good prospect of fabricating isolation devices with appropriate properties.

The present research was conducted under a contract given by the Ministry of International Trade and Industry.

5. References

- [1] Sawada Y. et al., 1989, " Seismic Isolation Test Program ", Trans. 10th SMIRT, to appear.
- [2] Ishida, E. et al., 1989, " Tentative Design Response Spectrum for Seismically Isolated FBR ", Trans. 10th SMIRT, to appear.

Seismic Analysis of Sliding Structures

D. Brochard, F. Gantenbein
CEA-CEN Saclay, Gif sur Yvette, France

1. INTRODUCTION

To limit the seism effects, structures may be base isolated. A sliding system located between the structure and the support allows differential motion between them.

The aim of this paper is the presentation of the method to calculate the response of the structure when the structure is represented by its eigenmodes, and the sliding phenomenon by the Coulomb friction model. Finally, an application to a simple structure shows the influence on the response of the main parameters (friction coefficient, stiffness,...).

2. COULOMB FRICTION MODEL

Let us consider a stiff mass, layed on an horizontal support and submitted to an external force F_e (parallel to the support). When F_e is smaller than a limit force F_0 , there is no differential motion between the support and the mass and the friction force balances the external force. The limit force is written: $F_0 = \mu F_n$ where μ is the friction coefficient and F_n the modulus of the normal force applied by the mass to the support (in this case, F_n is equal to the weight of the mass). When F_e increases and becomes equal to F_0 , sliding begins and the friction force F_f is directed in the opposite sense of the velocity, and is expressed as:

$$|F_f| = \mu F_n = F_0$$

3. EQUATIONS OF MOTION

Let us study the behaviour of a structure sliding on its seismically excited support. We are studying the case of a one contact point between the structure and its support.

The motion (absolute displacement X_a) of the structure may be expressed in the following way:

$$X_a(t) = Y_0(t) U + X(t)$$

where $Y_0(t)$ is the support motion, U a unit vector in the direction of the excitation and $X(t)$ the relative displacement (including the sliding) of the structure with respect to the support, which will be expanded on the basis of the eigenmodes of the structure. The boundary condition changes whether there is

sliding or not and we have chosen to use the basis corresponding to free boundary conditions at the contact point.

The equations of motion are derived in the same way as for the impact problems ([2] and [3]). For the modal coefficients, we obtain harmonic oscillators equations, coupled through the projection of the link force on each eigenmode. As for the seismic analysis, we are mainly interested by the low frequency behaviour of the structure, the modal basis is truncated and we keep only the first few eigen modes. The neglected high-order modes are supposed to have a static response. The set of equations to be solved are the following:

$$M \ddot{\alpha} + C \dot{\alpha} + K \alpha + B^T F_t = - \gamma_0 Q \quad (\gamma_0 = \ddot{y}_0)$$

- during a sliding phase:

$$F_t = \mu F_n \text{Sign}(\dot{B}\alpha)$$

- during a grip phase:

$$|F_t| < \mu F_n$$

$$\text{and } B\alpha + K_L^{-1} F_t = X_G$$

where: - M (resp K) is the diagonal generalised (resp stiffness) matrix
 - C is the modal damping matrix (assumed to be diagonal)
 - F_t is the link force
 - B a line matrix allowing to calculate the displacement of the contact point
 - Q is the vector of the generalised displacements
 - α the vector of the modal coefficients
 - K_L is the stiffness of the neglected high order modes, evaluated at the contact point
 - X_G is the sliding of the contact point at the end of the former sliding phase.

The last equation means that during the grip phase, due to the truncation, there is a relative displacement between the structure and its support at the contact point. The amplitude of this displacement will decrease when the number of modes in the basis will increase. Such effects due to the truncation has been observed for impact problems [2], [3], [4].

4. APPLICATION

The aim of this application is to study the behaviour of a simple structure sliding on its support (fig. 1) and to determine the influence of some important parameters like the friction coefficient, the stiffness and the characteristics of the structure.

First, we shall consider a rigid structure which will be represented by a mass m_t sliding on a support. Then we will study the behaviour of a structure which response is mainly influenced by one eigenmode. The structure will be represented by a 2 DOF model (fig. 1) composed of a sliding mass m_2 linked by a spring of stiffness k to another mass m_1 . The mass m_2 represents the mass of the

sliding stiff basis and the frequency $f_0 = \frac{1}{2\pi} \sqrt{k/m_1}$ is this first eigenfrequency of the structure with its basis clamped on the support, m_1 being the associated modal mass. Such model is fully described by its total mass $m_1 + m_2$, the ratio $r = m_2/m_1$ which represents the mass repartition and the frequency f_0 . When the mass m_2 is free, the model has two eigenmodes, the first one is the

rigid body motion (translation parallel to the support) and the second one corresponds to an opposite vibration of m_1 and m_2 with a frequency equal to: $f_1 = f_0[(1+r)/r]^{0.5}$.

The system is excited by the San Francisco seism normalized to 0.1 g. The parametric study has been performed for different values of the friction coefficient μ , the ratio r , and the frequency f_0 .

The modal damping coefficients of the free structure are equal to 2% and as the modal basis is complete, the stiffness K_L has no physical sense, and is chosen so that the frequency of the system linked with the spring K_L is far enough from the frequency range of interest.

Results

Only the main results are presented in this paper (see [5] for a detailed analysis).

We can observe that:

- it exists a residual sliding at the end of the excitation (fig. 2).
- the maximal value of the sliding decreases when μ increases; the stiffness of the structure increases the sliding in comparison with a sliding mass alone. This phenomenon is more sensitive for r small (fig. 3).
- in the case of the sliding mass alone for $\mu > 0.1$, there is no sliding and the Response Spectrum (fig. 4) of the sliding mass is equal to the excitation spectrum (except the peak at 55 Hz due to the modelisation of the grip phase with a spring). For $\mu = 0.01$, the spectrum is below the excitation spectrum and for intermediate values the spectrum of the sliding mass may be over the excitation one.
- for a deformable structure for small values of μ (0.01) a peak appears at the frequency f_1 of the 2nd eigenmode of the free structure (fig. 5, for $f_0 = 6$ Hz and $r = 0.5$, this peak is at 10.4 Hz). This peak may be observed on the response spectrum of the mass m_2 .
- the maximal value γ_{m_1} of the absolute acceleration of the mass m_1 as a function of the frequency f_0 represents the spectrum of an equivalent excitation taking into account the sliding phenomenon [6], [7]. γ_{m_1} is always smaller than the value corresponding to the clamped basis and the reduction increases when the ratio r becomes small (fig. 6).

5. CONCLUSION

This study has shown in a simple case the influence of the sliding and of the characteristics of structure on its response. The sliding reduces strongly the level of response and the stiffness of the structure amplifies the sliding.

For future studies, it would be interesting first to calculate the response of a structure having some high order modes located in the frequency range where there is an amplification due to the non linearity and to analyse the case of a more complex structure having several points of contact with the support where the sliding may occur independently.

REFERENCES

- [1] Antunes, J., Axiss, F., Beauffils, B., Guilbaud, D. Coulomb Friction Modeling in Numerical Simulation of Vibrations and Weir Work Rate of Multispan tube Bundles. Winter annual meeting ASME, Chicago, Dec. 1988, Vol. 5.
- [2] Brochard, D., Buland, P., Gantenbein, F., Gibert, R.J. Seismic Analysis of LMFBR Cores, Mock-up Rapsodie. SMIRT 9, Lausanne, 17-21 August 1987, Vol. E, pp. 33-42.
- [3] Brochard, D., Gantenbein, F., Gibert, R.J. Seismic Behaviour of LMFBR Cores. SMIRT 8 (Brussels 19-23 August 1985) EK 2/2.
- [4] Queval, J.C., Brochard, D. Analysis of Impact Phenomenon between PWR Fuel Assemblies in Earthquake Situations. PVP Pittsburgh, June 1988, Vol. 145.
- [5] Brochard, D., Gantenbein, F. Analyse sismique des structures glissant sur leur base. 2^{ème} Colloque national de Génie Parasismique et aspects vibratoires dans le Génie Civil, St-Rémy-lès-Chavreaux (FRANCE), 18-20 avril 1989.
- [6] Mostaghel, M., Tambakuchi, J. Response of Sliding Structures to Earthquake Support Motion. Earthquake Engineering and Structural Dynamics, Vol. II, 729-748 (1983).
- [7] Constantinou, M., Tadjibakhsh, F.G. Response of a Sliding Structure to Filtered Random Excitation. J. Structural Mechanics, 12 (3) 401-418 (1984).

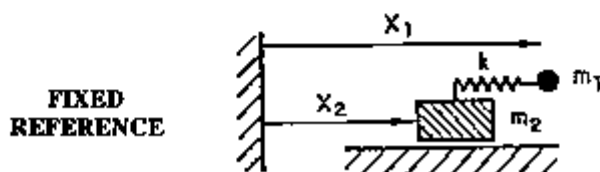


Fig.1 2 DOF model

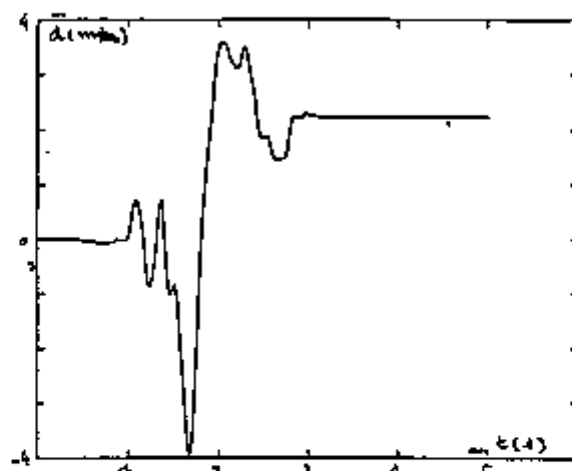


Fig. 2 Sliding mass displacement

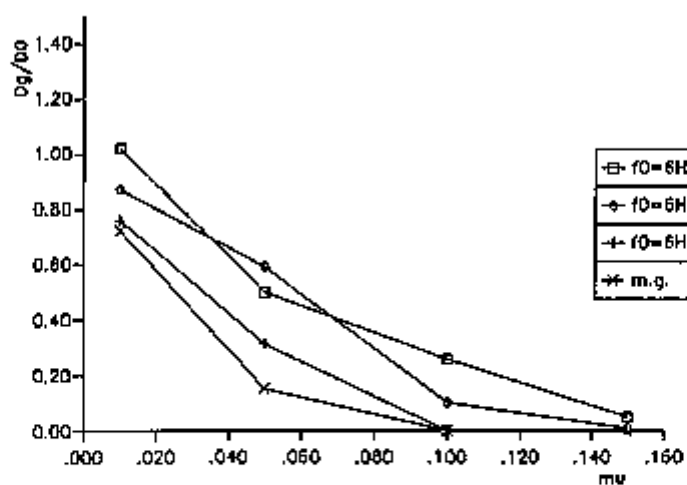


Fig. 3 Maximal sliding
(D_0 evaluation of $\max(Y_0(t))$)

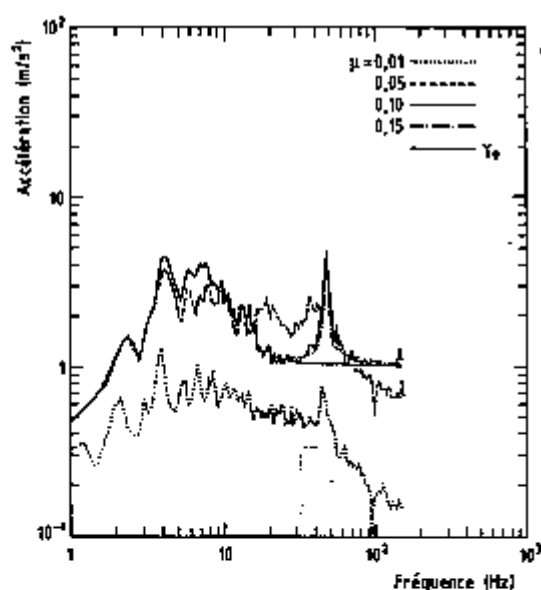


Fig. 4 Response spectrum of sliding mass.

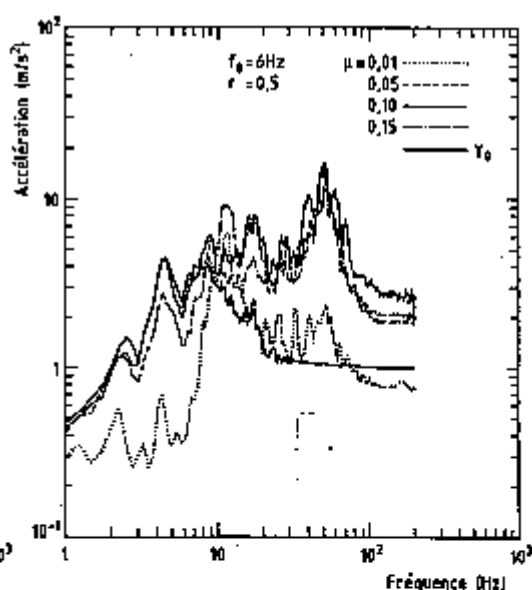


Fig. 5 Response spectrum of mass m_2

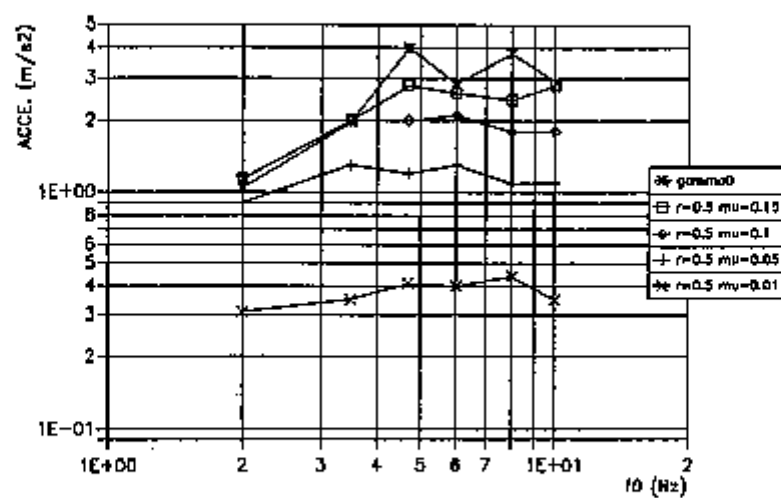


Fig. 6 Maximal absolute acceleration m_j

Subduing the Structural Shakes

Satya S. Sharma, Eddy L. Mercurio, Enrique Goldenberg
Bechtel Power Corporation, San Francisco, CA USA

INTRODUCTION

The evolution of seismic design practices is related to the occurrence of major earthquakes such as the 1906 San Francisco, 1923 Kanto, Japan, the 1925 Santa Barbara, the 1933 Long Beach, the 1940 El Centro, and the 1971 San Fernando earthquake. The amount of damage sustained by power equipment and structures during these earthquakes pointed out a necessity for the Power Industry to consider the dynamic behavior of equipment and structures and to reassess seismic design practices.

Conventional designs typically use codes whose main intent is life safety, and whose failure criteria is structural collapse. These methods allow the entire ground motion to be transmitted to the superstructure; absorbing the seismic energy through inelastic behavior which invariably gives rise to damage, both structural and non-structural. From the standpoint of the structure's essential function, conventional designs may reduce injury to people, but the corresponding damage to the building's equipment and other non-structural components may be catastrophic. The ideal solution for this seismic design problem is to provide a system which absorbs or mitigates the seismic forces before they enter into the structural system. Base isolation offers such an alternative.

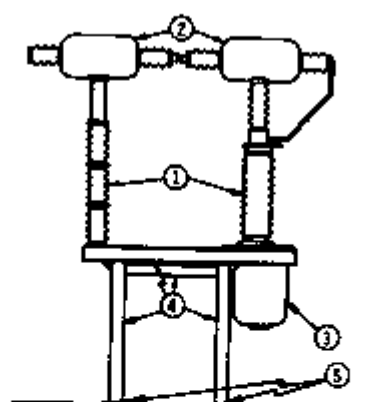
BASE ISOLATION CONCEPT

The base isolation concept used for mitigating seismic response in structures and equipment is both old and new. For years, aerospace and mechanical engineers have recognized the effectiveness of such systems which can isolate a structure from damaging vibrations.

Base isolation systems are an attractive and practical alternative. By using an isolation system, the structure's overall frequency is considerably reduced; in effect, deamplifying the floor spectra and virtually eliminating the damaging accelerations which act upon the equipment and its components. Of course, the equipment will see larger displacements relative to the ground, but these displacements can be controlled through the use of damping available in both the isolator and the equipment.

BASE ISOLATION SYSTEMS

During the past decade, several isolation devices have become available of which the elastomeric bearing offers the simplest method (Kelley 1986). The bearings, composed of steel plates bonded to vulcanized rubber possess the following characteristics (Derham 1986): 1) very stiff in the axial direction, supporting dead and live loads, 2) very flexible in the lateral direction, providing energy dissipation through the distortion of the bearing, 3) high

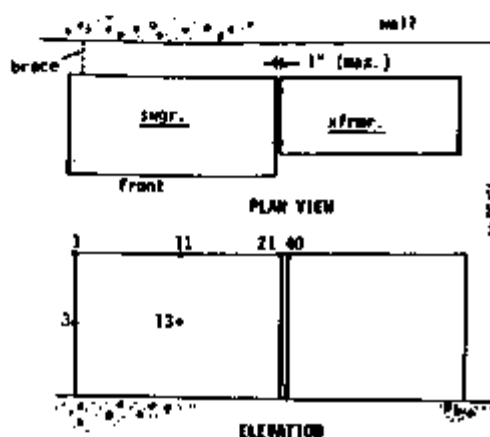


KEY (Kircher 1977):

- 1) Porcelain insulator
- 2) Breaker head
- 3) Liquid gas reservoir
- 4) Platform skid (steel structure)
- 5) Elastomeric bearings (proposed)

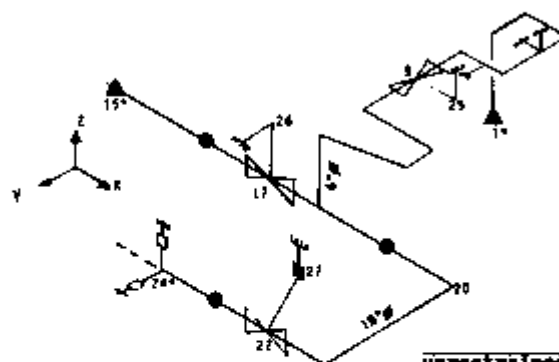
	Fundamental Frequency	Analytical Model Damping	Max. Accel. # Breaker
fixed	2.74 Hz	0.5%	9.7 g
isolated	0.3	10.0%	0.7

FIGURE 1: CIRCUIT BREAKER (Sharma et al., 1988)



	Fundamental Frequency	Analytical Model Damping	Max. Accel. # Mode 1
unbraced	4.5 Hz	2.0%	38 g
braced	9.3	2.0%	4.3
isolated	0.5	10.0%	1.7

FIGURE 2: SWITCHGEAR-TRANSFORMER ASSEMBLY (Sharma et al., 1988)



KEY:

- Rigid Hanger
- Spring Hanger
- Anchor
- Restraint
- Snubber

	Fundamental Frequency	Analytical Model Damping	Max. Accel. # Mode 20
unrestrained	3.4 Hz	2.0%	43 g
restrained	8.1	2.0%	28
isolated	0.3	10.0%	0.3

*Location of proposed elastomeric bearings

FIGURE 3: PIPE-VALVE ASSEMBLY (Sharma et al., 1988)

damping, 4) effective in main shock as well as aftershocks, 5) self centering, 6) minimum maintenance and inspection, and 7) available in different sizes, accommodating a variety of structures. In addition, elastomeric bearings have a long history of in-service performance with an existing large body of knowledge relating to their mechanical properties, quality control, and long-term reliability.

NEED FOR EQUIPMENT ISOLATION

In power plants, all structural systems and components important to safety are required to be designed to withstand the effects of earthquakes without loss of safety performance capability. These requirements point to the need for seismic qualification of equipment and systems to ensure structural integrity and functional capability during and after a seismic event. The current practice is to qualify such equipment by either testing them on a shake table or by performing detailed dynamic analysis. Equipment which has its fundamental frequency of vibration in the range of frequencies where the earthquake's energy is the strongest acts as an amplifier of the floor vibration, imposing excessive acceleration on the equipment and its devices and subcomponents. In several instances, the equipment requires stiffening or additional bracing to shift its fundamental frequency above the damaging frequency range of the earthquake. Such modifications are costly and, in many instances, difficult to implement because of the physical limitations of the equipment and its location in the plant.

COMPARATIVE STUDIES PERFORMED

The following equipment was analyzed to demonstrate the effectiveness of isolation systems: A) Circuit breaker (figure 1), B) Switchgear-transformer assembly (figure 2), and C) Pipe-valve system (figure 3). Each case was analyzed for conventional design, modified design using conventional stiffening methods, and finally base isolated design.

Circuit Breakers

Circuit breakers are vital components in switchyards which provide electrical power to large facilities. These facilities are completely dependent upon the performance of the circuit breakers. Therefore maintaining electrical power supply, especially during and after seismic events, is critical.

In California, many circuit breakers are located in seismically active areas and, in some cases, earthquake damage to circuit breakers has been extensive. Generally, circuit breaker failure has occurred due to failure of its main component, the porcelain insulator. This failure is so severe that restoring power to a switchyard is both a costly and time consuming process.

The dynamic characteristics of a 230 KV air blast circuit breaker determined from the experimental work of Kircher (1977) were used as typical values in this study. Utilizing these dynamic characteristics, a few simple analytical models were developed which had fixed base conditions representing current circuit breaker design and installation practice. The purpose of these analytical models was to simulate circuit breaker design and dynamic response characteristics. These models were subjected to the 1940 El Centro NS component. The dynamic analyses results for both the fixed base and base isolated analytical models are listed in Figure 4.

The dynamic analyses results of fixed base and base isolated circuit breaker models demonstrate the effectiveness of base isolation in the seismic design of circuit breakers.

Switchgear-Transformer Assembly

To further illustrate the case for base isolation, a problematic switchgear-transformer assembly was examined. The switchgear and transformer were originally tested and dynamically qualified separately, but when they were installed, the clearance between the two units was insufficient to accommodate

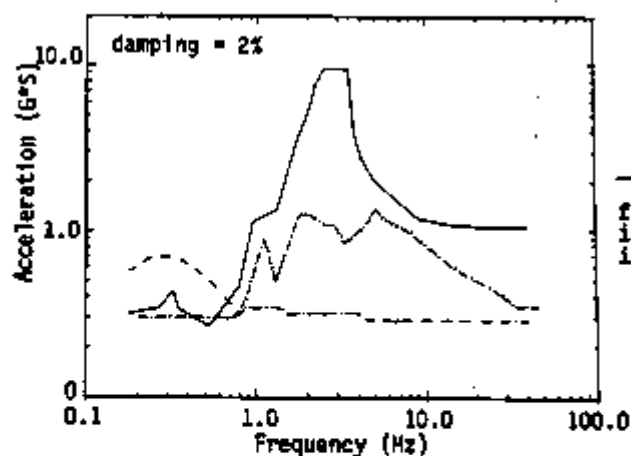


FIGURE 4
(Sharma et al., 1988)
CIRCUIT BREAKER

fixed	—————
isolated	- - - - -
input spectra	- · - · -

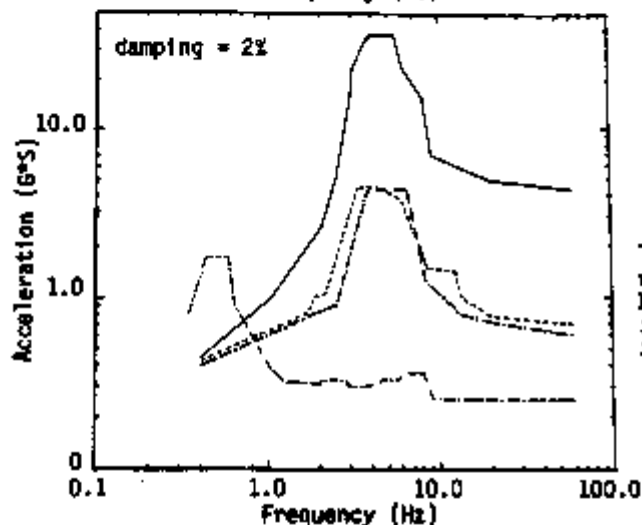


FIGURE 5
(Sharma et al., 1988)
SWITCHGEAR-TRANSFORMER
ASSEMBLY

unbraced	—————
braced	- - - - -
isolated	- · - · -
input spectra	- · · · -

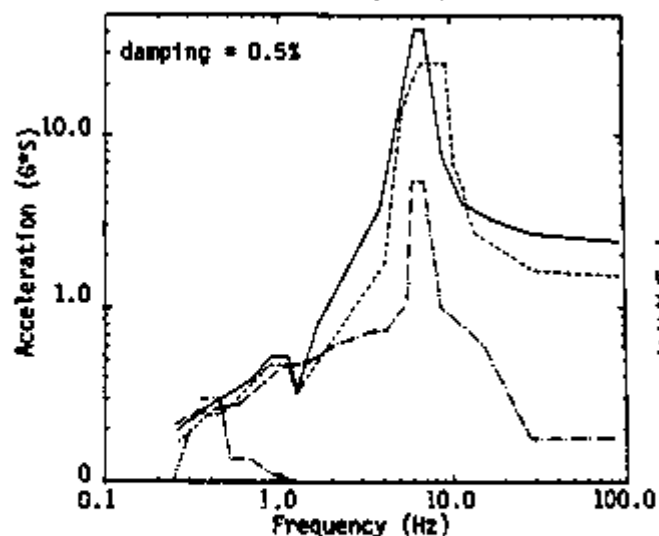


FIGURE 6
(Sharma et al., 1988)
PIPE-VALVE ASSEMBLY

unrestrained	—————
restrained	- - - - -
isolated	- · - · -
input spectra	- · · · -

the seismic displacements of the equipment. To dispel this problem, the two units were tied together by coupling mechanisms. A mathematical model of the coupled system was developed and analyzed. The analysis of this mathematical model revealed a dominant torsional mode which produced high acceleration values in the combined assembly (see figure 5). This meant that the panel mounted devices were not qualified for their actual installed condition. A solution was needed to resolve this problem.

The conventional stiffening approach was applied to the assembly by introducing a brace which connected the rear top corner of the switchgear to the wall located directly behind the two units (see figure 2). The assembly's retrofit reduced the device's required acceleration levels to within their qualified test levels (see figure 5). Although this stiffening approach produced the desired results for the above problem, it was a specific solution for this specific case. Future devices added to the panel would require minimum test levels of 9 g's (depending upon their panel location) which would be costly if not prohibitive. When there are a number of panels which require stiffening, this approach becomes very expensive since each panel must be examined on a case-by-case basis.

The same switchgear-transformer assembly (without bracing) was analyzed with base isolation. The analysis results of the base isolated system showed a significant reduction in the acceleration response (see figure 5). Base isolation effectively eliminated high accelerations in the switchgear-transformer assembly. If these units had been retrofitted with elastomeric bearings, not only would the problem of high acceleration response have been solved, but the future qualification of panel-mounted devices would have been made easier and less costly since the peak required acceleration would only be 1.7 g's.

Pipe Valve Model

Of equal relevance in the qualification of power plant equipment are valves and their associated piping system; their importance cannot be overstressed.

Valves, in certain zones of BWR nuclear power plants, are designed for dynamic loads from the combination of seismic and hydrodynamic loads. The combination of all these loads and the low damping associated with pipe systems create a potential for high acceleration response in the valves and pipe system. Many plants have undergone retrofit programs to upgrade equipment which were originally designed for seismic loads only, but require requalification for the above high frequency loads. For already installed equipment, requalifying and retrofitting is a difficult task based on both practical and cost reasons. A case in point was a torus attached pipe system reevaluated for hydrodynamic loads. In this case, the pipe system was stiffened in order to reduce the loads. Stiffening was achieved through the application of restraints at some valves, and springs, snubbers and restraints on the pipe (see figure 3). Adding restraints to a valve reduced the pipe's response, but created large reactions at the valve, overstressing it and inducing high accelerations at the valve operator. In order to resolve these problems, additional stiffness was added to the valves to increase their local frequency and reduce their component stresses. The numerous constraints of an operating plant created many design and installation difficulties.

An alternate to the extensive amount of work required to stiffen a pipe system is base isolation. The unrestrained pipe-valve system was analyzed with base isolation placed at some selected locations (see figure 3). The results of this analysis are shown in Figure 6. Not only does this approach alleviate the high responses in the pipe system, but it also eliminates the need for additional restraints.

SUMMARY AND CONCLUSIONS

From the results of these studies, the following conclusions are derived:

- 1) *Base isolation provides a very effective means of mitigating seismic and vibrational responses in the equipment and systems in nuclear power plants. Properly installed, isolation devices substantially lower*

seismic demand on equipment and piping systems, thereby eliminating the need for costly fixes and retrofiting. In addition, the system's energy absorption capacity is improved by virtue of its resilience. The reduction in response means that not just the structure but also its contents are given a similar degree of protection which is not possible without isolation.

- 2) *Isolation systems permit the analyst to preassign dynamic characteristics to the equipment, thereby making performance under seismic loads both predictable and controllable.* With base isolation systems, all significant deformations take place in the bearings whose properties are well documented and easily measured. This allows the engineer to optimize seismic design to improve equipment performance and reliability.
- 3) *Isolation systems do not require extensive detailed reanalysis for changing seismic demands on the systems, thereby saving time and cost.* Design studies are greatly simplified since the complexities of the structure, uncertainties of the structure's physical and material properties, and uncertainty in workmanship quality are greatly reduced. The analysis of an isolated structure is more reliable since the isolators can be tested for compliance with the design criteria after manufacture (Derham et al., 1986). The design analysis reduces to predicting the behavior of the bearings which is well understood, the behavior of the structure remains in the elastic range. In addition, experimental results have shown that design studies are extremely accurate in their predictions (Derham 1986).
- 4) *Seismic isolation is also effective for high frequency hydrodynamic loads and other in-plant vibrations, since most of these loads will be 'filtered' out.*

It is hoped that the preceding discussion will draw the attention of design professionals, utility owners, and researchers to the use of base isolation applications. Future studies into base isolation applications will include further examination of their interface requirements. The studies presented above demonstrate the effectiveness of isolation systems in power plant applications. Base isolation subdues the structural shakes.

ACKNOWLEDGMENTS

The authors wish to thank Julio Miranda and Armin Riaz who gave valuable contributions to the successful completion of these studies.

REFERENCES

- Derham, C. J., 1986, "Non-linear Natural Rubber Bearings for Seismic Isolation," ATC-17, Proceedings of a Seminar and Workshop on Base Isolation and Passive Energy Dissipation, Applied Technology Council, CA, pp. 315-322.
- Derham, C. J., Kelley, J. M., and Thomas, A. G., 1986, "Anti-Seismic Rubber Bearings with inherent Wind Restraint and Vibration Isolation Characteristics," SP-94, ACI Joint Sealing and Bearing Systems for Concrete Structures," Volume 1, pp. 151-165.
- Kelley, J. M., 1986, "Progress and Prospects in Seismic Isolation," ATC-17, Proceedings of a Seminar and Workshop on Base Isolation and Passive Energy Dissipation, Applied Technology Council, CA, pp. 29-37.
- Kircher, C. A., 1977, "Ambient and Forced Vibration Analysis of Full Scale Structures," Report No. 27, John A. Blume Earthquake Engineering Center, Stanford University, CA.
- Sharma, S. S., Lamore, E. M., Goldenberg, E. A., "Base Isolated Equipment - A Dynamic Solution," B8-JPGC/Pwr-25, presented at the Jt. ASME/IEEE Power Generation Conference, 9/88.